

Dissertation

submitted to the
Combined Faculty of Natural Sciences and Mathematics of
the Ruperto Carola University Heidelberg, Germany
for the degree of
Doctor of Natural Sciences

Presented by
M.Sc. Sanjana Singh
born in New Delhi, India

Oral Examination : December 6, 2019

Single-population transcriptomics as
a method to identify a network
regulating Golgi structure.

Referees :

Dr. Jonas Ries

Prof. Dr. Walter Nickel

ACKNOWLEDGEMENTS

To begin with, I would like to thank **Rainer Pepperkok** for his guidance, support and supervision during my PhD. I am grateful to him not only for the opportunity to work in his lab, but more so for teaching me how to do science. I thank you for the scientific discussions, inspiration and scientific principles that I will carry with me in my career henceforth. I would also like to thank **Walter Nickel**, **Yannick Schwab**, and **Wolfgang Huber** for their valuable input in my Thesis Advisory Committee (TAC) meetings, and additionally **Jonas Ries** and **Walter Nickel** for agreeing to be referees for my thesis. I thank **Joachim Wittbrodt** and **Martin Jechlinger** for agreeing to be on my defense committee.

During the course of my PhD, I have collaborated with several people. Among them, I would like to thank the ALMF, for training me on several microscopes and troubleshooting, as well as **Christian Tischer** for teaching me image analysis. In particular, **Volker Hilstenstein** and **Aliaksandr Halavatyi** for their help with automated microscopy. I would also like to thank **Richard Wombacher** for sharing plasmids with me. I am thankful to **Malte Paulsen**, **Diana Ordonez** and **Beata Ramasz** from the Flow Cytometry facility for the training, last minute appointments and their cooperation. A big thank you to the Genomics Core facility, especially **Vladimir Benes**, **Dinko Pavlinic** and **Bianka Baying** for bearing with and helping in the iterative troubles of the project. I am very grateful to **Jonathan Landry** for doing the sequencing data analysis for me, and patiently explaining each step. For teaching me data visualization, I want to thank **Matt Rogon**.

I have spent most of the last four years in the Pepperkok lab, where I have been fortunate to work with the best colleagues I could have hoped for. Coming into the lab with very little experience, I have to thank **Miriam** for taking me under her wing and teaching me so much, from tissue culture to German, and helping me become familiar with Heidelberg. I would also like to thank **Fatima** for her scientific as well as non-scientific help and guidance. I cannot thank enough my current colleagues – **Muzamil** for being an older brother to me, with his patient and valuable advice on matters scientific and otherwise. To **Magdalena**, for the runs, hugs, chocolate and more, thank you. To **George**, for the endless help, chats, laughs and coffees. To **Juan** for his quiet and wise advice. To **Joanna**, for taking over the project at a crucial moment and her undying optimism, it really helped. To **Alex**, for picking up this project and making it work, for always having time to troubleshoot and his quiet support. To **Lotte** and **Anthi** for their understanding and deep discussions. Thanks to **Karolina**, **Zehra** and **Cristine** for many interesting conversations. I have learned so much from you all.

I want to thank all my friends who made Heidelberg home, for the fantastic times in and outside of work. Thank you **Kuba**, **Sebastian**, **Carina** and many others for the support, advice, fun and laughter. I have been lucky to have found friends like you. Particularly special, thanks to **Ashna**, for her brilliant company as my roommate and best friend, and constant support between many frustrated chai breaks at work. You are one of the best things that happened to me at EMBL. Thank you, **Mircea**, for your boundless patience, encouragement and unending faith in my abilities. Thank you for making me smile through the stress, I could not have asked for more in a partner.

Not in the very least, I would like to thank my family. My parents, for all that they have taught me. Thank you, **Mom** and **Dad**, for making me unafraid of taking on challenges, giving me perspective, and never letting the distance get in the way of supporting me in any way possible. I am so grateful for you. A big thank you to **Gaurav**, the best little brother one could have, it's been great to see you more often. The past four years have been an incredible experience, with a lifetime's worth of lessons and memories.

SUMMARY

At the center of the secretory pathway lies the Golgi Apparatus, a uniquely structured organelle that plays a major role in protein and lipid modification, sorting and secretion. Morphologically, the Golgi is made up of cisternae which are stacked parallel to each other in eukaryotes. In vertebrates, these stacks are laterally arranged to form a peri-nuclear ribbon structure. This form of organization is hypothesized to contribute to more efficient transport and sorting of cargo. However, the exact mechanism of how Golgi organization is established, maintained and regulated is not completely clear. The presence of species without such Golgi organization, together with the dynamic nature of the Golgi suggest the presence large regulatory network in place to regulate Golgi organization. Nonetheless, so far, few studies have been able to explore such a regulatory network and major questions about the specific interactions in such a network remain unanswered.

This study was aimed at identifying regulators of Golgi organization based on their functional interactions with already established Golgi regulators. The groundwork to achieve this was laid by siRNA screens previously done in our lab and by others that revealed a large number of proteins which cause disruption of Golgi organization the knockdown. These screens, although responsible for identifying many key proteins involved in Golgi organization, did not provide information about the specific interactions. An interesting observation in these screens was however, that although the majority of the population responded a manner expected of the siRNA, a fraction of the population showed an uncharacteristic phenotypic response by retaining normal Golgi morphology.

The aforementioned observation was usually attributed to inefficient siRNA knockdown in these cells. Here, this assumption was challenged by analyzing protein levels in the two populations by immunofluorescence after siRNA knockdown, with the finding that the variability in phenotypes was not just due to transfection efficiency. Following this finding, a likely hypothesis was formulated proposing the presence of a compensation mechanism operating in these cells that enabled them to avoid Golgi disruption. Given such a scenario, comparing gene expression profiles of the dying phenotypes would highlight the proteins involved in such a compensatory mechanism, which were likely to be interactors of the protein being depleted by RNAi. Moreover, these would presumably be involved in regulation of Golgi organization at a steady state. This provided an impetus to devise a method for single-phenotype transcriptome analysis.

This was achieved by developing an advanced microscopy platform for automated detection of Golgi phenotypes using classifier-based recognition, followed by selective marking of phenotypic cells made possible by single-cell photo-activation. These two components were combined by coupling imaging with online image analysis and photo-activation of cells based on the image analysis, all in an automated fashion. The photo-activated cells were then isolated from the rest of the population by flow cytometry and processed for

transcriptome sequencing. The collection of cells could be done either in a single-cell modality or as pools of cells with the same phenotype. Thus, a generic pipeline capable of automated recognition of cellular morphology, marking and isolation of phenotypic single-cells for transcriptome analysis was developed. Two varying Golgi populations were collected in this fashion upon the knockdown of the Golgi protein USO1 and their gene expression profiles were compared.

On comparison of non-fragmented and fragmented Golgi phenotypes upon USO1 knockdown, we found a few key insights. Firstly, the two populations show an evident difference in gene expression. Conversely, little variability was observed between cells of the same phenotype. This means that there is a distinct phenotypic signature that can be detected at the transcription level. Second, both populations express USO1 at similar levels, which rules out an effect of knockdown efficiency. Lastly, and most importantly, non-fragmented cells reveal an up-regulation of a large number of signaling proteins, in particular those involved in chemokine signaling, clathrin-mediated endocytosis and many other kinases. In addition, two direct interactors of USO1 are significantly up-regulated as well, namely SEMA4F and PRKACA. These are compelling hits which will be followed up in the future. Altogether, we observe a network of signaling pathways expressed in cells that prevent Golgi fragmentation and these are likely to play a role in regulation of Golgi structure.

In conclusion, we show that variability in Golgi morphology upon siRNA treatment is not just a consequence of inefficient knockdown and describe a three-stage pipeline to perform single-phenotype transcriptome analysis. The pipeline was tested successfully on the protein USO1, which provides a promising data set for future experimentation.

ZUSAMMENFASSUNG

Der Golgi-Apparat ist das zentrale Organell im sekretorischen Weg. Er besitzt eine einzigartige Struktur und spielt eine wichtige Rolle für Protein- und Lipidmodifikationen, sowie deren Sortierung und Transport. In Eukaryonten ist der Golgi-Apparat aus einzelnen parallel übereinander gestapelten Zisternen aufgebaut. In Vertebraten sind diese Zisternenstapel in der Nähe des Zellkerns zu einem Golgi Band aneinandergereiht. Es wird angenommen, dass diese Form der Organisation des Golgi-Apparates einer effizienten Sortierung und Sekretion von Transportmolekülen zugrunde liegt. Die molekularen Mechanismen, mithilfe derer der Golgi-Apparat aufgebaut und seine Struktur erhalten und reguliert wird, sind weitgehend unbekannt. Die Tatsache, dass Organismen existieren, die solch eine Organisation des Golgi-Apparates nicht aufweisen, zusammen mit der hohen Dynamik der Golgi-Struktur, deutet darauf hin, dass Netzwerke von interagierenden Proteinen existieren, welche die Organisation des Golgi-Apparates dynamisch regulieren. Zurzeit gibt es nur wenige Studien, die solche regulatorischen Protein-Netzwerke untersucht haben, weshalb zentrale Fragen zur Funktionsweise dieser Netzwerke und den Wechselwirkungen zwischen den darin enthaltenen Proteinen noch unbeantwortet sind.

‘siRNA Screens’, wie sie in vielen Laboren in der Vergangenheit durchgeführt wurden, haben für eine große Anzahl von Proteinen ergeben, dass deren reduzierte Expression in der Zelle zu einer veränderten Morphologie des Golgi-Apparates führt. Obwohl der experimentelle Ansatz des ‘siRNA Screenings’ viele Proteine identifiziert hat, die bei der Organisation des Golgi-Apparates mitwirken, lässt sich daraus nicht ableiten, wie die einzelnen Proteine miteinander wechselwirken. Interessanterweise wird im Rahmen von ‘siRNA Screening’-Experimenten oft eine signifikante Anzahl von Zellen gefunden, die den mehrheitlich beobachteten Phänotyp nicht zeigen und eine normale Golgi-Morphologie aufweisen, obwohl das Zielprotein in seiner Expression unterdrückt ist.

Diese bisher unerklärte Variabilität der Phänotypen könnte ein Hinweis auf die Existenz kompensatorischer Mechanismen in Zellen mit einer normalen Golgi-Morphologie sein. Dabei sollten Gene, die in den verschiedenen Klassen von Phänotypen unterschiedlich exprimiert sind, mit großer Wahrscheinlichkeit an der Regulation der Golgi-Morphologie beteiligt sein. Diese Arbeitshypothese bildete die Grundlage für die hier beschriebene Entwicklung eines neuartigen experimentellen Ansatzes, mithilfe dessen das Transkriptom von einzelnen Zellen, die bei der Behandlung mit derselben siRNA verschiedene Golgi-Phänotypen aufweisen, quantitativ bestimmt werden kann. Im Rahmen dieser Arbeit wurde zunächst gezeigt, dass in allen untersuchten Golgi-Phänotypen das entsprechende Zielgen der siRNA in seiner Expression unterdrückt ist. Dieses Resultat bestätigt die oben beschriebene Arbeitshypothese.

Ziel der vorliegenden Arbeit war es deshalb, eine Methode zu entwickeln, die es erlaubt, morphologische Phänotypen in lebenden Zellen automatisch mit Hilfe eines Mikroskops zu

erkennen und deren transkriptionelles Profil zu bestimmen. Die dabei entwickelte vollautomatische Methode erkennt Phänotypen in lebenden Zellen mittels automatischer konfokaler Mikroskopie und Echtzeit-Bildanalyse, die auf computergestütztes Lernen basiert. Anschließend werden die phänotypischen Zellen ‘markiert’, indem ein im Zellkern exprimiertes, photoaktivierbares, fluoreszentes Protein (PA-FP) photoaktiviert und somit sichtbar gemacht wird. Die photoaktivierten Zellen können dann mittels Durchflusszytometrie als einzelne Zellen oder als ‘Zell-Pools’ vom Rest der Zellpopulation separiert, sowie anschließend mittels etablierter Methoden zur Bestimmung des Transkriptoms einzelner Zellen analysiert werden.

Die Machbarkeit dieser Methode wird in der vorliegenden Arbeit exemplarisch anhand des Zielgens *USO1*, welches mittels siRNA in seiner Expression unterdrückt wird, erprobt und nachgewiesen. Der im Rahmen dieser Experimente durchgeführte Vergleich von Zellen mit fragmentierter und nicht-fragmentierter Golgi-Morphologie lieferte wichtige Einsichten in die Regulierung des Golgi-Apparates. Beide Zellpopulationen weisen signifikant unterschiedliche Transkriptionsprofile auf, obwohl die Menge des exprimierten *USO1* vergleichbar ist. Im Gegensatz hierzu besitzen Zellen mit identischen morphologischen Phänotypen eine nur geringe Varianz ihrer Transkriptionsprofile. Diese Ergebnisse legen den Schluss nahe, dass morphologische Phänotypen nach Unterdrückung der Expression von *USO1* durch ihr transkriptionelles Profil gekennzeichnet sind. Zellen mit einer ‘normalen’ Golgi-Morphologie weisen eine drastische Erhöhung der Expression von Signalproteinen (insbesondere von Chemokinen, Regulatoren der Clathrin vermittelten Endozytose und vieler anderer Kinasen) auf. Weiterhin konnte nachgewiesen werden, dass in diesen Zellen zwei bekannte Interaktoren von *USO1* – nämlich *SEMA4F* und *PRKACA* – ebenfalls hochreguliert sind. Diese ‘Hits’ stellen besonders interessante Gene dar, die für zukünftige Untersuchungen von Interesse sind. Mit Hilfe der hier dargestellten Experimente konnten Signaltransduktionswege identifiziert werden, welche der Fragmentierung des Golgi-Apparates entgegenwirken und dadurch eine wichtige Rolle bei der Regulierung der Golgi-Morphologie spielen könnten.

Zusammenfassend konnte in der vorliegenden Arbeit gezeigt werden, dass die Variabilität der Golgi-Morphologie in einzelnen Zellen nach siRNA Behandlung nicht ausschließlich durch eine Variabilität der Transfektionseffizienz zu erklären ist. Die entwickelte Methode zur Korrelation von morphologischen Phänotypen mit Transkriptionsprofilen einzelner Zellen wurde anhand des Zielgens *USO1* erfolgreich getestet und stellt eine vielversprechende Grundlage für zukünftige Arbeiten dar.

CONTENTS

1	Introduction	18
1.1	The Early Secretory Pathway	19
1.1.1	ER to Golgi Transport	19
1.1.2	Golgi to ER transport	20
1.1.3	Intra-Golgi Transport	21
1.1.4	Golgi to Plasma Membrane transport	22
1.2	Golgi organization	24
1.2.1	Structure-Function Relationship of the Golgi Complex	26
1.2.2	The Golgi Complex as a dynamic organelle	26
1.3	Various Functions of the Golgi Complex	27
1.3.1	Protein and Lipid Biosynthetic center	27
1.3.2	Golgi as a calcium store	28
1.3.3	A Microtubule Nucleating Center	28
1.3.4	Signaling Platform	28
1.4	Regulation of Golgi Structure	30
1.4.1	Matrix Proteins: GRASPs	30
1.4.2	Golgins	32
1.4.3	Trafficking Proteins	34
1.4.4	Cytoskeleton	36
1.4.5	Self-Organization of the Golgi	37
1.5	Studying Golgi Organization	39
1.5.1	Why study Golgi organization?	39
1.5.2	Methods used to study Golgi organization	40
	Aims	42

2	Results	44
2.1	Examining variability in Golgi morphology upon siRNA knockdown	45
2.1.1	Different siRNA treatments have different effects on Golgi morphology	45
2.1.2	Golgi morphology is variable within single siRNA treatments	45
2.1.3	Hypothesis of a compensation mechanism to maintain Golgi structure	46
2.2	Experimental validation of hypothesis	48
2.2.1	Experimental test of the hypothesis	48
2.2.2	Characterization of Golgi populations upon siRNA knockdown	49
2.2.3	Validation of hypothesis	50
2.3	Pipeline for single-population transcriptomics of Golgi phenotypes upon siRNA knockdown	52
2.3.1	Identification of Golgi phenotypes	54
2.3.2	Selective marking of phenotypic cells	58
2.3.3	Automation of Golgi recognition and photo-activation	61
2.3.4	Collecting marked cells by Fluorescence-Activated Cell Sorting (FACS)	63
2.3.5	Preparation for RNA transcriptome analysis	67
2.4	Transcriptome Analysis	70
2.4.1	Global transcriptome analysis	70
2.4.2	Transcriptome analysis between two Golgi phenotypes	78
3	Discussion	90
3.1	Hypothesis Testing	91
3.1.1	The Hypothesis	91
3.1.2	Effect of siRNA knockdown efficiency on Golgi phenotypes	92
3.2	A method for single-phenotype transcriptome analysis	93
3.2.1	Detection of Golgi phenotypes	93
3.2.2	Selective marking of phenotypic cells	94
3.2.3	Automation of phenotype recognition and marking	95
3.2.4	Collection of marked phenotypic cells	95
3.3	Transcriptome Analysis	96
3.3.1	Global gene expression analysis	96
3.3.2	Single-phenotype sequencing	97
3.3.3	Differential expression analysis of Golgi phenotypes	97
4	Concluding Remarks	102
5	Materials and Methods	106
5.1	Materials	107
5.1.1	Cell Culture	107
5.1.2	Lab Reagents and Equipment	108
5.1.3	Antibodies	109

5.1.4	Oligonucleotides and Plasmids	110
5.1.5	Reagents for Flow Cytometry	111
5.1.6	Reagents for RNA sequencing	111
5.1.7	Kits, Analyzers and Softwares	113
5.2	Methods	114
5.2.1	Cell Biology	114
5.2.2	Microscopy	115
5.2.3	Flow Cytometry	117
5.2.4	RNA isolation	118
5.2.5	Data Analysis	122
6	Supplementary Material	126
6.1	Hypothesis testing and pipeline development	127
6.2	Transcriptome Analysis	128
6.2.1	Global Transcriptome Analysis	128
6.2.2	Single Population Transcriptome Analysis	128
7	Bibliography	164
8	Lists of Abbreviations, Figures and Tables	182

CHAPTER 1

INTRODUCTION

Compartmentalized cells rely on the secretory pathway to transport newly synthesized biomolecules from their site of synthesis to their functional destinations, be it another organelle or secreted outside the cell [1]. In its simplest form, the secretory system consists of the Endoplasmic Reticulum (ER), where protein and lipid cargo are synthesized and are then transported to the Golgi Complex (GC), where the cargo undergoes modification for functionalization. This cargo is then packaged for delivery to its target organelle or the plasma membrane at the Trans Golgi Network (TGN) [2]. This directional movement of cargo from the ER to the plasma membrane is known as anterograde transport, and is balanced by retrograde transport in the opposite direction by which membranes and resident proteins return to the ER and the Golgi. This essential process involves many intermediate compartments and vesicular structures, in conjunction with a plethora of essential and accessory proteins that co-ordinate endomembrane trafficking [3]. This thesis will focus mainly on the Golgi Complex, specifically on the organization and regulation of Golgi structure. However, in order to place the importance of Golgi structure in context, the thesis will begin with a general overview of the secretory pathway. I will subsequently narrow down and focus specific role of the Golgi Complex, finally addressing the structural aspect of Golgi structure and maintenance.

1.1 The Early Secretory Pathway

1.1.1 ER to Golgi Transport

The secretory pathway begins at the Endoplasmic Reticulum (ER). The ER is a large, continuous membrane bound organelle with specialized sub-domains employed to perform a multitude of functions inclusive of protein folding and degradation, lipid metabolism and cellular transport [4]. As newly synthesized proteins inserted into the ER in a post or co-translational manner, they undergo chaperone assisted folding and maturation. During this process proteins may form disulfide bonds, undergo oligomerization and/or associate in larger complexes [5]. The ER serves as the first point of quality control in cellular trafficking. At this stage, incorrectly folded proteins are withheld from proceeding forward for secretion. Properly folded proteins are allowed to proceed to specific ribosome-free sub-domains of the ER known as ER-exit sites (ERES) [6]. An important feature of ERES is the concentration of a group of vesicular coat proteins called COPII proteins. The COPII coat consists of five proteins – Sar1, Sec23, Sec24, Sec13 and Sec31 [7]. The formation of a COPII vesicle is initiated by the activation of the small GTP-binding protein Sar1[8] by the guanine nucleotide-exchange factor Sec12. Sar 1 interacts directly to recruit Sec23 and Sec24. These proteins drive cargo capture by direct binding of cargo to Sec24 adaptor subunits and assemble the inner coat of the vesicle by forming tight heterodimers [9]. Many cargo proteins have specific signal sequences that mark them for COPII transport, while others may be incorporated via bulk flow [10]. The final step in building a COPII

vesicle is the assembly of the outer coat, formed by the dimerization of Sec13-Sec31 [11], which envelope the inner coat proteins in a cage-like construction owing to the direct interaction between Sec31 and Sec23. After successful assembly of all the components, the COPII coated vesicles bud off the ER membrane as 60-70 nm structures and shed their coat proteins, often combining to form Vesicular Tubular Structures (VTC's)[12]. VTC's can range from 60nm to 200nm in diameter, which join together to form a compartment in their own right, called the ERGIC (ER-Golgi Intermediate Compartment)[13].

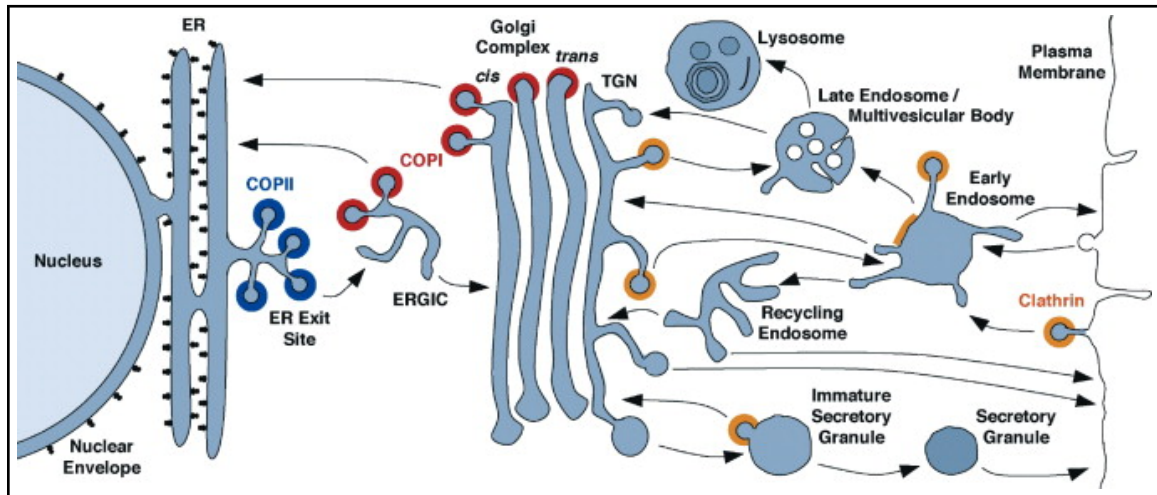


Figure 1.1: Overview of the Secretory Pathway, starting with the Endoplasmic Reticulum, where newly synthesized proteins and lipids are transported via vesicles to the Golgi Complex. This cargo undergoes modification and functionalization at the Golgi before being sorted to other organelles or for secretion. Adapted from Duden R. 2003 [14].

1.1.2 Golgi to ER transport

From the ERGIC compartment, ER resident proteins and membranes are recycled back to the ER. This is enabled by another set of vesicular coat proteins known as the COPI coat [15], which assembles on ERGIC and early Golgi membranes. The COPI coat is a heptameric structure comprising of COPA, COPB1, COPB2, COPD, COPE, COPG and COPZ subunits ($\alpha, \beta, \beta', \gamma, \delta, \epsilon, \zeta$). Subunits α, β, ϵ comprise the outer COPI coat, and the inner coat is formed by the β, δ, γ and ζ subunits [16]. This cytosolic protein complex is recruited by the GTP binding protein Arf-1 [17] which mediates the association of the coat proteins with the ERGIC/Golgi membranes in its GTP bound form. Arf-1 in turn requires activation by the Arf-Guanosine Exchange Factor (GEF). In Resident ER proteins usually carry a signal sequence that allow their retrieval into the ER. ER luminal proteins have a C-terminal KDEL sequence that is recognized by a KDEL receptor, which binds the COPI machinery to retrieve luminal ER proteins [18]. This receptor itself cycles between the ER and the Golgi Complex. Transmembrane proteins belonging to the ER are identified for retrieval using another signal sequence, characterized by the motif KKXX or KKKXX

at their C-terminals [19]. There are other such sequences that aid retrieval of proteins to the ER, and often mis-folded proteins that escape the first checkpoint of quality control are also brought back by retrograde trafficking from the ERGIC/Golgi back to the ER by molecular chaperones.

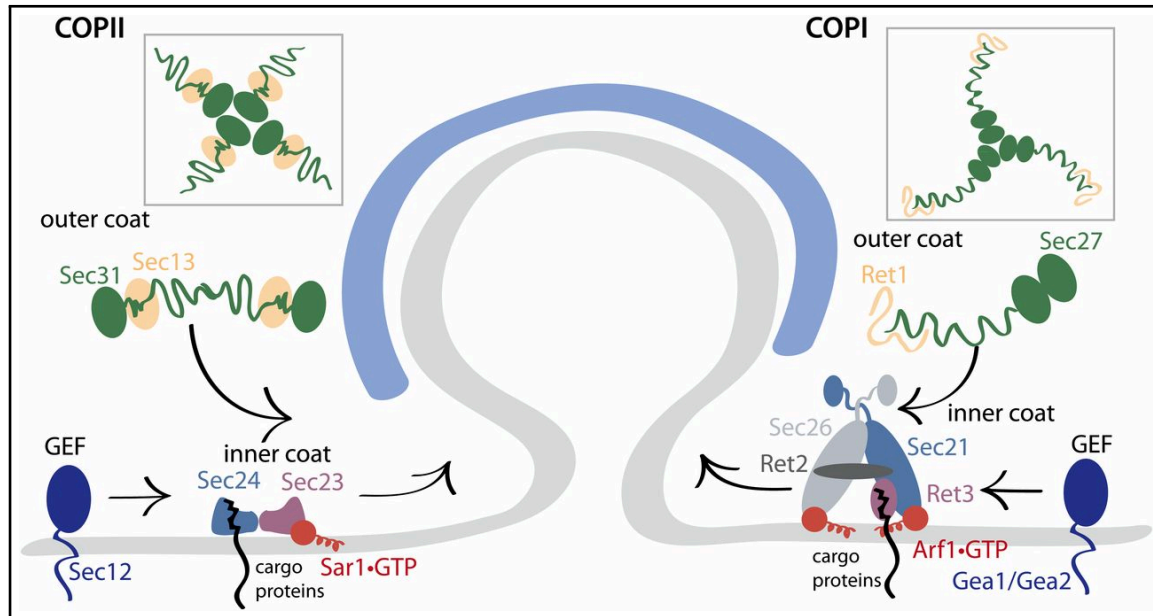


Figure 1.2: Components of the COPI and COPII vesicle coat proteins. COPII coat proteins assemble on special ER membrane sites and bud vesicles containing cargo directed to the Golgi Complex. COPI coat proteins assemble on early Golgi membranes to bud vesicles returning back to the ER. Adapted from Barlowe CK, Miller EA. [20].

1.1.3 Intra-Golgi Transport

How cargo travels once it arrives at the Golgi Complex has long since been a debated subject. Many models have been proposed to describe intra-Golgi trafficking, which have either been stand-alone transport models or combinatory models. Two major models in opposition are the Vesicular Model (VM) [21] and the Cisternal Maturation Model. The Vesicular model proposes that COP-I vesicles bud off from the Golgi membrane, un-coat, travel to the next Golgi cisterna and fuse with the distal membrane with the help of tethering proteins [22]. The primary facets of this model hypothesize that COP-I vesicles should be of comparable size to the cargo, and the cargo should be concentrated in these vesicles [23]. Moreover, if this model is accurate, there must be a way to target these vesicles to the correct Golgi cisterna. The Vesicular Model was not able justify its predictions and the Cisternal Maturation Model provided a better explanation for the experimentally observed data. This model regards Golgi cisternae as transient compartments that subsequently mature into the next cisterna [24]. This means that new cisternae are constantly formed at the *cis* face of the Golgi by fusion of vesicles with the ERGIC compartment and these gradually mature into *trans* cisternae, finally resulting in fragmentation into

secretory vesicles at the Trans-Golgi Network (TGN)[25].

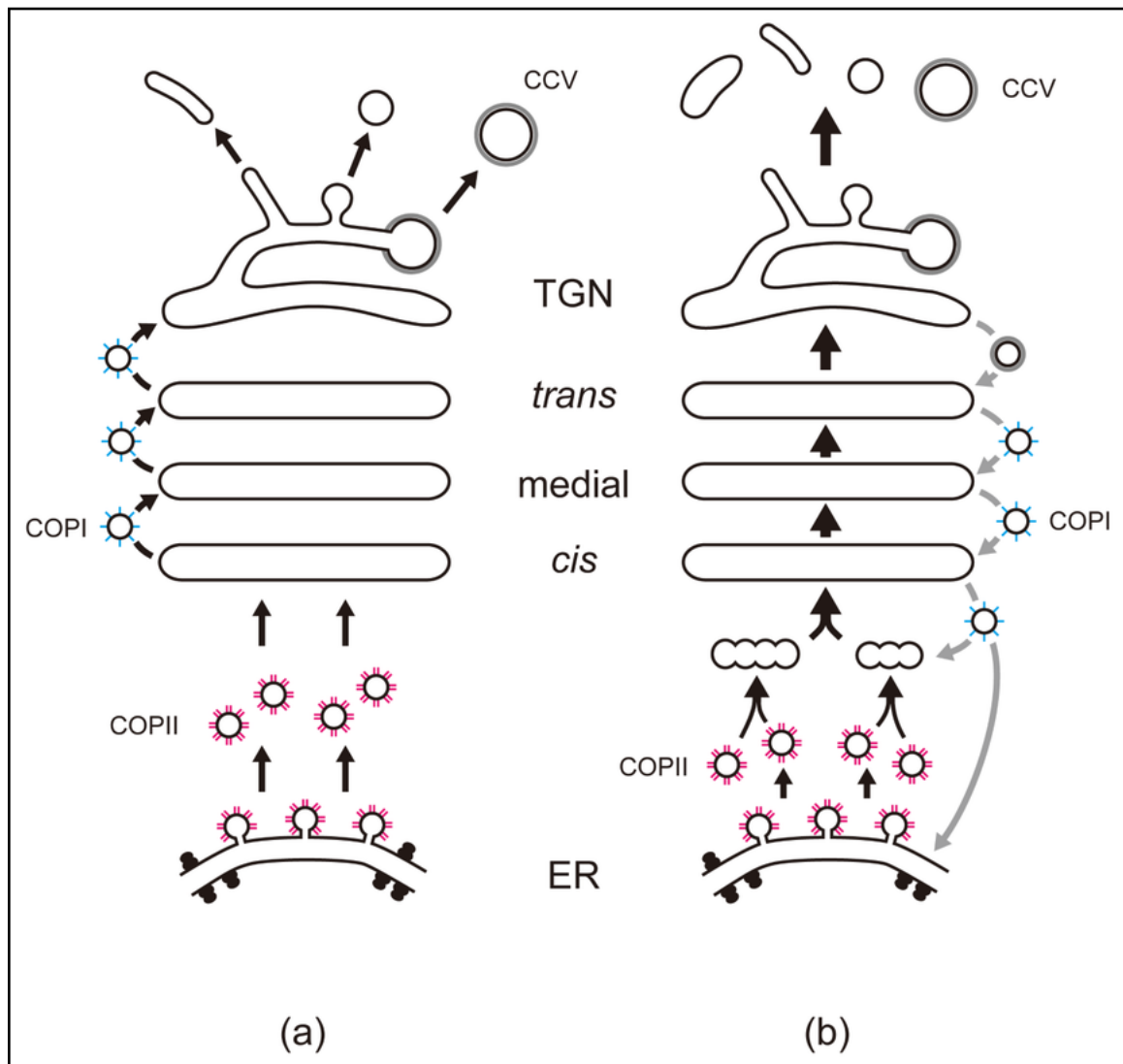


Figure 1.3: Two models of membrane traffic. Figure **a** depicts the vesicular model where cargo is carried through subsequent compartments of the Golgi by COPI vesicles that bud off each compartment. Figure **b** shows the cisternal maturation model, which claims that cisternae mature as they travel through a Golgi stack, and are transient compartments continually formed at the *cis*-Golgi. Adapted from Glick BS, Nakano A. [26]

1.1.4 Golgi to Plasma Membrane transport

At the Trans-Golgi Network (TGN), mature proteins and lipids are sorted for their forward journey towards the Plasma Membrane, endosomes and secretory granules or for retrograde transport to earlier Golgi cisternae or the ER [27]. The TGN also receives cargo from various endosomes for retrograde transport, providing a point of convergence of the secretory and endocytic pathways [27]. More than five pathways have been described for transport of cargo from the TGN in the anterograde direction, and there are

still other pathways that describe retrograde traffic towards the early Golgi. The TGN carries distinct membrane domains from which coated/uncoated vesicles as well as tubular structures carrying mature cargo emerge [28]. These structures are called Post-Golgi Carriers (PGC's). PGC's emerge by elongation of distinct cargo enriched domains of the TGN along microtubule tracks. These elongated structures undergo maturation, wherein cargo is segregated from Golgi resident proteins such as glycosyltransferases and transporters. Upon maturation, PGC's are severed from the Golgi membrane either simply by membrane elongation or with the help of the mechanoenzyme Dynamin-2 [29]. The specificity of the cargo destinations might be conferred in part by a class of Golgins at the TGN, identified by a GRIP domain. It is shown that these Golgins play a crucial role in anterograde (golgin-254 and golgin-97) as well as retrograde transport (GCC88 and GCC185) [30]. GCC185 has additionally been implicated in recruitment of the microtubule regulatory protein CLASP, providing a link between the cytoskeleton and the trans-Golgi Network. PGC's travel and fuse with the plasma membrane in a random fashion in non-polarized cells, while in polarized cells, cargo targeted to the basal plasma membrane bud from COP-I enriched Golgi cisternae [31].

1.2 Golgi organization

The Golgi Complex is fundamental feature of eukaryotic cells. The unique organization of the Golgi has both intrigued and puzzled biologists for decades. The basic constituents of the organelle are flattened membrane discs known as cisternae, which orient themselves along microtubules and have a diameter ranging between $0.7 - 1.1 \mu\text{m}$ [32]. These cisternae are ordered parallel to each other, giving rise to a pile of membranes known as a Golgi stack. A typical mammalian cell may contain between 4 to 11 cisternae in a stack, although the number of cisternae varies depending on the cell type [31].

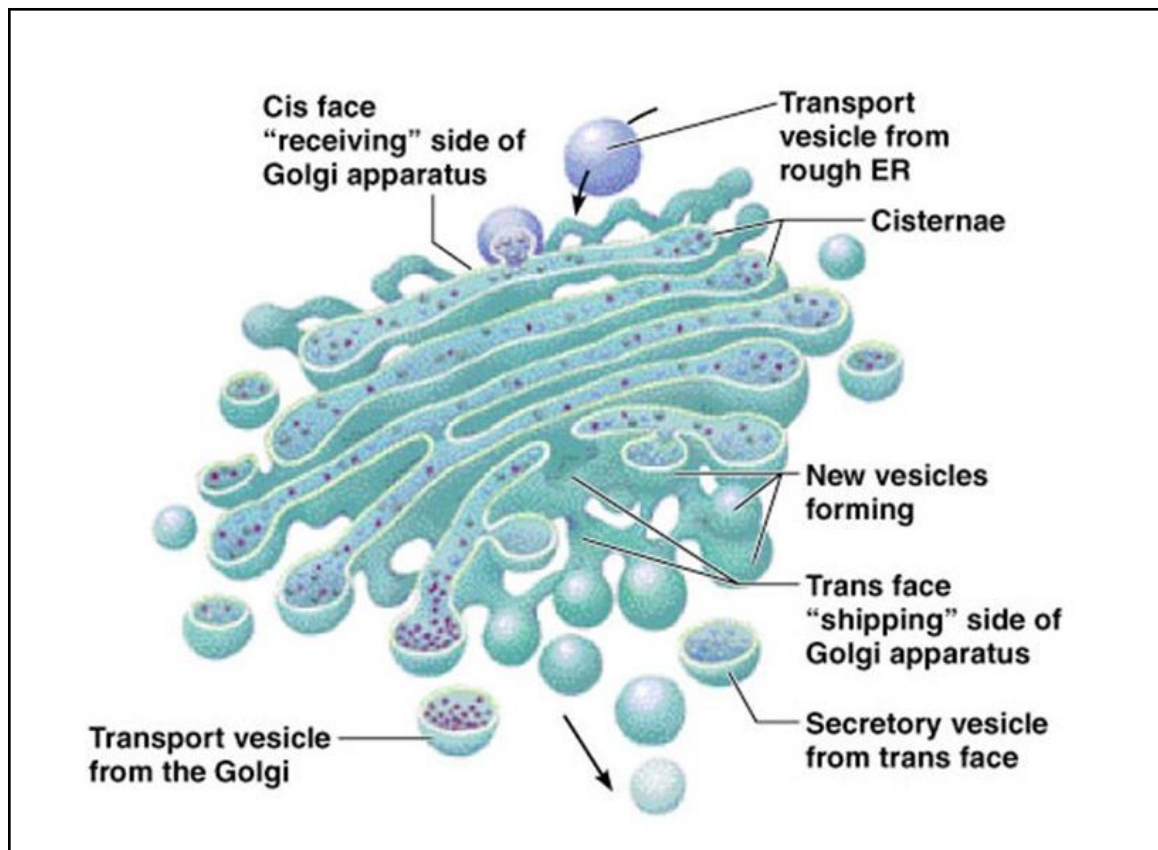


Figure 1.4: Organization of a single-stack of the Golgi Complex. This consists of a polarized stack of cisternae where material enters the stack through the *cis* face and exits through the *trans* face. Adapted from Benjamin Cummings, Pearson education 2008.

The cisternae can be divided into three main sub-compartments based on their location within the Golgi stack: *cis*, *medial* and *trans* [33]. The *cis* cisternae form a tubular network interacting with the ERGIC compartments whereas the *trans* cisternae interact with the TGN [34]. Cisternae along the Golgi stack differ not only in location, but in their membrane compositions, thickness, pH, as well as the enzymes they house. This results in several gradients operating through a Golgi stack [35]. Individual Golgi stacks are encapsulated in a ribosome-free protein matrix called the 'compact zone' of the Golgi,

which is speculated to contain proteins that maintain the structural integrity of the Golgi Complex[36].

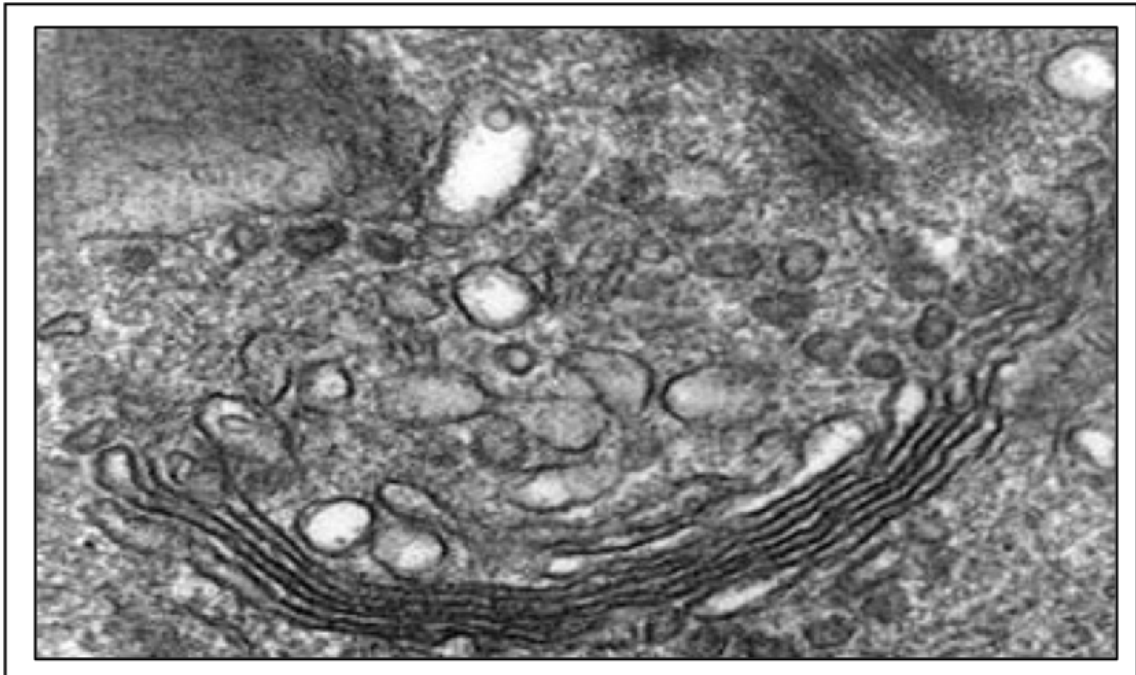


Figure 1.5: Electron micrograph of the Golgi Complex. Multiple Golgi stacks can be seen linked together to form a ribbon-like structure that typically localizes in the peri-nuclear area of mammalian cells.

The architecture of individual cisternae is narrow at the center and distended at the rims. At these rims, the cisternal membrane is punctured with holes called fenestrae, which can be as large as 100nm in diameter [37]. Cisternae show a particular pattern of fenestration – the holes are larger closer to the *cis* and *trans* ends of the Golgi and reduce both in number and size towards the center of the stack. These fenestrae and increase the surface-to-volume ratio, which play a role in the formation and partitioning of vesicular cargo [38]. From fenestrated rims of the Golgi stacks emerge tubules, forming a less organized, albeit large reticular network called the ‘non-compact zone’[39]. These tubules can connect cisternae within the same stack, and some tubules extend to laterally connect adjacent stacks. This configuration is seen in mammalian cells and is referred to as a Golgi ribbon [40]. The Golgi ribbon nests in the peri-nuclear area, in close proximity to the microtubule organizing center (MTOC). Unsurprisingly, the maintenance of the ribbon structure is closely dependent on the cytoskeleton and disruptions of actin or microtubule networks cause the ribbon to dismantle [41]. At either polar end (*cis* and *trans* faces), the Golgi associates with tubular networks such as Vesicular Tubular Structures (VTC’s) on the *cis* side and the Trans-Golgi Network (TGN) on the *trans* side that link different organelles of the secretory pathway [42]. The Golgi Complex in plants and

fungi lack the continuous ribbon organization, and present as individual stacks dispersed in the cytoplasm. Moreover, in some species like baker's yeast (*saccharomyces cerevisiae*), individual unstacked cisternae are found as tubular structures, lacking any of the sophisticated organization of the mammalian Golgi. Since such organisms still achieve effective intra-cellular transport[43], an important point of discussion is the relationship between the structure and the function of the Golgi Complex.

1.2.1 Structure-Function Relationship of the Golgi Complex

There are several speculations about the reasons for the unique organization of the Golgi complex. Firstly, different cisternae house different glycosylation enzymes in their optimal enzymatic environment [43]. Therefore, as cargo moves through different cisternae in a stack, it is sequentially exposed to modifying enzymes in a particular order [44]. This is, in part verified by the fact that species lacking Golgi stacks have fewer glycosylation enzymes[45]. The close proximity of cisternae in a stacked orientation makes the movement of cargo from one cisterna to the next faster and more efficient, as well allowing for iterative sorting of cargo[46]. The reduced distance between cisternae could also be important in regulating the flux of vesicles by limiting the membrane surface available for vesicle formation, indicated by observation that unstacked cisternae show a faster rate of vesicle formation [47]. The ribbon structure is seen only in vertebrates, and its loss does not have a dramatic impact on secretion. However, the ribbon is vital for directed secretion in polarized and migrating cells, as well for optimal centrosome positioning [48]. Another important function of the Golgi ribbon is as a cell cycle checkpoint. Normally the ribbon unlinks in the G2 phase in preparation for mitosis [49]. If ribbon breakdown is prevented, this process fails to occur resulting in mitotic arrest [50]. Altogether, these factors provide a reasonable explanation of the importance of Golgi organization, but further evidence is necessary to cement these inferences.

1.2.2 The Golgi Complex as a dynamic organelle

Despite the sophisticated architecture of the Golgi Complex, it is a highly dynamic organelle capable of rapid disassembly and reassembly. The most obvious case of this reorganization is during mitosis [50]. At the onset of mitosis, the Golgi ribbon is un-linked and peripheral membrane proteins are released into the cytoplasm. The individual Golgi stacks undergo unstacking and vesiculation [51]. This process is mediated by Arf1, and requires the phosphorylation of GM130 and GRASP65 by the mitotic kinases Cdk1 (Cyclin-dependent kinase 1) and Plk1 (Polo-like Kinase 1)[52][53]. Phosphorylation disrupts the tethering function of these proteins, causing Golgi disassembly [54][55]. Resulting Golgi vesicles are dispersed in the cytoplasm, and many are found to associate with astral microtubules at spindle poles. The Golgi membranes re-form their original stacked organization after during telophase and cytokinesis, mediated by SNARE-led membrane fusion (dis-

cussed later).

There is an ongoing debate as to whether Golgi vesicles remain as independent structures and are stochastically distributed or if they are reabsorbed into the ER and partitioned together with ER during metaphase. One theory maintains that these vesicles remain independent entities and serve as a template for Golgi biogenesis during mitosis [56] [57] [58][54]. The other argues that Golgi biogenesis occurs from ER, assembling the organelle *de novo* in the daughter cells [59] [60] [61] [62].

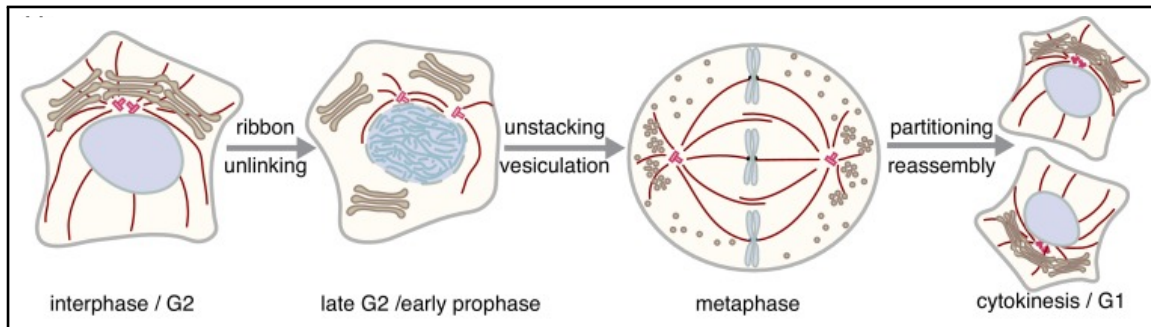


Figure 1.6: Breakdown of Golgi architecture at the onset of mitosis resulting in complete dispersal into a haze by metaphase. Consequently, the Golgi re-assembles in the two daughter cells. Adapted from Wei JH, Seemann J. [63]

1.3 Various Functions of the Golgi Complex

1.3.1 Protein and Lipid Biosynthetic center

A historically known fundamental role of the Golgi Complex is the modifications of proteins and lipids synthesized in the ER, in order to prime them for both further transport and function [64]. One of the major modifications that biomolecules undergo in the Golgi is glycosylation [65]. N-linked glycosylation begins in the ER, and upon arrival to the Golgi, further alterations are made by trimming/adding additional sugar residues. The gradient of enzymes in a Golgi stack ensures the sequential attachment of sugars such as N-acetylglucosamine, galactose, sialic acid and fucose [66]. The precise mechanisms by which resident enzymes are retained at specific cisternae, as well as the regulation of their activities is not well understood. There is evidence that glycosylation activity is coupled to nutrient levels and can drive certain cell-fate decisions. Some O-glycosylation enzymes respond to growth factor stimulation by increasing their activity to foster more cell-cell interactions. Needless to say, glycosylation of proteins is of prime importance, and glycosyltransferases at the Golgi regulate a variety of cellular process, directly or indirectly [67].

1.3.2 Golgi as a calcium store

A role traditionally attributed to the ER, it is now known that Calcium can be stored in the Golgi Complex, and released upon both extracellular cues as well as intracellular signal [68]. Calcium storage and release at the Golgi is mediated mainly by two classes of Ca^{2+} pumps, namely SERCAs (Sarcoplasmic/Endoplasmic Reticulum Ca^{2+} -ATPases) and the SPCAs (Secretory Pathway Ca^{2+} -ATPases) [69]. Ca^{2+} release from the Golgi has been shown to regulate ER-Golgi transport, intra-Golgi transport as well as Golgi-Plasma Membrane transport. The resulting change in luminal calcium levels would add a layer of regulation to the glycosylation and sorting of proteins within the Golgi. Lastly, Calcium release from the Golgi could also serve as a communication mechanism with neighboring organelles [70].

1.3.3 A Microtubule Nucleating Center

Microtubules (MTs) are essential for the movement of vesicular traffic in cells. Disruption of the MT network using the depolymerizing drug Nocodazole results in traffic defects and causes breakdown of the Golgi ribbon into mini-stacks [71]. The centrosome is regarded as the Microtubule Organization Center (MTOC), responsible for anchoring and nucleation of majority of the Microtubules. Although Golgi organization and function is dependent on centrosomal MTs [72], they are not optimal for directional cargo delivery. In 2001, the Christian Poüs group showed that the Golgi serves as an additional MTOC, nucleating two different classes of MTs [73]. These MTs have primarily two functions – adhesion of Golgi stacks to form the ribbon structure, and asymmetric delivery towards one end of polarized cells. MT nucleation at the GC is dependent on α -tubulin, similar to centrosome-derived MTs, as well as the scaffolding protein AKAP-9 (AKAP450). AKAP9 is recruited to *cis*-Golgi membranes by interacting with the Golgi protein GM130 [74]. Microtubules emanating from the Golgi are coated with a class of proteins called CLASPs (CLIP-associated proteins), which are responsible for stabilizing dynamic microtubules [75]. Golgi-derived MTs are the preferred tracks for vesicular cargo, since their minus ends are anchored at the Golgi.

1.3.4 Signaling Platform

The Golgi Complex acts as a signaling platform for a variety of cellular processes. These processes can either be related to Golgi structure and function, or be completely independent of trafficking. The Golgi responds to relayed signals originating outside the cell, cascades coming from other organelles as well as self-generated cues [76].

Plasma Membrane initiated signaling

The typical Ras/MAPK (Mitogen Activated Protein Kinase) is triggered by growth factors binding to Plasma Membrane receptors. Growth factor stimulation can also lead to Ca^{2+}

dependent activation of Ras at the Golgi Complex [77] [78]. This process is independent of trafficking and is triggered after Ras signaling is switched off at the Plasma Membrane by the same second messenger, i.e, Ca^{2+} [79]. In addition, Ras activation at the Golgi results in a different response to the Plasma Membrane activation [80]. It has been proposed that the type and duration of the signal plays a role in the outcome of signaling at the Golgi Complex, and the presence of Ras at the GC gives another view to look at the role of Golgi in oncogenic transformation and cancer [81][82] [83] [84].

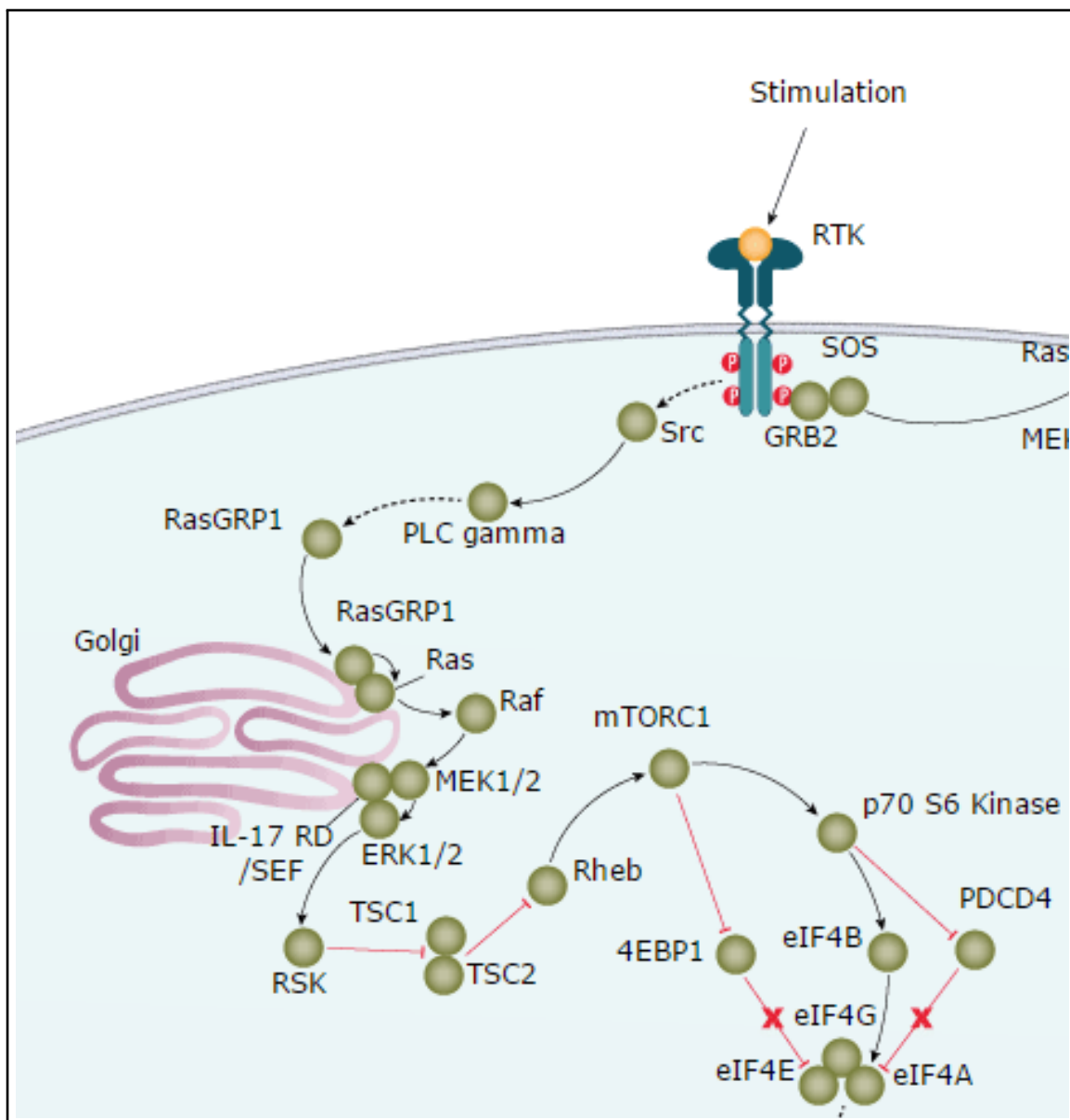


Figure 1.7: MAP Kinase signalling is an example of the many signaling pathways that involve the Golgi Complex to regulate a variety of cellular responses, including transcription. Modified from RnD Systems, Inc. 2014.

Organelle mediated signaling

The best example of signal-mediated regulation at the Golgi is shown in lipid homeostasis [85]. The sterol sensing pathway consisting of SREBPs (Sterol Regulatory Element Binding Proteins). At high sterol levels, SREBPs are kept inactive owing to their binding to SCAP (SREBP Cleavage Activation Protein). SREBP-SCAP is kept in the ER, and upon sterol depletion is transported to the Golgi Complex [86]. Here it undergoes cleavage to its active form which further translocate to the nucleus in order to activate sterol regulatory elements [87] [88]. In a similar fashion, the master regulator of the unfolded protein response – ATF6 is also moves from the ER to the Golgi for cleavage to its active form following translocation to the nucleus for activation of ER-stress response genes [89]. Another vital role played by the Golgi is in sensing the nutrient level of the cell and appropriate modulation of cell growth and trafficking [90]. A striking example of this is the mediation of both SREBP-2 and ATF6 by mTOR (mammalian Target Of Rapamycin) in response to low glucose levels resulting in inhibition of lipogenesis as well as activation of ER-stress pathways [91]. Another important example of such regulation is seen in the levels of PI4P (Phospho-Inositide-4-Phosphate) at the Golgi [92]. Interestingly, nutrition and growth status of a cell has a significant effect on PI4P levels, as maintained by respective kinases and phosphatases. PI4P in turn regulates a number of proteins that have an impact Golgi structure and function [93]. Needless to say, more and more examples of signaling at the Golgi are being discovered, opening the view of the Golgi as a vital signaling focal point.

Signaling from within the Golgi

Apart from responding and converging external signals, the Golgi also signals in response to cargo delivery by the ER. The KDEL receptor via which chaperones are trafficked back to the ER plays another role at the Golgi, activating a phosphorylation cascade that is required for intra-Golgi transport [94] [95]. This is probably one part of a network of auto-regulation that controls traffic at the Golgi Complex.

1.4 Regulation of Golgi Structure

The Golgi Complex is a highly organized and highly dynamic organelle, which suggest the presence of a large regulatory network capable of rapidly modulating Golgi structure. Therefore, it is no surprise that many factors are implicated in the maintenance of the Golgi complex, and the most extensively studied ones are detailed below.

1.4.1 Matrix Proteins: GRASPs

Golgi Reassembly and Stacking Proteins (GRASPS) are peripheral membrane proteins anchored to the cytoplasmic face of the Golgi Apparatus [36]. Mammalian cells express

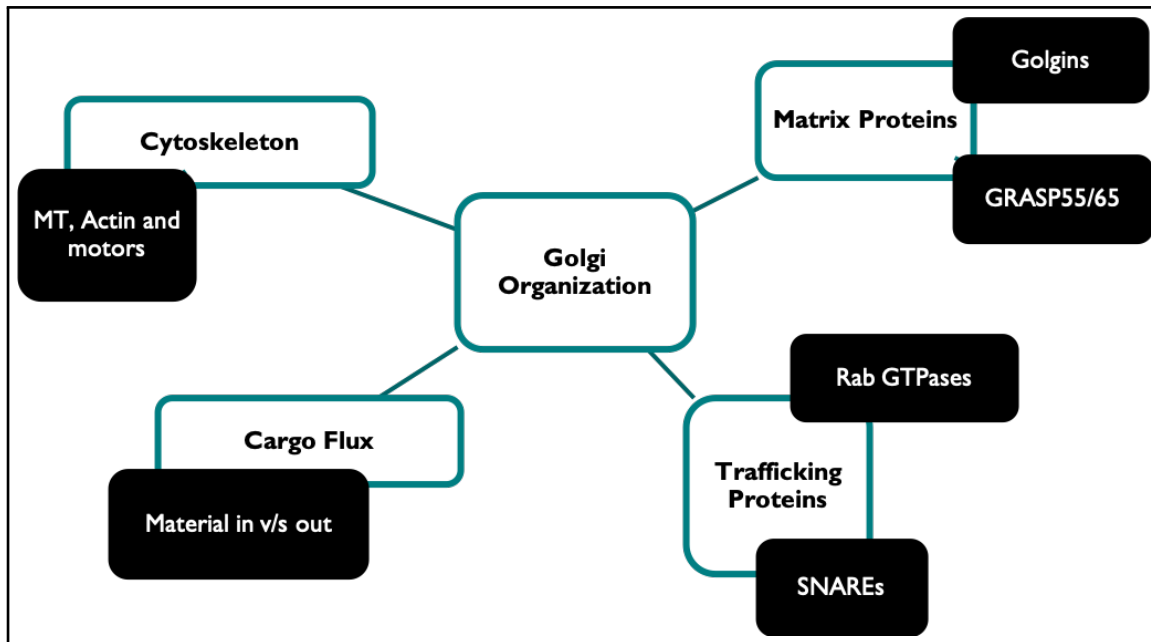


Figure 1.8: Golgi organization depends on various factors, including specialized matrix proteins, elements of the cytoskeleton, trafficking proteins and volume of cargo.

two GRASPs – GRASP55 and GRASP65, which are similar in structure and sequence, but differ in their location at the GC [96]. GRASP65 is found on *cis*-Golgi membranes, whereas GRASP55 is located at the medial cisternae. These two proteins have been significantly implicated in maintaining the stacked structure of the Golgi [39]. There are several reasons for this. Firstly, the size of the peripheral globular domain of GRASP proteins fits the small gap between the cisternae making them ideal stacking candidates. In addition, these globular domains form homo-dimers that then oligomerize with dimers from adjacent cisternae [97] [98]. Moreover, *in vitro* studies showed that when GRASP65 is coated onto the surface of beads, it causes the beads to aggregate [99] [100] and expressing GRASP65 on the outer membrane of mitochondria led to mitochondrial aggregation [101]. Also, microinjection of GRASP65 antibodies into cells inhibited post-mitotic Golgi reassembly [47]. Depletion of either GRASP by RNAi reduced the number of cisternae per stack (Sütterlin et al., 2005), which was rescued by expressing exogenous GRASP proteins [102]. Further evidence came from the simultaneous depletion of both GRASPs, which caused complete disassembly of the Golgi stacks [103] [104]. Although these studies seem convincing, more work in the last decade has shown equally convincing counter evidence, challenging the role of GRASPs as stacking factors. RNAi depletion experiments of either GRASP done by Linstedt and colleagues showed the loss of ribbon connectivity in depleted cells, with largely no effect on stacking [105]. This proposed a role of GRASPs in ribbon linking rather than stacking. A study from the Rothman lab used electron microscopy to show that efficient stacking occurs in the absence of GRASP65/55 when their respective binding partners- GM130 or Golgin-45 was overexpressed. They hypothesize that it is the

total adhesive energy provided by a large number of proteins that glues Golgi cisternae into a stack, rather than individual factors [106]. Golgi biogenesis experiments where the Golgi is removed from living cells using laser nanosurgery also revealed that siRNA depletion of either GRASP did not affect biogenesis, whereas co-depletion of both GRASPs resulted in a delay in biogenesis (Gayathri Vegesna, unpublished work). Regardless of their specific role in Golgi structure, GRASPs remain vital components in the network that regulates Golgi organization.

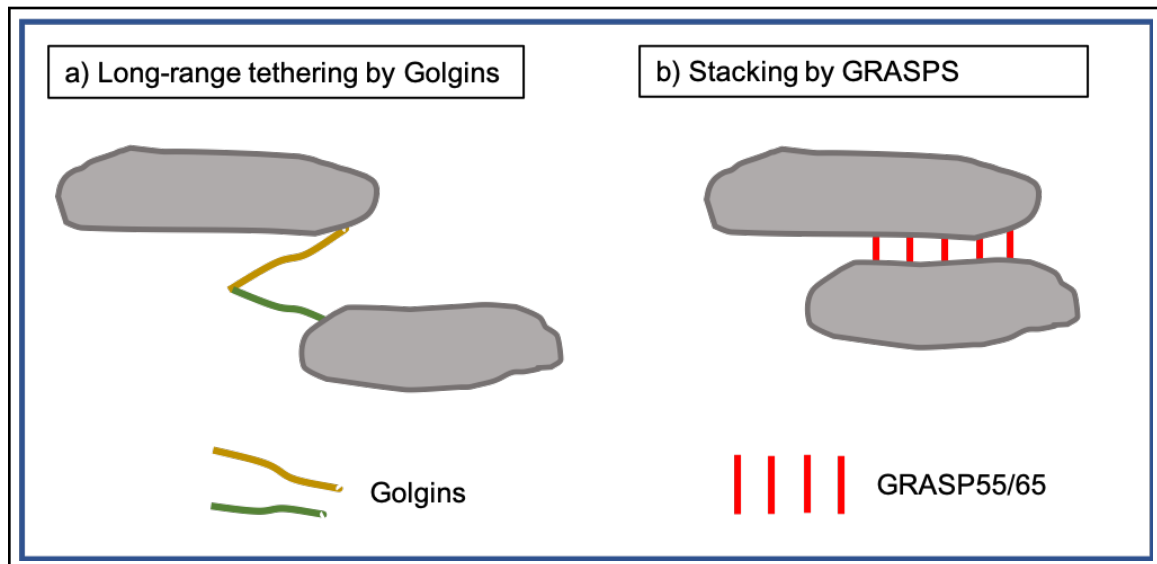


Figure 1.9: Schematic of Golgi organization by Golgins and GRASPs. Golgins mediate long-range tethering of different membranes and GRASPs operate at smaller distances, acting as a glue to hold the membranes close together.

1.4.2 Golgins

Golgins are a family of proteins characterized by their extensively coiled-coil domains that are known to form a rod-like structure. They were originally identified as Golgi-localized auto-antigens cytoplasmic face of the Golgi [107]. Another feature that Golgins have in common is that they interact with small GTPases [36]. Golgins make up a large family of proteins that vary considerably in structure and function. The coiled-coil nature of Golgins make them ideal tethering proteins [108]. They are capable of linking membranes over relatively long distances, which allows for efficient capture of cargo between compartments. Tethering not only serves to capture cargo for traffic, but is also required for cisternae formation and ribbon linking [109]. Upon long-range capture of membranes by Golgins, a GTPase dependent conformational change in the coiled-coil region that enables the Golgin to bend in order to bring the target membrane in close contact with the recipient membrane. This would be followed by SNARE pairing and subsequent membrane fusion. Some Golgins can interact directly with SNARE proteins, others interact with other tethering complexes such as the COG and TRAPP complexes [110] [111]. The

function of a few key Golgins are described below:

P115 (USO1)

USO1, also known as p115, is a tethering factor essential for ER-Golgi transport. p115 simultaneously binds the vesicle localized golgin Giantin and the Golgi localized GM130 for long range tethering [112], followed by direct interactions with SNARE proteins to facilitate docking of both COPI and COPII vesicles [113][114]. Depletion of this protein causes severe transport inhibition of cargo, causing it to accumulate in Vesicular Tubular Structures (VTC's) after ER exit [115] [116]. USO1 is also known to be essential for Golgi biogenesis [117], and RNAi mediated USO1 knockdown results in dramatic Golgi fragmentation, which is specifically attributed to loss of USO1-SNARE interactions. In addition to this, p115 is also a proposed cell cycle regulator, being phosphorylated during mitosis, which inactivates its docking function, thus halting traffic and fragmenting the Golgi Complex [118].

GM130

GM130 is one of the most extensively studied Golgins, originally identified using anti-sera from an autoimmune patient [107] as a part of the soluble Golgi fraction. GM130 is located at the *cis*-Golgi via its interaction with GRASP65, and interacts with p115 at its N-terminus. Perturbation of the GM130-p115 interaction deters both traffic and Golgi assembly, but siRNA mediated depletion of GM130 seems to have an effect on ribbon formation, but not stacking. Evidence indicates that GM130 is probably essential for ER to *cis*-Golgi transport [103]. The precise effect of GM130 depletion on secretion is unclear, as transport of certain cargo is affected while others remain unaffected [119]. Trafficking at higher temperatures is significantly affected in the absence of GM130, which supports the idea that it probably plays a major role under abnormal conditions but is compensated by other proteins under normal conditions [120].

Giantin

Giantin, as the name suggests, is a large (400 kDa) protein that localizes to the edges of the Golgi stack as well as COPI vesicles [121]. It is an integral membrane protein that also binds p115 at the same site as GM130 [122]. It is proposed that Giantin forms a complex with p115, GM130, rab1 and SNARE complexes to mediate tethering and membrane fusion of mainly COPI vesicles [123]. siRNA mediated depletion of Giantin was shown to cause increased cargo transport in conjunction with impaired glycosylation. Furthermore, depletion of Giantin also led to increased dispersion of Golgi stacks in nocadazole treated cells [124]. Although the exact role of this Golgin is yet to be elucidated, it is likely to play a role in both structural organization and glycosylation by the Golgi.

GMAP210

GMAP210 (Golgi Matrix Associated Protein 210) is a peripheral cis-Golgi protein that associates with the cytoskeleton [125]. Biochemical studies suggest the involvement of GMAP210 in sensing the curvature of membranes and tethering highly curved membranes to flat membranes [126]. The overexpression of GMAP210 leads to fragmentation of Golgi membranes and perturbs ER-Golgi trafficking [127]. In contrast, there are also reports of ribbon unlinking in response to depletion of GMAP210. Moreover, the role of this protein in secretion is also under debate, with some studies showing no effect of GMAP210 depletion on secretion, while other studies reported a blockage of transport [128] [125].

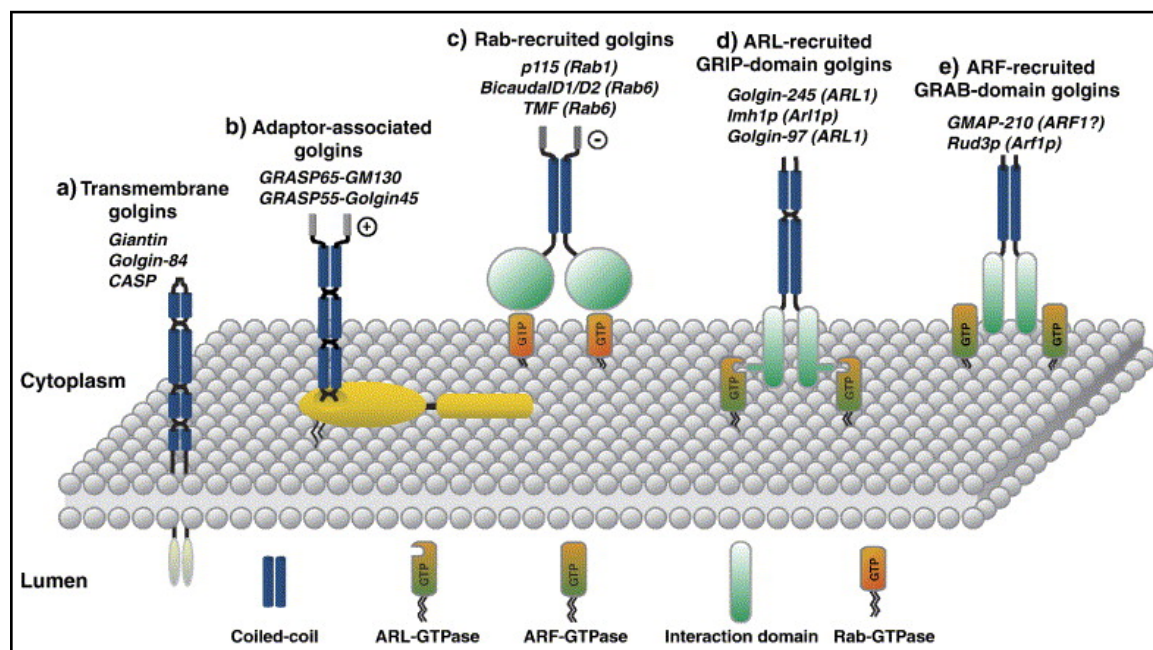


Figure 1.10: Mode of action of different Golgins. Different Golgins have different effector proteins that confer specificity to diverse tethering actions. Adapted from Short B, Haas A, Barr FA [129].

1.4.3 Trafficking Proteins

Apart from the matrix proteins, there are many trafficking proteins and tethering complexes which regulate Golgi organization by mediating cargo flux in and out of the Golgi. Therefore, it is no surprise that the absence of these proteins has an effect on Golgi morphology. The main functions of a few of these complexes are highlighted below.

Rab GTPases

Rab GTPases consist of a family of 60 small Ras-like GTP-binding proteins that recruit a variety of trafficking proteins, owing to their ability to switch between GTP and GDP bound states [130]. About 20 Rabs are localized at the Golgi Complex, including Rab

6A/A', Rab19, Rab33A, Rab33B, Rab34, Rab36 and Rab39 [131] [132]. Recent work has shown a subset of these function to correlate Golgi structure with protein transport. Rab6 is a widely studied protein implicated to do so. Rab6 and is involved in retrograde as well as anterograde transport, and is required for regulation of vesicle fission from the Golgi. Rab33B functionally overlaps with Rab6 to regulate intra-Golgi retrograde traffic and Golgi homeostasis [133] [134]. Rab1 and Rab2 are also key regulators of Golgi structure, being essential for ER-Golgi trafficking and ribbon maintenance, respectively. Rab43 and Rab18, as trapping them in their inactive GDP bound form leads to Golgi fragmentation [135]. It is likely that more Rabs will be implicated in Golgi maintenance in the future.

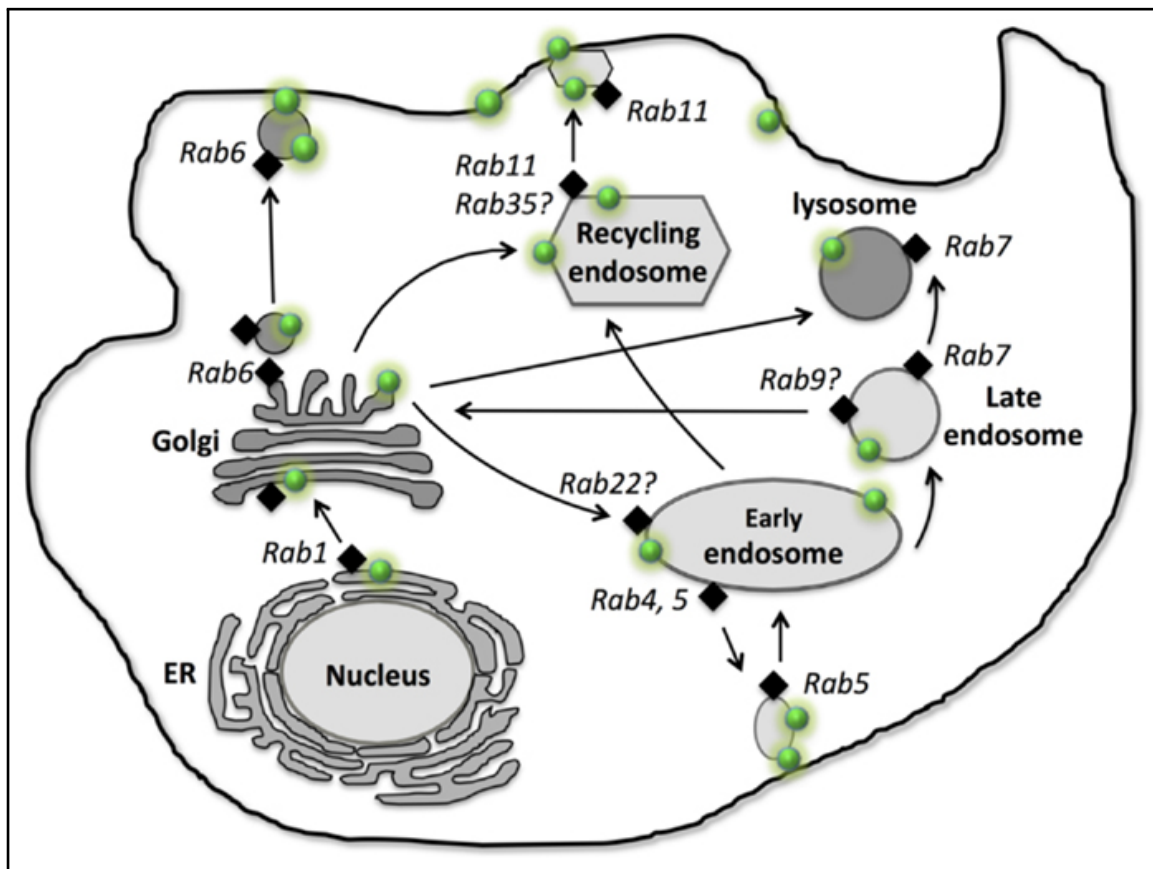


Figure 1.11: Several Rab proteins operate along the secretory pathway. They are involved in several trafficking steps as well organelle homeostasis. About 20 Rabs are located at the Golgi Complex. Taken from Fu, D. (2013) [136]

SNAREs

SNAREs (SNAP-REceptor) are a family of membrane proteins containing a coiled-coil SNARE domain. These proteins form complexes that are the primary driving factor for membrane fusion [137]. Functionally, SNAREs are categorized as t-SNAREs or v-SNAREs depending on whether they are found on the target or vesicle membrane [138]. Pairing between specific t-SNAREs and v-SNAREs is required for membrane fusion, thus

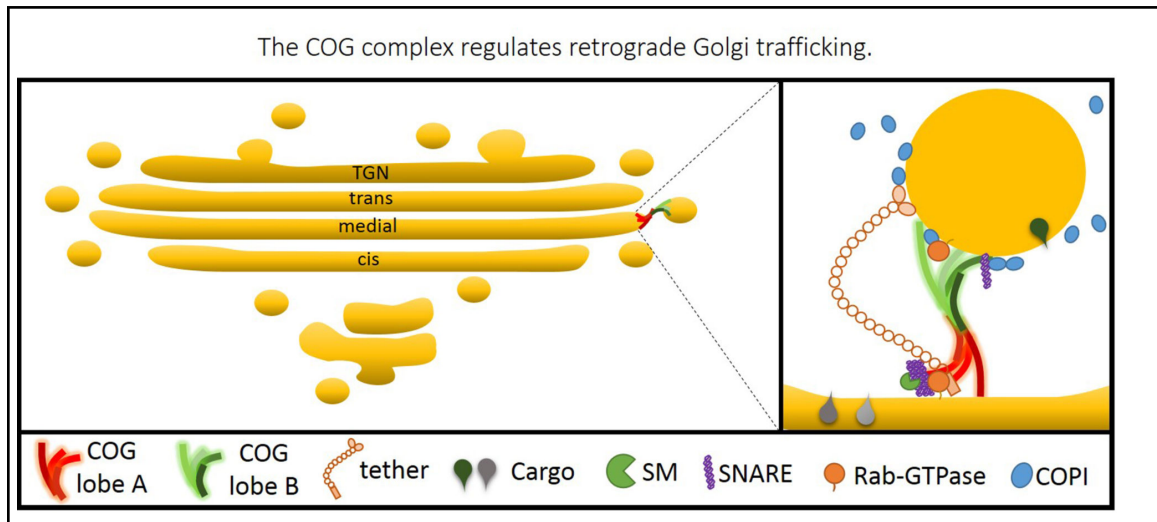


Figure 1.12: Proteins forming the COG complex play a role in vesicle tethering to the Golgi complex, along with other tethering factors, making them key players in Golgi organization. Taken from Vladimir Lupashin, <https://physiology.uams.edu/faculty/vladimir-lupashin/>.

conferring specificity of membrane fusion. These proteins form distinct complexes, operating at different locations [139]. A single SNARE protein is not limited to one complex, and can be a part of many complexes [140]. The dependency of membrane fusion events on SNARE proteins make them indirect, but important regulators of Golgi organization.

COG Complex

The Conserved Oligomeric Golgi (COG) Complex constitutes 8 proteins (COG1-8) that are involved in vesicle tethering during retrograde intra-Golgi transport [141]. The complex consists of two lobes formed by COG1-4 and COG5-8 respectively, bridged by the interaction between COG1 and COG8 [142]. Glycosylation of proteins is impaired in the absence of a functioning COG complex, since vesicles containing glycosylation enzymes rely on these proteins for tethering and membrane fusion [143]. The COG complex closely interacts with the SNARE complex, and therefore the structure of the Golgi depends on the COG complex [144] [145] in similar relation to the SNAREs, which is regulation of trafficking flux.

1.4.4 Cytoskeleton

The cytoskeleton plays a critical role in the formation and maintenance of Golgi organization [146]. Both microtubule and actin networks operate and interact to orchestrate this process [147]. The role of the microtubule network in Golgi transport and organization has been long since known and well-studied, whereas actin and its associated proteins have been implicated in this process relatively recently.

Actin Cytoskeleton

The role of the actin in Golgi organization was first seen when cells treated with actin polymerizing drugs such as latrunculin and cytochalasin displayed a compacted Golgi [148]. On the other hand, depletion of other actin associated proteins caused fragmentation of the Golgi (e.g. members of the formin family of proteins)[149]. γ -Spectrin III plays an important role in Golgi structure, and its knockdown causes Golgi fragmentation and dilation of the resulting membranes [150]. Actin associated motors-i.e. the myosin family are also essential for Golgi transport and organization [151] [152]. Myosin I, II and IV are known to play a role in vesicle localization, fission and movement and thus indirectly are implicated in Golgi structure. Moreover, the unconventional myosin 18A (Myo18) binds GOLPH3 and this interaction generates membrane tension that facilitates the maintenance of the extended Golgi ribbon organization and flattens Golgi cisternae [153]. It is likely that actin-associated proteins are important for the mechanical stability of cisternae and prevent their expected spontaneous swelling due to the hyperosmotic conditions in Golgi stack [154] [149].

Microtubule Cytoskeleton

Microtubules (MTs) are essential for the movement of vesicular traffic in cells. Disruption of the microtubule network using the depolymerizing drug Nocodazole results in traffic defects and causes breakdown of the Golgi ribbon into mini-stacks [41]. The centrosome is regarded as the main Microtubule Organization Center (MTOC), responsible for anchoring and nucleation of majority of the Microtubules. In addition, the Golgi is capable of nucleating and stabilizing microtubules [73]. These self-generated set of microtubules are important for ribbon maintenance as well as directed secretion [156]. There are several proteins that play a role in anchoring microtubule arrays at the Golgi- the chief protein being AKAP9 (AKAP450). AKAP9 interacts with the Golgin GM130 at the *cis*-Golgi and together with proteins γ -tubulin, myomegalin and CAMSAP2 regulates the formation of tubulin arrays [157]. Minus end tracking proteins called CLASPs are recruited to the trans Golgi by GCC185 and play an important role in stabilization of the microtubule array [75].

1.4.5 Self-Organization of the Golgi

As described in the previous section, there are many factors that contribute to the regulation of Golgi organization. However, it is probable that Golgi structure operates on some self-organizing principles in addition to these forces. Self-organization is a process by which several components of a system come together in an ordered fashion in space and/or time [159]. This means that the whole system has characteristics that differ qualitatively from those of the component parts, and the interactions between the individual components give the system unique characteristics [160]. Evidence that self-organization is a process

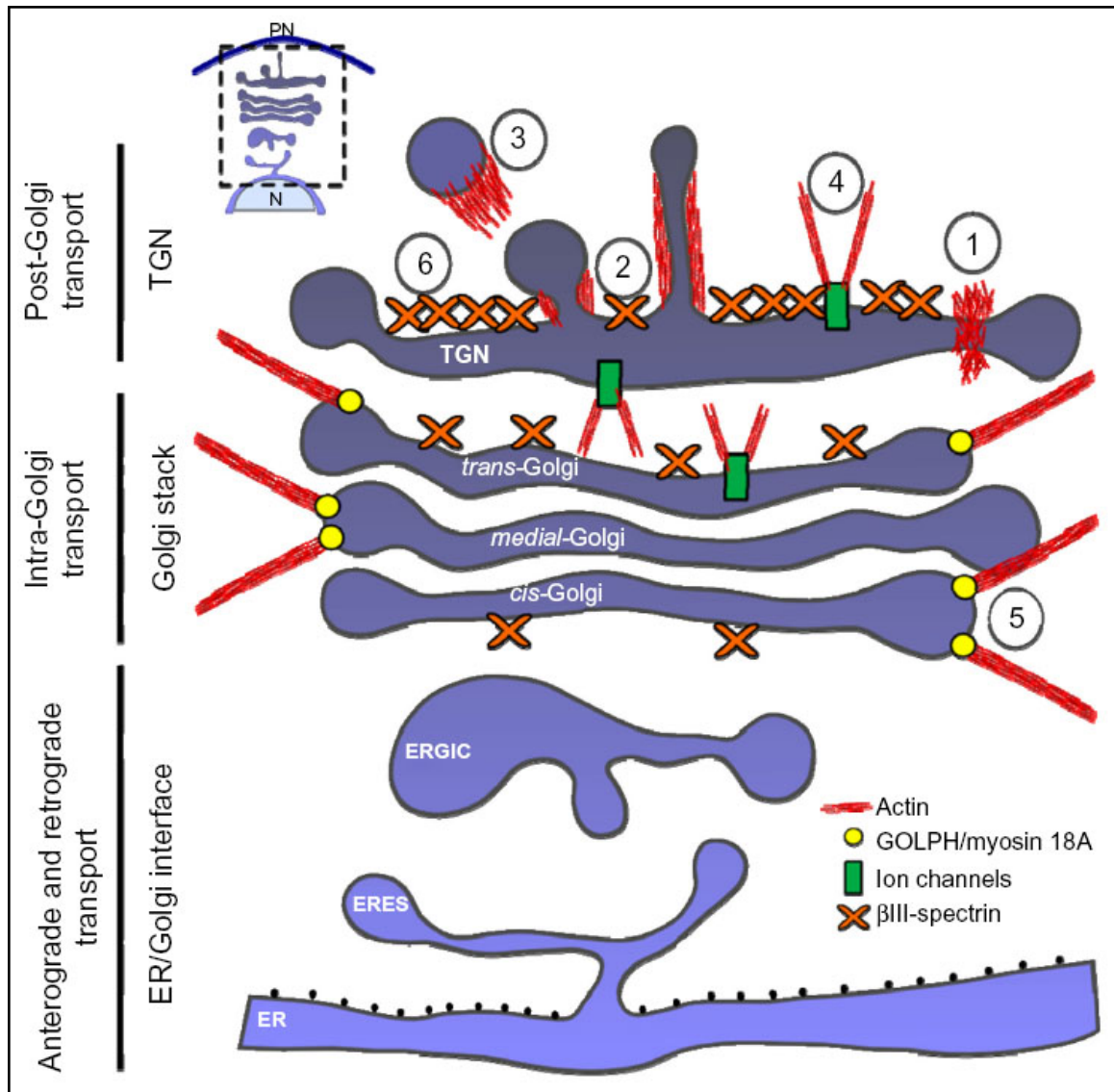


Figure 1.13: Actin, myosin and associated proteins such as spectrin and ankyrin play a role in anchoring different sub-compartments of the Golgi Complex. Adapted from Egea, Gustavo, et al. [155]

at play in Golgi structure comes from a few studies. In one such study, Golgi biogenesis experiments were done where the Golgi is removed from the cell using laser nanosurgery [59]. In these experiments, the *de novo* assembly of Golgi structures is evident [161]. In yet another study, it was shown that organization of core Golgi material is independent of ER to Golgi transport [162]. Moreover, a three-dimensional simulation based on the coarse-grained membrane model was done [163] to understand Golgi reassembly after mitosis. They were able to simulate the assembly process and show that three factors: vesicle aggregation speed, membrane fusion speed and membrane relaxation speed are important for this process. However, it is likely that self-organization is one of the factors playing a role in regulating a complex organelle such as the Golgi.

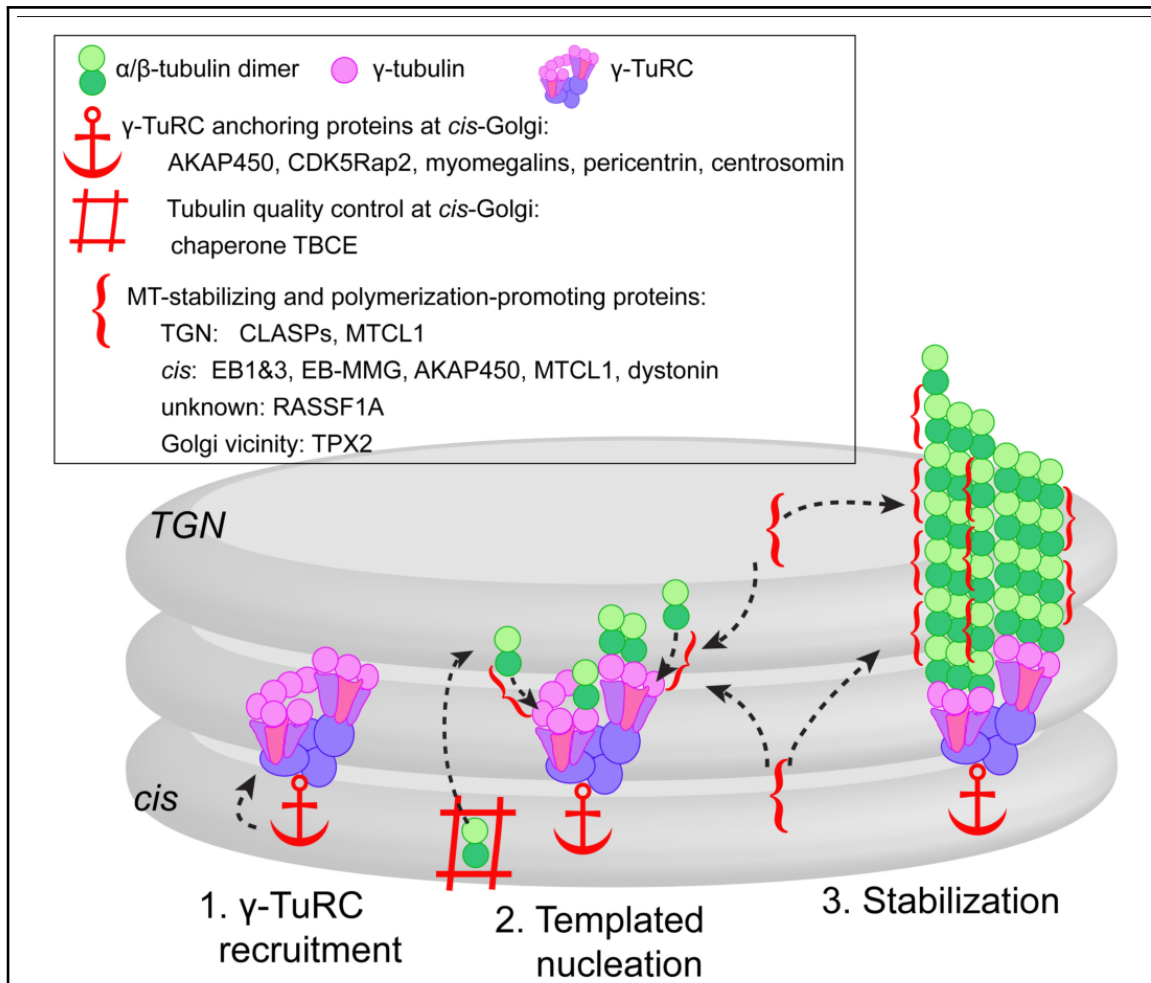


Figure 1.14: Microtubule cytoskeleton, originating both from the centrosomes as well as from the Golgi Complex are essential for maintenance of Golgi architecture as well as trafficking. Adapted from Sanders AA, Kaverina I. [158]

1.5 Studying Golgi Organization

1.5.1 Why study Golgi organization?

The importance of the Golgi Complex in the secretory pathway makes it a key participant in the regulation of cellular homeostasis. Indeed, malfunction of the Golgi Complex has been implicated in innumerable diseases, ranging from neurological disorders to arthritis [164] [165] [166]. The organization of the Golgi is relevant here due to its impact on Golgi function [167]. Alterations in Golgi structure negatively affects certain types of cargo transport, and loss of function of a Golgi structural protein can cause impairment of trafficking with far reaching effects on physiology [168]. Many neurodegenerative diseases arise from improper export of material from the Golgi, causing the debilitating presentations seen in dementia, Alzheimer's and Parkinson's disease [169] [170] [171]. Another way in which Golgi organization contributes to disease is by impairment of the glycosylation function of the Golgi in that cause a glycosylated protein to lose it's function, or act on

the wrong targets, etc. Improper glycosylation is responsible for a whole range of diseases ranging from skeletal muscle disorders to cystic fibrosis, reviewed in [172]. Moreover, there have been several reports of altered Golgi architecture seen in tumors [173] [174] [175] [176]. Although more and more studies are showing links between Golgi morphology, function and disease, we are far away from a comprehensive picture that allows a look at the pathway regulating Golgi structure, making such information a vital starting point to address the many pathologies that can be caused by its malfunction.

1.5.2 Methods used to study Golgi organization

Many methods have been used to study Golgi organization and its regulation. These include, but are not limited to – Chemical perturbation, transport assays, biochemical methods and Microscopy techniques [177] [178] [179] [180]. Within the domain of microscopy, a number of imaging modalities have been used to study Golgi structure, organization and dynamics. These include live imaging of fluorescent-tagged proteins, laser nanosurgery, correlative light and electron microscopy and genome-wide screening approaches [161][181] [182] [183]. Genome-wide screening approaches using RNAi (RNA interference) have been instrumental in identifying many key trafficking regulators. They have also described many proteins that cause disruption of Golgi morphology upon depletion, as well as determined key regulatory proteins that play a role in maintaining Golgi organization [184] [185] [186] [187] [135] [188]. Genome-wide siRNA screens looking at Golgi morphology therefore serve as a profitable starting point in further investigating Golgi organization. However, siRNA-based screens identify individual candidates and cannot provide information about how these proteins interact with one another to orchestrate Golgi organization. As in case of many cellular processes, Golgi organization is dependent upon proteins that upon depletion, might be compensated by another protein, such as a homolog. With single gene knockdowns, this is information that is missed. In order to understand how Golgi regulatory proteins, interact with one another to function as regulatory machinery, it is important to supplement information from a single gene knockdown with additional information about the trajectory of its associated proteins. An effective way of obtaining network information is to combine siRNA knockdowns with transcriptome analysis. The goal of this PhD project has been to find proteins that play a role in Golgi organization based on their interaction with already known Golgi regulators by using the tools of siRNA mediated depletion, imaging and transcriptome analysis.

AIMS

The overarching goal of the project was to identify proteins that interact with known regulators to form a network that senses and regulates the structure of the Golgi. The approach taken to achieve this was to compare transcriptome profiles of different Golgi phenotypes seen in a singular siRNA treatment affecting Golgi morphology. This approach stemmed from the observation made in previous siRNA screens- in most siRNA knock-down, cells showed variability in Golgi morphology, rather than a homogenous phenotype throughout the treatment well.

Our hypothesis was that cells expressing different phenotypes upon the same siRNA treatment express different genes. These differentially expressed genes are likely to be themselves involved in Golgi organization, or may interact with the knocked down gene to influence Golgi organization.

With this rationale, the following aims were set:

- To develop a pipeline capable of comparing the transcriptome profiles of varying Golgi phenotypes within the same treatment.
- To identify genes that were differentially expressed (upregulated or down regulated), between cells that have a normal Golgi and those having a disrupted Golgi after the same siRNA treatment.
- To identify candidate genes/pathways from the above list that are likely to play a role in Golgi organization by rescue experiments combined with a literature search.

CHAPTER 2

RESULTS

2.1 Examining variability in Golgi morphology upon siRNA knockdown

2.1.1 Different siRNA treatments have different effects on Golgi morphology

A variety of cellular responses, both physiological and pathological lead to a change in Golgi structure[189]. This change in Golgi structure is not of a single nature, and different triggers result in alteration of the typical stacked-ribbon structure into different altered arrangements[187]. The loss of function of a single gene can lead to such a distortion of Golgi architecture, as have been observed in RNA-interference experiments wherein a single gene is knocked down using siRNAs[184, 134]. A few well characterized presentations of such alterations- referred to here as ‘Golgi Phenotypes’ are dispersed, fragmented and compact (Fig 2.1). Many perturbations can result in a particular phenotype, and the ensuing alteration may or may not have an effect on the ability of the Golgi to transport different cargo [190, 191].

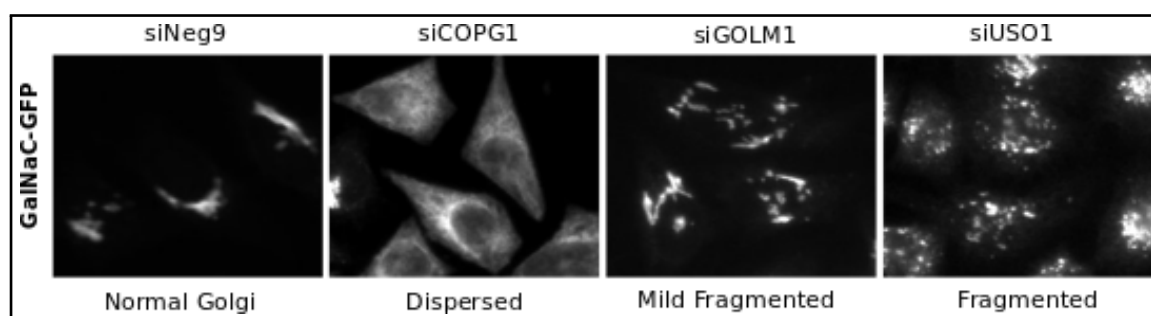


Figure 2.1: Different siRNA treatments affect Golgi morphology differently, as seen in siRNA mediated knockdown of HeLa cells overexpressing GalNaC-GFP. siNeg9 depicts normal Golgi morphology as viewed under a widefield microscope with a 20X objective. siCOPG1 causes a dispersed Golgi phenotype whereas siGOLM1 and siUSO1 both cause fragmentation of the Golgi, albeit to different extents.

2.1.2 Golgi morphology is variable within single siRNA treatments

Previously, siRNA screens were performed in our lab with the purpose of identifying individual genes that caused a change in Golgi morphology[187]. An interesting observation in these screens was the variability in Golgi morphology within a single siRNA treatment well (Fig 2.2), whereby a population of cells retained normal Golgi morphology despite treatment. Also, similar variability was consistently observed in all such Golgi-affecting siRNA treatments. This observation raises the question whether the variability seen has a biological basis based on different behavior of cells to the same siRNA treatment .

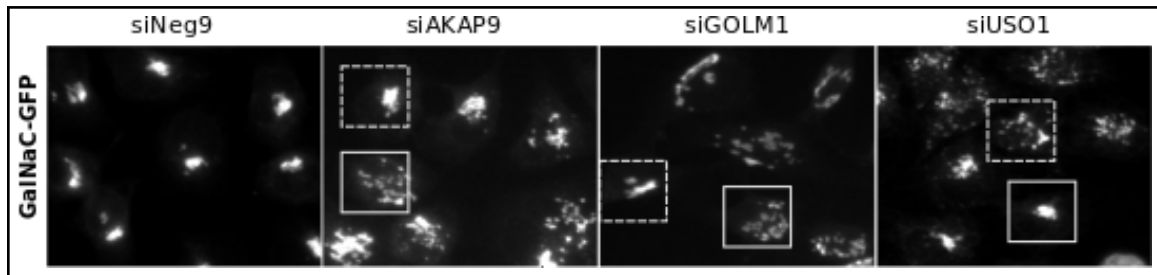


Figure 2.2: Golgi morphology shows variability within a single siRNA treatment. As seen in the images above, some cells retain their normal Golgi morphology upon siRNA treatment as seen in case of siAKAP9, siGOLM1 and siUSO1 (dotted boxes), while majority cells show characteristic response to the siRNA (solid boxes)

2.1.3 Hypothesis of a compensation mechanism to maintain Golgi structure

In view of these observations, we hypothesize a likely scenario whereby a population of cells are able to bypass or compensate the Golgi-disrupting effect of the siRNA by activation of certain regulatory pathways. If this were indeed the case, identifying the genes that were expressed differently between cells showing altered morphology and those showing normal Golgi morphology could shine light on the genes involved in such a compensation mechanism. Moreover, it is likely that these differently expressed genes in the non-responsive population interact with the gene being targeted in the siRNA treatment. Thus, differential transcriptomics of these two populations could be a valuable tool to illuminate some of these interactions at play and ultimately to find networks that operate to organize and maintain Golgi structure (Fig 2.3).

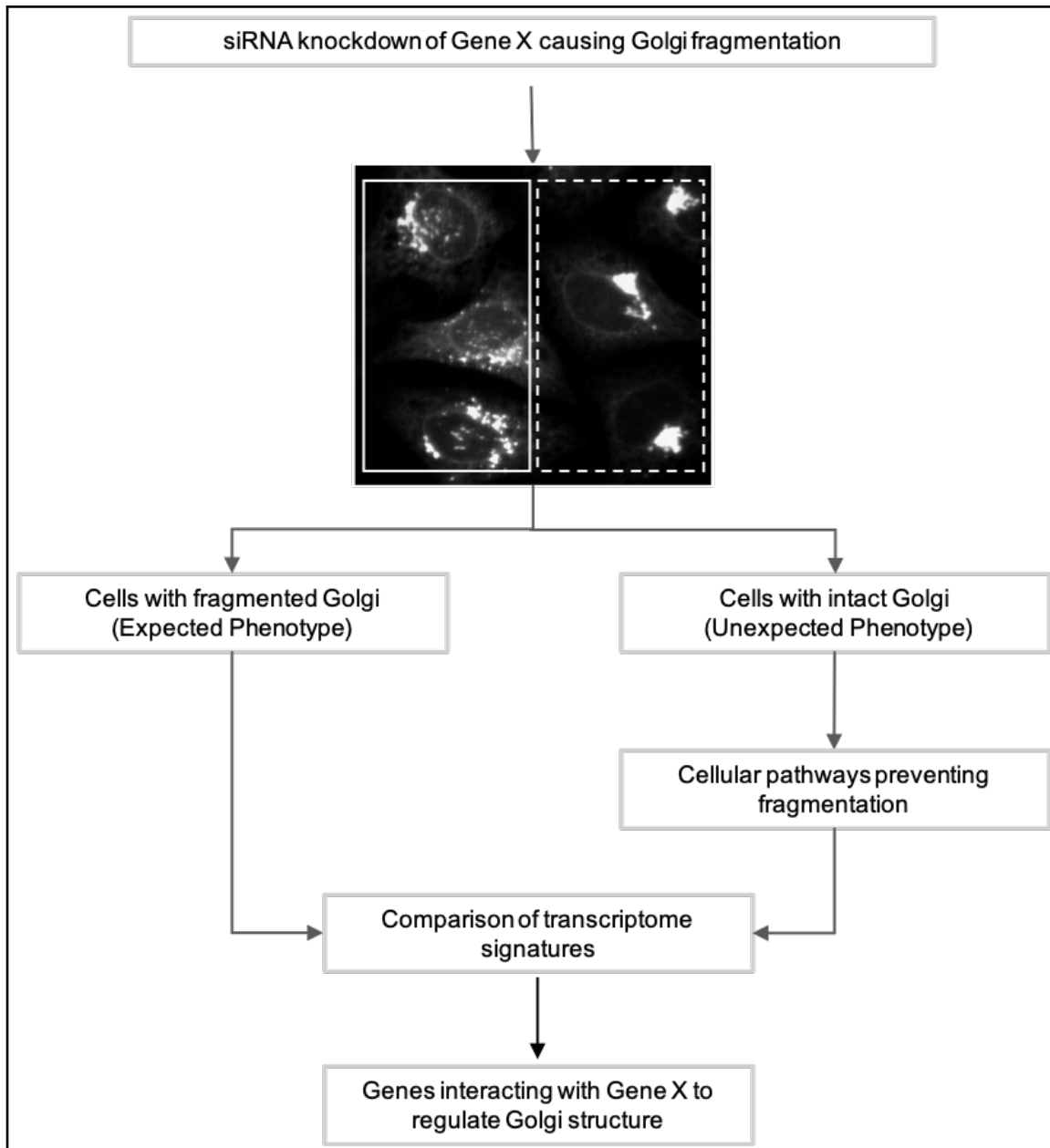


Figure 2.3: Hypothesis: a compensation mechanism operates in the cells that do not display characteristic siRNA knockdown morphology upon siRNA treatment. This implies that the cellular mechanisms by which these cells preserve Golgi organization are probably involved in maintenance of Golgi structure, in combination with the knocked-down gene.

2.2 Experimental validation of hypothesis

Prior to comparing Golgi phenotypes on the transcriptome level, it was imperative to test if the phenotypic variability observed in siRNA treatments was just an effect of inefficient knockdown in the non-phenotype expressing cells and therefore would not be a biologically relevant explanation for lack of change in Golgi structure.

2.2.1 Experimental test of the hypothesis

In order to test the hypothesis, 20 Golgi-localized proteins (Table 3.1) were selected based on the availability of siRNAs and good fluorescent antibodies against the proteins. These proteins were systematically knocked down in HeLa cells expressing an GFP-tagged version of the Golgi enzyme N-acetyl Galactosyltransferase, referred to henceforth as GalNaC-GFP. After 72 hours of siRNA treatment, cells were fixed and stained with the antibody against the targeted protein (Fig 2.4). First, cells were first analyzed for the effect on Golgi morphology, with the result that 6 of the 20 siRNA knockdowns induced a visible and reproducible disruption in Golgi morphology (Fig 2.5). These 6 conditions were further analyzed by image analysis at a single cell level for the levels of remaining targeted protein levels, measured by antibody staining. For each of the 6 siRNA conditions, a ‘knocked down’ population was defined based on comparison with control-siRNA treated cells stained with the same antibody. Once the percentage of cells classified as ‘knocked down’ (Fig 2.6) was defined, the Golgi morphology within this population of cells was evaluated.

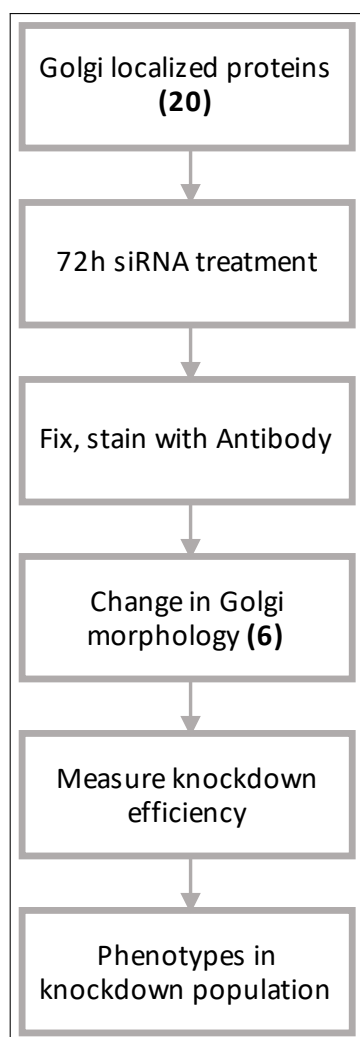


Figure 2.4: Hypothesis testing. 20 Golgi localized proteins were chosen and each one knocked down for 72 hours in HeLa-GalNaC-GFP cells. After this, cells were fixed and stained with an antibody against the knocked-down protein. Cells were then analyzed for change in Golgi morphology. Those which showed a change in Golgi morphology were further characterized for Golgi phenotype variability in knocked-down cells.

2.2.2 Characterization of Golgi populations upon siRNA knockdown

The resulting observation was that each siRNA treatment had a small percentage of cells that showed normal levels of the targeted protein. In other words, these cells were not knocked down, owing to transfection efficiency. However, the majority of the cells in all cases displayed much lower levels of the targeted protein as compared to control-siRNA transfected cells, measured by the intensity of the antibody stains. Within this ‘knocked down’ population, defined as 3 standard deviations away from the median of control-siRNA stains, we observed cells displaying both siRNA-typical and normal Golgi morphologies, with varying percentages (Fig 2.7).

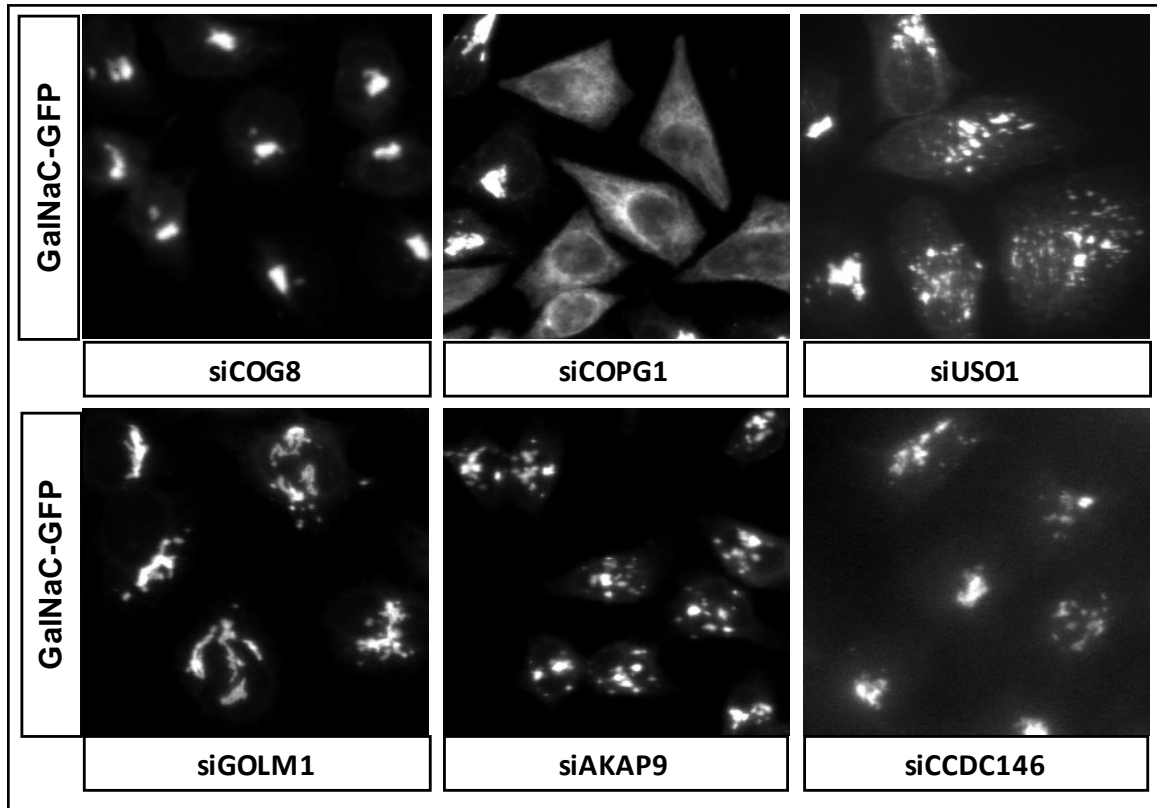


Figure 2.5: 6 out of the 20 siRNA treatments caused a strong change in Golgi morphology. These were siCOG8, displaying condensed Golgi, siCOPG1, showing dispersed Golgi morphology and siUSO1, siGOLM1, siAKAP9 and siCCDC146 which all caused Golgi fragmentation to a different extents. Each of the six siRNA treatments also had a population of cells that did not show the knockdown phenotype. Images were taken and analyzed on the ScanR with a 20X objective.

2.2.3 Validation of hypothesis

In view of these observations, we can conclude that knockdown efficiency alone cannot explain the presence of a population of cells that do not respond in the expected fashion to a given siRNA treatment. This strengthens the hypothesis that a compensation mechanism might be operating in these cells, allowing them to evade Golgi disruption. To study this further, a pipeline was developed with the goal of analyzing transcriptome changes between the populations showing different Golgi morphology upon knockdown. In the end, a three-step pipeline was established comprising microscopy, flow cytometry and single-phenotype transcriptome analysis which is discussed in detail in the following section.

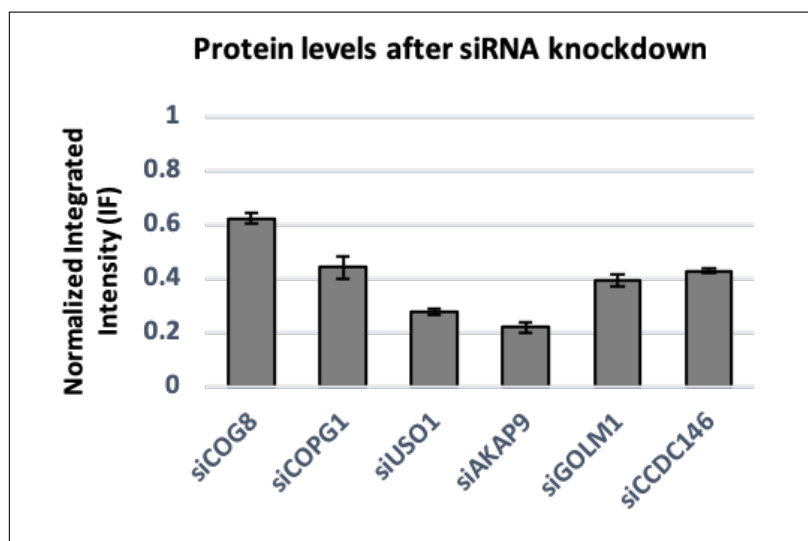


Figure 2.6: Analysis of protein levels after knockdown. In the six treatments that had showed a change in Golgi morphology, the extent of the knockdown in the population was quantified by analyzing the antibody staining in these cells and comparing it to the respective antibody levels in non-treated cells. Shown here are the normalized integrated intensities of these proteins.

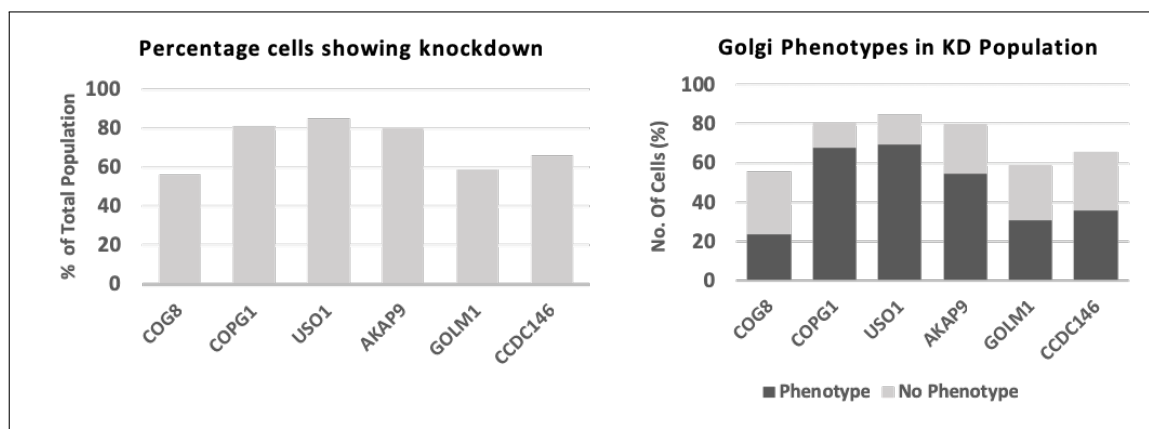


Figure 2.7: The percentage of cells showing a knockdown was calculated by taking the mean intensity values of antibody staining in normal conditions, and setting a threshold to 3 standard deviations below this value. This value was then used to threshold the antibody staining in each siRNA treatment to arrive at the number of cells defined as 'knocked-down' in each treatment. Once this population was defined, each cell defined as knocked down was analyzed for its Golgi morphology and assigned a phenotype using Cell Profiler. In this way, populations of knocked down cells showing different Golgi phenotypes were ascertained.

2.3 Pipeline for single-population transcriptomics of Golgi phenotypes upon siRNA knockdown

With the aim of finding genes differentially expressed between two cell populations with different Golgi phenotypes, a workflow was developed that allowed for automated classification of Golgi phenotypes at the microscope and selective marking of a particular phenotype using photo-conversion. Cells marked in this way were then detected by flow cytometry and sorted into single-cells for further transcriptome analysis. The general workflow is described in Fig 2.8. The development of this workflow formed the major part of the project and is discussed in the forthcoming sub-sections in detail.

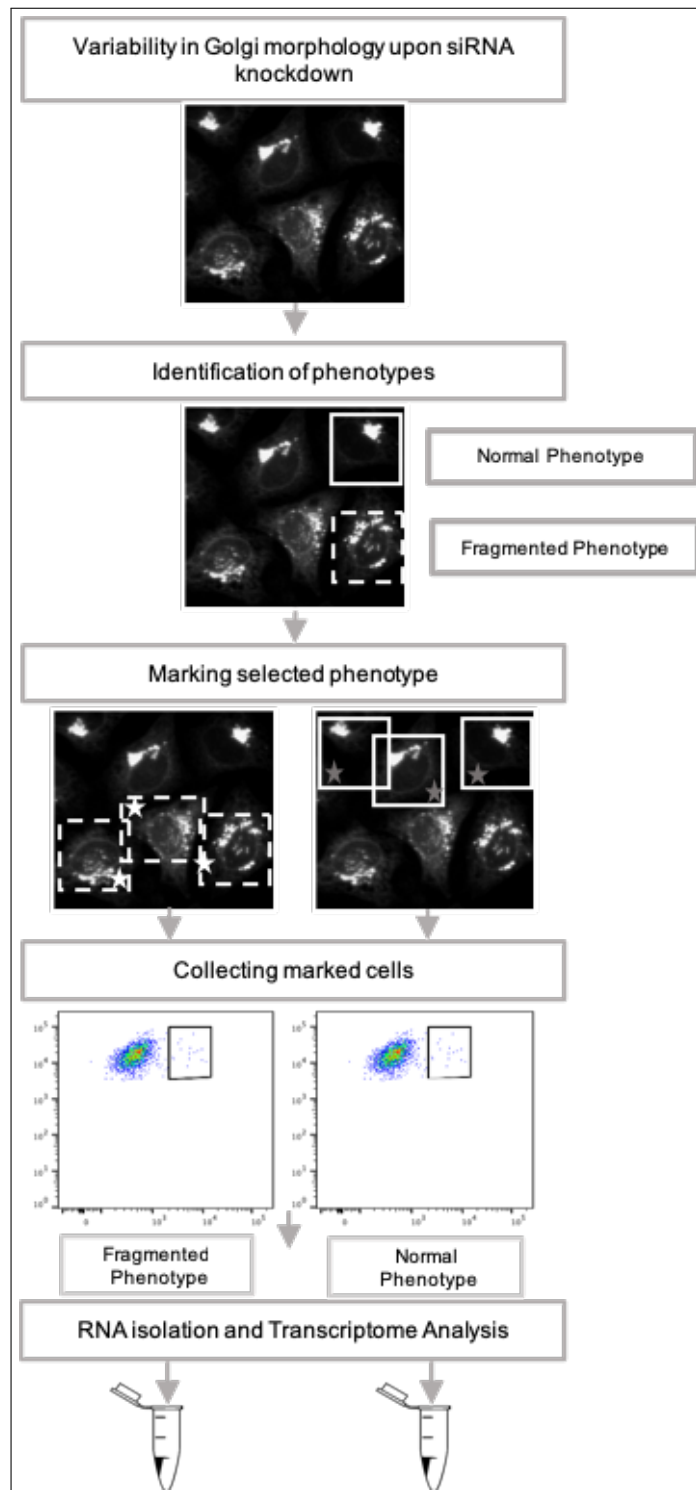


Figure 2.8: Schematic overview of a pipeline for transcriptome analysis of Golgi phenotypes upon siRNA knockdown. The pipeline aims at detecting various Golgi phenotypes using microscopy, and subsequent marking of one desired phenotype. The marked cells can then be detected using flow cytometry, followed by sorting and subsequent transcriptome analysis.

2.3.1 Identification of Golgi phenotypes

Two candidates were used to set up the pipeline : USO1 and AKAP9, as both proteins caused strong Golgi fragmentation upon knockdown. Hence, two Golgi phenotypes were of immediate interest to us in order to set up the pipeline, namely “normal” and “fragmented” Golgi morphologies. While manual detection of these phenotypes is straightforward and possible, it is time consuming and prone to user bias. To overcome this, an automated phenotype recognition process was set up by combining imaging with the image analysis process. For image analysis, we used CellCognition, a computational framework used for supervised annotation and classification of cell morphologies [192]. The working of CellCognition is shown in Fig 2.9.

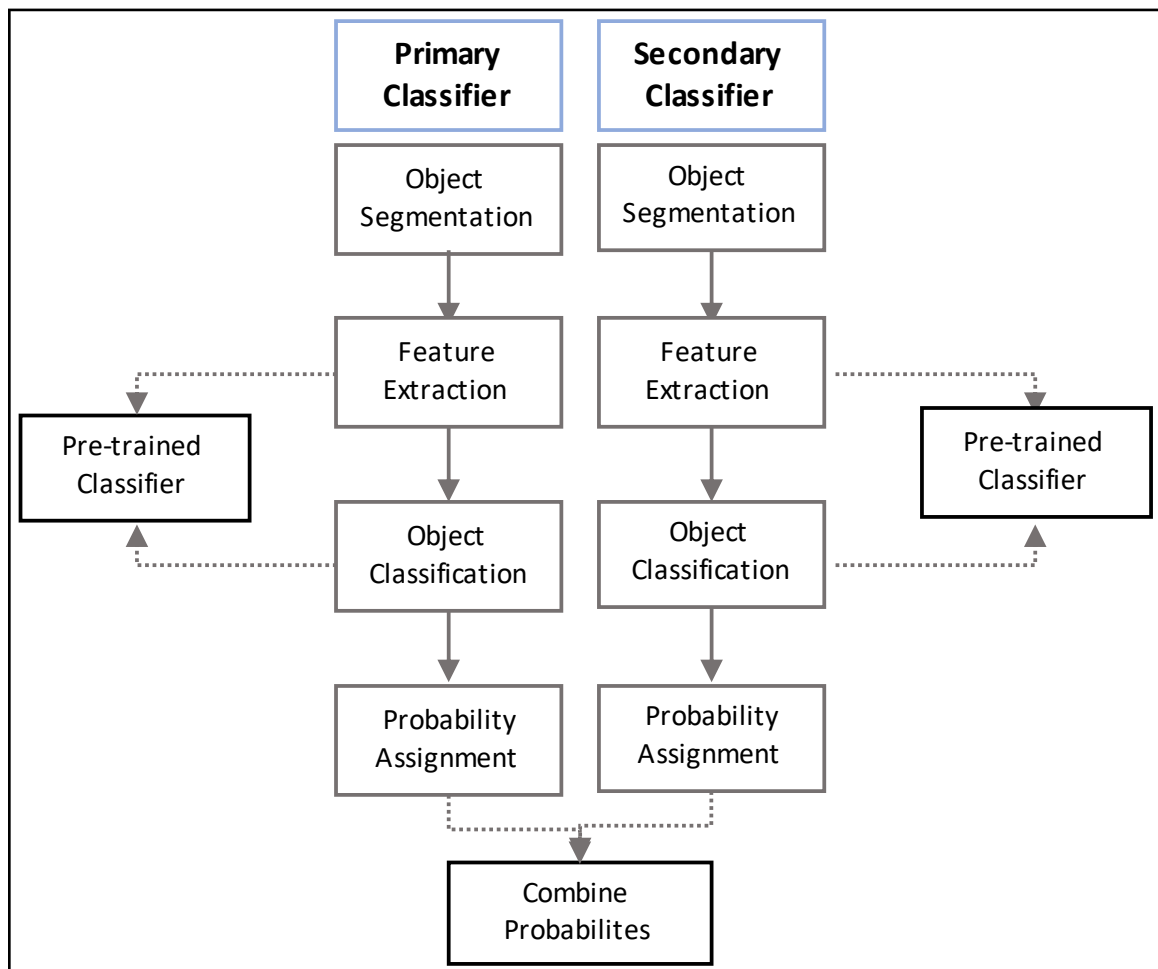


Figure 2.9: Workflow of automated classification of phenotypes in CellCognition. CellCognition relies on a pre-trained classifier with manually defined classes and annotations for each class. Here, we use a two-channel classifier, with the nuclear channel as the Primary Classifier and the Golgi channel as the Secondary Classifier. The classifier goes through stages of segmentation, feature extraction and classification of the identified objects into the pre-defined categories, each with a certain probability value.

The first step in automation recognition was acquisition of a training set of images to train the classifier on. For this, 72-hour siRNA treated HeLa-GalNaC-GFP cells were stained with Hoechst and wide-field images in both nuclear (Hoechst) and Golgi (GFP) channels were acquired at the Leica SP5 with a 40X objective in a 2048 x 2048 format for optimal resolution. Around 30 two-channel images were acquired in this manner and further used as a training set for CellCognition.

Next, the acquired training set was renamed and imported into CellCognition. A classifier was set up for both the nuclear and Golgi channels (two-channel classification). Here, they were annotated manually into user defined classes. Two classes were defined for the nuclear channel – namely “normal”, where most nuclei were annotated and “discard”. Mitotic nuclei as well as multi-nucleated/abnormally shaped nuclei were annotated into the “discard” class. About 70 nuclei from the training set were annotated into each class to obtain a robust confusion matrix. For the Golgi channel, three classes were defined namely “normal”, “fragmented” and “discard”. Cells having a compact or ribbon-shaped Golgi located in the peri-nuclear area were annotated as “normal”. Cells classified as “fragmented” were those displaying 5 or more clearly visible Golgi fragments scattered around the nucleus. Overly dispersed or hazy Golgi morphology, as well as cells not showing a Golgi signal were annotated as “discard”. For this channel, 100 cells were manually annotated into each class to get a precision rate of about 85% for each class (Fig 2.10).

The software was allowed to extract all features except intensity from the annotated samples, and then tested on the same image set (training set). This automated classification was overseen and error rates were noted, and then confirmed by a second person. Cells were iteratively annotated until a satisfactory error rate of less than 5% was observed and these annotations were then tested on a newly acquired image set. Once the software was able to classify samples on a new image set with an error rate less than 5%, the classifier settings were saved for further use. An example of the classification on a test image is shown in Fig 2.11. The classifier assigned a certain probability of a cell belonging to a pre-defined class, and the probability map of one image is shown in Fig 2.12. These probability values were later used to set thresholds for selection of a certain phenotype. For example, in the case of a fragmented phenotype, cells classified as having a normal Nuclei with a probability of over 0.5 combined with a probability of 0.75 for a fragmented Golgi were taken for selective marking and further analysis.

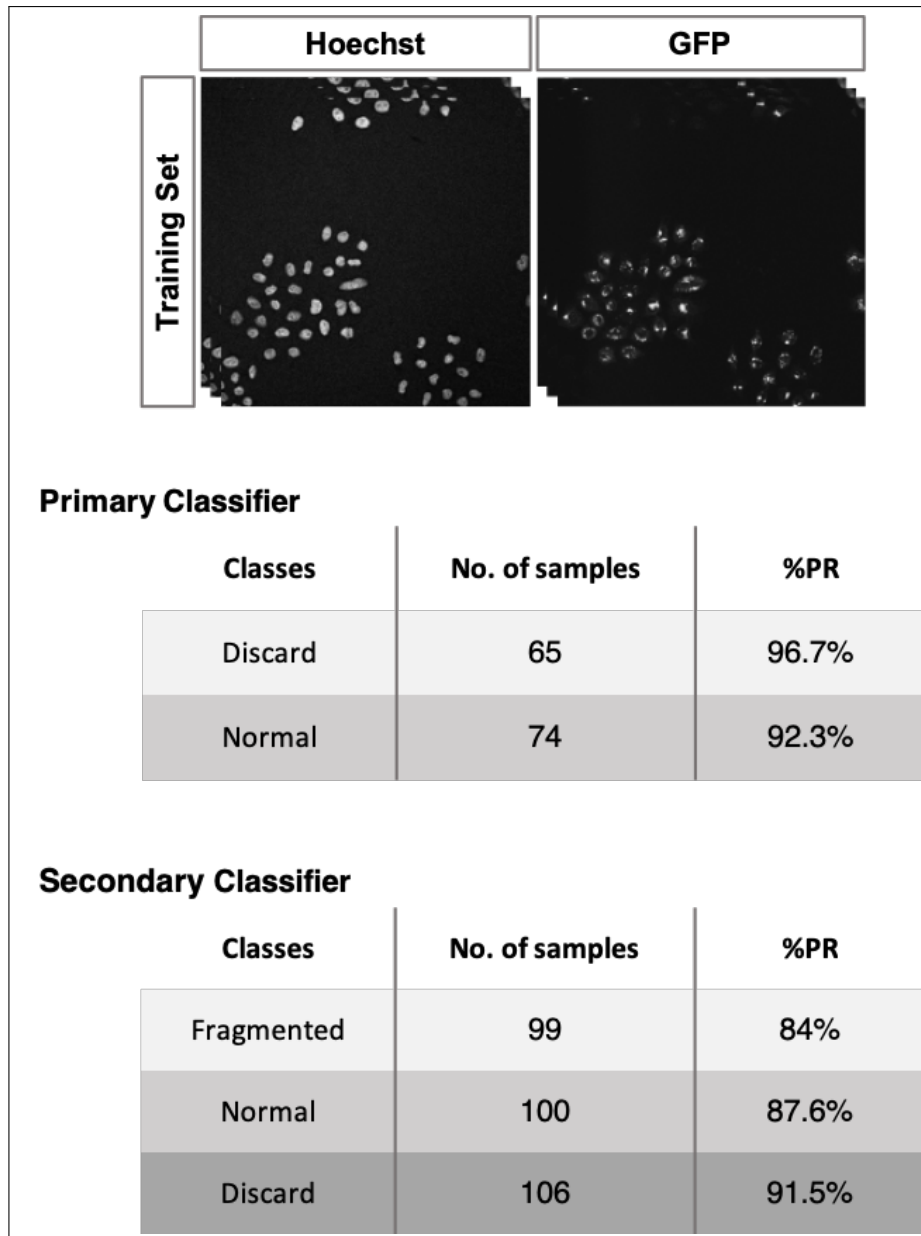


Figure 2.10: Training the CellCognition classifier. First, a set of images were acquired termed the 'training set'. These images were loaded onto CellCognition, where two classes were defined for the Primary Classifier (nucleus) namely discard and normal. For the Secondary Classifier (Golgi) three classes were defined and cells belonging to each class manually annotated.

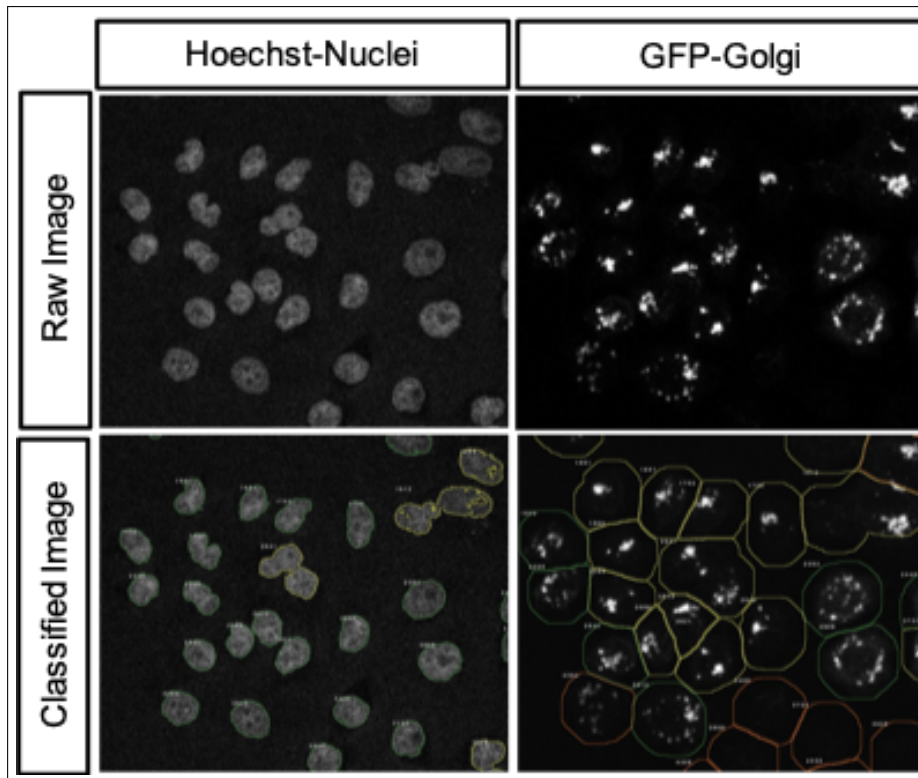


Figure 2.11: An example of classifier testing for its quality and accuracy of phenotype identification. After several iterations of training, the classifier was able to reliably recognize the right Golgi phenotypes.

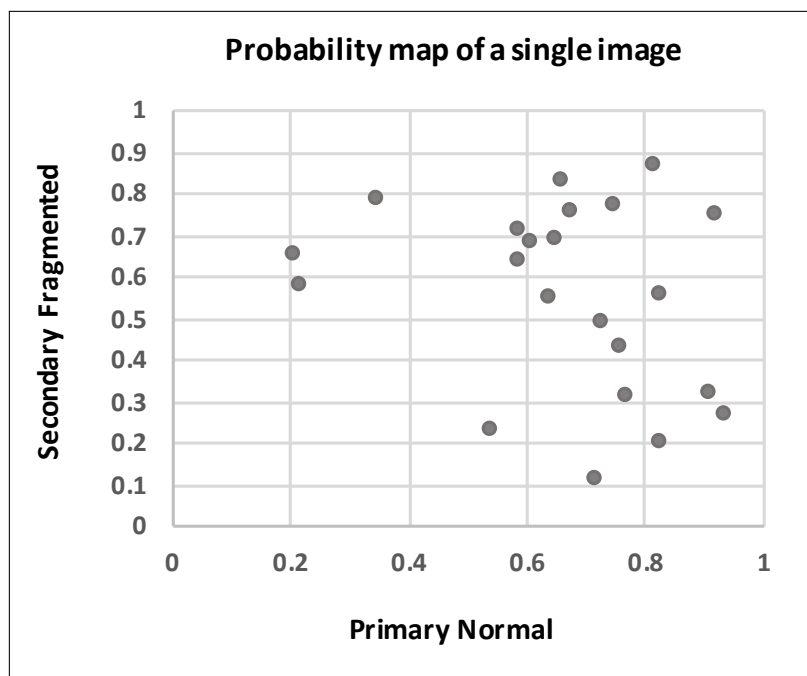


Figure 2.12: Probability map of one classified image after siUSO1 treatment, showing that most cells had a high probability of a normal nucleus and a fragmented Golgi.

2.3.2 Selective marking of phenotypic cells

Once Golgi phenotypes could be reliably identified in an automated fashion, it was imperative to select cells of a certain phenotype from the mixed population of phenotypes, which required marking them in a distinguishable manner. This was done using the photo-activatable marker H2B-PAmCherry, which comprises the inactive form of the red fluorescent protein mCherry tagged to the nuclear localizing histone protein H2B. This plasmid was a kind gift from Richard Wombacher at the University of Heidelberg. Non-fluorescent in its nascent form, this marker changed to active mCherry upon UV illumination (Fig 2.13) so that marked cells could easily be identified with a red nucleus.

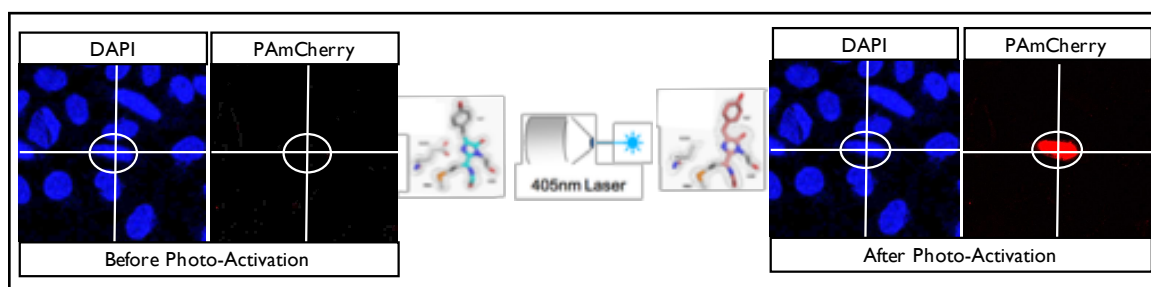


Figure 2.13: H2B-PAmCherry used as a selective marker that converts from dark to red when activated with UV light (405nm). The marker localizes to the nucleus and can be detected after activation using a 561nm laser.

This marker was first transfected into cells, which resulted in poor transfection efficiency in combination with siRNA transfection. Ultimately, high transfection efficiency of the marker could be achieved by electroporation of the plasmid into the cells prior to siRNA transfection (Fig 2.14), without adversely affecting siRNA transfection efficiency.

Photo-activation parameters were optimized on both fixed and live cells, with an effort to minimize UV exposure in live cells (Fig 2.15). The final parameters used to activate single cells were carefully chosen keeping cell viability, time and resulting strength of mCherry signal in consideration and are listed in Table 2.1.

Parameter	Value
Objective	40X air
Zoom Factor	40
Scan Speed	10 Hz
Line Average	2

Table 2.1: Optimal parameters for photo-activation of single live cells in order to prevent cell stress and unwanted activation of neighbouring cells.

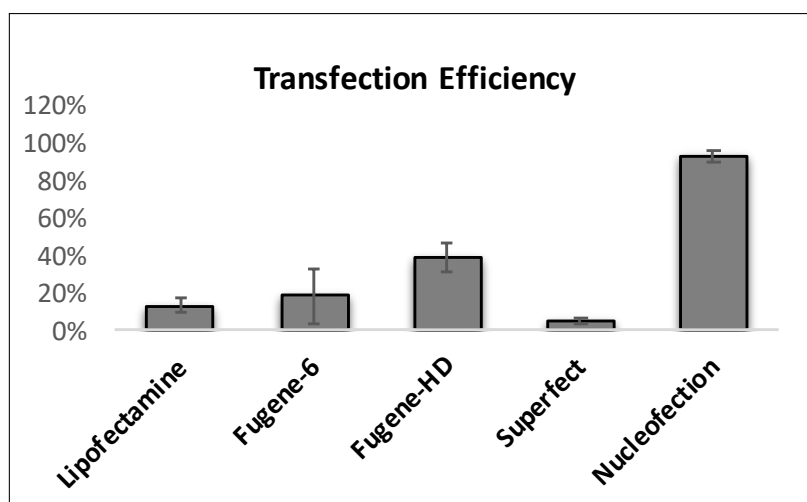


Figure 2.14: Optimizing transfection of H2B-PAmCherry. Lipid-based transfection reagents showed poor transfection efficiency when combined with siRNA transfection. Nucleofection was highly efficient (over 90%) and did not interfere with subsequent siRNA transfection.

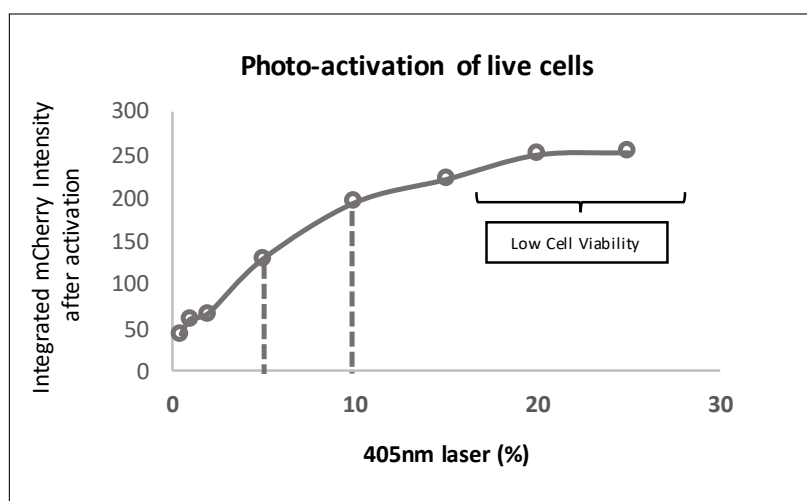


Figure 2.15: Optimization of photo-activation in live cells. Photo-activation was optimized using different percentages of laser power with optimal averaging to achieve a bright mCherry signal while causing as little damage to the cells by UV exposure. Although the activated intensity of PAmCherry was higher at high UV laser powers, it caused low cell viability, and 5% laser was deemed optimal for a detectable signal with low damage.

Photo-activation of single-cells could be achieved by zooming into the nucleus of a single cell. This was optimized with a digital zoom factor of 40 in combination with a 40X air objective on the Leica SP5 microscope with an aim to prevent UV undesired activation of neighboring cells. This allowed for selection of specific cells with the desired phenotype by sequential activation of the desired single-cells as seen in Fig 2.16.

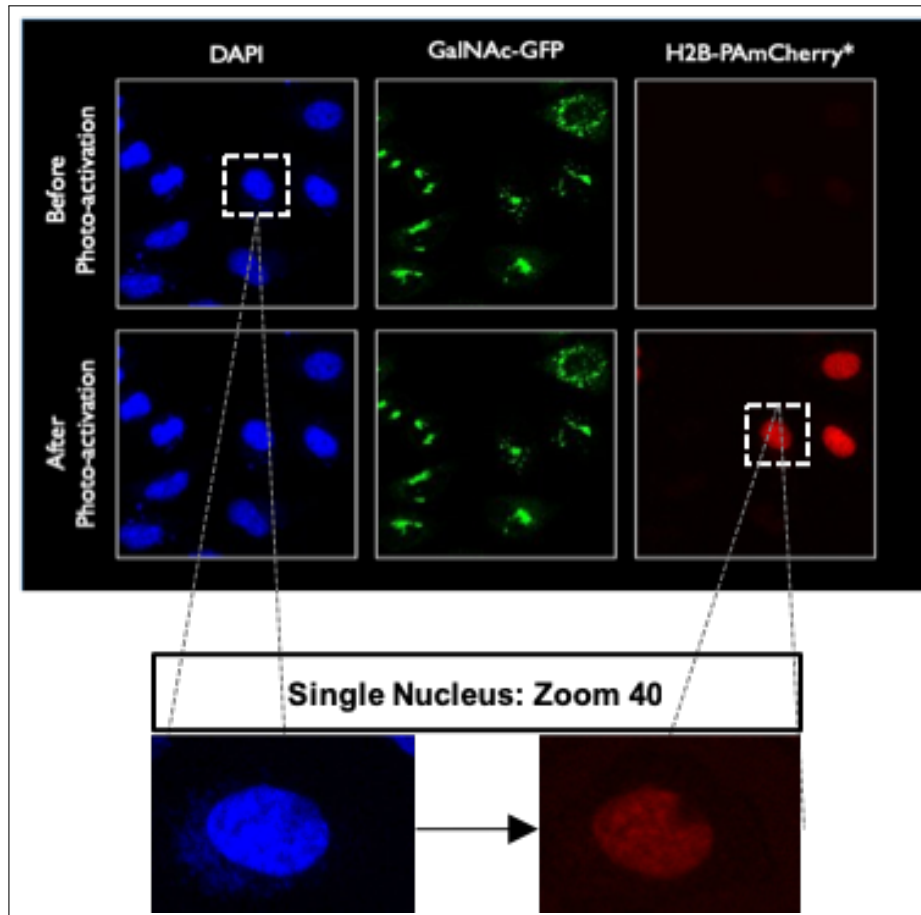


Figure 2.16: Photo-activation of a single cell. In order to activate a single-cell, the nucleus was zoomed into by a factor of 40 before UV exposure. This ensured that no neighbouring cells were activated.

2.3.3 Automation of Golgi recognition and photo-activation

After Golgi phenotype recognition and selective marking using photo-activation was established, they were combined by automated feedback microscopy. This was done on the Matrix Screener module of the Leica microscope software. The imaging software was connected to the image analysis software (CellCognition) using the CAM server option on the imaging software which allowed communication of the microscope with an external program and enabled images to be sent to CellCognition through a GUI called CeCogLink developed by Volker Hilsenstein and Alex Halavyati from the Advanced Light Microscopy Facility at EMBL Heidelberg.

In this set-up, an initial image would be taken in a 'search' pattern designed to autofocus the field of view and capture a 2048x2048 image of both the nucleus and Golgi channel. This image would then be sent to CellCognition, where the image would be analyzed for Golgi morphology based on the pre-defined training set. The output of the image analysis would be selection of cells that belong to the class specified by the user in the GUI. The co-ordinates of these selected cells would be returned to the microscope.

Post image analysis, CellCognition communicated with the imaging software to initiate another pattern of imaging, namely the 'photo-activation' pattern. In this sequence, the co-ordinates of one selected single-cell were first centered, and then the image was re-focused with a software zoom of factor 3 to ensure that the correctly identified phenotypic cell was in the center of the field of view. A sequential scan was done in three channels: Nucleus :405nm, Golgi:488nm, and PAmCherry: 561nm. This was done for two purposes- firstly, to check that the correct phenotype indeed had been selected by CellCognition. The second reason was to ensure no signal in the PAmCherry, ruling out previous photo-activation. This sequence was named 'Before Photo-activation'.

Next, the centered cell was zoomed into further to a final factor of 40, such that light only reached the nucleus of the single centered cell. At this time, the cell was photo-activated using 5% of the 405nm laser. Once photo-activation has occurred, another sequence of images are taken with the exact same way as 'Before Photo-activation' to ensure efficient photo-activation of the single-cell without damage, and without any activation effect on neighboring cells. The same pattern was then run on until all selected cells were photo-activated. Once all selected cells in the search image were activated, the microscope automatically moved to the next field of view in the sample well and the process began again. In total, it took about one hour for activation of 80-100 cells, and was highly dependent on the number of cells displaying the Golgi phenotype being marked. The whole process is depicted in Fig 2.17.

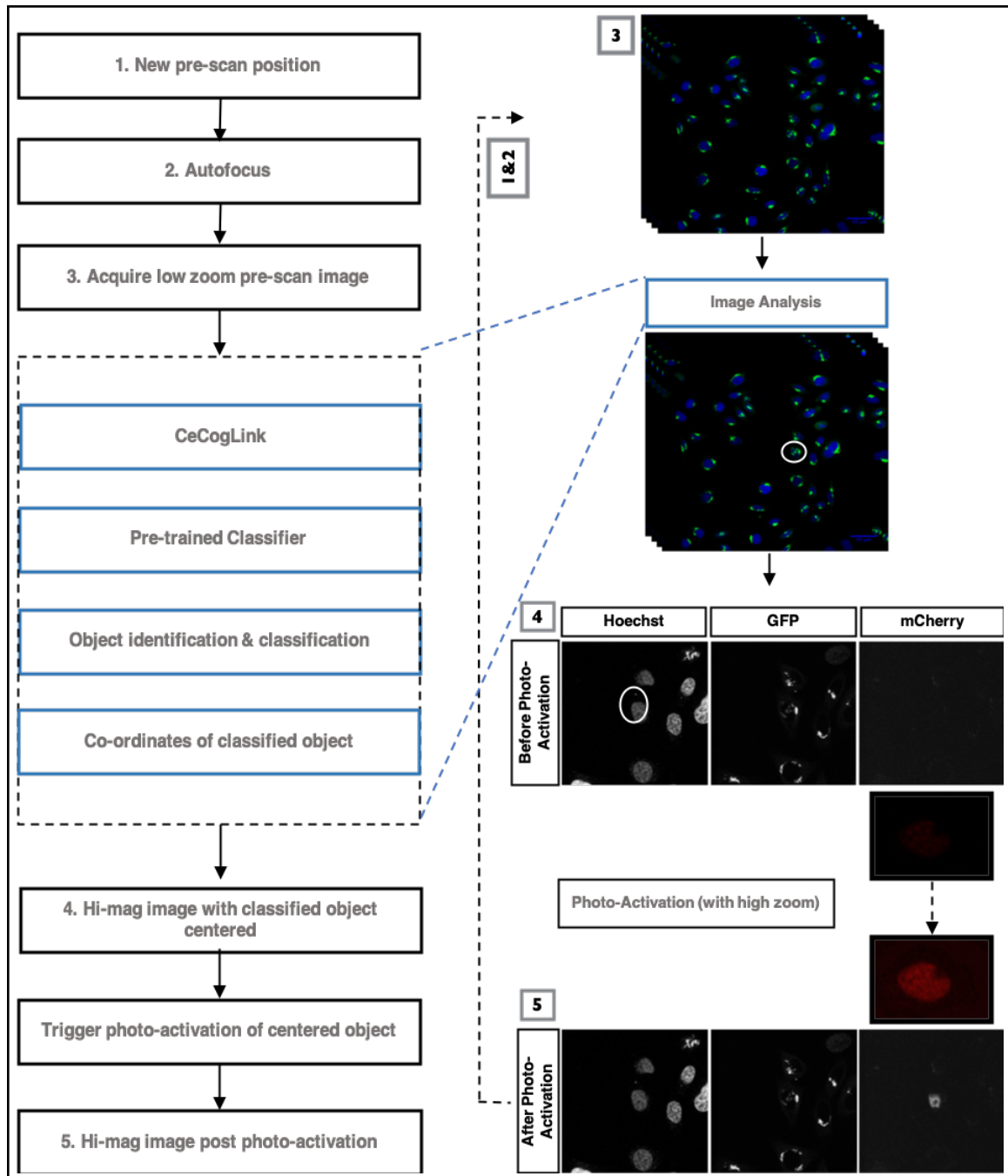


Figure 2.17: Automation of phenotype recognition and selective photo-activation. The imaging process was coupled to the image analysis software CellCognition via the GUI CeCogLink. This enabled images to be classified online, and the results of the classified objects were then taken as co-ordinates for the next step of photo-activation. After one cycle of analysis and photo-activation, the process began at the next position.

2.3.4 Collecting marked cells by Fluorescence-Activated Cell Sorting (FACS)

Once sufficient cells of each phenotype were collected in individual wells, the wells were trypsinized, spun down and washed with cold PBS. After this, they could either be prepared for live-cell sorting or be fixed and suspension for Flow Cytometry and/or sorting. For preparation of fixed cells, a modified version of the Maris* protocol was used. Although initially both fixed and live preparations were tested, the decision was made to proceed with live cells, as the mRNA yields from live cells were much higher.

For live cells, the centrifuged cell pellet is re-suspended in cold FACS staining buffer with an RNase inhibitor. The cells were kept on ice and sorted as soon as possible after preparation. There was an observable cell loss between microscopy and flow cytometry, where about 60-70% activated (PAmCherry positive) cells were typically detected at the cytometer (Fig. 2.18). This could be attributed to cell loss during trypsinization and washing steps.

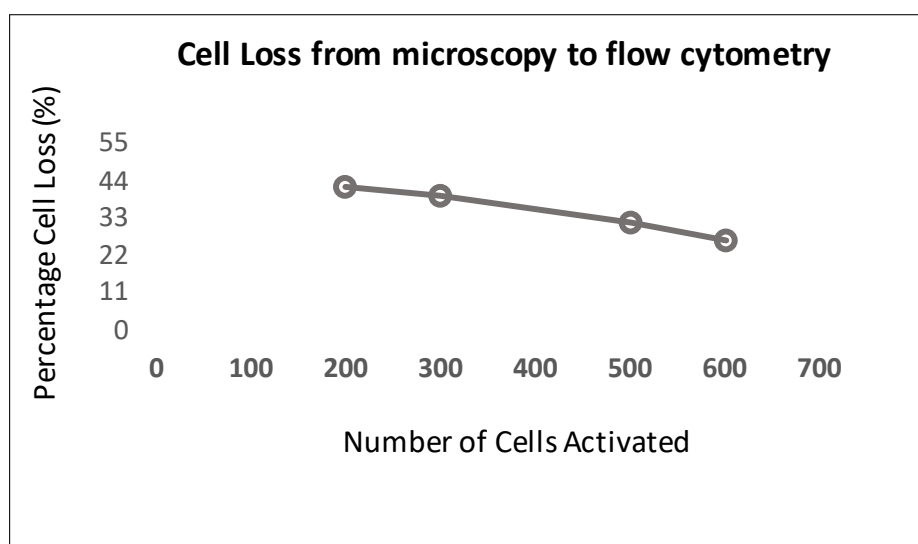


Figure 2.18: Cell loss between microscopy and flow cytometry. Considerable cell loss is seen while processing cells from microscopy to flow cytometry at low cell numbers (100-200) which gets lower as a high number of activated cells are present. This was attributed to trypsin and washing steps during FACS sample preparation.

The aim was to sort cells that showed a GFP signal corresponding to the Golgi channel, an mCherry signal corresponding to a photo-activated cell and a Hoechst signal since the dye was added to all cells i.e Hoechst, GFP and mCherry triple positive cells. Prior to sorting, positive and negative controls for all three fluorophores were assayed on the sorted so as to set the voltages for their detection and define strict gates. Since the mCherry positive cells (photo-converted) were the limiting factor in sorting cells of interest, extra care was taken to define a narrow gate for this channel to avoid low-signal mCherry pos-

itive cells. This was mainly done because transfection of the photo-convertible marker itself created a small but detectable signal in the mCherry channel, even without any photo-conversion.

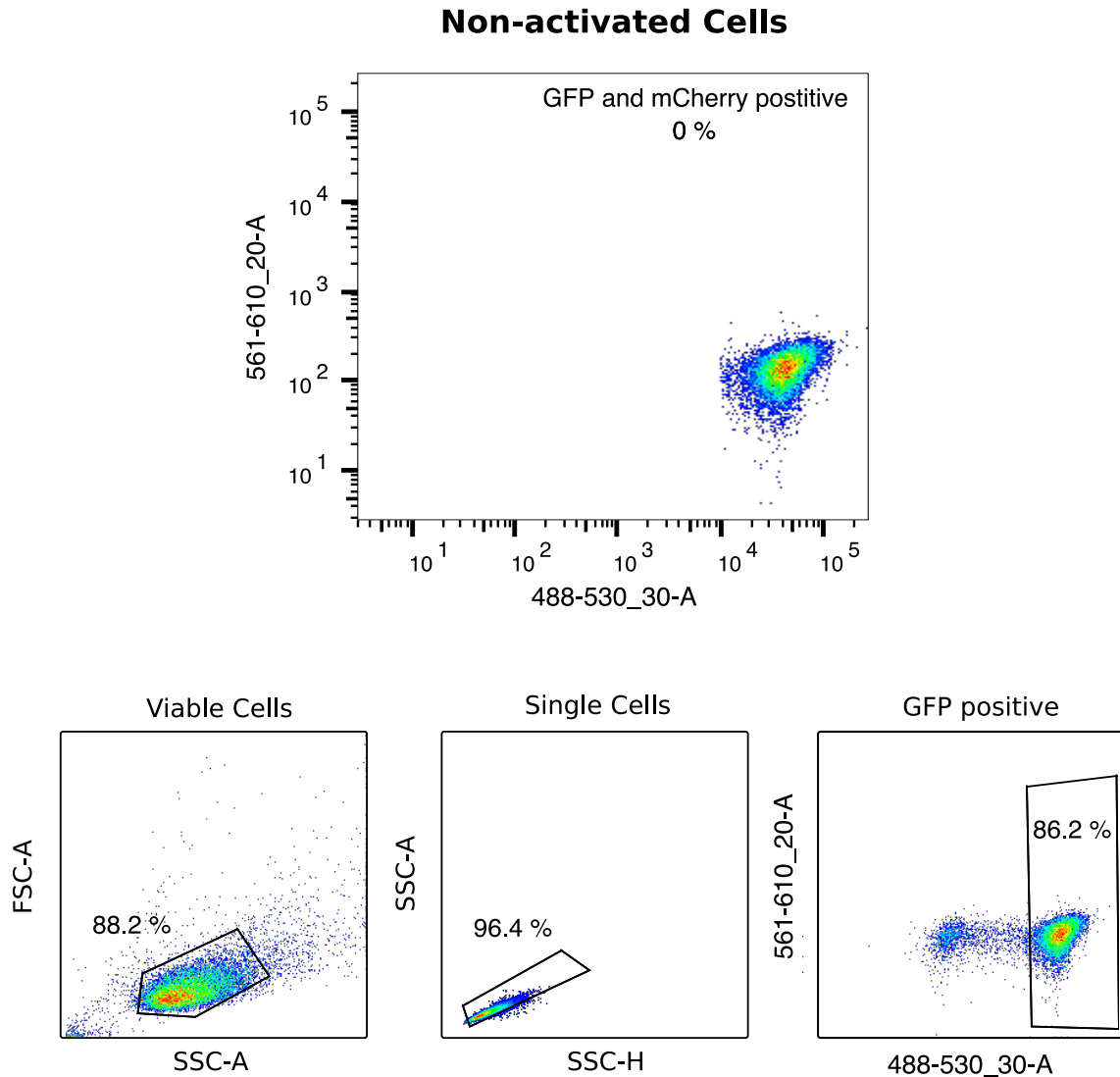


Figure 2.19: Flow cytometry plots of non-activated HeLa-GalNaC-GFP cells. This was used to define the negative population in order to set up gates for the mCherry positive, activated cells. The lower panel shows the back-gates that were defined in order to select, first viable cells, then single-cells (doublet-exclusion) and GFP-positive cells only.

Photo-activated Cells Normal Phenotype

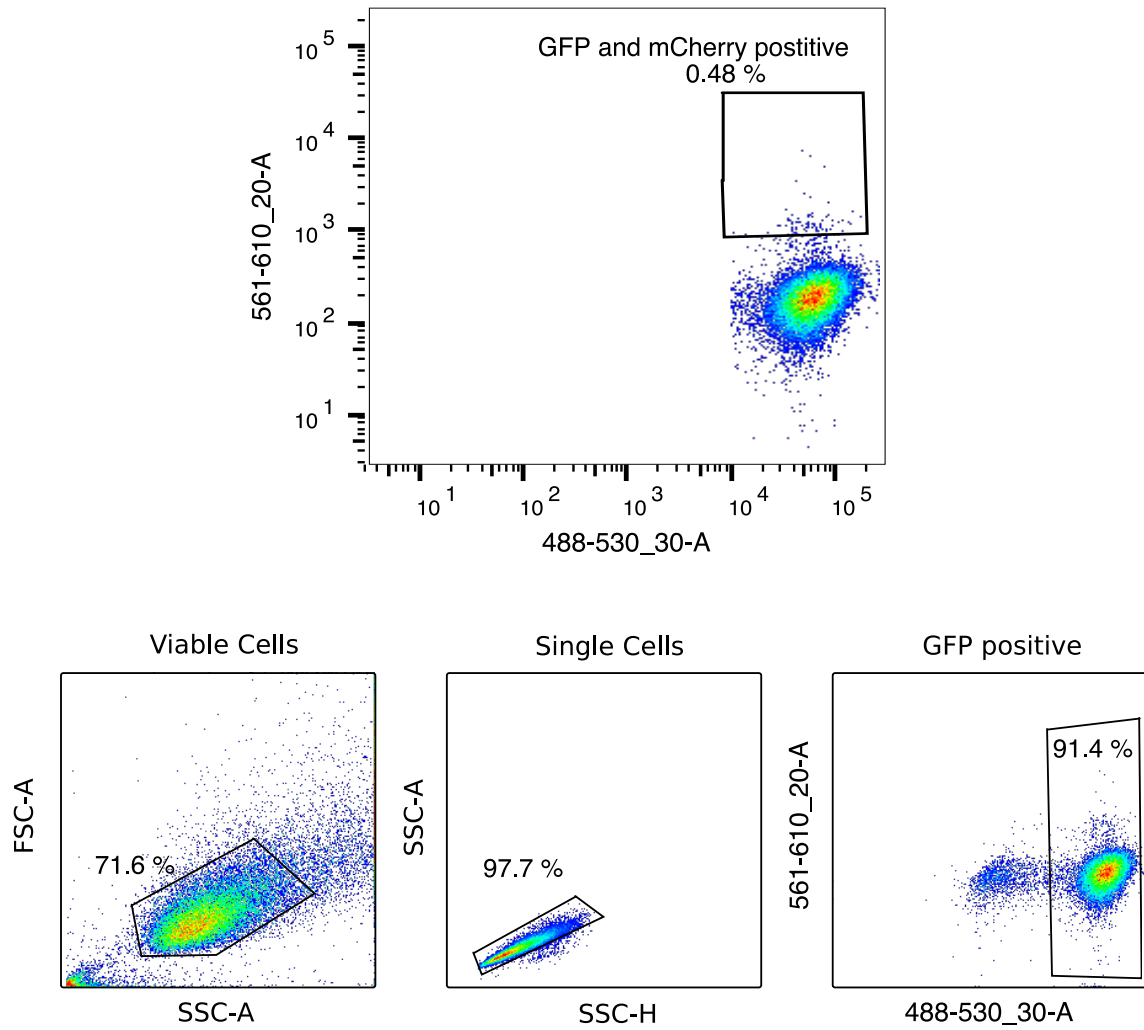


Figure 2.20: Flow cytometry plots of activated HeLa-GalNaC-GFP cells showing a normal phenotype upon USO1 knockdown. This population was sorted out into single cells as well as pools of 20 cells. The lower panel shows the back-gates that were defined in order to select, first viable cells, then single-cells (doublet-exclusion) and GFP-positive cells only.

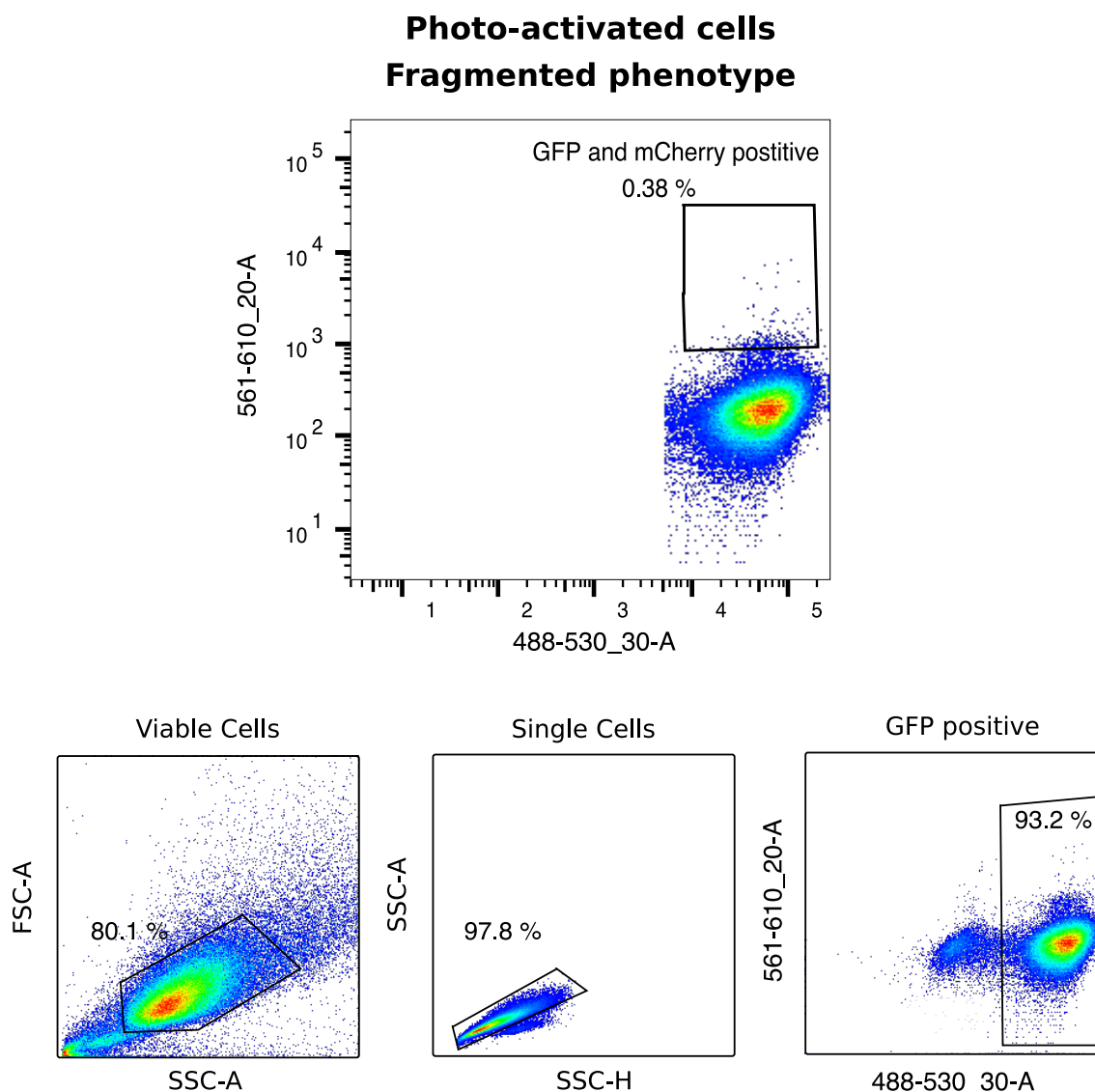


Figure 2.21: Flow cytometry plots of activated HeLa-GalNaC-GFP cells showing fragmented phenotype upon USO1 knockdown. This population was sorted out into single cells as well as pools of 20 cells. The lower panel shows the back-gates that were defined in order to select, first viable cells, then single-cells (doublet-exclusion) and GFP- positive cells only.

Sorting was performed at the EMBL Flow Cytometry core facility, and sorters were cleaned and cooled to 4°C before use. Cells were sorted in two modalities: as single cells into a 96-well plate or as a pool of 20 cells of one phenotype into each well of a 96-well plate. The second modality was required since single-cell collection was inefficient for further processing to cDNA for sequencing. Prior to each sort, the sort accuracy was tested in empty wells to ensure correct alignment as sensitivity of the instrument. The collection plate contained lysis buffer as per the SmartSeq2 protocol [193] that was used further on for cDNA library preparation. Immediately after sorting, plates were sealed and frozen in dry ice before transferring into -80°C until further use.

2.3.5 Preparation for RNA transcriptome analysis

Preparation of bulk samples for sequencing

Before proceeding with single-phenotype low-input mRNA sequencing, a Global transcriptome analysis was performed for two putative candidates as a baseline: USO1 and AKAP9, since the siRNA knockdowns of both these proteins caused significant Golgi fragmentation, and had a population of cells which did not show the typical fragmented phenotype within the treatment. For comparison, another Golgi protein TRIP11 was chosen for bulk sequencing post knockdown. The reason behind this was that TRIP11 knockdown did not result in visible Golgi fragmentation upon knockdown and it would be a good comparison to see the particular signature of Golgi fragmentation alone. Along with these three protein knockdowns, a control siRNA with no target (siNeg9) and transfection controls were sequenced for their transcriptomes and the results are discussed in a following section. These samples were prepared by performing a 72-hour knockdown on HeLa-GalNaC-GFP cells followed by mRNA isolation using the RNA EasyKit from Invitrogen. Samples were then submitted to the EMBL Genomics Core facility for library preparation and sequencing.

Preparation of single-phenotype and single-cells for sequencing

The cells collected after FACS were prepared in different ways depending on whether they were live or fixed. Fixed samples were first reverse-crosslinked to break down the protein mesh-work generated by paraformaldehyde treatment and then RNA was extracted using a modified version of manual Trizol extraction (Fig.2.22). This approach was ultimately discarded due to low mRNA recovery rates.

Live cells were directly assayed with the SmartSeq2 protocol which included reverse transcription and PCR amplification of the product to obtain cDNA . Further, cDNA libraries were prepared by tagmentation using a homemade version of the Tn5 enzyme. Although single-cell cDNA could be obtained in both the fixed and live cell protocols, the final pipeline was run using the live cell protocols due to higher efficiency. The highest efficiency of cDNA preparation was obtained, however, with live cells with 20 cells sorted per well (Fig.2.23).

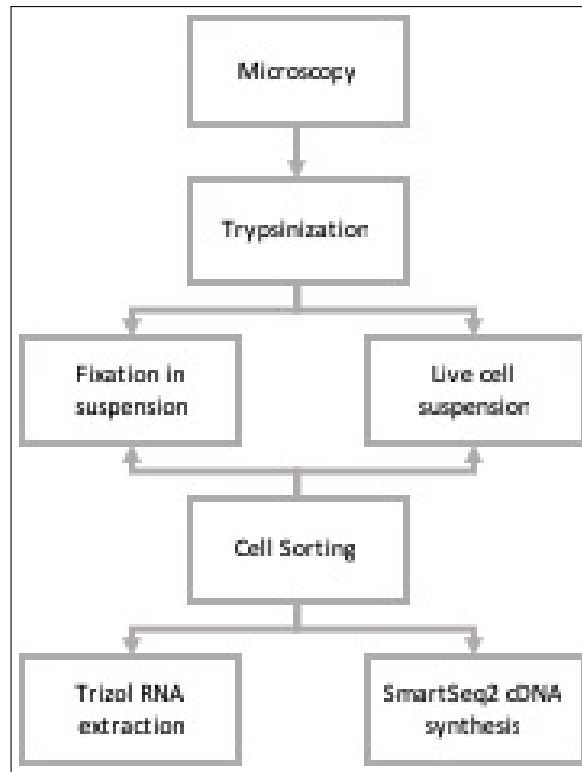


Figure 2.22: Processing of cells for transcriptome sequencing. Cells were either fixed in suspension or sorted live. Fixed cells were reverse cross-linked and live cells were sorted directly into lysis buffer, followed by the SmartSeq2 protocol.

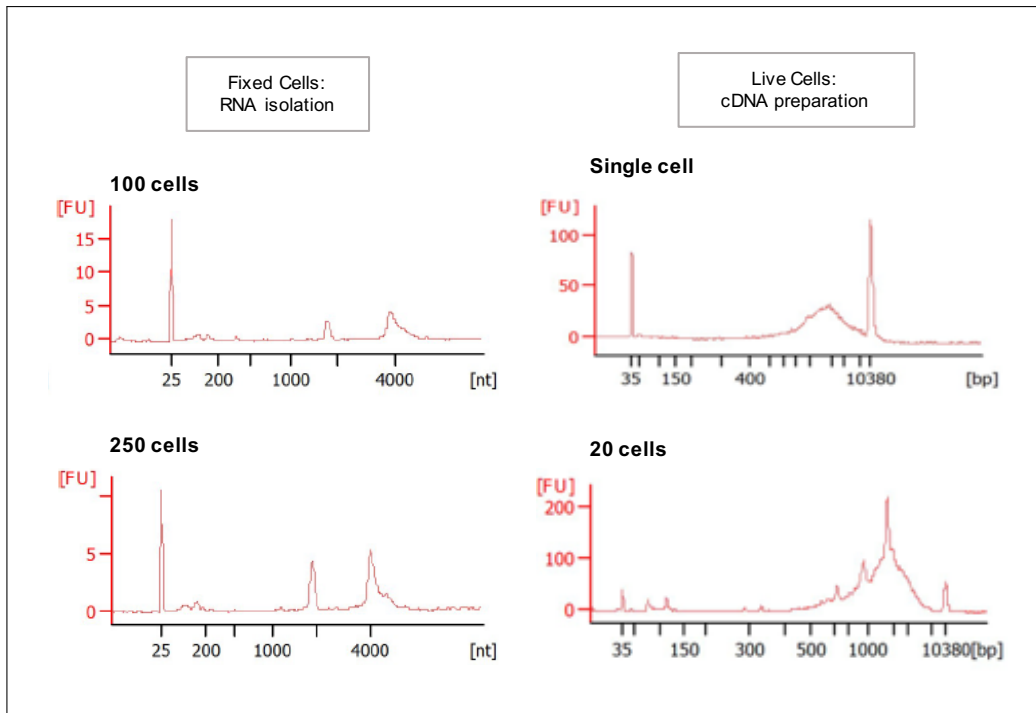


Figure 2.23: Left: Bioanalyzer plots of a RNA pico-chip analysis of RNA isolated from 100 and 250 PFA fixed cells, respectively. Right: Bioanalyzer plot of a high sensitivity DNA chip analysis to detect reverse transcribed mRNA from a 1 and 20 cells, respectively.

2.4 Transcriptome Analysis

2.4.1 Global transcriptome analysis

The effect of changes in Golgi morphology on the transcriptome have not been studied before. Before comparing different phenotypes within a siRNA treatment, it was important to understand the transcriptome changes occurred when a protein affecting Golgi structure was knocked down. For this purpose, two proteins were chosen from the 6 proteins that showed an effect on Golgi morphology upon knockdown (shown in Fig. 2.5). These were siAKAP9 and siUSO1. Since both these treatments resulted in Golgi fragmentation, another Golgi protein :TRIP11, which does not cause Golgi fragmentation upon siRNA knockdown was chosen alongside to compare non-morphology related changes in trafficking etc. An siRNA with no targets in the genome (**siNeg9**) was included, as well as a sample treated only with the transfection reagent (**TC**) without any siRNA to look for transcriptome changes upon adding the lipid reagent alone. A final control was the cells treated with the transfection media alone (**OptiMEM**) (Table: 2.2). Each sample consisted of 1 million cells, and three replicates were sequenced per sample.

Sample Name	siRNA	OptiMEM	Oligofectamine	Golgi morphology
OptiMEM	-	X	-	Unchanged
TC	-	X	X	Unchanged
siNeg9	Neg9	X	X	Unchanged
siUSO1	USO1	X	X	Fragmented
siAKAP9	AKAP9	X	X	Fragmented
siTRIP11	TRIP11	X	X	Unchanged

Table 2.2: Samples and corresponding negative controls for an understanding of the transcriptomic signature to lipid-based siRNA knockdown of proteins affecting Golgi structure.

Analysis of negative controls and normalization

The first step in analysis of sequence data from bulk samples was to see sample-to-sample variability both within and across treatments. About 11,000 genes were detected across all samples (Fig. 2.24, meaning that samples could be compared without much bias. A PCA plot (Fig. 2.25 shows the variance between all sequenced bulk samples. As is seen in this plot, both siUSO1 and siAKAP9 cluster away from the controls, confirming that the siRNA knockdown had a significant effect on the transcriptome. It was interesting to note that siUSO1 and siAKAP9 show complete different transcriptome profiles, despite the fact that both treatments cause Golgi fragmentation. Cells treated with siTRIP11 are, however clustered close to the control samples. Within the different controls, there seems to be little difference between the OptiMEM, TC and siNeg9 samples, which can

be interpreted as having little effect of adding the lipid-based transfected reagent (TC), or the un-targeted siRNA (siNeg9) *vis-a-vis* addition of only the media (OptiMEM).

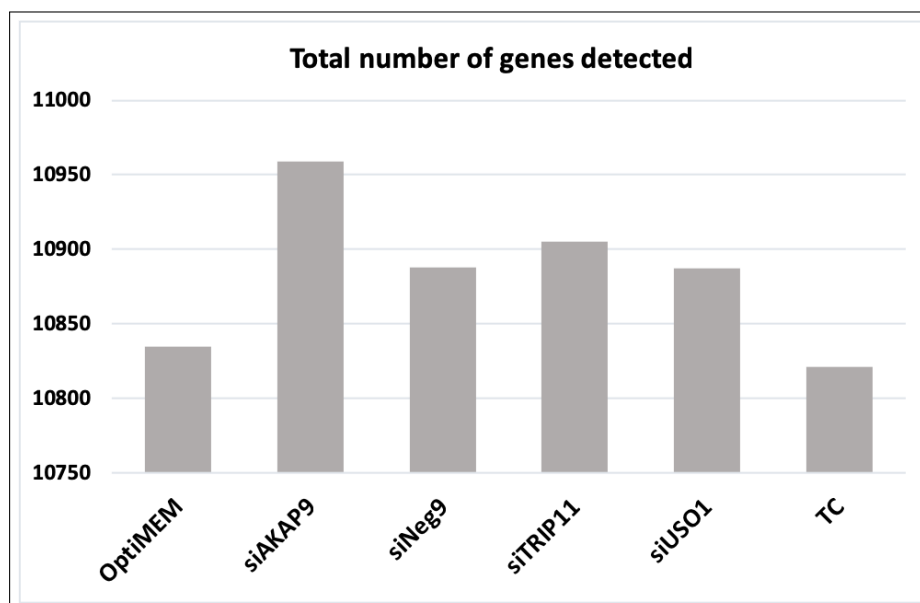


Figure 2.24: Number of genes detected in each treatment for global expression analysis. All samples show a consistent value around 11,000 genes.

Since siNeg9 was the closest negative control to the siRNA treatments, it was used to perform a differential expression analysis for all the other siRNA treatments. This means, read counts of genes were normalized to those in siNeg9 to come up with a genelist for each treatment showing all genes that were significantly upregulated or downregulated. This was performed by Jonathan Landry at the Genomics Core Facility at EMBL Heidelberg using the R package DESeq2 [194]. As seen in Fig. 2.26, the other negative controls, namely OptiMEM and Transfection Control (TC) showed only a few genes differently expressed from siNeg9, whereas the siAKAP9 and siUSO1 had strong differences in gene expression from the siNeg9, indicating that Golgi fragmentation indeed had a large effect on global gene expression. This was especially confirmed by the fact siTRIP11, that does not cause Golgi fragmentation showed a much lower extent of change in gene expression.

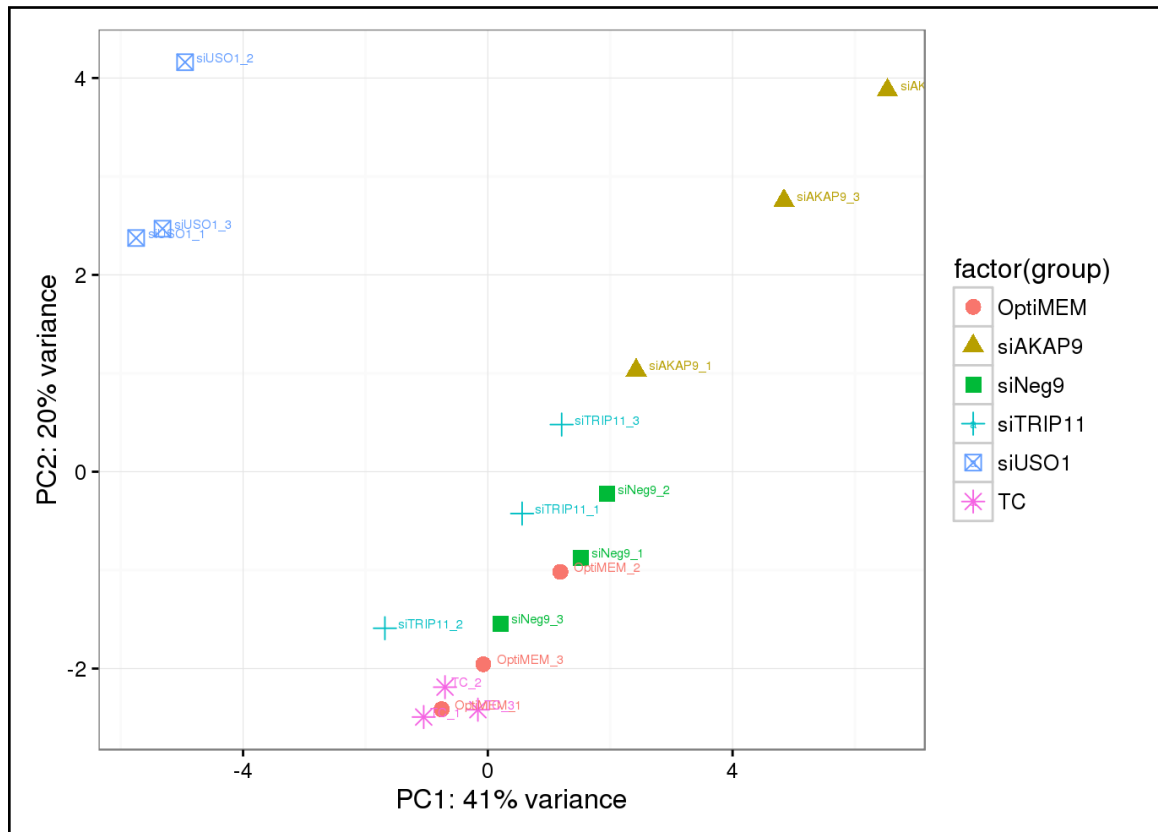


Figure 2.25: PCA plot representing variation across and within samples in the global transcriptome analysis. Replicates cluster closely except in the case of siAKAP9, shows the most variance from the other samples. The negative controls are found to cluster close to each other, as well as with TRIP11.

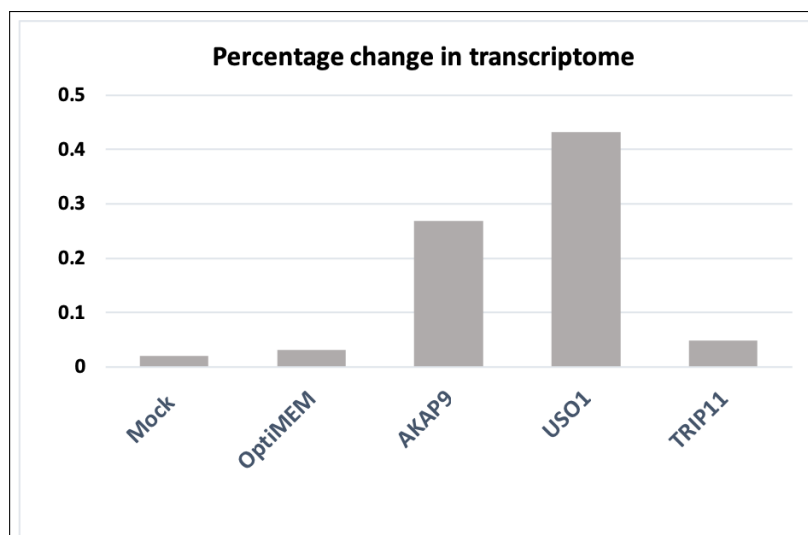


Figure 2.26: Comparison of changes in transcriptome upon siRNA knockdown normalized to Neg9. The most drastic change is seen in siUSO1, followed by siAKAP9. OptiMEM and TC samples show a very minor change in comparison to siNeg9.

Functional analysis of enriched pathways

To assess the biological impact of the siRNA treatments, the genes differentially expressed in each treatment were first thresholded to filter out any genes that were not significant (pvalue greater than 0.05). Also, only genes that were up/down regulated at least 1.5 times the normal value were considered (Log 2 FoldChange of ± 0.58). With these constraints in place, a functional enrichment analysis was performed using the ClueGo application in Cytoscape. The pie charts below represent a global picture of the pathways that are detected as enriched in the transcriptome of each siRNA treatment (both up and down-regulated genes)(Fig. 2.27, 2.28, 2.29).

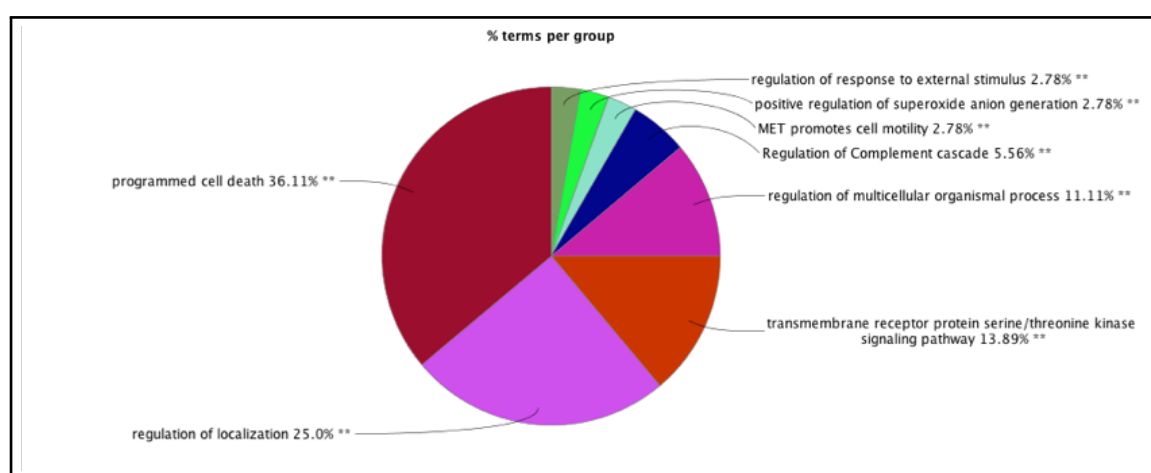


Figure 2.27: Pie chart representing functional clusters found in significantly expressed genes after AKAP9 knockdown.

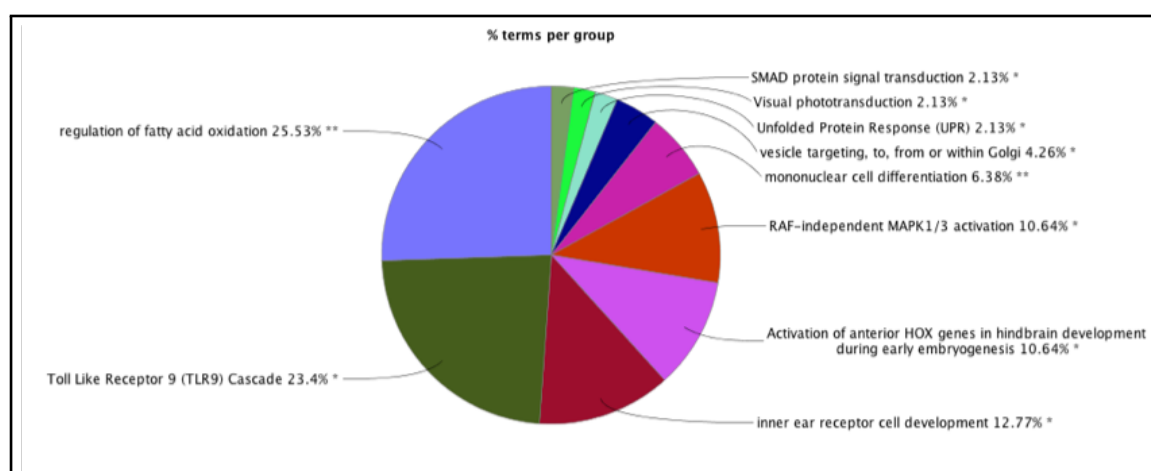


Figure 2.28: Pie chart representing functional clusters found in significantly expressed genes after TRIP11 knockdown.

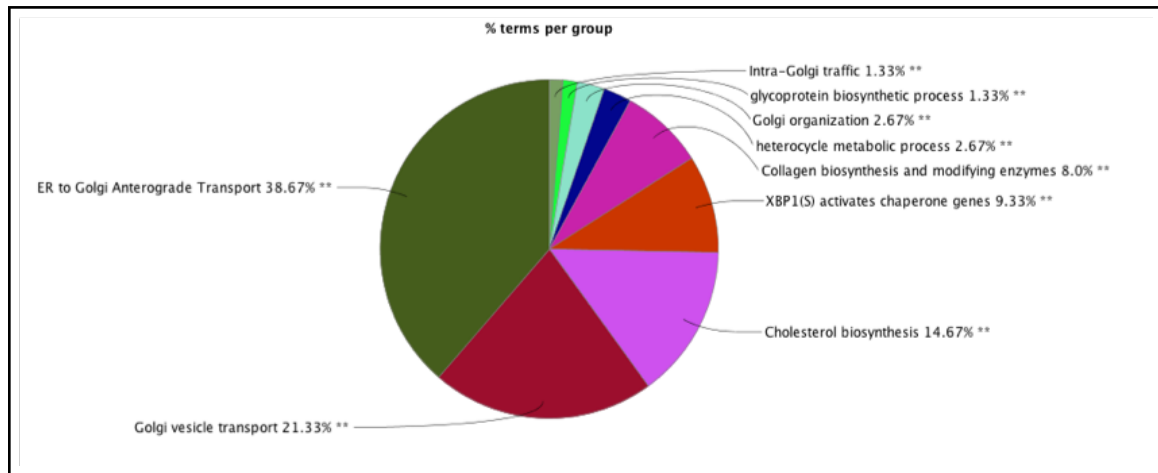


Figure 2.29: Pie chart representing functional clusters found in significantly expressed genes after USO1 knockdown.

In all three siRNA knockdowns, the up-regulated pathways were particularly interesting (Fig. 2.30, 2.31, 2.32). siTRIP11 and siUSO1 showed similar pathways such as ER-Golgi transport, Intra-golgi transport and vesicle transport that were up-regulated at the transcriptome level. This was particularly interesting as although both these proteins function at a similar location with similar function of vesicle tethering, their knockdown has different effects on Golgi morphology. On the contrary, siAKAP9 showed a high expression of apoptosis-related genes, despite showing the same Golgi phenotype as USO1. From this result, we can interpret that there different cellular mechanisms that lead to fragmentation, and could have completely different implications for the cell. For example, it could be in the case of siUSO1 and siTRIP11, cells sense the defect in trafficking upon the knockdown and up-regulate trafficking machinery to compensate. Whereas in the case of siAKAP9, the cell senses a problem with cell division and therefore apoptotic pathways are triggered.

Although similar pathways are up-regulated in siUSO1 and siTRIP11, the effect size of this up-regulation is much milder in siTRIP11. This could be an explanation for lack of Golgi fragmentation in siTRIP11, where there simply are other proteins that could compensate for its absence. A detailed comparison between the two treatments is not performed here, as it was not the purpose of this study. However, such an analysis could potentially provide exciting insights into regulation of the early secretory pathway.

The global transcriptome changes seen could either be the cause or effect of the Golgi phenotype observed. Therefore, a comparison of cells with and without the Golgi phenotype upon the same siRNA treatment was required to complete the picture of how these correlated and find pathways specific for control of Golgi phenotype (i.e, Golgi organization).

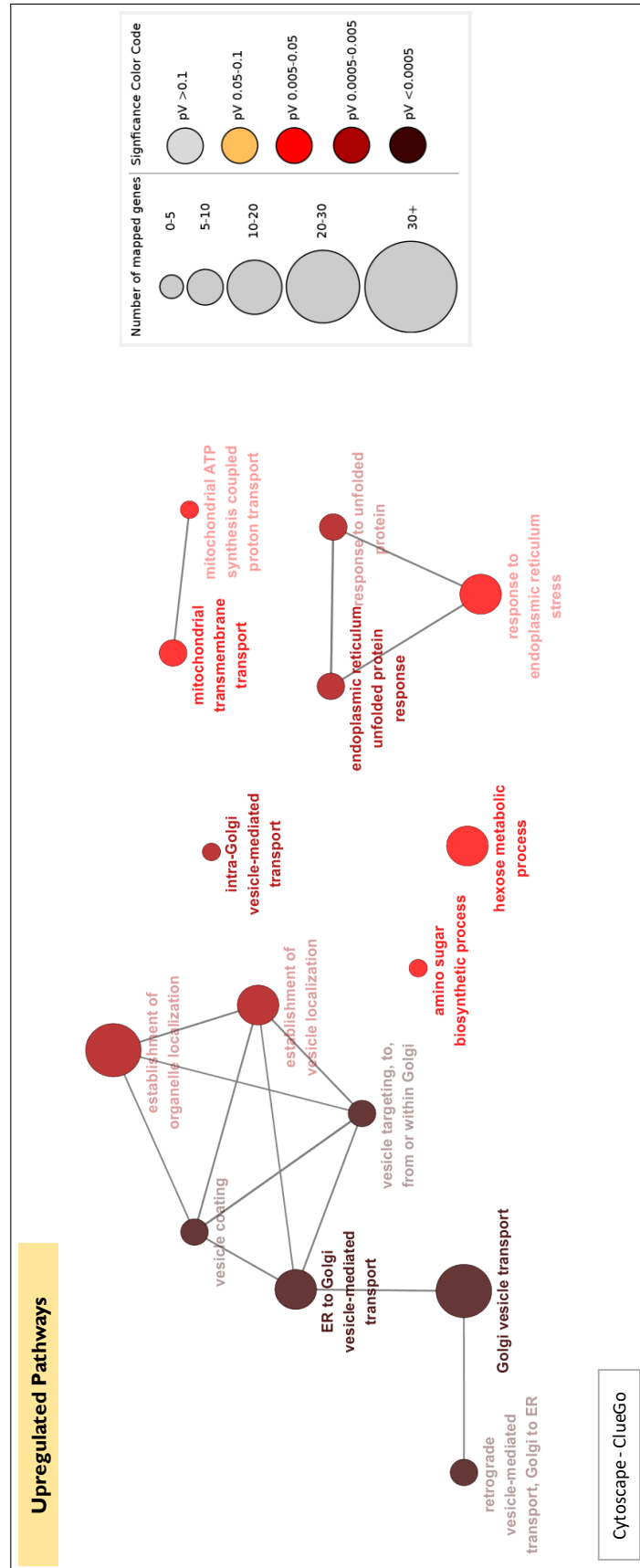


Figure 2.31: Up-regulated pathways upon TRIP11 knockdown. ER-Golgi transport and intra-Golgi transport are enriched in the geneset.

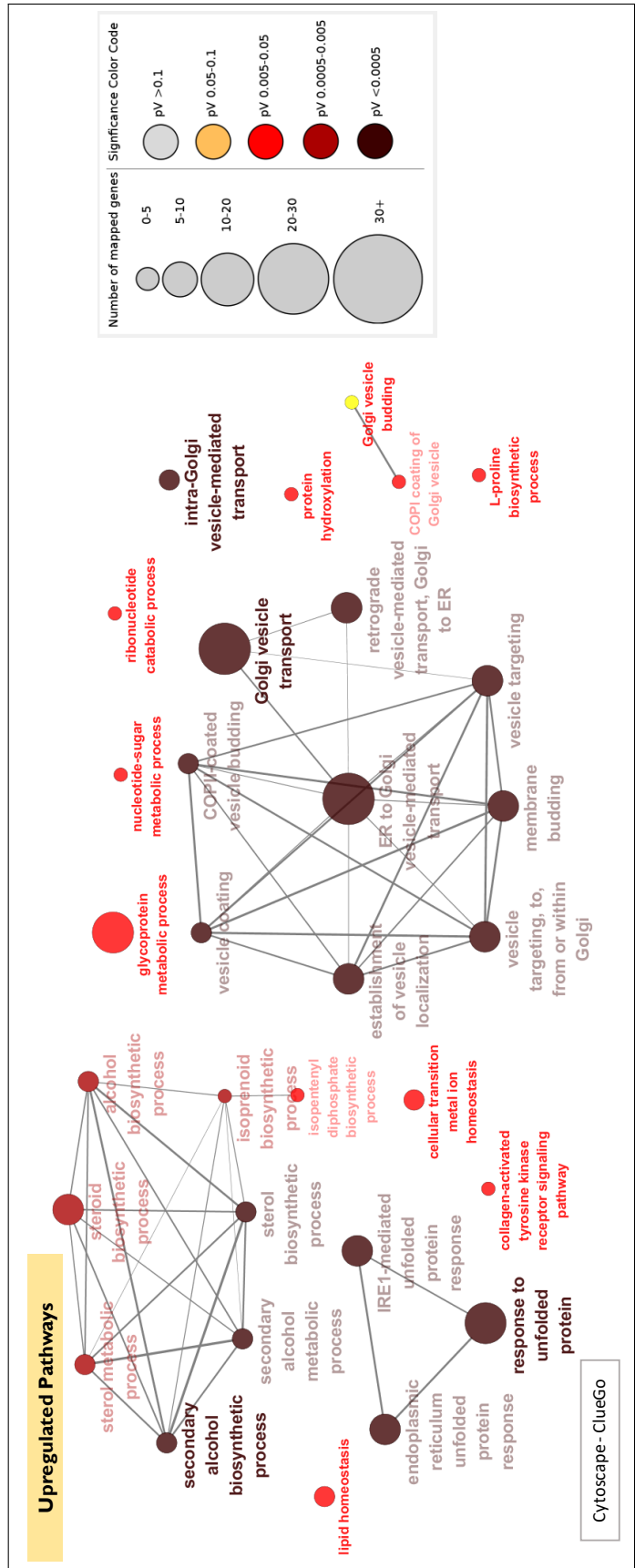


Figure 2.32: Up-regulated pathways upon USO1 knockdown. An enrichment is seen in ER-Golgi transport, Golgi vesicle, and intra-Golgi transport, among others.

2.4.2 Transcriptome analysis between two Golgi phenotypes

siUSO1 was chosen to perform transcriptome analysis between different Golgi phenotypes. The reason for this choice was the large number of genes and pathways relating to trafficking appear upon USO1 knockdown, combined with the strong Golgi fragmentation seen.

Therefore, the developed pipeline for differential transcriptome between two Golgi phenotypes was run after 72 hours of USO1 knockdown. In total, 100 cells of each phenotype were collected after photo-activation, in pools of 20 cells. 20 cells were collected in a single well by flow cytometry due to inefficient library preparation of single-cells. These were then sequenced by Hi-Seq and a differential expression analysis between the two phenotypes was performed at the Genomics Core Facility at EMBL Heidelberg.

Estimating variability between phenotypes

In order to assess the extent of changes in the transcriptome between the phenotypes 'normal' and 'fragmented', a principal component analysis (PCA) was done on all samples. The resulting PCA plot is shown in Fig. 2.33. In this plot, a significant difference is observed between the sample 'Fragmented 2' and all other samples (PC1). All the other samples do not show great variability between each other, and further samples of the same phenotype cluster together. Given that the sample 'Fragmented 2' behaved drastically different from all other samples, it was removed from further analysis and the PCA was re-plotted (Fig 2.34).

Estimating variability within phenotypes

The PCA plots provided a first glance into the difference between the two phenotypes, and provided some insight into variability between samples of the same phenotype. However, in order to perform further analysis, a more robust measure of same-phenotype sample variability was required. This was measured by correlating the expression levels of each gene in a particular sample with the same gene in another sample to generate a correlation plot of all genes detected. Such pairwise correlation was done for every pair of samples of the same phenotype and are shown in Figures 2.36 and 2.35.

Both phenotypes showed a high degree of similarity between samples within their phenotype. This, along with the difference between phenotypes observed in the PCA plot, laid the ground for robust analysis to be performed to get differential expression analysis between the two phenotypes.

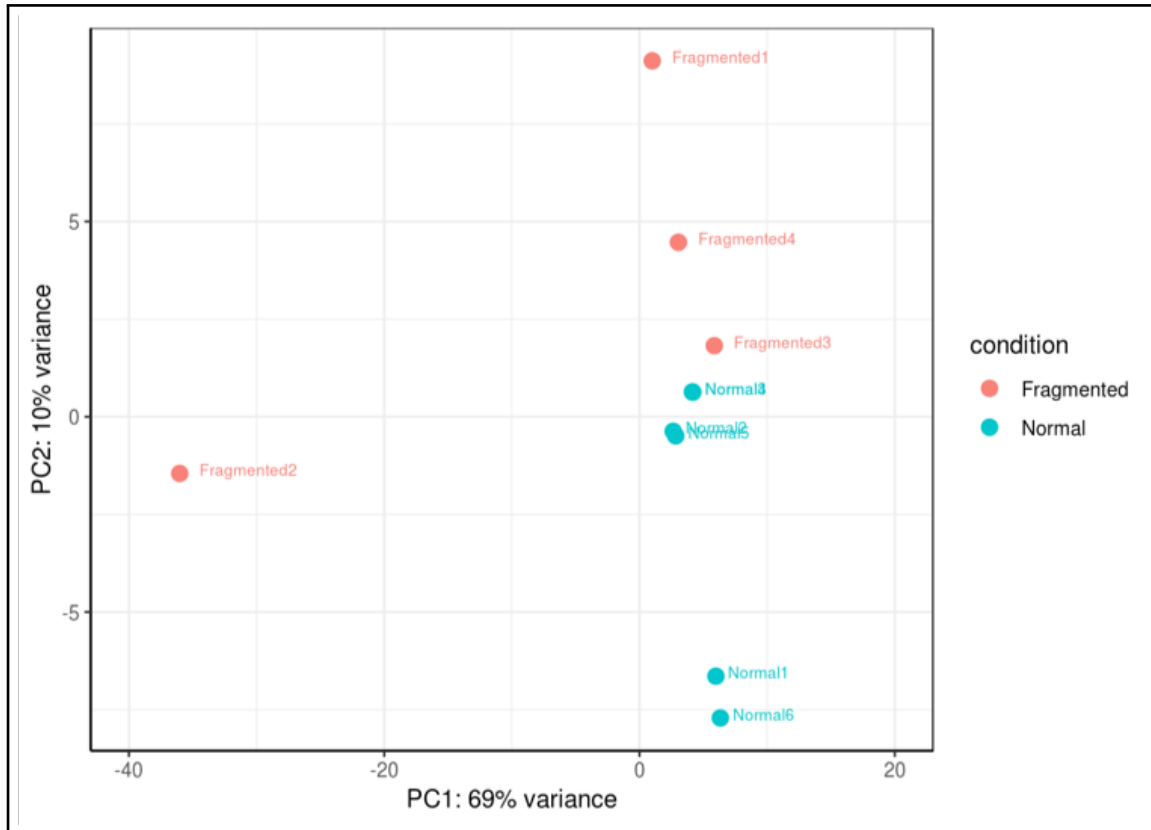


Figure 2.33: PCA plot of phenotype-based transcriptomics. As seen on the X-axis of this plot, the maximum variance (69%) seems to be between the sample 'Fragmented 2' and all other samples. In contrast, there is a maximum of 10% variance seen between all other samples.

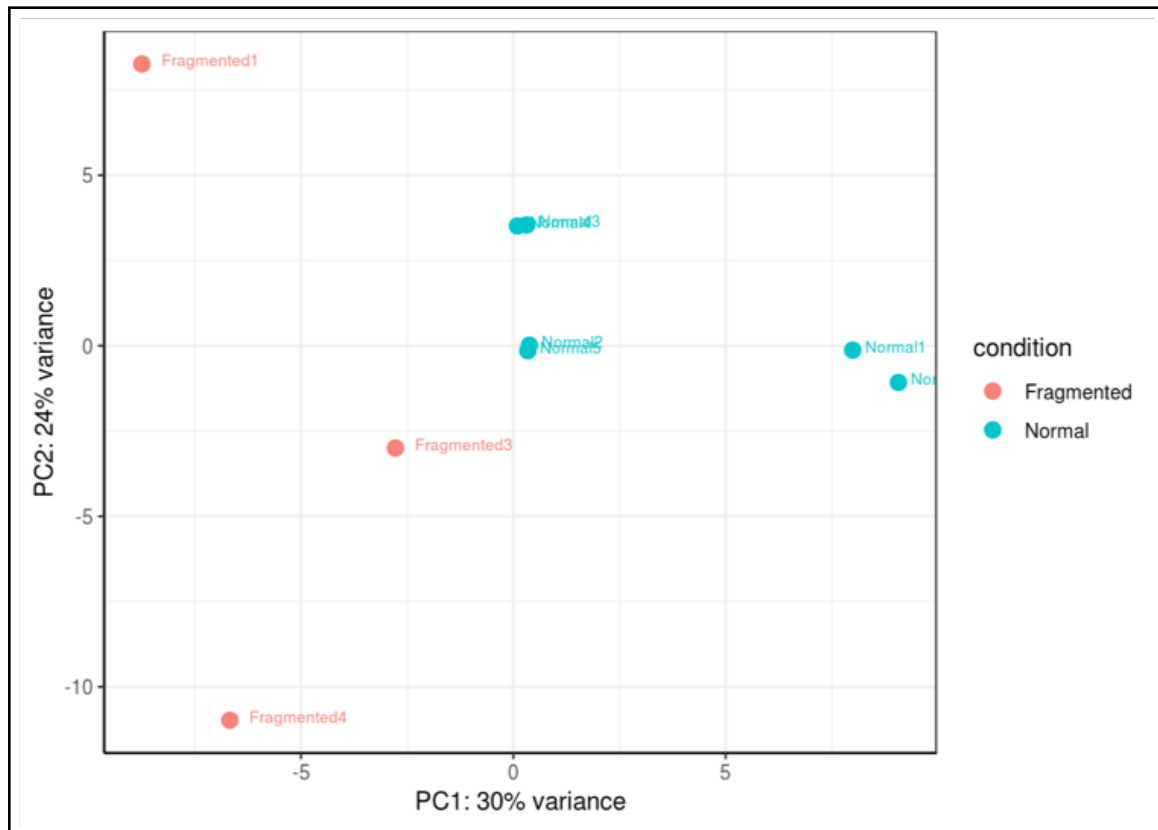


Figure 2.34: PCA plot of after removal of sample 'Fragmented 2'. This plot shows a 30% variance on the PC1 axis, which separates phenotypes distinctly. The second axis shows a variance of 24%, which is mainly seen among different Fragmented samples, whereas the normal samples seem to cluster in close proximity.

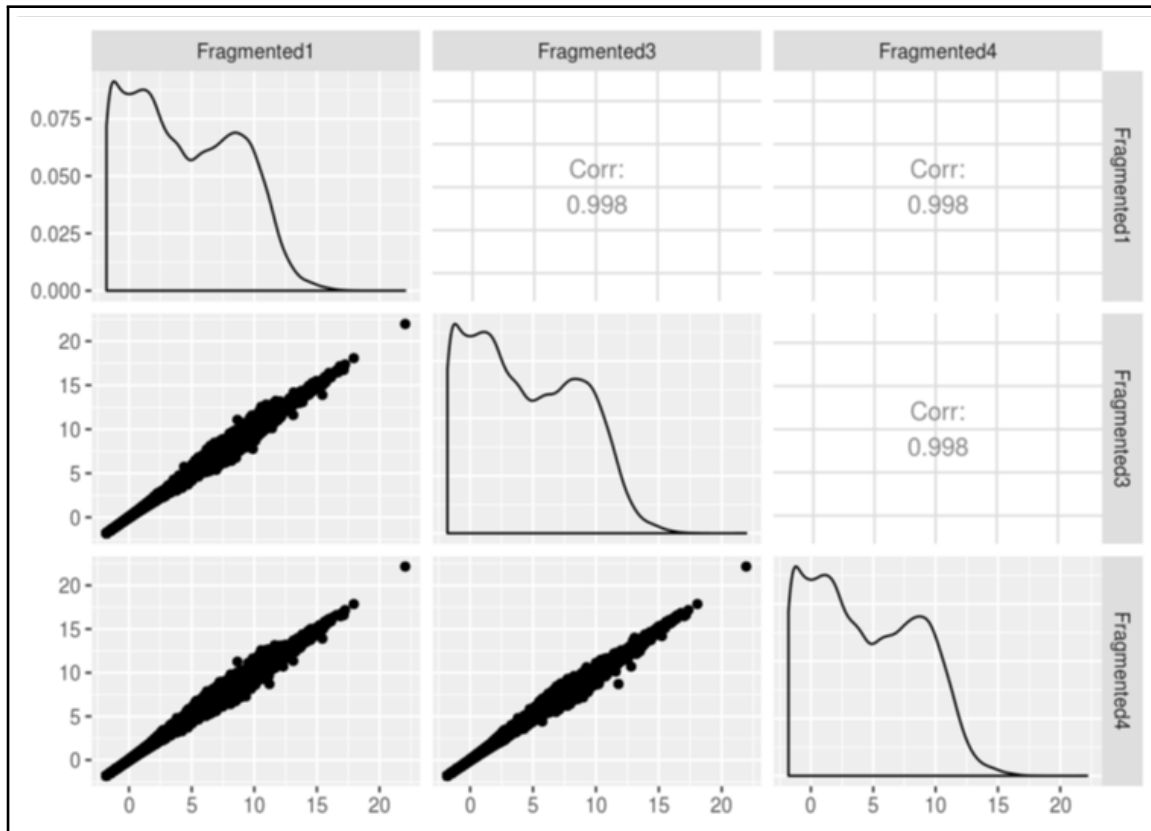


Figure 2.35: Scatterplots of transformed counts for pairwise correlation of same phenotype samples. High correlation coefficients are seen for all pairwise comparisons within the Fragmented phenotype.

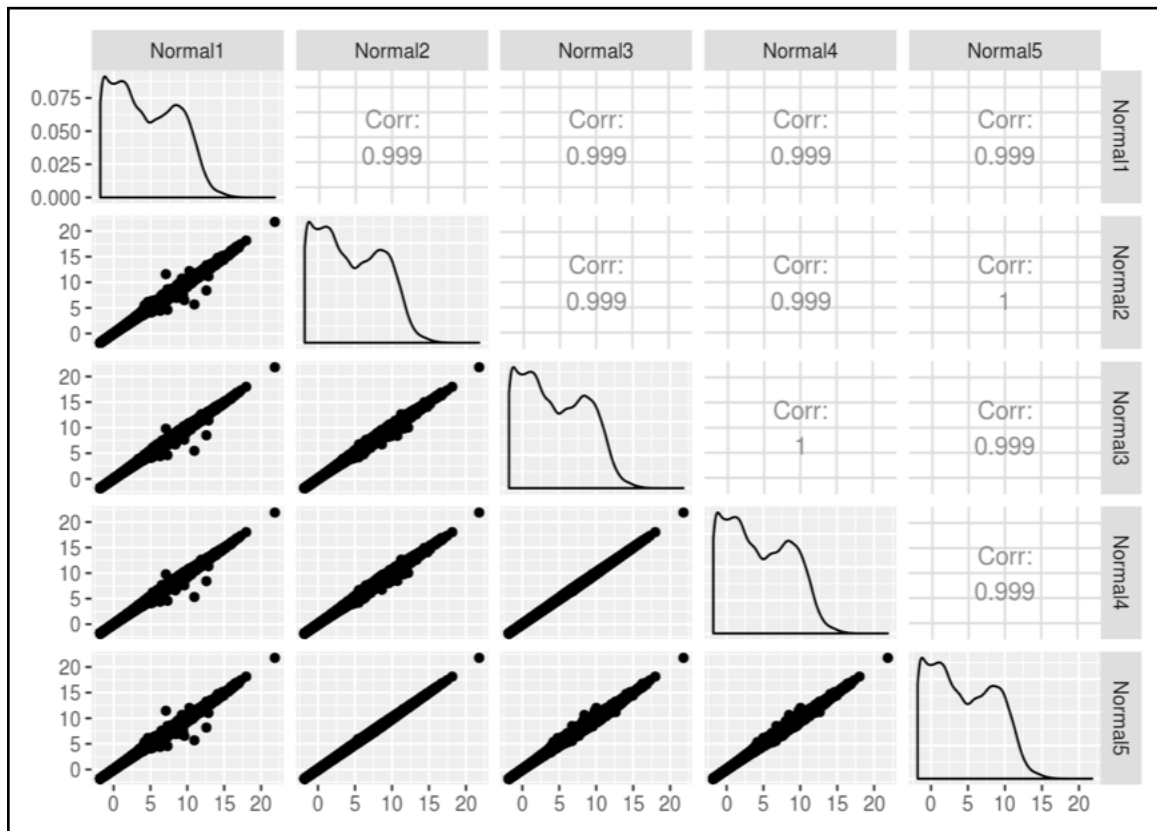


Figure 2.36: Scatterplots of transformed counts for pairwise correlation of same phenotype samples. High correlation coefficients are seen for all pairwise comparisons within the Normal phenotype.

Estimating USO1 knockdown in each phenotype

The basis of our hypothesis is that the two Golgi phenotypes observed upon siUSO1 treatment indeed have this gene knocked down. Prior to this moment in the pipeline, it was not possible to assess the knockdown level of USO1 in either population. Therefore, it was imperative to compare the levels of USO1 at the transcriptome level, to make sure the phenotype difference is not an effect of transfection efficiency or insufficient knockdown (Fig.2.37). The comparison of Fragments Per Kilobase Million (FKPM) values shows similar expression levels of USO1 in both phenotypes.

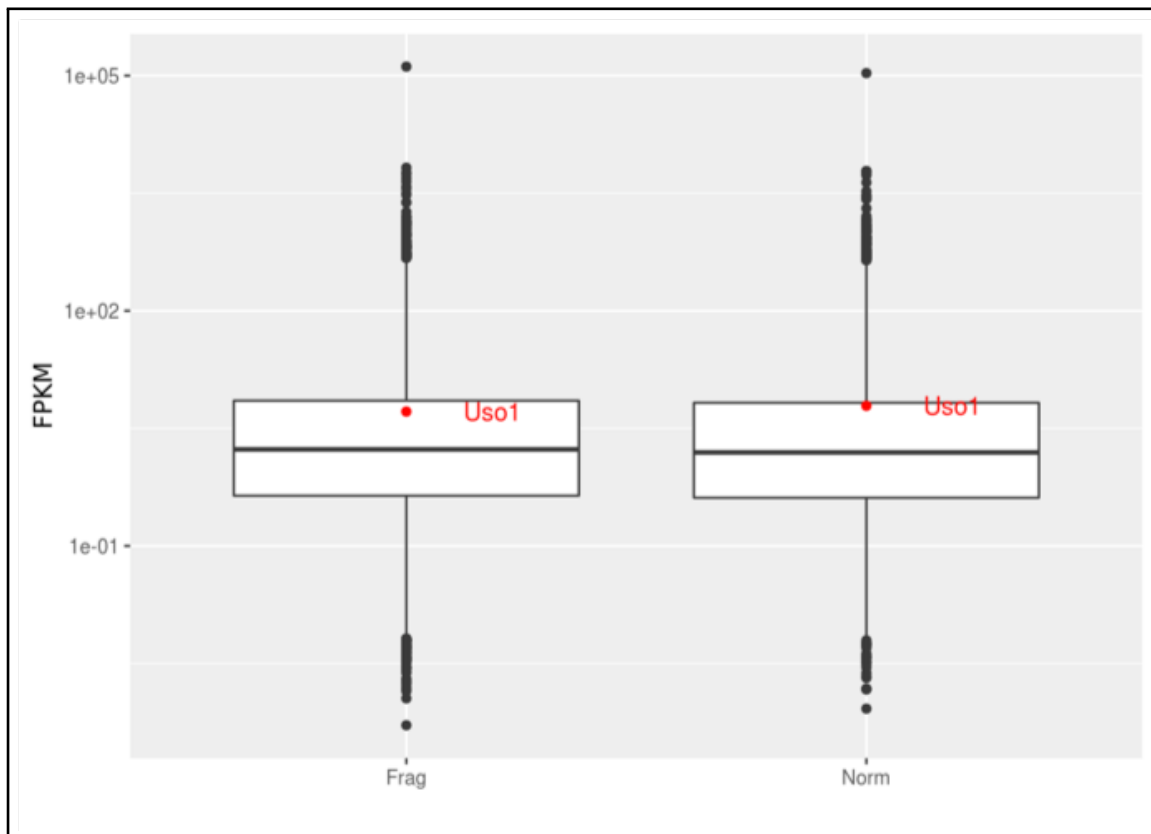


Figure 2.37: Fragments Per Kilobase Million (FKPM) values for USO1 in normal and fragmented phenotypes. Both phenotypes show similar levels of USO1.

FKPM	Fragmented	Normal
Median gene expression	15.80	14.73
USO1 expression	5.170489	6.125937

Table 2.3: FKPM values for expression of USO1 in both fragmented and normal phenotypes in comparison with the median expression level of all genes in the respective phenotypes.

Moreover, the expression of USO1 in both genes is significantly lower than the median level of gene expression in both the phenotypes, shown in Table 2.3. This is also in contrast

to usual levels of USO1 expression in HeLa cells, which is five-fold higher than the levels seen here. This confirms that both phenotypes are knocked down for USO1 to similar levels. With this confirmation, differential expression analysis between the two populations could be performed.

Differential expression analysis

Differential expression analysis between the normal and fragmented phenotype was performed by Jonathan Landry at the Genomics Core Facility at EMBL Heidelberg. The R studio package DEseq2 [194] was used. In total, 18,910 genes were compared in the two samples. A list of differentially expressed genes between all samples of the two phenotypes was generated. A few filtration steps were performed on this dataset before biological analysis (Table 2.4). First, genes were filtered so only genes with adjusted p.value ≤ 0.05 were considered. This was automatically done while DEseq2 analysis and therefore was not required as an additional step. The data set was not thresholded by the usual Log 2 Fold Change value of ± 0.58 due to low input mRNA (few cells), where any differences might be important. The last filtration step was to remove genes with unknown IDs, as they had no known product and could not be investigated at this stage.

Number of Genes	No filter	Log2 Fold Change $\geq \pm 0.58$	Known Gene IDs
Upregulated	728	630	452
Downregulated	345	257	210

Table 2.4: Number of genes upregulated and downregulation between normal and fragmented phenotypes. Number of genes after thresholding on expression fold change and removal of unknown gene IDs.

The differential expression analysis resulted in a list of all genes that were significantly up or down regulated in non-fragmented cells with reference to the fragmented cells. Around 700 genes came up as differentially regulated between the two Golgi phenotypes. This was about 4% of all detected genes in the samples. This indicates that although a small percentage of the transcriptome changes between the two phenotypes, this change has a large effect size. For functional analysis, a significance threshold was placed at p-value less than or equal to 0.05.

First, we looked for changes in the major components of the secretory pathway. This included the Golgins, SNARE proteins, COP components, Rab proteins, COG proteins, clathrin components as well as cytoskeletal proteins associated with the secretory pathway. Since USO1 operated at the ER to Golgi stage of anterograde transport, it was expected that other proteins in this pathway are differentially expressed. However, no significant changes were found in any major groups of proteins involved in the secretory

pathway, apart from a group of clathrin components, which were found to be significantly up-regulated in non-fragmented cells as compared to fragmented cells. These clathrin components are listed in Table 2.5.

Gene	Log2 FC	Function
AP2B1	0.3976	Links clathrin to receptors in coated vesicles
WASL	0.4686	Regulates actin polymerization
DNAJC6	0.7430	Promotes uncoating of clathrin-coated vesicles
FCHSD2	1.0520	Involved in mid-late stage clathrin vesicle budding
FNBP1L	0.6994	Coordinates membrane tubulation with actin reorganization
GPR107	0.4619	Involved in Golgi-to-ER retrograde transport
PIP5K1C	1.5883	Role in membrane ruffling and assembly of clathrin-coated pits at the synapse.
KIAA1107	4.3964	Involved in synaptic vesicle recycling in mature neurons

Table 2.5: Role of proteins found transcriptionally up-regulated in fragmented phenotype belonging to the cluster of clathrin-mediated endocytosis.

Next, we looked for differential expression of known interactors of USO1. A list of USO1 interactors and whether they were differentially expressed between the two Golgi phenotypes (Table 2.6). As seen in this table, only two direct interactors were found up-regulated in non-fragmented cells, namely SEMA4F and PRKACA.

Third, we looked at other pathways that were differentially expressed between the two phenotypes. Both the upregulated and downregulated gene sets were individually analyzed for their involvement in a biological process in attempt to find pathways connecting these genes. Majority of the genes did not cluster under any common molecular function or pathway, which was not surprising given the low amount of input RNA for sequencing. However, some biological pathways did emerge with a subset of genes involved. These are depicted in Tables 2.8 and 2.9. One striking observation was the up-regulation of chemokine-mediated signaling in the non-fragmented cells. A second observation was a significant enrichment in signaling kinases also up-regulated. The majority of these kinases belonged to the Serine/Threonine family of kinases, and their functions were varied, although it is likely that they all ultimately regulate cell proliferation, survival and cell cycle. The third, and possibly most interesting observation was the up-regulation of clathrin mediated endocytosis, as observed in our first analysis (Table 2.5).

Gene	Upregulated/Downregulated	Log2 FC
STX5	-	-
Sec16A	-	-
PRKACA	Upregulated	2.047346228
GOSR1	-	-
GOSR2	-	-
GOLGA2	-	-
TRAF3	-	-
SEMA4F	Upregulated	6.394658935
SCFD1	-	-
Giantin	-	-
RNF114	-	-
EFNB2	-	-
TRAF3	-	-
BET1	-	-

Table 2.6: List of top USO1 direct interactors their expression between the two Golgi phenotypes

symbol	geneName	log2FoldChange
CAMK2A	calcium/calmodulin dependent protein kinase II alpha	4.845467265
CDK10	cyclin dependent kinase 10	0.999405641
CDK20	cyclin dependent kinase 20	6.989662338
DGKQ	diacylglycerol kinase theta	4.453314025
ERBB3	erb-b2 receptor tyrosine kinase 3	7.154670763
MAP2K3	mitogen-activated protein kinase kinase 3	0.691619885
MAP3K6	mitogen-activated protein kinase kinase 6	6.547710693
PIK3IP1	phosphoinositide-3-kinase interacting protein	1 7.129075723
PKIG	cAMP-dependent protein kinase inhibitor gamma	0.994088928
PRKACA	protein kinase cAMP-activated catalytic subunit alpha	2.047346228
PRKAG2	protein kinase AMP-activated non-catalytic subunit gamma 2	1.111130879
RPS6KA3	ribosomal protein S6 kinase A3	1.477685793
PLK2	polo like kinase 2	0.841505166
PLPP1	phospholipid phosphatase 1	0.518500466
PLPP7	phospholipid phosphatase 7 (inactive)	6.323214679
PPM1M	protein phosphatase, Mg ²⁺ /Mn ²⁺ dependent 1M	6.437439702
PPP1R35	protein phosphatase 1 regulatory subunit 35	0.715038231
PPP2R1B	protein phosphatase 2 scaffold subunit Abeta	0.670347207
PRKACA	protein kinase cAMP-activated catalytic subunit alpha	2.047346228
PRKAG2	protein kinase AMP-activated non-catalytic subunit gamma 2	1.111130879
PRKCG	protein kinase C gamma	5.103120536
RPS6KA3	ribosomal protein S6 kinase A3	1.477685793
SRPK2	SRSF protein kinase 2	0.403008098
STK31	serine/threonine kinase 31	5.8336817
TNIK	TRAF2 and NCK interacting kinase	3.962497628

Table 2.7: List of signaling kinases and phosphatases found to be up-regulated in non-fragmented cells upon differential expression analysis.

Id	Term	In Population	In StudySet	Std. Error
GO:0070098	chemokine-mediated signaling	44	9	0.0111
GO:0072583	clathrin-dependent endocytosis	36	8	0.0110

Table 2.8: Biological processes that are upregulated in the non-fragmented phenotype compared with the fragmented phenotype.

Id	Term	In Population	In StudySet	Std. Error
GO:0070370	cellular heat acclimation	5	3	0.0041
GO:0035089	establishment of cell polarity	16	4	0.0028
GO:0010729	hydrogen peroxide biosynthesis	3	2	0.0016
GO:0035666	TRIF-dependent TLR signaling	28	4	0.0066
GO:0090071	regulation of ribosome biogenesis	4	2	0.00278

Table 2.9: Biological processes that are downregulated in the non-fragmented phenotype compared with the fragmented phenotype.

While the other pathways that appear up- or downregulated are equally interesting and worthy of investigation, for the sake of time only the clathrin-dependent endocytosis pathway has been explored here. Our data demonstrates that cells having a non-fragmented phenotype have up-regulated endocytic genes as compared to cells with a fragmented Golgi phenotype. By up-regulating clathrin-mediated endocytosis, these cells could increase retrograde flux into the Golgi, thus balancing out the lack of anterograde flux from the ER owing to USO1 knockdown. which might be carefully balanced by the lack of anterograde flux owing to knockdown of the ER-Golgi transport protein USO1. However, this is a hypothesis that requires testing. Blocking clathrin-mediated endocytosis could be a way to see if non-fragmented cells can indeed become fragmented would prove that that increasing retrograde flux is indeed a way for cells to prevent fragmentation.

The purpose of this study was to devise a method to analyze the transcriptome changes between different Golgi phenotypes after siRNA knockdown and find pathways that could potentially be involved in regulating Golgi structure. This method was developed, and potential pathways have been outlined. This has provided a rich data-set with many potential follow-up proteins and pathways that could play a role in regulation of Golgi structure. Further experiments will be performed in the future to confirm the results and follow-up the pathways found here with phenotype rescue experiments.

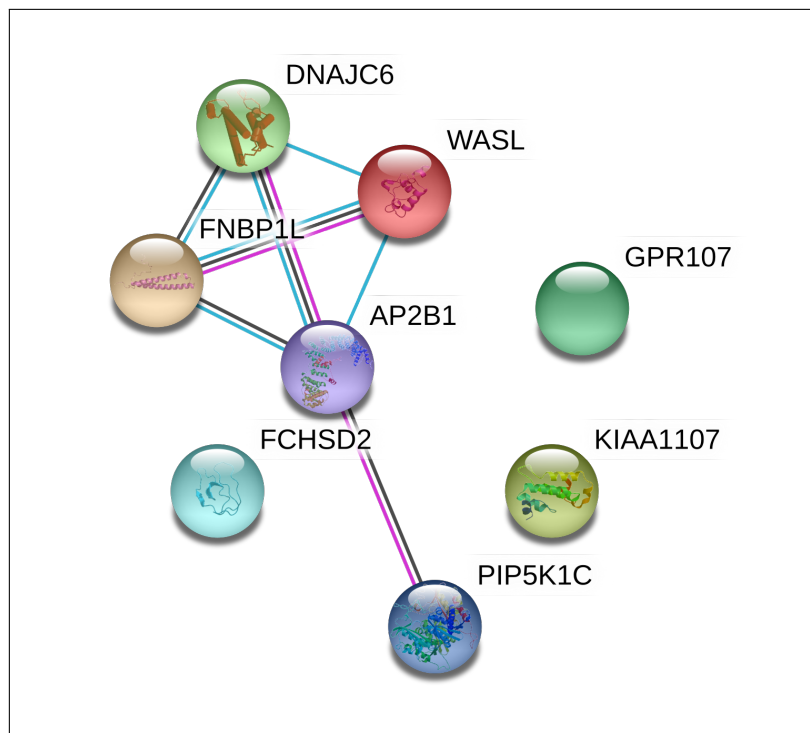


Figure 2.38: Genes upregulated in the fragmented phenotype that play a role in clathrin mediated endocytosis.

CHAPTER 3

DISCUSSION

The Golgi Complex is a fundamental feature of eukaryotic cells that plays a pivotal role in functionalization, sorting and secretion of lipids and proteins. Apart from being vital to cellular homeostasis, the Golgi Complex is a uniquely structured organelle, displaying remarkable dexterity in re-arrangement of its stacked membrane structure under various circumstances. The exact relationship between the structure and function of the Golgi complex, however, is not implicitly known, although there is mounting evidence that Golgi organization contributes significantly to efficient transport.

The Golgi has been studied in context of its structure and function for over a century. Over the years, a number of proteins have been identified that contribute to Golgi structure. These proteins range from specialized Golgi structural proteins called matrix proteins to proteins involved in different stages of trafficking, regulatory kinases, cell cycle proteins and cytoskeletal proteins [184] [185] [186] [187]. It is likely that all these seemingly diverse pathways communicate with one another to constitute a regulatory mechanism for Golgi architecture and dynamics. However, some proteins are probably more vital in this regulatory role than others, which are likely to be either downstream effectors or indirect influencers of Golgi structure. In the end, how these pathways coalesce and interact with each other is largely not understood.

The impetus to find such networks comes not only from an academic appetite to gain a deep understanding of cellular regulation. A myriad of diseases are caused by dis-regulation of the secretory pathway, as is expected if proteins are not effectively transported to their functional sites. Many other disorders are caused due to improper glycosylation of proteins, that is, because of improper Golgi function [164] [165] [166]. If Golgi function and structure are indeed so closely linked, it becomes imperative to better understand regulation of architecture [168]. Moreover, an increasing number of diseases, including many cancers have been reported to have altered Golgi morphology and distribution, further strengthening the case for investigation pathways of Golgi regulation [174] [175] [176]. All of these reasons, taken together created the motivation this project aimed at isolating network information about Golgi regulation.

3.1 Hypothesis Testing

3.1.1 The Hypothesis

In the attempt to find networks relating to Golgi regulation, a good starting point was given by looking at already existing information about Golgi organizers. RNAi based screens previously performed in our lab had been fruitful in identifying many proteins which, when knocked down in HeLa cells, disrupted Golgi morphology [187] [184]. In these

screens, an interesting observation was made, which was the presence of a population of cells that did not show the characteristic response of the siRNA treatment. In other words, in an siRNA treatment causing Golgi disruption most cells, there remained a population that still displayed intact Golgi morphology. This pattern was observed consistently across all such siRNA treatments.

Two possible theories could explain the behavior of the cell population not displaying characteristic morphology of the siRNA treatment. The first one being inefficient knock-down of the cells that do not display the expected phenotype. The second and more interesting one being the existence of a compensatory mechanism operating in the subset of cells that retained their morphology despite knockdown. If this were indeed true, looking at the genes expressed between the two populations under the same siRNA treatment would identify the genes involved in such a compensation mechanism. These genes were not only likely to be regulators of Golgi organization, but also be interacting with the siRNA targeted gene in order to maintain normal Golgi architecture.

3.1.2 Effect of siRNA knockdown efficiency on Golgi phenotypes

To test which two theories were true, we selected 20 Golgi-localized proteins for which siRNAs and antibodies were available in the lab. Each of these proteins were knocked down and stained for the knocked down protein. Out of 20 siRNA treatments, 6 treatments reliably showed a significant effect on Golgi morphology. Golgi localized proteins were chosen to be sure that they had a major role to play in Golgi function and therefore their effect on Golgi morphology was less likely to be an indirect effect of a non-Golgi related pathway. It was not surprising that only 30% of the treatments had a drastic effect on Golgi morphology, as many Golgi localized proteins may not play a role in Golgi organization, or be compensated by other proteins in their absence.

For these 6 proteins, the levels of protein remaining after knockdown was assessed by antibody staining and comparison with normal protein levels in untreated cells, measured using a self-developed CellProfiler [195] pipeline. A threshold was set individually for each treatment as three standard-deviations lower than the respective untreated antibody levels. This way, the percentage of cells showing knockdown was determined and within this population, CellProfiler was again used to ascertain the number of cells with the knock-down phenotype/ normal phenotype. This importantly showed that cells showing similar or same protein levels after siRNA knockdown could display different Golgi phenotypes, one being the disrupted morphology characteristic of the siRNA treatment and the other being normal Golgi morphology. We were able to therefore conclude that siRNA transfection efficiency was not the sole cause of the population retaining intact Golgi morphology.

This strengthened the hypothesis that a compensation mechanism could be operating in these cells, allowing them to evade Golgi disruption.

The reasoning to uncover this compensation was that it would likely lead to pathways controlling Golgi organization. In this attempt, the next step was to develop a pipeline that allowed for the comparison of transcriptome profiles of the two populations. This required the selection of cells based on their Golgi phenotype and collecting them for RNA sequencing.

3.2 A method for single-phenotype transcriptome analysis

In order to set up such a pipeline, one of the 6 siRNAs having a strong effect on Golgi morphology – USO1, was chosen. There were a few reasons for this choice. To begin with, USO1 knockdown had a dramatic effect on Golgi morphology, showing strong Golgi fragmentation. This made the phenotype relatively easy to detect reliably. Moreover, the siRNA had a high transfection efficiency, which meant that we were less likely to get cells showing normal Golgi morphology due to inefficient knockdown. Lastly, USO1 is a Golgi localized, important trafficking factor which has been well-studied in its role in ER-Golgi traffic [113][114] [112]. Therefore, it would be easier to build interaction networks around this protein with the resulting transcriptome data.

3.2.1 Detection of Golgi phenotypes

The first step in developing the pipeline was to reliably identify Golgi phenotypes after USO1 knockdown. This was done by manual training of a classifier in CellCognition [192] along with Aliaksandr Halavaty and Volker Hilsenstein of the ALMF at EMBL Heidelberg. Two classifiers, one for the nucleus and Golgi channel each were set up, as it provided more flexibility in annotating cells, not only based on Golgi phenotype, but also by nuclear structure. This was imperative in the case of mitotic cells, which showed a fragmented Golgi phenotype, but ideally should not be recognized and the exclusion of mitotic nuclei could easily be made in the nuclear channel. Cells were annotated into each defined class for both channels and the classifier were iteratively tested. Unfortunately, even after iterative class definition, annotation and testing, a precision rate of only 85-90% was reached. This efficiency could be improved by using multiple image sets to train the classifier. Another way to improve recognition would be addition of a cell-surface marker to ascertain the cell boundary, making correlation of nuclei to their respective Golgi easier. For this study, we decided to go forward with this rate, as another parameter was used at the time of selection to further fine-tune selection of the right phenotype, which was probability of classification. For each identified object- nucleus or Golgi, the classifier assigned

a probability value of it belonging to a given class. By setting the threshold on this probability value very high, we were able to pick cells that the classifier had high confidence in belonging to a certain class, and was also the correct phenotype. This way, we could get a high overall precision rate of phenotype recognition. Although CellCognition [192] was used in this case, another image analysis platform, such as CellProfiler [195] could also be used for this step.

3.2.2 Selective marking of phenotypic cells

The next step was to selectively mark phenotypic cells upon siRNA knockdown. A photo-activatable plasmid was used for this purpose. This plasmid was a kind gift from Richard Wombacher at the University of Heidelberg and consisted of a photo-activatable version of the red fluorescent protein mCherry called PAmCherry. PAmCherry is an inactive form of mCherry, which can be converted to active mCherry upon UV exposure, owing to a conformational change in the protein structure. This was originally developed by the Lipincott-Scwartz group [196]. The given plasmid had PAmCherry was tagged to the histone protein H2B, which caused the protein to localize to nucleus. This was ideal because the activation location was the nucleus, which is easy to identify and did not interfere with Golgi recognition. A photo-convertible marker such as Dendra [197] was not used in our case because the Golgi marker GalNaC was stably expressed with a Green Fluorescent Protein (GFP) and therefore any marker that was green to red convertible would interfere with Golgi recognition in the GFP channel. An attempt was made to make a double stable cell line with HeLa GalNaC-GFP and H2B-PAmCherry, which was not successful, as the cells did not express the later marker with time, even with antibiotic selection. Next, the PAmCherry plasmid was introduced into cells using lipid transfection reagents such as lipofectamine, Fugene, etc. This method resulted in very poor transfection efficiency of the plasmid (15-20%), especially in combination with siRNA knockdown, which was done using the lipid reagent Oligofectamine. After many rounds of optimization, electroporation of the H2B-PAmCherry was most effective in combination lipid-based siRNA transfection, with about 95% efficiency.

Activation of cells was then optimized first on fixed cells followed by live cells. This included the wavelength of activation, intensity and time required to fully activate the nuclei. The intensity and time were then adapted for live cells to minimize UV damage. Activation of a particular phenotype warranted activation of single-cells, which was optimized next. In the end, a single nucleus was activated using a high software zoom, such that no neighboring cells were activated by stray UV light. Since this marker was only previously described for two-color photoactivated localization microscopy (PALM) [196], the parameters for widefield microscopy were set up without any previous knowledge from literature.

3.2.3 Automation of phenotype recognition and marking

With Golgi recognition as well as photo-activation parameters optimized, the two elements were connected to couple automated phenotype recognition direct photo-activation of the desired phenotype. This was done using a graphic user interface (GUI) developed by Volker Hilsenstein and Aliaksandr Halavatyi called CeCogLink. This GUI connected the imaging software on the Leica SP5 to the CeCogAnalyzer from CellCognition by sending each image to the analysis software and once phenotype were recognized by the software, each selected cell was individually photo-activated. The GUI allowed the user to define the phenotype desired to be activated as well as the probability with which cells should be classified in order to be activated.

With this setup, around 80-100 cells could be activated in an hour. The most time-consuming component was the actual activation step, which was performed at a low scan speed. The time could have been decreased increasing the UV laser power, but would have negative repercussions on cell health. The time taken also highly depended on the frequency of the phenotype in question, as well as the stringency of the probability threshold. These parameters could probably be further fine-tuned for faster activation. Between 400-500 cells were activated in a single experiment, which means 200-250 cells of each phenotype (in different wells). Microscopy time was restricted to 4-5 hours to avoid big changes in the transcriptome of cells activated in the beginning versus the end, as well as to keep cells as healthy as possible for further processing.

3.2.4 Collection of marked phenotypic cells

Following activation of cells, they were prepared for flow sorting as per standard protocols for RNA sequencing. Due to washing steps during sample preparation, as much as 30% of the activated cells were lost/ or not detected on the sorter. The samples were always supplemented with RNase inhibitor to prevent RNA damage, and all material used for preparation was kept RNase-free. The sorter tubing was usually cleaned thoroughly before sorting, and the chamber was kept at 4°C. Cells were sorted in either single-cell modality or in batches of 20 cells per well of a 96-well which contained lysis buffer.

Single-cell sorting was problematic at the RNA sequencing levels, because less than 50% of the collected cells usable amounts of cDNA after reverse transcription and amplification. This continued to be the case even after making sure that each droplet sorted contained exactly one cell, meaning that a cell was definitely sorted into each well. The reason for not obtaining cDNA in these samples could be because the cell was either sorted

outside the lysis buffer or splashed out of the buffer after being sorted. To overcome this, 20 cells were collected into each well instead and taken for differential phenotype analysis.

Taken together, a generic pipeline to perform single-phenotype transcriptome analysis was developed here, which, by simple tweaking of the image analysis platform could be applied to a wide range of biological questions. This is particularly relevant since there has been a paradigm shift in cell biology where exploring cell-to-cell variability is increasingly used to uncover new biological mechanisms [198] [199]. Such an approach is valuable as it does not necessarily require an external perturbation, as intrinsic variability in cellular morphology itself can be used to probe cellular pathways and interactions [200] [201].

3.3 Transcriptome Analysis

3.3.1 Global gene expression analysis

There have not been any studies so far investigating the effect of changes in Golgi morphology on the transcriptome. Therefore, before comparing two phenotypes within a treatment, it was necessary to define the general global response of cells to siRNA-mediated knockdown of Golgi proteins and the subsequent change in Golgi structure. We found that the knockdown of both AKAP9 and USO1 proteins caused a drastic change in the transcriptome of cells as compared with negative control siRNA treatment. Moreover, it was interesting that the nature of the response was completely different in the case of siAKAP9 and siUSO1, despite the effect on Golgi morphology being the same. However, there might be differences in Golgi ultrastructure in the two treatments that cannot be seen using light microscopy, and electron microscopy would be required to understand the subtle differences in structure between the two treatments. Another explanation could be the activation of different pathways in the two knockdowns, depending on the process causing Golgi phenotype.

Even more surprising was the similarity in transcriptome profiles between siUSO1 and siTRIP11, which both operate in ER to Golgi transport [202] [114] [203] [127], except that siTRIP11 did not cause Golgi fragmentation. Both treatments showed genes of ER-Golgi transport up-regulated. This can be interpreted as follows: cells sense a defect in ER to Golgi transport owing to the missing proteins, and up-regulate transport machinery to compensate for this defect. However, the extent of the upregulation was much higher in USO1, indicating that it had a stronger effect. It is possible that the effect of TRIP11 was not strong enough to elicit Golgi fragmentation, or another protein was able to compensate partially for its function. It is also possible that the Golgi is indeed disrupted at some level upon TRIP11 knockdown, but these changes cannot be observed by light microscopy. Electron microscopy studies have demonstrated that overexpression

of TRIP11 causes Golgi fragmentation, contrary to USO1 [127]. Yet another possibility for the differences between Golgi morphology upon knockdown of USO1 and TRIP11 is different kinetics of protein degradation, which could mean that after 72 hours of siRNA treatment, there still might be enough TRIP11 protein left in cells that can mediate at least some of the essential functions and therefore prevent fragmentation.

The global transcriptome contained plenty of exciting data which could be followed up in many different directions, and it would be potentially be of interest to look at the transcriptome changes in many such siRNA treatments targeting the Golgi to find a common signature for Golgi fragmentation, as well elucidate connections within the secretory pathway. Unfortunately, this data could not answer whether the resulting transcriptome was a cause or the result of Golgi fragmentation, since a variety of cellular perturbations can lead to Golgi fragmentation, and the resulting transcriptome could just be a consequence of that particular perturbation, as opposed phenotypically correlating response [204]. For this, we would have to look to a comparison of two phenotypes within a singular treatment, and the established pipeline was used for this purpose for one siRNA treatment, siUSO1.

3.3.2 Single-phenotype sequencing

The global transcriptome analysis showed that siUSO1 had a strong effect on the transcriptome, particularly on secretory transport, cytoskeleton and Golgi proteins, all of which are likely to contain key regulators of Golgi structure. Hence, it was taken for differential expression analysis of Golgi phenotypes.

Although the ideal way to sequence the two populations was to collect them in a single-cell modality, to provide a higher resolution and prevent averaging of phenotypes occurring due to inefficient knockdown. This was especially important since the knockdown efficiency could not be measured at any stage during the pipeline except in the transcriptome data. Unfortunately, collection of single-cells proved to be problematic at the cDNA preparation stage after sorting, as discussed before, and 20 cells were of a single phenotype were pooled instead.

3.3.3 Differential expression analysis of Golgi phenotypes

Differential expression analysis of the two Golgi phenotypes revealed about 700 genes as significantly differentially expressed. The fact that comparison of only 100 cells of each phenotype showed such large differences between the two phenotypes indicates that there was in fact a considerable change in gene expression between the two populations. This was strengthened by the high degree of transcriptome similarity within the same phenotype, especially since cell-to-cell variability is usually a problem in low-input transcriptome

analysis, often making conclusions from the data difficult [205] [206]. Also, the changes detected in the phenotype comparison were many magnitudes higher than the changes observed in the global transcriptome analysis of USO1 knockdown. Thus validating the claim that important information might be lost in the averaging out of cells that respond differently and giving impetus to this method of comparing expression profiles on the basis of cellular phenotype.

On analysis of the genes differentially expressed between non-fragmented and fragmented cells, we observed that there was no significant difference in any of the trafficking components, especially those operating at the ER to Golgi stage. This gives the impression that no other Golgins were up-regulated in order to compensate for the lack of USO1. Such an observation indicates that the lack of Golgi fragmentation is unlikely to be a direct effect of a simple compensation by another protein. This is surprising at a first look, since Golgins are known to operate in a redundant manner where different Golgins can tether the same cargo, and little effect of their individual depletion is seen especially on ER-Golgi trafficking [110] [207] [208]. However, our observation with the other literature on USO1, where studies have shown that USO1 is vital for cellular traffic and USO1 deficiency is lethal during mouse development, naming USO1 an indispensable trafficking factor [118].

It is likely that a larger network is involved in maintaining Golgi integrity upon USO1 knockdown, and this hypothesis is supported by the large number of signaling proteins that are up-regulated in these cells. The dataset is particularly enriched in chemokine signaling proteins, MAP Kinase pathway components and calcium mediated signaling kinases. The kinases upregulated do not point towards a singular pathway or function, further indicating that more than one cellular pathway is involved in this network. Further, our findings are in agreement previous screens revealing a large signaling network regulating Golgi structure. [184].

A surprising observation in the differential analysis was the upregulation of clathrin components in non-fragmented cells. Within our gene list are clathrin components that seem to act the TGN-endosome stage as well as the plasma membrane stage [209], [210]. This suggests that endocytosis or endosomal trafficking steps are involved in the compensatory mechanism of non-fragmented cells. Supporting this is the up-regulation of syntaxin 3 and syntaxin 7, both of which are SNARE proteins that promote vesicle fusion [211]. Syntaxin 7 is said to mediate traffic from early to late endosomes/lysosomes [212], and Syntaxin 3 operates at the plasma membrane and is involved in exocytosis as well as establishment of cell polarity [213]. It is curious that disturbance of ER-Golgi traffic resulted in an endosomal/plasma membrane trafficking response in cells with normal Golgi morphology, and it could be possible that two-way flux to the Golgi is being carefully regulated in these cells to maintain Golgi structure.

In summary, we observe a significant difference between the transcriptome profiles of the two Golgi phenotypes upon USO1 knockdown. However, most components of the usual trafficking machinery are not expressed differently. On the other hand, a large number of signaling proteins are up-regulated in non-fragmented cells, indicating that a signaling network is indeed in place to prevent fragmentation. In addition, two direct interactors of USO1 – SEMA4F [214] and PRKACA [215] are significantly up-regulated in this phenotype, which make them extremely interesting candidates to follow up. SEMA4F belongs to a category of semaphorin proteins containing a transmembrane domain. Most semaphorins are involved in neuronal connectivity, cell migration and immune modulation [216] [217]. Preliminary data from our lab describes a possible role for SEMA4F in cholesterol regulation, given that it changes localization from the ER to the plasma membrane upon sterol depletion. PRKACA is the catalytic subunit of Protein Kinase A, which has a wide range of effectors mediated by the second messenger cAMP [218]. Both these proteins would be interesting to follow up in the context of their roles in Golgi organization. This data provides us with a strong base to further explore the interactions and networks that could be significant for Golgi regulation.

There are a few key questions that need to be answered to provide strength to our data set for a firm conclusion. One such question is whether trafficking is impaired in cells showing non-fragmented Golgi to a similar extent as to the fragmented cells. This would tell us whether the Golgi phenotype is linked to the trafficking ability of the cell. In other words, if USO1 is indeed being compensated by another protein/group of proteins, or if the lack of fragmentation is isolated from the effect of USO1 down-regulation on secretory trafficking.

A second important question is to check how the differentially expressed genes between the two phenotypes compare with the levels expressed in untreated cells. This would be key information to see how significant the differences we observe between the two phenotypes are, and further narrow down the list to genes that deviate most from untreated cells.

The future focus of this project will be to answer these key questions, in addition to providing a larger data set to confirm the present findings. The key candidates and pathways will be investigated in a combined approach of literature mining and co-knockdown experiments along with USO1. Altogether, this body of work provides a tool to perform single-phenotype transcriptome analysis of the Golgi complex, and can be applied not only to phenotypes upon siRNA treatment, but also to drug treatments, or simply morphological differences seen in different conditions. Moreover, in principle this method of image-based phenotype/morphology identification and subsequent gene expression analysis can be applied to different organelles, cell types and even organisms, such as bacteria

etc. However, our focus would stay on learning more about Golgi structure, its regulation and the connections to Golgi function in the secretory pathway in the future with additional experimentation using this method.

CHAPTER 4

CONCLUDING REMARKS

In this study, a method was developed to correlate cellular morphology visualized by microscopy with gene expression analysis. This method was then used in the specific biological context of comparing gene expression profiles of cells showing different Golgi morphology upon siRNA knockdown.

To achieve this, first, an advanced microscopy platform was developed that coupled live-cell imaging with online image analysis to identify cellular phenotypes, additionally allowing marking of individual cells using a photo-activatable marker previously introduced into these cells. In this way, morphologically different cells could be selectively photo-activated based on a robust recognition system. Moreover, the entire process, including photo-activation was automated, which removed user bias and was more time efficient. More importantly, automation offers the prospect of future upscaling up of the method.

To analyze the gene expression of a cellular phenotype, the marked cells were collected by flow cytometry. Although a single-cell modality is not yet usable in a robust manner for sequencing, future effort will be aimed at achieving single-cell resolution for gene expression profiling, where the response of each cell can be evaluated individually and combined with cell cycle and knockdown level information for a more comprehensive picture.

This pipeline was used to compare two Golgi phenotypes: fragmented and normal (non-fragmented) upon knockdown of one candidate protein -USO1. The differential expression analysis between the two phenotypes revealed about 700 genes significantly differently expressed between them, indicating that Golgi phenotype was indeed accompanied by large transcriptomic changes. Moreover, USO1 was knocked-down to a similar extent in both populations, confirming our hypothesis that the phenotypic variability is not an effect of transfection efficiency. Further strength was given to the dataset by the fact that cells within the same phenotype showed extremely similar gene expression profiles, meaning that the genes expressed between phenotypes were not simply a result of cell to cell variability.

On further examination, a number of signaling proteins were observed to be up-regulated in cells which displayed intact / non-fragmented Golgi morphology. These included proteins involved in chemokine mediated signaling, clathrin-mediated endocytosis in addition to many kinases and phosphatases responsible for regulation of a plethora of vital processes. It is likely that among these proteins there lie a few key regulators of Golgi morphology, whereas most other proteins are indirect effectors or are seen as a consequence of the phenotype.

Of particular interest in the context of this study was the upregulation of two direct interactors of USO1, namely SEMA4F and PRKACA, in non-fragmented cells, which makes

them very likely candidates as key proteins for regulation of Golgi morphology. Following up these two proteins is therefore a compelling starting point to explore the dataset. The combined siRNA mediated knockdown of USO1 and SEMA4F or PRKACA and resulting change in phenotypic populations will be crucial indicators of the nature and potency of these interactions.

Although this pipeline was developed with the purpose of identifying Golgi phenotypes upon siRNA treatment, one of the major advantages of such a platform is its broad applicability. This method can be applied to any biological question where phenotypic variability is observed either in response to a particular stimulus, even intrinsic variability. This would only require a change in the image analysis pipeline in order to recognize the phenotype of choice. Furthermore, the availability of a range of photo-convertible plasmids and dyes provides many choices for selective marking of organelles as well as cells in tissues. Therefore, with simple changes, a wide range of processes could be probed by correlating visual phenotype with gene expression.

In conclusion, a general pipeline for single-phenotype transcriptome analysis is described here, which was specifically applied to study the differences between Golgi phenotypes upon siRNA knockdown. This pipeline was successfully tested on one protein critical for Golgi morphology- USO1, which provided an intriguing dataset with promising candidates for key proteins involved in regulation of Golgi architecture.

CHAPTER 5

MATERIALS AND METHODS

5.1 Materials

5.1.1 Cell Culture

Bacterial Cell Culture

Bacterial cell line: XL1-Blue E. Coli.

Reagent	Cat. No.	Source
L-Agar plates with Ampicillin	-	Media kitchen, EMBL
LB (Luria Bertani) Media	-	Media kitchen, EMBL
Ampicillin	A0166-54	Sigma

Table 5.1: List of reagents used for bacterial cell culture

Mammalian Cell Culture

Mammalian cell line: HeLa-GalNaC-GFP

Reagent	Cat. No.	Source
DMEM	31885-023	Gibco
OptiMEM	51958	Gibco
FCS	10270	Gibco
0.05% Trypsin-EDTA	25300-054	Gibco
Geneticin	10131	Gibco
CO2 Independent medium	ME080051L1	Gibco
L-Glutamine	G7513	Sigma
TryPLE Express	12604013	Gibco

Table 5.2: List of reagents used for mammalian cell culture

Media	Composition
Normal Culture Media	DMEM + 10% (v/v) FCS + 1% (v/v) L-Glutamine
Serum Free Media (SFM)	DMEM + 1% (v/v) L-Glutamine
Imaging Media	CO2 Independent Media + 10% (v/v) FCS + 1% (v/v) L-Glutamine
Freezing Media	DMEM + 20% (v/v) FCS + 10% (v/v) DMSO

Table 5.3: Composition of media used for mammalian cell culture

5.1.2 Lab Reagents and Equipment

Equipment	Source
Centrifuge 5804R	Eppendorf
10cm cell culture dishes	Nunc
0.5 ml, 1.5 ml, 2 ml tubes	Eppendorf
15 ml and 50 ml Falcon tubes	BD Biosciences
Glass bottom dishes	MatTek
Cryotubes 1.5 ml	Nunc
24 well Glass-Bottom Plates	CellVis
Incubator	Binder
Water bath	GFLR
Table centrifuge	Sarstedt
Cell counting chamber	Marienfeld
Hard Shell 96-well PCR plates	Bio-Rad

Table 5.4: List of lab equipment used

Reagents	Cat. No.	Source
DMSO	102952	Merck
Hoechst	33258	Sigma
Mowiol	475904	Calbiochem
4% Paraformaldehyde	15710	Electron Microscopy Sciences
Oligofectamine	12252-011	Invitrogen
Saponin	47036	Gibco
BSA	A9576	Sigma
RNasin Plus RNase Inhibitor	N261B	Promega
Triton X-100	T9284	Sigma
dNTPs (10mM)	R1092	ThermoScientific
oligodT (5 μ M)	Custom sequence	Sigma
Trizol	15596-026	Invitrogen
GlycoBlue Co-Precipitant	AM9515	Invitrogen
Chloroform	600-006-00-4	EMSURE
Ethanol (absolute)	1.00983.2500	EMSURE
Isopropanol	1.09634.1000	EMSURE

Table 5.5: List of reagents used

5.1.3 Antibodies

Protein	Antibody ID	Host	Dilution
ACBD3	HPA015594	rabbit	1:54
CCDC146	HPA020082	rabbit	1:200
GCC1	HPA021323	rabbit	1:100
BICD2	HPA024452	rabbit	1:10
GAK	HPA027463	rabbit	1:50
GORASP2 (GRASP55)	HPA035275	rabbit	1:43
GOLGA5 (Golgin 84)	HPA000992	rabbit	1:69
AKAP9	HPA008548	rabbit	1:222
TMF1	HPA008729	rabbit	1:72
GOLM1	HPA010638	rabbit	1:32
GOLGB1 (Giantin)	HPA011008	rabbit	1:600
SYNGR2	HPA014742	rabbit	1:87
RASGEF1A	HPA035593	rabbit	1:159
TMEM165	HPA038299	rabbit	1:88
USO1 (P115)	HPA038282	rabbit	1:31
COPG1	HPA037866	rabbit	1:50
TMCO3	HPA039561	rabbit	1:98
COG8	HPA049429	rabbit	1:55
GORASP1 (GRASP65)	Martin Lowe	Sheep	1:3000
COPB2	HPA058180	rabbit	1:40
TRIP11 (GMAP210)	Martin Lowe	sheep	1:500
GOLGA1 (Golgin 97)	molecular probes #A21270	mouse	1:800
GM130	BD #610822	mouse	1:400

Table 5.6: List of primary antibodies for immunofluorescence

All secondary antibodies used were conjugated with AlexaFluor and obtained from Molecular Probes

Antibody	Host	Dilution
AlexaFluor 568-mouse	donkey	1:200
AlexaFluor 647-mouse	donkey	1:200
AlexaFluor 647-sheep	donkey	1:200
AlexaFluor 568-rabbit	donkey	1:200
AlexaFluor 647-rabbit	donkey	1:200
AlexaFluor 568-sheep	donkey	1:50

Table 5.7: List of secondary antibodies for immunofluorescence.

5.1.4 Oligonucleotides and Plasmids

Gene	siRNA ID
ACBD3	s34848
CCDC146	s33493
GCC1	s35832
BICD2	s23497
GAK	s5529
GORASP2 (GRASP55)	s24914
GOLGA5 (Golgin 84)	s19321
AKAP9	S10746
TMF1	s444246
GOLM1	s27833
GOLGB1 (Giantin)	s5951
SYNGR2	s17477
RASGEF1A	s47933
TMEM165	s31678
USO1 (P115)	s16390, s16391
COPG1	s22430
TMCO3	s29958
COG8	s38958
GORASP1 (GRASP65)	s34818
COPB2	s17737
TRIP11 (GMAP210)	s17813
CLASP2	s23082
GOLGA1 (Golgin 97)	s5941
GM130	s5942
Neg9	s444246

Table 5.8: List of siRNAs used

Plasmid	Source	Selection
pcDNA4-TO-Puromycin-mVenus-MAP	Addgene #44118	Puromycin
H2B-mPACCherry	Richard Wombacher	Geneticin

Table 5.9: List of plasmids used

5.1.5 Reagents for Flow Cytometry

Buffer compositions for fixed cells

Fixation/Permeabilization Buffer: 4% PFA + 0.1% Saponin in PBS + 1:100 (40U/ μ l) RNasin Plus

Wash Buffer: PBS + 0.2% BSA + 0.1% saponin + 1:100 (40U/ μ l) RNasin Plus

Staining Buffer: PBS + 1% BSA + 0.1% saponin + 1:25 (40U/ μ l) RNasin Plus

Sort Buffer: PBS + 0.5% BSA + (40U/ μ l)1:25 RNasin Plus

Buffer compositions for live cells

Wash Buffer: PBS + 1:100 (40U/ μ l) RNasin Plus

Sort Buffer / Cell Lysis Buffer: 0.4% Triton X-100 in PBS + 1:20 (40U/ μ l) RNasin Plus + 10mM dNTP mix + 5 μ M Oligo dT

5.1.6 Reagents for RNA sequencing

Buffer and Master Mixes

SmartSeq2 Reverse Transcription Master Mix

- 2.0 μ l of SSRT II Buffer
- 0.5 μ l of 100mM DDT
- 2.0 μ l of 5M Betaine
- 0.1 μ l of 1M MgCl₂
- 0.25 μ l RNase Inhibitor
- 0.5 μ l SSRII enzyme
- 1.0 μ l Template Switching Oligo (10 μ M)

Pre-Amplification Master Mix

- 10 μ l cDNA
- 12.5 μ l of 2X KAPA HiFi HotStart Ready Mix
- 0.20 μ l of 5 μ M ISPCR Primers (optional)
- 2.30 μ l Nuclease Free Water

Annealing Buffer

- 50 mM NaCl
- 40 mM Tris-HCl pH 8.0

Tagmentation Buffer

- 40 mM Tris-HCl pH 7.5
- 40 mM MgCl₂

Reagent	Source	Cat. No.
dNTPs	Kappa Biosciences	KK1017
Kappa HiFi Hot start ReadyMix	Kappa Biosciences	KK2601
100% DMF	Sigma	68-12-2
0.2 % SDS	Sigma	151-21-3
100 % DMSO	Sigma	67-68-5
SPRI beads	Beckman Coulter	B23319
Betaine	Sigma	B0300-1VL
MgCl ₂	Ambion	AM9530G
Illumina i5 and i7 adapter index primers	Illumina	
RNAse inhibitor 40U/ μ l	Clontech Takara	2313A

Table 5.10: List of reagents for cDNA library preparation.

Reagent	Sequence
TSO/LNA	5'-AAGCAGTGGTATCAACGCAGAGTACATrGrG+G-3'
Oligo-dT30VN	5'-AAGCAGTGGTATCAACGCAGAGTACT30VN-3'
ISPCR oligo	5'-AAGCAGTGGTATCAACGCAGAGT-3'
Tn5-fw (BamHI)	5'-GATCGGATCCATGATTACCAGTGCACCTGCATCG-3'
Tn5-rev (HindIII)	5'-GATCAAGCTTTTAGATTTTAATGCCCTGCGCC-3'
Tn5ME-A	5'-TCGTCCGCAGCGTCAGATGTGTATAAGAGACAG-3'
Tn5ME-B	5'-GTCTCGTGGGCTCGGAGATGTGTATAAGAGACAG-3'
Tn5MErev	5'-[phos]CTGTCTCTTATACACATCT-3'
PE1.Smart-seq2	5'-AATGATACGGCGACCACCGAGATCTACACAAGCAGTG GTATCAACGCAGAGTACCCAA-3'
polyA-seq	5'-AAGCAGTGGTATCAACGCAGAGTACCCAA-3'

Table 5.11: List of Oligonucleotides for cDNA library preparation. All sequences were ordered from Sigma, except for TSO/LNA, which was ordered from Exicon.

5.1.7 Kits, Analyzers and Softwares

Kit	Source	Use	Cat. No
Amaza SE Cell Line 4-D Nulceofection Kit	Lonza	Electroporation	V4 XC-1024
RecoverAll Total Nucleic Acid Isolation	Invitrogen	RNA isolation	0052541
Velocity DNA polymerase	Bioline	PCR amplification	PL371-13027910
Kappa HiFi Hot start ReadyMix Kit	Kappa	cDNA preamplification	KK2601
Qubit HS dsDNA kit	Thermo Fisher	DNA detection	Q32854
High Sensitivity DNA kit	Agilent	DNA electrophoresis	5067-4626

Table 5.12: List of analyzers used

Analyzer	Developer
Zeiss CellObserver HS widefield Laser scanning microscope SP5 MSA	Zeiss Leica
ScanR microscope (Automated screening)	Olympus
BD FACSMelody Cell Sorter	BD Biosciences
BD FACSAria Fusion Sorter	BD Biosciences
Aligent 2100 Bioanalyzer	Aligent
Illumina Sequencer	Illumina

Table 5.13: List of kits used

Software	Developer
Image J	Wayne Rasband, National Institutes of Health (NIH)
CellProfiler 3.0	Broad Institute, Cambridge
CellCognition	ETH Zurich, EMBL Heidelberg
Rstudio	Free software foundation Inc., Boston
Cytoscape 3.6.1	Institute for Systems Biology (Open)
FlowJo 10	Becton, Dickinson and Company (BD)
ApE 2.0.53c	Wayne Davis, University of Utah
Leica LAS AF	Leica Camera AG

Table 5.14: List of software used

5.2 Methods

5.2.1 Cell Biology

Cell Culture

All eukaryotic cell culture was done under a laminar flow hood sterilized prior to use. HeLa GalNac-T2 cells were cultured in low glucose (1g/l) DMEM supplemented with 10% FCS and 1% L-Glutamine. 400 μ g/ml Geneticin was added to the cells to maintain selection pressure of the GFP tagged enzyme and cells were kept at 37°C and 5% CO₂. Cells were passaged upon reaching 80% confluence by removing medium from the culture dish, washing the cells with Trypsin-EDTA and adding 2ml of Trypsin-EDTA solution to a 10cm dish. Cells were incubated with Trypsin for 5 minutes at 37°C till they detached from the dish. To stop trypsin activity, 8 ml media was added and the cell suspension was dispensed into new dishes at appropriate dilutions for use. Cells were passaged this way for a maximum of 15 cycles before being discarded.

Plating Cells

Cells in suspension after trypsinization (described above) were counted using a hemocytometer and plated onto 24-well glass bottom dishes at 16,000 cells per well to achieve appropriate cell numbers for experimentation after approximately 84 hours (72-hour siRNA transfection).

Freezing and Thawing Cells

Cells were frozen in liquid nitrogen for long term storage. In order to freeze cells, a confluent 10cm dish was treated with Trypsin-EDTA and cells were resuspended in DMEM up to 10ml. The cell suspension was centrifuged (5804R) at 1000rpm for 5 minutes to obtain a cell pellet. The supernatant was carefully discarded and the pellet was resuspended in 0.5ml cold FCS and 0.5ml cold freezing media. This suspension was transferred to pre-chilled cryotubes and the tubes were placed in a cell-freezing container at -80°C for a few days before transfer to a liquid nitrogen tank (-160°C).

Electroporation of Cells

In order to introduce plasmids into cell at a high efficiency, the plasmid was added to a cell suspension and subject to an electric field to puncture temporary holes in the cell membrane using the 4D-Nucleofector™ X Unit (Lonza). The cells were prepared using the Lonza Amaxa SE Nucleofection 4D kit in the 100 μ l format. For this, cells were detached into a suspension and pelleted. A nucleofection solution was made by mixing 82 μ l of the provided nucleofection solution and 18 μ l of supplement (total 100 μ l solution). The cell pellet was resuspended into this nucleofection solution and 2 μ g of the desired

plasmid was added. The suspension was transferred to a cuvette (closed lid) and the C114 program was run on the nucleofector. The cells were then removed from the cuvette and transferred to a tube containing 400 μ l serum free medium for 10 minutes before being plated in the appropriate plates using complete DMEM.

siRNA Transfection of Cells

Small interfering RNAs (siRNAs) were used to selectively inhibit the re-synthesis of desired proteins in order to assay the effect of their depletion. This one using lipid-based delivery agents. Two solutions were prepared as shown below (for 1 well of a 24 well plate). One contained the diluted delivery reagent and the other a diluted siRNA of interest. The two solutions were incubated separately for 5 minutes and then combined. The resulting mix was incubated for 20 minutes at room temperature. Prior to addition to cells, the media was replaced with 200 μ l serum free media. The reagent-siRNA mix was then added dropwise to the cells and incubated for 4 hours at 37°C and 5% CO₂. After 4 hours, 250 μ l DMEM containing 20% FCS and 1% L-Glutamine was added to make up the final volume in the well.

Transfection Volumes: Solution 1: 0.25 μ l of a 30 μ M stock siRNA + 45 μ l OptiMEM
Solution 2: 0.5 μ l Oligofectamine + 4.5 μ l OptiMEM

Immunostaining

In order to visualize proteins of interest, cells were incubated with protein specific antibodies linked to fluorescent reporters. To achieve this, cells were first fixed using 4% Paraformaldehyde for 20 minutes at room temperature. The fixative was washed off with PBS, followed by cell permeabilization in a solution of the detergent saponin (0.1% Saponin and 10% BSA in PBS). The primary antibody was diluted in the saponin solution and incubated for 1hr on the bench. After this, the primary antibody was washed away using PBS and the similarly diluted secondary antibody (containing the fluorophore) was added to the cells. Cells were incubated for 1 hour (in the dark) and the antibody was washed away with PBS. Cells were then incubated with the nuclear stain Hoechst at a 1:2000 dilution in PBS for 10 minutes. After this, cells were washed with PBS. If cells were in a multi-well plate, they were left in PBS until imaging. Cells grown on glass coverslips were mounted on glass slides using Mowiol and left to dry overnight at room temperature before proceeding with microscopy.

5.2.2 Microscopy

Live-Cell Imaging

Live cell imaging was performed at the Leica SP5 MSA confocal microscope with an open pinhole (600 μ). The environment chamber was heated to 37°C prior to use. HeLa-GalNac-GFP cells were cultured in a 24-well glass bottom plate and the media was replaced to

phenol-red free, CO₂ independent media 30 minutes before imaging. Hoechst was added to the wells at a dilution of 1:2000 to stain live nuclei. A 40X objective was used for imaging, and the lasers used are provided in the table below. Automated live imaging was performed on the Matrix Screener module of the Leica SP5 software. The initial X and Y co-ordinates of the well were saved, and a (—) distance was set between imaging fields. To perform automated feedback microscopy, two ‘patterns’ were set up: namely- search and photoactivate. The search pattern consisted of:

1. An autofocus scan used in a 64 X 64 format in order to focus on nuclei in the 405nm channel.
2. A sequential scan was set up in two channels – Hoechst and GFP in a 2048 X 2048 format at a scan speed of 600Hz. Additionally, frame averaging of 2 frames was set up for the GFP channel.

Photo-activation

Cells were transfected with the photo-activatable marker H2B-PAmCherry using either lipid transfection reagents or electroporation (detailed in the previous section). The cells were transfected at least 12 hours prior to further treatment / fixation. Fixed cells were photo-activated mainly to observe and optimize the transfection efficiency of the photo-activatable marker as well as the optical parameters for photo-activation such as light intensity, activation time, etc. Transfected cells were fixed with 4% Paraformaldehyde for 20 minutes at room temperature. After this, the paraformaldehyde was washed away and the cells were washed twice with PBS, and then left in PBS at 4°C until imaging. Once fixed, cells were activated at the Zeiss CellObserver microscope using the fluorescence lamp under a 20X objective. The fluorescent lamp was used along with a UV filter of 405nm. Photo-activation of live cells was done usually at the Leica SP5A microscope, in a single-cell modality. For this, cells transfected with H2B-PAmCherry were placed in live-cell imaging media with Hoechst under a 40X air objective. A single-cell was photo-activated by first moving the nucleus of the desired cell in the center of the field of view. Next, the nucleus was zoomed into by a factor of 40 (software zoom) and illuminated with 5% of the 405 nm laser at a scan speed of 10Hz in a 64 X 64 format, with each line scanned 3 times and averaged.

Automated classification of Golgi phenotypes

Classification of Golgi morphology into phenotypes was done using CellCognition. This comprises a classifier that can be manually trained with a set of images. Therefore, first a training set of images were acquired in the same way as the ‘search’ pattern described in section (). These images were re-named using the renaming tool developed by Volker Hilsenstein (ref) and then input into CellCognition. CellCognition performed cell segmentation by identification of the Nucleus and then dilating the Nucleus to define a cell

boundary. The Golgi channel was then overlaid on this to obtain a segmented cell containing a Nucleus as well as a Golgi. Once cells were segmented, cells were manually annotated into user defined classes. Two separate classifiers were trained, one for the Nucleus – called the ‘primary classifier’ and another for the Golgi – called the ‘secondary classifier’. In the primary classifier, two classes were defined: Normal and Discard. Nuclei that appeared normal in shape were annotated under the Normal class whereas nuclei appearing mitotic, irregular and multi-nucleated cells were annotated as Discard. In the secondary classifier, three classes were defined: Normal, Fragmented and Discard. Cells having an intact Golgi localized close to nucleus were annotated as Normal. Cells showing a fragmented Golgi phenotype – that is 5 or more fragments displayed around the nucleus, were annotated under the Fragmented class. Cells appearing to have a dispersed Golgi or not showing a prominent phenotype were annotated under Discard. Once these classes were defined and annotations manually made, the classifier was trained by allowing feature extraction. All features except intensity were allowed to be taken for classifier training, as intensity could be slightly variable in each experiment. Once the classifier was trained, it showed the precision rate of classification with the classification and the error rate. Both the primary and secondary classifiers were iteratively trained until a low error rate and high precision rate was achieved (above 85%). The classifier was first tested on the training set to validate it, followed by a new set of images.

5.2.3 Flow Cytometry

Sample Preparation

Cells were detached from the glass bottom well using 200 μ l TryPLE Express and resuspended in 800 μ l complemented DMEM to make up the volume of the suspension to 1ml in an Eppendorf tube. The cell suspension was centrifuged (5417R) at 1000 rpm at 4°C for 5 minutes to obtain a cell pellet. The cell pellet was washed with cold FACS wash buffer and centrifuged as before. The supernatant was discarded and the pellet was resuspended in 250 μ l cold FACS staining buffer. Samples were kept on ice to prevent cell lysis. The sort buffer/cell lysis buffer was prepared meanwhile and 4 μ l of the buffer was dispensed into each of 48 wells in a 96-well plate (Bio-Rad). A box of dry ice was also required to freeze cells immediately after sorting.

Single-cell Sorting

Single-cell sorting was performed on the BD FACS Melody at the FACS core facility at EMBL, Heidelberg. Samples prepared as described above were transferred to flow cytometry tubes (Falcon). The FACS machine was prepped beforehand as per the manual. The software was set to the single-cell sort mode. A negative control sample (mCherry negative) was used to determine the population of viable cells, after which doublets were excluded from the sort analysis. After this, the population of GFP cells were gated. The

positive control (mCherry positive) was used to set up a gate to determine where the activated cells would be found. The sample was then loaded and Cells positive for both GFP and mCherry (double-positive) were selected for sorting based on previously set gates. The flow rate was set to 10 because of low sample volume and the sample was vortexed while being sorted (Agitation mode). These cells were sorted into the pre-prepared 96-well plate containing lysis buffer. As soon as the sort was complete, the plate was immediately placed in dry ice, then sealed and placed at -80°C until RNA isolation.

5.2.4 RNA isolation

RNA was performed as follows from both PFA fixed as well as live, single cells:

Manual Trizol extraction from fixed cells

SORTING

- Sort cells (10,50,100 and 250 cells) into 5-10 μl of PKD+1/16 Proteinase K
- Spin down
- Freeze samples at -80°C (or proceed directly to rev.crosslink)

activate proteinaseK solution incubating 10 min @ 37°C , then keep on ice.

EXTRACTION (All steps were performed on ice, unless indicated otherwise)

- Thaw samples for 5 minutes at room temperature
- Incubate samples for 1hour at 56°C on thermomix for reverse crosslinking to remove PFA induced protein crosslinks
- Add 100 μl of cold TRIreagent to each sample
- Incubate 2-3min at room temperature then transfer to alu-racks on ice
- Add 20 μl chloroform and shake vigorously
- Incubate 3min at room temperature
- Centrifuge at 12000rpm for 5min at room temperature and immediately transfer back to alu-racks on ice
- Transfer aqueous phase into new 1.5ml Eppendorf tube
- Add 0.5 μl glycobblue reagent in 75 μl isopropanol (1:150), shake vigorously
- Precipitate overnight at 80°C
- Centrifuge @13000rpm 1 hour at 4°C
- Remove the supernatant (keep on cooled metallic holder)
- Add 100 μl of 70% ethanol (freshly made)
- Centrifuge at 13000rpm for 15 minutes at 4°C
- Remove most of the ethanol. Give the tubes a quick spin and remove the remaining ethanol with a P20 pipette.
- Air-dry for 1-2 minutes
- Resuspend the pellet in 5 μl of Smart-Seq2-buffer and proceed with Smart-Seq2 protocol.

cDNA preparation from live single-cells

SORTING

- Sort cells (1, 20) into 4 μ l of lysis buffer
- Spin down
- Snap freeze at -20°C and then transfer to -80°C overnight

REVERSE TRANSCRIPTION AND AMPLIFICATION

- incubate plate at 72°C (on a heating block) for 3 minutes
- Add 6.75 μ l of the Reverse Transcription Master Mix to each sample
- start the Reverse Transcription PCR reaction:

90min at 42°C

10 cycles of (2 min at 50°C, 2 min at 42°C)

15 min at 70°C

- Add 15 μ l of Amplification mix to each sample
- Run the Amplification PCR as follows:

3 min at 98°C

18 cycles of (20 sec at 98°C, 15 sec at 67°C, 6 min at 72°C)

5 min at 72°C

BEAD PURIFICATION

- Make up the volume of each sample to 50 μ l using distilled water
- Add 30 μ l SPRI beads to each sample and pipette to mix evenly
- Let the mix stand at room temperature for 10 minutes
- Place the samples on a magnetic stand for 5 minutes for the beads to adhere to the wall
- Remove the supernatant and add immediately add 13 μ l water to each sample, directly on top of the spot of magnetic beads.
- Remove the samples from the magnetic stand and resuspend the beads thoroughly in the water
- Let the mix stand for 5 minutes at room temperature for elution
- Place the samples back on the magnetic stand and wait 5 minutes for the beads to re-adhere to the walls
- Elute 10 μ l of the water once the magnetic beads are completely separated and transfer to new tubes/a new plate
- Measure cDNA concentration and quality using a High Sensitivity DNA chip on the Aligent Bioanalyzer

Tagmentation-based NGS library preparation

This protocol describes the workflow of the Tn5 loading and tagmentation-based library preparation for dual indexing i5/i7 NGS

1. Annealing of the linker oligonucleotides Tn5ME-A/Tn5MErev and Tn5ME-B/Tn5MErev

A. Resuspend lyophilized oligonucleotides in annealing buffer to a stock concentration of 100 μM and mix one volume of Tn5ME-A or Tn5ME-B with one volume of Tn5MErev (working stock, 50 μM). Distribute the mix in 10-20 μl aliquots for storage at -20°C .

B. Run the following PCR program in a thermocycler for the annealing of the oligonucleotides:

95 $^{\circ}\text{C}$ 5 min

slowly cool down to 65 $^{\circ}\text{C}$ (0.1 $^{\circ}\text{C}/\text{sec}$)

65 $^{\circ}\text{C}$ 5 min

slowly cool down to 4 $^{\circ}\text{C}$ (0.1 $^{\circ}\text{C}/\text{sec}$)

C. Store the annealed linker oligonucleotides at -20°C .

2. Loading of the Tn5(R27S),E54K,L372P with Tn5ME-A/Tn5MErev and Tn5ME-B/Tn5MErev

A. Thaw the annealed linkers on ice. Add 0.5 μl of each annealed linker at a concentration of 35 μM to 10 μl of the Tn5 stock (0.2 mg/ml - 0.4 mg/ml). Mix well.

B. Incubate linker-Tn5 mix at 23 $^{\circ}\text{C}$ under constant shaking at 350 rpm in a thermomixer for 30-60 min.

**Make sure to keep the temperature constant at 23 $^{\circ}\text{C}$*

Do not exceed 60 minutes of loading as the Tn5 enzyme will gradually lose activity

Proceed immediately with the tagmentation reaction or supplement the loaded Tn5 with glycerol to a final concentration of 50% glycerol and store at -20°C for several days.

C. Tn5 dilutions can be prepared with nuclease-free water. A final concentration in the range of 20-40 ng/ μl is suitable for the tagmentation of cDNA.

3. Tagmentation-based library preparation

A. Dilute the cDNA in nuclease-free water to a concentration of 100 pg/ μl – 200 pg/ μl

B. Mix one volume of the 4x tagmentation buffer with one volume of 100% DMF, referred to as tagmentation mix.

** The tagmentation mix should be prepared fresh. As DMF is unstable in solution, we find decreased Tn5 activity in tagmentation mix prepared 30 minutes prior to experimentation.*

C. Assemble the tagmentation reaction and mix

2.50 μ l tagmentation mix

1.25 μ l 100 pg/ μ l – 200 pg/ μ l cDNA

1.25 μ l Tn5 at desired concentration

5.00 μ l in total

D. Perform tagmentation reaction with SDS

** make sure that the thermomixer is pre-heated to 55° C*

SDS inactivation results in higher yields after PCR enrichment

heat inactivation ensures same tagmentation time for all samples in large scale experiments and reduces hands-on time.

55°C for 3 minutes in a pre-heated thermocycler

cooling down to 10°C

1.25 μ l 0.2 % SDS

incubate at room temperature for 5 min

E. PCR enrichment (HiFi HotStart ReadyMix)

Add 10 μ l of the PCR mastermix to each sample and run the following PCR program

** for multiplexing: Add a unique pair of i5 and i7 adapter index primers separately to each sample.*

KAPA HiFi HotStart ReadyMix

6.75 μ l 2x KAPA buffer

0.75 μ l 100 % DMSO

1.25 μ l 10 μ M i5 adapter index primer

1.25 μ l 10 μ M i7 adapter index primer

10.00 μ l in total

** the gap filling step at 72° C for 3 min is essential to filling the 5' overhangs of the single stranded linker oligonucleotides to allow for the binding of adapter primers and the amplification of the tagmented cDNA library.*

72°C 3 min

95°C 30 sec

98°C 20 sec

58°C 15 sec: 12 cycles

72°C 30 sec

72°C 3 min

10°C hold

F. Remove residual dNTPs, primers, and the polymerase by adding one volume of SPRI beads to the sample (1:1 v/v) and follow the manufacturer's instructions. Elute with 10 μ l nuclease-free water.

G. Determine the concentration of the tagmented cDNA libraries using Qubit HS dsDNA and check the quality of the libraries on the Agilent 2100 Bioanalyzer using the Agilent High Sensitivity DNA Kit.

5.2.5 Data Analysis

Cell Profiler pipeline

The following pipeline was used to define protein knockdown levels after siRNA treatment as well as to classify Golgi phenotypes in the knocked down populations.

LoadImages

RescaleIntensity

RescaleIntensity

IdentifyPrimaryObjects

IdentifySecondaryObjects

ImageMath

Morph

IdentifyPrimaryObjects

MeasureImageQuality

ImageMath

RelateObjects

RelateObjects

FilterObjects

MeasureObjectSizeShape

RelateObjects

MaskImage

MeasureObjectIntensity

DisplayDataOnImage

DisplayDataOnImage

MeasureObjectIntensity

FilterObjects

ImageMath

ApplyThreshold

SaveImages

SaveImages

ExportToSpreadsheet

RNA sequencing analysis

The purpose of a test for differential expression is to test whether the data provides sufficient evidence to conclude that this value is really different from zero. DESeq2 performs for each gene a hypothesis test to see whether evidence is sufficient to decide against the null hypothesis that there is zero effect of the treatment on the gene and that the observed difference between treatment and control was merely caused by experimental variability (i.e., the type of variability that you can expect between different samples in the same treatment group).

As usual in statistics, the result of this test is reported as a p value, and it is found in the column pvalue. A p value indicates the probability that a fold change as strong as the observed one, or even stronger, would be seen under the situation described by the null hypothesis.

DESeq2 uses the Benjamini-Hochberg (BH) adjustment [219] as implemented in the base R `p.adjust` function; in brief, this method calculates for each gene an adjusted p value that answers the following question: if one called significant all genes with an adjusted p-value less than or equal to this gene's adjusted p-value threshold, what would be the fraction of false positives (the false discovery rate, FDR) among them, in the sense of the calculation outlined above. These values, called the BH-adjusted p values, are given in the column `padj` of the `res` object.

The FDR is a useful statistic for many high-throughput experiments, as we are often interested in reporting or focusing on a set of interesting genes, and we would like to put an upper bound on the percent of false positives in this set.

- Input data overview
 - 1.1 Reads
 - 1.2 Fastq QC

- 1.3 Alignments
- 1.4 Read counting
- Differential expression
 - 2.1 R and analysis software
 - 2.2 DESeq2
 - 2.3 Data preparation
 - * 2.3.1 Gene Counts table
 - * 2.3.2 Describing conditions in sample table
 - * 2.3.3 Principal component analysis
 - 2.4 Differential expression analysis
- GO analysis for gene enrichment analysis
 - 3.1 Enrichment
- Plotting genes of interest - USO1
 - 4.1 USO1 expression level
 - 4.2 Summary stats for all genes for Fragmented and Normal samples
 - 4.3 Summary stats for USO1 express for Fragmented and Normal samples
- 5 Comparison to first experiment (USO1 KO and Neg9)
 - 5.1 Input
 - * 5.1.1 Gene Counts table
 - * 5.1.2 Describing conditions in sample table
 - * 5.2 Create Deseq object
 - 5.2.1 PCA
 - 5.3 Differential expression analysis vs Uso1 KD samples
 - 5.4 Differential expression analysis vs Neg9 samples

CHAPTER 6

SUPPLEMENTARY MATERIAL

6.1 Hypothesis testing and pipeline development

List of proteins used for validation of the hypothesis as depicted in Fig. 2.4 is shown below in Fig. 6.1

Protein	Name	Localization
ACBD3	Acyl-CoA binding domain containing 3	Golgi, mitochondria
CCDC146	Coiled-coil domain containing 146	Golgi, Vesicles
GCC1	GRIP and coiled-coil domain containing 1	Golgi, Plasma Membrane, Cytosol
BICD2	Bicaudal D homolog 2	Plasma Membrane, Golgi, cytoskeleton
GAK	Cyclin G associated kinase	Golgi, Vesicles, Plasma Membrane, ER
GORASP2 (GRASP55)	Golgi reassembly stacking protein 2, 55kDa	Golgi
GOLGA5 (Golgin 84)	Golgin A5	Golgi
AKAP9	A kinase (PRKA) anchor protein 9	Golgi, Centrosome, Vesicles, Cytoplasm
TMF1	TATA element modulatory factor 1	Golgi, nucleus
GOLM1	Golgi membrane protein 1	Golgi, endosomes
GOLGB1 (Giantin)	Golgin B1	Golgi
SYNGR2	Synaptogyrin 2	Golgi, synaptic vesicles
RASGEF1A	RasGEF domain family, member 1A	Golgi
TMEM165	Transmembrane protein 165	Golgi, vesicles
USO1 (P115)	Vesicle transport factor p115	Golgi, cytoplasm, nucleus
COPG1	Coatomer protein complex, subunit gamma 1	Golgi, nucleoplasm, cytosol
TMCO3	Transmembrane and coiled-coil domains 3	Cytosol
COG8	Component of oligomeric golgi complex 8	Golgi
GORASP1 (GRASP65)	Golgi reassembly stacking protein 2, 55kDa	Golgi
COPB2	Coatomer complex, subunit beta 2 (beta prime)	Golgi, Vesicles
TRIP11 (GMAP210)	Thyroid Hormone Receptor Interactor 11	Golgi
CLASP2	Cytoplasmic Linker Associated Protein 2	Golgi, centrosome
GOLGA1 (Golgin 97)	Golgi Autoantigen, Golgin Subfamily A, 1	Golgi
GM130	Golgi Matrix Protein 130	Golgi

Figure 6.1: Golgi proteins selected for siRNA treatment. The following proteins were chosen for systematic siRNA knockdown and antibody staining to see their effect on Golgi morphology as well as quantify the level of the knockdown in different phenotypes.

6.2 Transcriptome Analysis

6.2.1 Global Transcriptome Analysis

Attached here are the genelists with upregulated and downregulated genes in every treatment. All these genelists are in comparison to the negative control, Neg9. Genelists have been thresholded on the basis of a Log2 Fold Change value of either 0.25 or 0.50 for upregulated genes, and -0.25 or -0.50 for downregulated genes. The basis for this selection depended on the number of genes that were within this bracket. For USO1, a threshold of 0.25 would be too low, as there were over 800 genes in this bracket, so 0.50 was used instead. Conversely for TRIP11, 0.50 was too high a threshold, with no genes occurring above this value. Therefore, 0.25 was used instead. Shown in these lists are the gene symbols, their base mean values, the Log2 Fold Change from the negative control, the normal as well as adjusted p-values for the change measured.

6.2.2 Single Population Transcriptome Analysis

Attached thereafter are the genelists comparing Normal golgi phenotype with fragmented phenotype. The data has been thresholded using a Log2 Fold Change value of less than or equal to 0.58 and -0.58 for upregulated and downregulated genes, respectively. This value corresponds to a fold increase or decrease of 150% from the original value.

AKAP9_Global_Upregulated

symbol	baseMean	log2FoldChange	pvalue	padj
ID2	137.3936906	1.425093842	1.58E-42	3.16E-39
PSCA	672.749052	1.360045668	6.60E-36	8.59E-33
HR	254.8737586	1.298796744	6.76E-36	8.59E-33
CFB	117.0974649	1.252409358	1.21E-28	8.02E-26
ADGRG1	1399.749981	1.149140948	2.77E-84	3.86E-80
MCF2L	432.1912451	1.100229835	1.74E-43	4.86E-40
KRT17	704.3925025	1.028769197	3.29E-28	1.77E-25
MMP12	1428.301218	1.005805539	1.13E-18	3.51E-16
TRAPPC3L	324.6026463	1.003120403	3.56E-28	1.84E-25
FOLR1	30840.91866	0.975709593	1.26E-50	4.42E-47
TINCR	614.487324	0.964724432	1.32E-21	4.86E-19
MYO7B	388.3110115	0.957938326	3.41E-22	1.32E-19
PSG4	325.5250575	0.913337986	2.70E-26	1.30E-23
PTGES	1285.871917	0.882885184	3.72E-40	6.49E-37
LOC1001304	146.6653659	0.853567817	6.29E-18	1.87E-15
SAMD11	103.0100218	0.828536691	1.73E-13	2.69E-11
MFAP5	135.0862711	0.819897148	1.70E-14	3.25E-12
HKDC1	691.0305341	0.803034931	2.99E-28	1.74E-25
LYPD3	3430.127742	0.802280665	1.29E-33	1.20E-30
DLX3	87.00766261	0.788179897	5.35E-12	6.34E-10
ID1	1876.191923	0.780657841	7.22E-12	8.34E-10
ECM1	962.2125227	0.767933043	1.32E-38	2.06E-35
VTN	2310.497202	0.766276387	2.40E-34	2.40E-31
SLC12A3	591.3066734	0.751610914	9.55E-31	7.02E-28
DUSP2	1693.643955	0.748564901	3.13E-28	1.75E-25
NA	585.4733983	0.746161887	6.83E-11	6.62E-09
NME5	48.09887459	0.745510734	5.99E-11	5.90E-09
PSG5	52.84873718	0.740962981	5.40E-11	5.43E-09
BMP2	3748.663939	0.723683669	1.67E-34	1.79E-31
PGBD5	53.30364184	0.720102736	2.89E-10	2.49E-08
HK1	921.9220038	0.713121919	1.22E-35	1.42E-32
ATOH8	1212.615711	0.713023831	5.37E-24	2.27E-21
ZNF385A	326.8243849	0.695218606	6.03E-14	1.03E-11
ALPI	257.4445049	0.680388445	3.42E-12	4.19E-10
PLEKHS1	35.51098076	0.671132572	6.17E-10	4.71E-08
ID3	8354.371543	0.669581546	7.76E-17	1.97E-14
MGP	1751.974923	0.649953997	2.69E-29	1.88E-26
NA	145.444443	0.645678244	3.81E-10	3.15E-08
CD70	1364.558425	0.640632792	1.46E-12	1.90E-10
WISP2	4162.196147	0.638425498	6.31E-13	8.74E-11
DUSP1	4457.494877	0.637383621	2.04E-20	7.31E-18
F2RL1	250.0704101	0.636847748	3.07E-11	3.17E-09

AKAP9_Global_Upregulated

FIBCD1	125.7159894	0.635905538	1.11E-08	6.75E-07
ADIRF	57.38194908	0.635828892	1.99E-08	1.11E-06
FSTL3	12093.65778	0.635804727	5.53E-14	9.53E-12
PROCR	570.1076884	0.631154612	1.52E-15	3.43E-13
PAG1	203.5786234	0.626718419	1.45E-11	1.60E-09
GPR1	126.7065233	0.617116283	1.86E-08	1.05E-06
GCNT3	515.899726	0.616858916	4.95E-10	3.92E-08
PDK4	6893.405546	0.610662828	1.87E-22	7.48E-20
TPPP	483.875802	0.604639651	1.94E-14	3.67E-12
TSPAN10	782.4672965	0.603228798	5.86E-09	3.81E-07
NA	54.08166357	0.599752579	1.28E-07	5.91E-06
ACER2	149.2708977	0.596251118	1.12E-08	6.78E-07
TNS4	795.1396393	0.594071768	1.17E-17	3.21E-15
ZNF831	2138.681368	0.592785715	5.57E-22	2.11E-19
SMAD6	2317.600547	0.588036907	3.67E-15	7.66E-13
ZNF488	79.93305285	0.586577469	1.11E-07	5.18E-06
NA	110.4917427	0.58169664	1.65E-07	7.29E-06
LOC1005066	279.0033894	0.563185392	3.12E-11	3.21E-09
CSDC2	83.93698242	0.561891396	8.21E-07	3.02E-05
ATP8B2	1550.983714	0.544420879	8.59E-14	1.41E-11
LINC01531	26.04390688	0.543907565	4.25E-07	1.69E-05
PRRG4	131.5318551	0.542297123	1.46E-07	6.59E-06
PLAU	67.82763759	0.540289009	2.28E-06	7.49E-05
FGFBP1	174.8018271	0.535073795	2.74E-08	1.49E-06
KIAA1644	51.62442538	0.532964776	3.11E-06	9.71E-05
GPER1	694.5108875	0.529580689	7.45E-07	2.78E-05
ACP5	95.79748268	0.526330264	1.79E-06	6.10E-05
PAX8-AS1	91.21195132	0.52179738	4.85E-06	0.00014415
NA	131.2056397	0.520957013	5.72E-07	2.20E-05
C15orf65	260.7676761	0.520244321	4.29E-08	2.24E-06
SLC12A7	2695.058373	0.516260264	1.77E-12	2.27E-10
F2R	266.7526743	0.515036878	1.23E-08	7.31E-07
UNC13D	444.5658157	0.514288847	5.37E-08	2.75E-06
S100P	6070.981574	0.513338098	4.69E-19	1.60E-16
CIART	59.320286	0.511972729	6.11E-06	0.00017611
ABTB1	791.7215605	0.511811913	2.59E-12	3.23E-10
SERPING1	137.5981855	0.50979383	1.02E-06	3.67E-05
TSPAN1	286.5211345	0.507047138	1.34E-07	6.11E-06
ACOT11	300.5757642	0.504569747	5.71E-08	2.89E-06
FAM105A	2253.971445	0.504513863	2.02E-16	4.78E-14
APOD	23.23099434	0.503774443	1.92E-06	6.46E-05
ZBED1	14861.18377	0.502157703	4.51E-13	6.37E-11
TBC1D2	1933.101081	0.500064493	5.17E-12	6.18E-10

AKAP9_Global_Downregulated

symbol	baseMean	log2FoldChange	pvalue	padj
AKAP9	6154.313503	-1.407712854	5.40E-72	3.77E-68
C4BPA	354.1035175	-0.976605345	2.90E-27	1.45E-24
SPARCL1	262.2982093	-0.710916243	2.61E-13	3.84E-11
LGSN	79.21071593	-0.649415128	6.11E-09	3.95E-07
LTBP1	190.8419805	-0.639072196	9.37E-11	8.97E-09
INTU	835.8467578	-0.630063334	8.78E-19	2.85E-16
LRIG1	501.5088925	-0.626248027	8.00E-18	2.28E-15
C9orf152	99.40092837	-0.621645226	3.76E-08	1.98E-06
SORCS2	445.7554334	-0.616209577	1.98E-13	3.00E-11
MGC39584	1194.163169	-0.612541779	4.66E-12	5.62E-10
MARCKSL1	1274.182448	-0.608547806	2.28E-20	7.95E-18
STC2	1026.87982	-0.605293931	7.62E-16	1.75E-13
KCTD12	1636.346118	-0.574118194	8.12E-14	1.37E-11
PPP3R1	4225.713191	-0.556862527	1.03E-16	2.58E-14
IL32	100.4588251	-0.556285969	9.11E-07	3.33E-05
YBX3	9978.742804	-0.538478438	2.61E-55	1.22E-51
CEP135	808.9557008	-0.537104433	4.30E-16	1.00E-13
DSC2	2857.805899	-0.527616342	3.72E-18	1.13E-15
BAG2	4685.146763	-0.525436161	2.03E-24	9.14E-22
COL27A1	152.4361484	-0.503382514	2.61E-06	8.33E-05
SLC9A7	255.4961252	-0.501354605	2.90E-08	1.56E-06
LAMC3	1345.753741	-0.500982304	4.49E-09	2.96E-07
LEPR	707.1755953	-0.49562839	1.90E-11	2.04E-09
SMARCD3	437.9479911	-0.480412552	2.55E-09	1.75E-07
SLC23A2	1857.487319	-0.477303126	1.99E-14	3.70E-12
NA	114.9401432	-0.477296586	8.39E-06	0.000228933
NA	85.0534098	-0.466063107	3.67E-05	0.000769792
GCNT2	3353.174087	-0.464829887	4.97E-24	2.17E-21
CADM1	629.6362707	-0.463864864	1.69E-12	2.19E-10
PLAGL1	3325.146983	-0.458022693	2.82E-17	7.42E-15
MRO	560.8644175	-0.45531371	1.22E-10	1.15E-08
FBXO10	89.11930047	-0.451511959	7.31E-05	0.001348174
CTSC	7610.903103	-0.449500345	7.39E-33	6.45E-30
ZNF106	14227.59977	-0.448946402	1.22E-22	5.01E-20
ARRDC4	243.8279663	-0.446844731	4.89E-06	0.000145045
HMCN2	78.05571362	-0.439562083	9.42E-05	0.001657512
FAM69A	520.0064464	-0.430897668	1.54E-07	6.87E-06
EFHD1	452.0683715	-0.427526761	9.93E-07	3.58E-05
PRG4	207.9417416	-0.426761598	2.72E-05	0.000601284
SELT	4219.011338	-0.425586847	1.75E-15	3.89E-13
CRABP2	651.1733718	-0.422413295	1.81E-07	7.86E-06
NEGR1	2756.296143	-0.421851384	6.64E-08	3.31E-06

AKAP9_Global_Downregulated

TBC1D5	2615.060748	-0.419657167	6.00E-11	5.90E-09
PEG10	29284.29592	-0.419295785	1.95E-28	1.24E-25
TSPAN3	8027.995345	-0.418924796	8.25E-31	6.40E-28
DNMT3A	186.6311988	-0.416551225	2.81E-05	0.000615095
SCML1	3086.530039	-0.414811192	2.57E-11	2.72E-09
FCGBP	174.4282685	-0.414536739	4.57E-05	0.000924266
PLEKHA3	914.0577989	-0.414145736	4.97E-10	3.92E-08
GTDC1	453.2470819	-0.411959222	9.59E-09	5.98E-07
ULBP1	149.6818463	-0.408609355	8.46E-05	0.001509909
ZNF721	162.6758081	-0.406141891	2.67E-05	0.000591709
ROR1	915.2453819	-0.405565341	1.24E-11	1.37E-09
GAL	1673.867157	-0.403649674	1.32E-08	7.73E-07
LINC00641	549.291272	-0.400822381	1.83E-06	6.21E-05
TP73	163.9540412	-0.399788651	9.97E-05	0.001724438
RNF157	122.3232883	-0.393961066	0.00015667	0.002512943
LRRC32	71.68443468	-0.393339438	0.00054276	0.006706087
SIGLEC1	120.6491153	-0.392138005	0.00034768	0.004744573
CENPQ	1167.951888	-0.39146626	7.44E-07	2.78E-05
ARHGAP28	560.2111977	-0.390955758	2.65E-06	8.45E-05
RIMS4	838.8782914	-0.390311585	3.57E-10	2.97E-08
ACTL8	12766.99019	-0.389074464	5.82E-08	2.94E-06
GPD1L	4036.526374	-0.38892777	1.34E-14	2.65E-12
GABRE	1681.027689	-0.387383139	5.03E-10	3.95E-08
S100A1	318.9909155	-0.383154764	9.52E-06	0.00025434
CASP1	127.1637182	-0.381766966	0.00037317	0.004980541
NEK6	1570.369939	-0.381255211	5.44E-15	1.12E-12
POP1	3933.734028	-0.380980256	5.01E-19	1.67E-16
NRP1	83.3740003	-0.376191708	0.00078191	0.008868105
NT5E	592.1104466	-0.373440724	4.47E-06	0.000134673
CREB3L1	19104.45748	-0.373350541	4.65E-08	2.41E-06
FKBP5	3388.322397	-0.37021465	2.07E-13	3.12E-11
C3	196.3199137	-0.369778906	0.00017897	0.002791247
BACE1	480.4468764	-0.367789449	5.81E-06	0.000168327
SLC26A9	129.7882203	-0.367770231	0.0007446	0.008576202
LINC00052	83.72918115	-0.366140017	0.00098388	0.010682743
NR2F1	1417.551698	-0.366021739	1.18E-07	5.47E-06
LPL	19576.96099	-0.364910479	2.77E-12	3.43E-10
MEST	3670.590989	-0.364696446	6.41E-17	1.66E-14
P4HA3	253.4648766	-0.362787107	2.73E-05	0.000602584
VAV3	2956.903687	-0.360249894	7.90E-13	1.07E-10
ARHGAP19	1242.458513	-0.360077466	4.04E-10	3.28E-08
LRRC8B	479.1454398	-0.359473805	0.0003614	0.004838949
LHX6	184.7807088	-0.358095615	0.00020419	0.003115005

AKAP9_Global_Downregulated

SPTBN2	1700.286441	-0.35669154	5.03E-06	0.000148578
GALNT1	5797.995209	-0.355652215	3.14E-10	2.69E-08
FOXP4-AS1	55.88135877	-0.35558375	0.00184575	0.017149309
CBX5	16556.63572	-0.355085654	5.16E-09	3.39E-07
NA	52.22813671	-0.354195321	0.00194107	0.01777487
MYO7A	36.70728277	-0.353964263	0.00173947	0.016346573
SVEP1	6591.895596	-0.352762509	3.33E-14	5.97E-12
ME2	3991.90604	-0.350378749	1.51E-10	1.40E-08
SLC38A5	325.2482765	-0.349323206	9.91E-05	0.001717292
DBNDD1	95.27844101	-0.347740725	0.00179418	0.016759285
NA	61.1671955	-0.346929109	0.00232329	0.02027838
MAPT	61.10959386	-0.344684564	0.00254828	0.021700013
RTKN2	848.0678617	-0.343994427	0.00010452	0.001792578
P2RY6	5989.293252	-0.343431901	1.20E-07	5.55E-06
NA	162.5841607	-0.343254077	0.00065257	0.007682385
MARCKS	5568.000392	-0.34318425	5.54E-05	0.0010773
IL17REL	178.0088564	-0.341480573	0.00100174	0.01083462
TP63	88.59347841	-0.339744947	0.00222719	0.019635816
PPL	1665.272547	-0.339482394	3.06E-08	1.64E-06
GHRLOS	59.23474238	-0.338755213	0.00296103	0.024239878
PI3	265.3006311	-0.337808535	0.00028882	0.004076724
ASNS	5798.277498	-0.337561463	1.93E-09	1.37E-07
MEX3A	345.6633826	-0.33740674	1.84E-05	0.000437228
KATNAL2	356.5685626	-0.336673419	1.22E-05	0.000307526
VAV2	1929.342422	-0.336041686	2.70E-10	2.34E-08
LBR	6122.598673	-0.33565135	3.06E-09	2.07E-07
NA	99.42721487	-0.334504152	0.00215327	0.019217577
WDR78	143.2562606	-0.333205036	0.00091574	0.01010784
TNS3	4751.565282	-0.332951167	1.94E-13	2.98E-11
NA	81.88535732	-0.331498062	0.00350211	0.027571001
MLXIPL	350.1331259	-0.331057074	0.00035386	0.00477766
ADAM11	175.5401391	-0.330425461	0.00149048	0.01459559
GALNT7	4668.638395	-0.32819466	1.80E-07	7.86E-06
PPIF	7242.988302	-0.3278568	1.45E-14	2.82E-12
NECTIN1	660.9424354	-0.327123523	6.13E-06	0.000176309
TEX9	168.5035208	-0.326683468	0.00230177	0.020166132
CMYA5	43.89112867	-0.326648128	0.00425599	0.031957634
POLN	235.0515883	-0.326265739	0.0001936	0.002976197
DEPTOR	361.7614737	-0.325276132	5.87E-05	0.001124758
KRT18	34272.9113	-0.325144601	7.26E-06	0.000202541
ACSL4	6009.23636	-0.324629849	9.20E-08	4.39E-06
SESN1	2038.791773	-0.324332071	1.14E-09	8.38E-08
ARL5A	1115.974041	-0.323723028	0.00041953	0.005468805

AKAP9_Global_Downregulated

SOCS2	939.1540128	-0.322949039	8.63E-09	5.43E-07
PI15	41.17862709	-0.321945642	0.00454141	0.033641804
LYRM7	1116.416313	-0.321046742	0.00025012	0.003644558
ABCA3	388.6935701	-0.320872062	0.00011018	0.00186625
TOP2A	41658.17861	-0.320168589	3.45E-09	2.32E-07
APLN	29.97067022	-0.320071715	0.0033994	0.027026676
SOX4	2877.175854	-0.316313741	3.51E-10	2.95E-08
ODC1	7463.481565	-0.315876292	1.90E-12	2.41E-10
FAT1	9435.236391	-0.315306207	9.57E-08	4.53E-06
NA	109.3386028	-0.31501759	0.00376883	0.029161476
BIRC3	469.3836304	-0.314797564	0.00042119	0.005485302
CCND1	4100.211708	-0.314790504	8.79E-10	6.57E-08
DCUN1D4	2788.598572	-0.313588571	2.18E-05	0.000502875
RRP15	3087.647263	-0.313280129	1.13E-06	4.01E-05
DHRS7C	217.642176	-0.311840487	0.00101697	0.010960956
NA	529.9180818	-0.311790892	1.89E-05	0.000448046
CHML	4479.396036	-0.311502081	0.0029445	0.024118654
SYPL1	7215.890546	-0.311475124	3.09E-06	9.68E-05
TMEM64	1863.526419	-0.309799535	8.41E-06	0.000229015
NA	388.4138708	-0.308994967	0.00258302	0.021915642
PLD1	1990.803689	-0.308976046	7.11E-13	9.74E-11
U2SURP	13431.78642	-0.30785258	1.15E-05	0.000295014
ARHGFB40	188.4507247	-0.306273342	0.00300107	0.024510171
NA	124.6738792	-0.304808816	0.00692622	0.045568273
HTRA1	2764.181971	-0.304762635	6.62E-09	4.24E-07
NUP210	22208.8704	-0.304704115	3.57E-07	1.46E-05
NA	640.6793363	-0.304427122	7.60E-05	0.001390738
FMNL3	470.315952	-0.304235201	0.00012683	0.002107459
CLYBL	391.2987651	-0.303955407	0.00060738	0.007285417
ABCA1	84.9723952	-0.30329771	0.00688137	0.045465821
OTUD6B	1391.370682	-0.303231586	0.00022105	0.003310591
COL16A1	383.2757951	-0.303006458	0.00094429	0.010333171
FAM132B	29.53988225	-0.302558005	0.00550339	0.038723271
GLB1L2	24.91614585	-0.302318625	0.00552211	0.038797609
MINPP1	1815.88647	-0.3017883	7.40E-06	0.000206103
CXCL16	114.7607398	-0.301585081	0.00519535	0.037192517
NDUFA5	2707.657839	-0.301390614	6.60E-05	0.001237662
HOOK1	2329.424415	-0.301094605	5.04E-06	0.000148578
NA	148.771272	-0.300641814	0.0039664	0.030271153
ARNTL2	311.1890396	-0.298981864	0.0005324	0.006613065
TMEM170B	2090.237065	-0.298723438	0.00023278	0.003439609
SMARCA1	165.9102507	-0.298545036	0.00275354	0.022944498
ZMYM1	2320.894495	-0.298427251	0.00046423	0.005941608

AKAP9_Global_Downregulated

C8orf22	2765.655519	-0.297423954	1.02E-09	7.54E-08
WNT10B	552.1890897	-0.297325804	5.51E-05	0.001075018
MCC	1268.912572	-0.29700556	4.34E-07	1.73E-05
DOPEY2	1344.969222	-0.29682825	2.71E-07	1.15E-05
TRIM14	921.9234595	-0.296072211	2.95E-06	9.31E-05
NETO2	3256.031345	-0.295999704	2.89E-13	4.17E-11
UBE2K	6126.129822	-0.295604243	7.95E-08	3.87E-06
LAMB1	13978.54443	-0.295372042	2.18E-13	3.25E-11
FAM117B	1441.850321	-0.294146593	1.56E-07	6.91E-06
NA	275.6039399	-0.293055267	0.00207815	0.018671067
TCF7L1	255.1008653	-0.292829044	0.00126642	0.012898684
UNC13B	10734.2651	-0.292764057	1.13E-17	3.16E-15
THBS1	2571.69464	-0.291124043	2.52E-11	2.68E-09
LCN2	69.3220389	-0.290560277	0.01100402	0.063201854
NWD1	96.45589332	-0.290294958	0.00948217	0.057311354
TATDN1	706.7429732	-0.289892492	0.00020137	0.003082064
PGM2L1	767.3657301	-0.289409277	1.90E-05	0.000449617
WDR35	1865.454358	-0.289190398	6.48E-07	2.46E-05
ZSCAN30	423.8171224	-0.288889777	0.00041171	0.005397083
CNOT6L	2245.848076	-0.288765941	0.00017387	0.002729889
JAG2	993.4375643	-0.288222699	0.00571204	0.039751004
ANK1	273.698438	-0.28801938	0.00059344	0.007155047
SNED1	385.022152	-0.287951892	0.00108613	0.011437536
LRRC40	5069.133082	-0.287854861	6.58E-05	0.001234938
TERT	30.78820851	-0.287623589	0.0082658	0.051796539
ADCY7	107.6109255	-0.286105348	0.01131349	0.064423247
RBP2	34.43438283	-0.285354024	0.01048918	0.061354444
NA	82.83764715	-0.285038602	0.01258417	0.069754518
NUCKS1	40709.1363	-0.284864775	5.57E-05	0.00108091
CCDC13	36.90114512	-0.284624045	0.01225876	0.068439449
IQCH	113.2706553	-0.284533622	0.00857614	0.053334648
ATP11C	7823.339224	-0.284134415	1.81E-07	7.86E-06
NA	156.7657193	-0.283637017	0.00781563	0.049756517
SLC29A4	158.0177343	-0.283497064	0.0073543	0.047578244
11-Sep	2545.777874	-0.283318413	1.93E-06	6.48E-05
SCRN3	699.5916315	-0.283157556	0.000191	0.00294269
HMGB1	8836.45582	-0.282718567	2.86E-05	0.000623718
CCDC169	151.4970614	-0.282335896	0.0061953	0.042313381
MOB4	784.8925088	-0.282233162	0.00292575	0.02404207
PPAT	2776.629976	-0.281878645	1.80E-08	1.02E-06
TSNAX	2496.889918	-0.281725528	2.80E-05	0.000613934
SACS	3230.01123	-0.281493322	0.00012465	0.002076127
C11orf80	263.8219866	-0.279045307	0.00137733	0.013737869

AKAP9_Global_Downregulated

RIDA	917.8291818	-0.278723481	4.26E-05	0.000869294
PKP2	1145.274693	-0.278395871	1.31E-05	0.000324895
ADGRG6	2132.838925	-0.278107995	2.68E-06	8.54E-05
MEGF9	5126.139295	-0.277840298	1.43E-12	1.88E-10
ZNF146	9752.014839	-0.276758341	7.04E-08	3.49E-06
NDC1	12118.55879	-0.275678462	2.33E-09	1.63E-07
BMPR1B	131.8909063	-0.27561811	0.01042035	0.061028509
LOC285556	27.52552394	-0.27492675	0.00985629	0.058935311
FRMD4B	345.9341909	-0.274843577	0.00047082	0.005997446
SPOPL	1248.872136	-0.274805626	2.20E-05	0.000505389
MGAT4A	878.4651862	-0.27429058	6.89E-05	0.001277997
CLIC4	9367.812877	-0.273511374	0.00030223	0.004222404
CCDC18	4649.17226	-0.273436972	1.43E-06	4.93E-05
CYP17A1	37.29065696	-0.273249309	0.01625803	0.083464245
NA	66.98513974	-0.272598721	0.01649244	0.084182294
SVIL	4808.623607	-0.272357258	1.50E-08	8.69E-07
CCDC88A	5770.311003	-0.27218225	8.46E-05	0.001509909
TAP2	1155.095651	-0.270949071	5.68E-07	2.19E-05
ZNF271P	2627.360656	-0.270730408	1.89E-08	1.06E-06
NA	64.56998951	-0.27064245	0.01791615	0.08925498
CSTF3	4230.878989	-0.269509283	7.33E-08	3.61E-06
UBE2Q2	969.0569062	-0.269374433	7.47E-05	0.001371912
WDR3	13279.22547	-0.26919117	7.53E-07	2.80E-05
RAP2A	1130.395329	-0.26886161	0.0001521	0.002459925
HMGB2	7300.838335	-0.268650092	2.55E-09	1.75E-07
HPD	68795.49598	-0.268603117	0.00097141	0.010579669
SNTB1	915.2850561	-0.267766818	3.00E-06	9.42E-05
NUDT4	1468.775412	-0.26771374	4.77E-05	0.00095712
GAREM2	143.4280566	-0.267336919	0.01066121	0.06192008
NFATC2	110.314949	-0.26732273	0.0156639	0.081491951
RAB3D	1627.406178	-0.267067521	2.28E-07	9.78E-06
MB	161.5822064	-0.266920966	0.00904426	0.055456143
SYNGR3	132.8218248	-0.266759592	0.01432965	0.076516046
JAG1	806.7457942	-0.266592107	1.23E-05	0.000309256
TXNIP	8313.908432	-0.265701558	0.00131985	0.013307017
CAMK2D	863.2378468	-0.265691884	9.64E-06	0.000256512
HSD17B12	1058.510488	-0.265670969	0.00027315	0.003902895
KIF15	2719.162179	-0.265195298	3.70E-05	0.000772923
LIFR	31406.9004	-0.265169319	1.30E-05	0.000322403
CYCS	8719.164809	-0.265030129	0.0014361	0.014192424
SP2-AS1	80.47535151	-0.264704141	0.02041797	0.097698409
SLC18B1	1410.419606	-0.264529591	7.22E-06	0.000201697
SERPINE2	51.60466754	-0.264021933	0.02010078	0.096824624

AKAP9_Global_Downregulated

MDC1	10288.88093	-0.263789771	5.69E-06	0.000165606
NOC3L	3304.401817	-0.262671995	2.61E-05	0.000583201
TFPI	2260.474821	-0.262398765	2.27E-06	7.47E-05
FAH	769.3425685	-0.261816792	0.00346077	0.027322474
NA	125.27255	-0.261773056	0.01270682	0.070294963
GAGE1	1838.06288	-0.261652369	9.40E-07	3.42E-05
C1orf198	2895.864022	-0.261381662	1.67E-10	1.52E-08
NALCN	632.236201	-0.261050619	0.00025503	0.003693017
UBE2E3	1876.630112	-0.260995464	6.69E-09	4.27E-07
NA	237.7956597	-0.260760556	0.0034529	0.027291198
USP46	1322.241348	-0.260615388	5.99E-05	0.001138988
DCP2	2565.247413	-0.260526414	0.00024359	0.003579359
MAK16	2606.215952	-0.260449289	6.56E-08	3.28E-06
CCDC159	289.9095761	-0.260000963	0.00325152	0.026218582
COLQ	34.17584987	-0.259860895	0.01978257	0.095787132
ZNF239	763.9937115	-0.259679122	0.00023285	0.003439609
ABCC6	94.72710473	-0.259574315	0.01658105	0.08453249
NLN	5081.958135	-0.259266875	2.47E-06	7.99E-05
AK4	10111.00013	-0.256503334	2.16E-07	9.27E-06
LYPLA1	3842.302203	-0.256314224	0.00056766	0.006921822
ELL2	4829.380448	-0.255399091	5.63E-06	0.000164201
RNF138	1215.250673	-0.254889836	0.00340836	0.027061562
KPNA5	507.3210481	-0.254849236	0.00368018	0.028634064
MND1	762.9780495	-0.254572928	0.00013621	0.002239277
TNFSF4	135.3120678	-0.254500555	0.01378811	0.074305822
DDX10	2757.480761	-0.253821593	3.03E-07	1.26E-05
LIN9	2789.401485	-0.253786325	1.16E-05	0.000295047
HELB	424.1517099	-0.253724494	0.00529536	0.037755821
CDCA8	4574.017144	-0.253191936	3.31E-08	1.77E-06
NA	170.9506705	-0.253051137	0.01308212	0.07169003
DDAH1	11477.91102	-0.253042459	5.53E-06	0.000161945
HSPD1	78438.74169	-0.252445951	1.24E-06	4.37E-05
KIAA1958	1330.019269	-0.251618495	5.19E-05	0.001024975
GTPBP10	1492.698089	-0.251352103	0.00010894	0.001849655
NA	25.01805739	-0.250731613	0.01719514	0.087091302
NT5DC3	932.3175007	-0.250340065	0.00019451	0.002986903

TRIP11_Global_Upregulated

symbol	baseMean	log2FoldChange	pvalue	padj
GCNT3	515.899726	0.448848834	6.58E-06	0.00154369
TINCR	614.487324	0.44810004	1.03E-05	0.00203293
STRA6	89.45308779	0.447989554	6.53E-05	0.00730598
NA	97.34266926	0.413989444	0.00020444	0.01578085
CASC15	66.96856818	0.412899199	0.00025384	0.01779241
CREB5	151.0888963	0.411885836	7.08E-05	0.00751141
ZNF831	2138.681368	0.408365439	4.34E-11	4.81E-08
PPP1R26-AS1	88.15252345	0.406193497	0.00028009	0.01893972
MFAP5	135.0862711	0.400495495	0.00021375	0.01599327
WIPI1	1356.067291	0.398757646	1.73E-16	3.01E-13
ORAI2	128.2081028	0.39657005	0.00011153	0.01042101
PI3	265.3006311	0.395178301	1.51E-05	0.00275982
LOC10192694	158.1611302	0.393286152	9.76E-05	0.00975953
NA	131.2056397	0.389681961	0.00021322	0.01599327
DUSP5	632.809439	0.38431079	1.91E-06	0.00055473
TRAPPC3L	324.6026463	0.381553076	4.32E-05	0.00560742
DUSP4	756.6491695	0.378157479	2.01E-06	0.00057036
NA	145.444443	0.376587681	0.00031537	0.02009592
KDELR3	3922.569937	0.367507292	1.50E-16	3.01E-13
RCN3	4213.445562	0.36647198	1.72E-06	0.00053491
DOX1	113.6858372	0.363267881	0.00110087	0.04416516
HKDC1	691.0305341	0.362973195	1.04E-06	0.00037297
MANSC1	248.2135201	0.361658648	5.61E-05	0.00663776
PPARA	1630.208282	0.358901591	1.31E-06	0.00045748
C15orf65	260.7676761	0.357544335	0.00019818	0.0153951
INHBE	125.940046	0.357365777	0.00147091	0.05260753
SEC24D	7271.067358	0.354506401	3.63E-30	2.21E-26
RNF145	4091.111089	0.353954317	8.11E-20	3.30E-16
MYO7B	388.3110115	0.347981406	0.00050286	0.02667883
CCDC64	315.0247589	0.346896089	0.00023348	0.01694978
APBB1IP	301.67714	0.341155949	2.87E-05	0.0043147
PSG4	325.5250575	0.340657408	0.00011763	0.01070652
SDR16C5	903.1264293	0.340548657	3.13E-07	0.00015437
GSDMB	255.7472499	0.340164858	0.00023738	0.01702959
LGALS8	565.4778559	0.3364433	3.78E-05	0.00523209
GDF15	1779.449648	0.336295333	0.0032393	0.08496024
LURAP1L	516.5943347	0.33497709	0.00099189	0.0415707
C15orf62	104.8542373	0.33466198	0.00205019	0.06548896
HIST1H2BK	861.6286254	0.330768887	0.00014093	0.01239143
HIST1H2BN	156.7048838	0.328938623	0.00098254	0.04155815
PAX8-AS1	91.21195132	0.32855317	0.00396493	0.09556569
NA	553.1866025	0.324220556	0.00072763	0.03374228
PDE2A	83760.42151	0.318776955	0.00011284	0.01042101
PRKAG2	947.2676463	0.318302758	9.28E-06	0.00199587
ZNF432	610.4732673	0.317519561	0.00011364	0.01042101
NA	195.9550892	0.315746727	0.00165991	0.05734919
COL7A1	1937.534765	0.314335735	6.73E-05	0.00736764

TRIP11_Global_Upregulated

RELL2	128.6263267	0.313988593	0.00390365	0.09427511
PPARG	346.2843743	0.31398587	0.00033654	0.02104846
LPCAT1	19891.94264	0.31259542	6.45E-08	4.14E-05
HIST1H1C	1864.634576	0.311837059	0.00098906	0.0415707
MIR34AHG	94.22421321	0.311830825	0.00426116	0.09912386
IFT20	1333.563549	0.310866335	9.82E-06	0.00199587
JUN	753.9362233	0.307645067	0.00290048	0.0802137
ZNF75A	151.8057114	0.307552182	0.00357786	0.08946817
PDE4DIP	1724.630348	0.303848324	1.05E-11	1.29E-08
MAFF	949.6125568	0.303651008	1.22E-05	0.00237108
NA	200.1470798	0.30172134	0.00192006	0.0633192
KIAA0513	248.8541666	0.300496533	0.003341	0.08669539
YPEL2	393.5060059	0.298935137	7.24E-05	0.00760763
N4BP3	471.2751033	0.293944207	0.00115752	0.04553899
DNAJC12	352.2064439	0.293864167	0.00030295	0.01985628
KIAA1024	277.9056079	0.293123855	0.0005753	0.02926207
MAGED2	10401.54832	0.291950758	1.47E-09	1.19E-06
RORC	1218.166578	0.288556768	1.56E-06	0.00052739
MURC	242.3130426	0.288124117	0.0032951	0.08568663
PLPP5	1345.991866	0.287361572	3.27E-07	0.00015437
SAMD4A	263.35902	0.286912817	0.00070855	0.03334828
FAM114A1	3292.80082	0.283859804	9.16E-10	8.59E-07
NA	548.4072952	0.282794608	0.00015491	0.0132023
STX3	2009.819555	0.28266384	5.31E-07	0.00023111
REPS2	836.156532	0.282115188	2.68E-05	0.00429973
PLPP3	733.2764524	0.281800414	3.17E-05	0.0045437
EIF2AK3	3980.458371	0.280411154	1.58E-13	2.41E-10
HMOX1	3129.225662	0.278526563	0.00196926	0.06414554
IER3	4424.377427	0.276375988	0.00041164	0.02376915
HSD17B6	511.7121094	0.273901068	0.0010444	0.04274334
ARHGEF28	1075.625024	0.273794879	2.80E-05	0.0043147
PELI3	647.6157163	0.271970274	0.00288774	0.08004284
ALPK2	1735.209792	0.271718105	4.15E-05	0.0055004
S1PR3	1030.496311	0.265681381	0.00095216	0.04088906
TMEM243	1845.279758	0.262345379	1.28E-05	0.00242385
PPEF1	627.3676242	0.259565395	0.00377562	0.09216119
ARL3	1262.115151	0.257949138	2.39E-05	0.00398849
YPEL5	1641.272146	0.257886331	4.79E-05	0.00595852
SLC17A5	3246.36658	0.256030111	6.18E-07	0.00025786
DUSP1	4457.494877	0.25566912	0.00021515	0.01600009
TCP11L2	338.6432542	0.254430982	0.00144746	0.05222844
BHLHE40	2721.873718	0.251470606	3.92E-08	2.66E-05

TRIP11_Global_Downregulated

symbol	baseMean	log2FoldChange	pvalue	padj
TRIP11	2721.596558	-1.322994279	1.7552E-76	2.14062E-72
HMCN2	78.05571362	-0.414918365	0.00023643	0.01702959
SH3BP1	125.2607873	-0.391325656	0.00042213	0.024057671
SDC4	3703.888052	-0.37647421	4.4864E-19	1.36792E-15
ASIC1	93.76839769	-0.35290627	0.00124603	0.047938564
IL1RAP	4793.709968	-0.346434113	1.4642E-08	1.11607E-05
HSPB7	4429.176339	-0.343445911	1.0757E-07	6.2472E-05
LEPR	707.1755953	-0.340352193	4.3101E-06	0.001051316
NA	148.771272	-0.336329845	0.00138434	0.05085372
LGSN	79.21071593	-0.332990429	0.00282516	0.07866582
NA	99.42721487	-0.331909622	0.00245791	0.071919462
PSD2	72.206674	-0.326829527	0.00381436	0.092669155
UNC13D	444.5658157	-0.319490281	0.00094265	0.040810031
CRLF1	440.5563953	-0.310926461	0.00057584	0.029262066
CHML	4479.396036	-0.304482392	0.00366403	0.090458472
SLC12A3	591.3066734	-0.302801685	1.5161E-05	0.002759825
NPTX1	22969.79603	-0.296855869	1.6146E-17	3.93823E-14
DHODH	960.3182498	-0.29113821	0.00010871	0.010277849
CSPG4	1782.010075	-0.282404633	0.00016439	0.013455783
POLR2L	5622.658096	-0.274370679	0.00010796	0.010277849
FAM46C	5869.175319	-0.272976331	1.1947E-09	1.04076E-06
MACROD1	644.5649999	-0.270915628	0.00170697	0.058642869
GPCPD1	3615.431602	-0.269430622	0.00126461	0.048400162
KRT8	27311.96295	-0.264172821	7.4142E-07	0.000280732
P2RY6	5989.293252	-0.262798997	5.2252E-05	0.006247652
ENO3	3016.916552	-0.260883569	0.00019306	0.01509355
EFHD1	452.0683715	-0.26046925	0.00293289	0.080592151
SLC44A2	2743.777391	-0.260343871	3.0581E-05	0.004440003

USO1_Global_Upregulated

symbol	baseMean	log2FoldChange	pvalue	padj
PLXNA3	104.4141633	2.189961607	1.09E-90	2.63E-87
RCN3	4213.445562	1.328909673	4.89E-68	5.17E-65
AGR2	3489.213935	1.298588925	2.86E-56	1.73E-53
KDELR3	3922.569937	1.149583639	2.51E-152	1.42E-148
SEC24D	7271.067358	1.078363916	4.61E-275	3.90E-271
SIGLEC1	120.6491153	1.057166016	3.04E-23	3.28E-21
CRABP2	651.1733718	1.049658814	2.62E-41	6.92E-39
PLPP5	1345.991866	1.024294333	2.43E-78	3.43E-75
YIPF2	3073.295445	1.014296429	5.99E-43	1.69E-40
DOX1	113.6858372	1.003550666	7.88E-20	6.51E-18
MAGED2	10401.54832	0.9747267	1.36E-91	3.82E-88
MAPK15	243.7960798	0.960893491	4.87E-20	4.06E-18
FKBP14	2460.646182	0.948338091	1.28E-43	3.74E-41
ABCA1	84.9723952	0.934588886	1.84E-17	1.23E-15
CERCAM	4148.414496	0.921609764	2.11E-45	6.37E-43
BBOF1	199.7716786	0.919646168	1.84E-24	2.21E-22
COG6	1811.693435	0.907516281	2.00E-52	9.39E-50
C16orf71	125.721115	0.903497911	5.58E-17	3.64E-15
FAM114A1	3292.80082	0.884297876	9.55E-84	1.47E-80
RORC	1218.166578	0.879153931	1.12E-50	4.73E-48
ARF4	19399.96341	0.878603888	8.74E-57	5.48E-54
PDE4DIP	1724.630348	0.872635059	2.78E-90	5.89E-87
IFT20	1333.563549	0.86814424	7.40E-36	1.72E-33
SPARCL1	262.2982093	0.862761377	9.96E-21	8.78E-19
EAF2	180.5551852	0.860695279	2.64E-19	2.08E-17
CCL28	610.6335296	0.828787655	1.81E-21	1.66E-19
HSD17B13	220.9712685	0.824830849	5.80E-14	2.77E-12
TMEM45A	2634.074092	0.82212719	2.22E-41	5.97E-39
GOLGA3	6229.511819	0.820478901	1.62E-61	1.31E-58
MGC39584	1194.163169	0.809717893	1.60E-20	1.40E-18
ERLEC1	6259.519635	0.808522881	5.37E-84	9.10E-81
CCDC186	2229.125648	0.793159857	2.36E-33	4.81E-31
HHIPL2	60.29465286	0.791180295	3.04E-12	1.20E-10
SLC15A2	46.22732358	0.786132442	5.87E-12	2.23E-10
PGM3	5069.133573	0.779997199	1.61E-45	4.95E-43
KDELR2	24391.01798	0.779204649	1.17E-66	1.17E-63
GSDMB	255.7472499	0.778557852	1.08E-17	7.34E-16
CLIP4	217.1041919	0.776513325	1.46E-12	5.92E-11
WIP1	1356.067291	0.771546951	8.35E-60	6.15E-57
STRA6	89.45308779	0.767934282	5.94E-12	2.25E-10
YIF1A	6657.141256	0.762225495	2.08E-28	3.23E-26
FKBP10	33014.19801	0.760315689	2.05E-40	5.17E-38
RRBP1	13250.97519	0.753056075	2.26E-71	2.95E-68
GMPPA	2707.252334	0.750692635	4.28E-54	2.26E-51
PRRC1	5427.949168	0.748237696	9.89E-34	2.09E-31
NUCB2	4503.132839	0.740345717	1.38E-52	6.66E-50
S100A14	259.7370613	0.738431056	1.85E-16	1.15E-14

USO1_Global_Upregulated

LOX	3237.900417	0.735589194	5.14E-62	4.58E-59
SLC39A13	932.5100746	0.735358727	6.94E-24	7.99E-22
ARFGAP3	2982.866637	0.717256315	6.30E-47	2.15E-44
TMEM263	8570.268923	0.715451517	2.27E-18	1.64E-16
GPX8	6002.60463	0.709650349	2.76E-59	1.94E-56
CAPS	112.5915189	0.707829179	5.41E-12	2.07E-10
FAM83E	17.22302017	0.706442391	1.00E-12	4.21E-11
SLC17A5	3246.36658	0.697648219	7.48E-43	2.08E-40
TMEM151A	38.05052214	0.691310557	4.39E-10	1.29E-08
SEC13	14605.41134	0.688807636	4.28E-55	2.34E-52
FAM83F	37.7956603	0.685898887	1.16E-09	3.19E-08
SEC24A	3688.197329	0.678049338	1.01E-45	3.23E-43
PDXDC2P	119.4993765	0.67783649	2.08E-10	6.51E-09
AIM1	409.7803953	0.672541256	1.06E-14	5.65E-13
CLU	18804.94744	0.669655122	2.65E-26	3.66E-24
KIAA1024	277.9056079	0.669625966	9.68E-16	5.59E-14
ALDH3A1	1833.418494	0.668746997	1.22E-28	1.91E-26
ARCN1	17156.61594	0.663852509	1.18E-70	1.42E-67
LMAN1	21295.64714	0.663732532	1.56E-29	2.61E-27
TVP23B	1301.239222	0.662945108	2.33E-22	2.28E-20
USP3-AS1	124.7970852	0.662076185	1.13E-09	3.13E-08
GOLGA2	11535.06394	0.66062451	1.21E-69	1.37E-66
OGN	595.697426	0.660324408	7.98E-13	3.40E-11
CDR2	2484.999106	0.658613373	2.77E-49	1.12E-46
MGP	1751.974923	0.658290705	8.71E-30	1.51E-27
TMF1	7106.246511	0.655240643	3.37E-56	1.97E-53
PDXDC1	12158.33225	0.651807007	1.55E-98	5.26E-95
RWDD2A	714.8663079	0.648911862	1.99E-22	1.97E-20
COPA	40341.21663	0.646971776	1.87E-64	1.76E-61
WDR5B	368.0900935	0.646091775	2.16E-15	1.20E-13
CASC4	4828.463364	0.644225659	8.20E-29	1.30E-26
TMEM39A	2655.566135	0.642570974	3.07E-47	1.08E-44
COL20A1	21.48312681	0.638662482	2.25E-10	7.01E-09
DNAJB9	1013.042121	0.638291754	1.76E-21	1.62E-19
RABAC1	4006.36854	0.637247926	1.76E-08	3.88E-07
ARFGAP1	8502.601893	0.636163672	3.31E-30	5.90E-28
MATN1-AS1	174.1687373	0.633439631	4.59E-11	1.56E-09
GFPT1	9878.479896	0.631919489	6.33E-47	2.15E-44
SEC23A	8736.344936	0.630891188	5.76E-54	2.96E-51
CREB3	2626.224267	0.630315114	2.10E-31	4.04E-29
FAM229A	438.6303126	0.628436561	6.60E-16	3.85E-14
GPR180	2519.387224	0.628429202	9.16E-27	1.34E-24
SLC37A3	2708.82083	0.627930612	4.49E-41	1.17E-38
FAM63B	1083.523199	0.62740997	2.48E-12	9.84E-11
PPM1K	415.6331204	0.626993904	2.25E-14	1.14E-12
RAPGEF3	82.75747563	0.625953673	1.31E-08	2.98E-07
CFAP44	313.0195833	0.624438777	1.08E-13	4.98E-12
SLC35A2	4916.996955	0.623964636	4.82E-30	8.51E-28

USO1_Global_Upregulated

P3H1	4854.32898	0.623556338	5.17E-33	1.03E-30
SRA1	1384.789922	0.621999165	7.61E-30	1.33E-27
PLCD4	113.3978835	0.621995002	1.26E-08	2.88E-07
SERP1	13657.11993	0.621836261	3.65E-22	3.56E-20
FAM8A1	2000.478542	0.620721847	6.90E-22	6.53E-20
TRAPPC3L	324.6026463	0.619361897	2.13E-11	7.51E-10
SPINK4	93.76078199	0.615820444	1.82E-08	4.01E-07
COPB2	25402.28656	0.614234628	1.37E-129	5.80E-126
FOSB	180.4275826	0.612884879	1.75E-09	4.73E-08
MFSD2A	77.97407366	0.610080982	5.73E-08	1.16E-06
GOLGA5	2916.913357	0.609511234	2.67E-49	1.10E-46
TEF	671.4099394	0.606252276	3.38E-18	2.39E-16
CRIPAK	466.1749068	0.604380041	4.32E-14	2.10E-12
C11orf24	3145.026207	0.603986366	6.37E-31	1.19E-28
FGF21	60.58969026	0.603732625	1.26E-07	2.35E-06
NPIP15	127.2052973	0.601057533	1.29E-08	2.95E-07
SLC31A1	9601.242444	0.601017635	1.16E-57	7.54E-55
ARL1	7193.56402	0.600375035	1.89E-47	6.81E-45
CFB	117.0974649	0.59954052	1.26E-07	2.36E-06
TSPAN13	7506.854047	0.596999477	2.81E-20	2.42E-18
SSR3	26449.21324	0.593310869	1.50E-25	1.94E-23
PLPPR2	3489.575035	0.592890053	5.06E-13	2.21E-11
SPDEF	910.4858879	0.591806384	1.54E-11	5.54E-10
SLC1A1	666.8847856	0.590844036	2.28E-20	1.97E-18
LOC10192694	158.1611302	0.587883408	4.28E-09	1.08E-07
MCEE	726.9828726	0.587285777	7.72E-20	6.41E-18
INHBE	125.940046	0.586136253	1.69E-07	3.05E-06
MORC4	2176.915224	0.581297433	2.08E-20	1.81E-18
COL5A1	8749.665158	0.580479868	4.58E-16	2.72E-14
ARL3	1262.115151	0.579550384	7.10E-22	6.68E-20
ZNF70	287.971699	0.578170336	8.62E-12	3.19E-10
MFSD6	1207.336166	0.576783961	2.32E-23	2.52E-21
SLC35C1	2775.216578	0.576489926	1.74E-26	2.46E-24
COG3	1648.05161	0.575263997	2.18E-25	2.80E-23
P3H4	5533.624356	0.575208399	3.56E-21	3.17E-19
SYTL3	51.14872765	0.574952945	4.85E-07	8.07E-06
TMEM214	7985.813293	0.571786014	8.12E-26	1.07E-23
TPST1	224.4491618	0.571507308	6.25E-09	1.52E-07
CALU	37548.4501	0.571289094	1.58E-58	1.07E-55
TM4SF1-AS1	108.6647483	0.569783518	7.13E-08	1.40E-06
ZNF841	930.0543975	0.569581899	3.17E-24	3.70E-22
EIF2AK3	3980.458371	0.568933242	8.08E-52	3.51E-49
GLCE	1515.563164	0.567323162	4.02E-23	4.28E-21
FAM83A	159.1931076	0.56657676	1.43E-07	2.63E-06
POFUT2	1416.003519	0.564484307	4.03E-26	5.42E-24
LCA5L	158.8984519	0.563827312	2.30E-08	4.94E-07
SELM	2110.1332	0.558055223	7.25E-07	1.16E-05
TJP3	473.1696224	0.557637952	3.86E-09	9.85E-08

USO1_Global_Upregulated

MAP3K9	2244.458137	0.556201939	7.82E-35	1.74E-32
TMED3	5852.925349	0.553885943	5.98E-34	1.28E-31
ATP8B2	1550.983714	0.553771201	3.71E-14	1.83E-12
FGD4	594.3410395	0.553336996	2.47E-14	1.24E-12
COPG1	21948.75437	0.553310523	4.02E-28	6.13E-26
SEC22B	8822.378485	0.552601103	4.47E-56	2.52E-53
FAM98A	7224.164279	0.552139781	1.29E-48	4.87E-46
CCDC110	45.93733966	0.551595241	1.09E-06	1.68E-05
MMP12	1428.301218	0.550386424	1.38E-06	2.08E-05
YIPF5	3398.670134	0.549264108	5.62E-25	7.11E-23
SLPI	3073.876738	0.54837558	4.89E-34	1.08E-31
SEC31A	24690.20991	0.547683872	4.17E-46	1.36E-43
LBX2-AS1	65.16693845	0.547530661	1.52E-06	2.28E-05
TMEM243	1845.279758	0.547165867	4.49E-20	3.76E-18
GBF1	12590.23189	0.545300058	8.03E-42	2.19E-39
NDEL1	4021.868076	0.545174047	2.62E-26	3.63E-24
FKBP7	378.4970381	0.54369723	1.60E-10	5.05E-09
ELN	16.66874442	0.543245811	5.89E-08	1.18E-06
C4BPA	354.1035175	0.543034481	1.70E-10	5.38E-09
MED8	4055.619888	0.542325021	7.89E-29	1.26E-26
TMEM184A	2614.910354	0.540791074	1.81E-11	6.46E-10
SLC16A4	84.43169144	0.537585236	1.53E-06	2.28E-05
PPARA	1630.208282	0.535618493	4.34E-13	1.92E-11
SAR1A	14345.51683	0.533550857	2.57E-32	5.01E-30
PSD	76.2894839	0.533550463	2.86E-06	4.06E-05
TNS2	2403.162998	0.532898247	1.50E-17	1.01E-15
SEC61A1	30925.95527	0.531468706	6.75E-49	2.66E-46
OSBPL2	3330.013984	0.530366388	4.82E-23	5.07E-21
LARP1B	1970.454173	0.529987531	3.77E-22	3.65E-20
GOLGB1	16202.70251	0.529855076	1.35E-17	9.08E-16
BTN3A3	798.2272342	0.529418632	8.43E-19	6.40E-17
SLC39A7	26353.09847	0.529341889	3.20E-52	1.42E-49
IKBIP	4301.060906	0.528995876	8.75E-19	6.58E-17
TTC3	15100.37798	0.527614299	1.32E-24	1.61E-22
ARHGEF37	484.9165172	0.526869342	2.02E-13	9.16E-12
ENTPD7	2089.22595	0.525939014	1.35E-33	2.79E-31
SLC41A2	1206.061843	0.5229909	3.87E-14	1.90E-12
GLT8D1	3392.476686	0.521955192	3.53E-35	7.96E-33
SERPINF2	235.8579206	0.520067191	1.35E-07	2.50E-06
UGT3A1	272.3759921	0.519669205	3.65E-09	9.32E-08
ALDH18A1	13339.15197	0.518008379	5.10E-34	1.11E-31
STXBP2	1363.315205	0.517630042	5.87E-12	2.23E-10
MOGS	7025.540991	0.517568752	1.53E-24	1.85E-22
CUL7	4902.654322	0.51568208	1.03E-18	7.65E-17
AKTIP	419.2937047	0.514668981	1.06E-12	4.44E-11
KDELR1	14430.8733	0.513877486	2.68E-26	3.66E-24
ARL2BP	2996.051712	0.513077552	1.07E-29	1.84E-27
DAP	20087.75341	0.512525821	7.77E-29	1.25E-26

USO1_Global_Upregulated

EPOR	1612.944108	0.510360195	1.11E-12	4.59E-11
FBN3	54.45081934	0.510320182	7.80E-06	0.000100698
LINC00888	299.4443278	0.509676401	4.34E-10	1.28E-08
PAG1	203.5786234	0.508853263	6.08E-08	1.22E-06
COPB1	27031.77351	0.508828335	1.59E-36	3.80E-34
BET1	1832.948125	0.508072293	5.58E-14	2.69E-12
TXNDC15	2489.146466	0.505621701	1.26E-33	2.63E-31
ALDH1L2	137.94768	0.504944401	9.53E-06	0.00012098
MAST4	638.9460969	0.503632882	4.78E-13	2.09E-11
PPP2R5B	473.9860179	0.502559298	2.07E-09	5.50E-08
ZNF449	519.6967772	0.502524852	3.58E-12	1.40E-10
JAK3	290.841445	0.502161657	3.37E-09	8.64E-08

USO1_global_Downregulated

symbol	baseMean	log2FoldChange	pvalue	padj
USO1	7202.0684	-2.247346497	1.40E-291	2.37E-287
RPS10	807.660574	-1.538181018	4.28E-88	8.05E-85
MARCKSL1	1274.18245	-0.764745338	1.80E-30	3.28E-28
CRLF3	1271.00855	-0.764562714	1.01E-47	3.72E-45
KLHL38	243.468009	-0.76382378	4.20E-14	2.05E-12
STT3B	19929.7012	-0.763073031	4.70E-53	2.34E-50
MCF2L	432.191245	-0.747034077	6.53E-18	4.50E-16
GLUD2	117.569506	-0.732974917	8.27E-12	3.07E-10
AP1M2	4101.05112	-0.73217155	5.86E-62	4.96E-59
HSP90B2P	75.4717256	-0.68844544	1.06E-09	2.93E-08
C8orf4	666.857322	-0.674337818	6.72E-15	3.60E-13
MACROD1	644.565	-0.672130167	1.30E-14	6.84E-13
LGSN	79.2107159	-0.668610296	2.46E-09	6.45E-08
SLC29A4	158.017734	-0.651071532	1.28E-09	3.51E-08
FHL1	291.222144	-0.64131418	2.01E-11	7.15E-10
EFHD1	452.068372	-0.628158676	1.34E-12	5.47E-11
ELFN2	192.733094	-0.622704763	8.44E-09	2.01E-07
THBS1	2571.69464	-0.599319153	5.68E-41	1.46E-38
ACSS2	3475.15121	-0.599067198	1.85E-27	2.74E-25
SLC16A6	2062.02507	-0.598721179	1.09E-15	6.29E-14
KREMEN2	153.12647	-0.596901619	2.42E-08	5.19E-07
RPL23P8	52.4828635	-0.595409026	1.72E-07	3.10E-06
FOS	665.957486	-0.592786863	5.66E-16	3.34E-14
NR4A1	3660.6025	-0.587083532	5.70E-19	4.39E-17
PABPC3	68.3897316	-0.586651479	2.30E-07	4.07E-06
SV2B	32.7469029	-0.582067572	2.02E-07	3.59E-06
PLAT	456.558861	-0.581975914	1.36E-10	4.40E-09
ACAT2	8461.49067	-0.581638136	2.56E-46	8.51E-44
PXYLP1	1019.84607	-0.578738056	3.02E-20	2.57E-18
HSPB7	4429.17634	-0.564124349	2.99E-18	2.13E-16
MT2A	1428.26489	-0.558277285	7.43E-11	2.46E-09
NDUFA13	226.122181	-0.55710737	2.18E-08	4.72E-07
RPL13AP5	304.111643	-0.551005182	2.80E-09	7.28E-08
IRS1	908.361183	-0.550830076	2.86E-19	2.24E-17
MFAP5	135.086271	-0.549288838	6.44E-07	1.04E-05
LSS	7622.01098	-0.545867242	6.32E-31	1.19E-28
HDAC5	2607.14103	-0.5449246	1.77E-16	1.11E-14
UBASH3B	1948.56718	-0.543648251	5.27E-19	4.08E-17
APOBEC3B	1316.66958	-0.540739944	6.86E-25	8.54E-23
KRAS	3546.38086	-0.536808997	4.30E-17	2.81E-15
MVD	3695.99856	-0.536381656	5.72E-11	1.92E-09
TIMP3	1414.58667	-0.533088688	8.69E-19	6.57E-17
COL9A2	237.764123	-0.530421789	6.38E-07	1.04E-05
SCART1	71.2227037	-0.525110472	3.32E-06	4.66E-05
GADD45B	469.326333	-0.524732231	4.77E-10	1.39E-08
CPNE2	288.168007	-0.523882004	2.32E-08	4.99E-07
NT5E	592.110447	-0.521127413	2.50E-10	7.69E-09

USO1_global_Downregulated

TRIM14	921.92346	-0.520581371	8.50E-16	4.94E-14
APC2	170.062551	-0.519000144	3.72E-06	5.14E-05
NEXN	2406.96948	-0.513798217	4.26E-16	2.56E-14
HR	254.873759	-0.510734933	1.88E-06	2.76E-05
NFATC2	110.314949	-0.506273194	5.51E-06	7.36E-05
FCMR	70.4667453	-0.503906435	9.74E-06	0.00012336
HSD17B7	1808.06194	-0.500975039	3.72E-20	3.15E-18

USO1_Normal vs Fragmented_Upregulated

symbol	baseMean	log2FoldChange	pvalue	padj
IFI44	36.3484323	20.15028704	1.02E-10	1.61E-07
IGFL1	97.4056574	9.250167558	0.002999066	0.067716545
CXCL8	66.4739571	8.72039718	1.42E-08	7.06E-06
SAMD9L	58.5951357	8.538721391	8.18E-16	7.74E-12
CXCL10	54.5978432	8.436146056	1.32E-07	4.53E-05
OASL	797.22557	7.862927456	0.000330616	0.017274681
SERPING1	26.7634274	7.407587945	3.10E-05	0.003119931
TNF	24.9513223	7.306464498	0.000279054	0.015593626
CAPN10	23.8909276	7.242766792	6.13E-11	1.05E-07
MID2	23.8603116	7.242111369	2.19E-10	2.96E-07
NECTIN4	23.1816484	7.200947435	0.001184928	0.039173045
FXSD3	22.5196927	7.157975354	3.06E-11	7.22E-08
ERBB3	22.4569146	7.154670763	4.91E-09	3.50E-06
PIK3IP1	22.078789	7.129075723	4.62E-09	3.50E-06
STARD5	21.1889455	7.070619871	2.37E-09	2.14E-06
CDK20	33.0593681	6.989662338	5.81E-11	1.05E-07
ZNF182	19.9106992	6.981818136	8.80E-09	5.12E-06
IL6	19.2684788	6.934925977	8.30E-08	2.96E-05
PRSS8	18.6803166	6.889427558	5.19E-08	2.06E-05
GPR87	18.5223498	6.877459289	0.000595478	0.024967808
ZEB1-AS1	18.0712683	6.84241945	5.24E-08	2.06E-05
CCL20	17.9963932	6.835689542	0.002370033	0.058584726
C1orf127	28.4756029	6.768763528	4.57E-07	0.000120116
ADAMTS13	16.6872376	6.729288088	8.70E-09	5.12E-06
NPTXR	16.5438969	6.712989064	2.17E-07	6.61E-05
SLC2A5	16.1848626	6.683528662	2.87E-07	8.48E-05
FAM46B	15.9395957	6.659180636	1.75E-06	0.000324419
ANK3	15.5621482	6.626189824	0.00089308	0.03237061
PGGHG	25.5741901	6.611647518	1.06E-09	1.18E-06
CXCL3	15.3361244	6.603366886	3.57E-07	9.93E-05
CD36	15.2191005	6.594523789	3.12E-07	9.08E-05
MAP3K6	14.762087	6.547710693	8.75E-07	0.000194588
ZNF8-ERVK3	14.2180379	6.495407212	3.17E-09	2.50E-06
LOC1019281	14.0866186	6.483247501	1.54E-06	0.000299904
STPG4	14.0746652	6.480273173	0.003106546	0.0692745
SRPX2	13.9036065	6.462257453	0.000286226	0.015872518
PPM1M	13.6519865	6.437439702	0.001207507	0.039642275
LOC1053787	13.259934	6.394689031	0.00137972	0.043189342
SEMA4F	13.2505846	6.394658935	1.19E-08	6.23E-06
CELP	12.6876398	6.332048487	1.26E-05	0.001477713
PLPP7	12.6197349	6.323214679	0.001950454	0.052700018
PRR7	12.5852439	6.318303678	4.54E-07	0.000120116
VTCN1	12.4149823	6.300025698	0.001631632	0.047273907
A2M-AS1	12.3960317	6.298568513	0.000148396	0.009846192

USO1_Normal vs Fragmented_Upregulated

KDM8	12.341502	6.289563208	0.000100032	0.007658347
TNFSF4	11.8894593	6.234875227	3.39E-08	1.39E-05
CCDC153	11.6306788	6.202435688	5.43E-06	0.00078989
MUC12	11.4303381	6.181002908	4.83E-06	0.000724629
SPNS3	11.3921307	6.177299932	7.24E-07	0.000169098
SLC35D2	11.316801	6.16435969	1.81E-06	0.000328565
LINC01819	11.2733593	6.159413495	1.68E-05	0.001850348
ADAM21	11.121683	6.141309913	0.003452246	0.073819362
TMEM145	11.1054349	6.139435505	3.28E-05	0.003215775
TDRD6	11.0049874	6.123967293	8.66E-05	0.006909653
DIO3OS	10.6510559	6.078175475	0.000647295	0.026318693
GPR3	17.681159	6.075998943	5.37E-06	0.000787631
LINC00638	10.5991337	6.071614854	0.0027759	0.064328766
MAP1A	10.5843173	6.068874667	0.000824136	0.030738497
BATF3	10.5057026	6.057610005	8.29E-06	0.001060604
PACERR	10.3344928	6.037023774	6.07E-07	0.000145338
LOC1053786	10.2050036	6.016965527	0.000776525	0.029545435
CCL26	9.65912918	5.937118671	1.12E-06	0.000240505
GKN1	9.46450501	5.91056007	1.95E-06	0.000341169
SLC27A1	62.2106919	5.909358937	8.74E-18	1.65E-13
KRT13	9.45790444	5.90425227	2.28E-06	0.000387984
PCOLCE	9.39565454	5.902557737	2.31E-06	0.000389472
ARHGAP9	9.32278544	5.890350512	2.59E-06	0.000426514
LOC1052743	9.35426824	5.889658855	1.71E-06	0.000324419
SULT2B1	9.36059586	5.887007882	2.14E-07	6.61E-05
SPINK13	9.30055082	5.882448037	0.003710385	0.076980874
SPARC	9.18950308	5.865335537	0.003940594	0.08003934
ICA1	9.07979204	5.852048505	3.91E-06	0.000610389
RNF208	9.01682519	5.840272657	7.84E-06	0.001024635
LINC00870	8.99371698	5.836474085	1.54E-07	5.12E-05
STK31	9.02611325	5.8336817	1.95E-06	0.000341169
RFX3	8.93221847	5.821981678	7.83E-06	0.001024635
ZNF112	8.8536228	5.814141917	0.000172529	0.010948058
SLC28A3	8.73415455	5.793698765	0.000728917	0.028361773
TFF2	8.65258473	5.778430085	0.005096937	0.094032265
HPX	8.48795834	5.755020491	1.89E-06	0.000340542
CYP3A5	8.29971722	5.720483886	0.000114727	0.008474562
LOC1053791	8.27830856	5.718643677	1.02E-05	0.001240079
MATN1	8.28061841	5.714922943	5.27E-06	0.000779268
ACTG2	13.6853894	5.700959243	0.002395927	0.058967572
MYOZ2	8.14632969	5.692138681	0.005333452	0.096223047
GPD1	8.02967912	5.676164914	1.44E-06	0.000284129
GJB5	7.82582537	5.633294816	0.001398526	0.043496916
IL16	7.83295888	5.632588374	1.26E-06	0.000257976
TIMM29	19.8161624	5.626373655	4.03E-06	0.000622861

USO1_Normal vs Fragmented_Upregulated

AMHR2	7.75236756	5.619297711	7.03E-05	0.00588162
BEST3	12.7695352	5.598170279	0.000181169	0.011306616
TMEM40	7.59974084	5.59353392	0.000504666	0.022245301
KSR1	7.49912522	5.571232307	0.002074099	0.054473918
LOC1053701	7.44000419	5.564470367	0.000135628	0.009463898
ISM1	7.31931614	5.535994521	0.000206577	0.012560665
IL17REL	7.28092732	5.528952906	3.77E-06	0.000594836
UNC5C	7.26468741	5.526244642	0.002208121	0.056426437
MOV10L1	12.0969291	5.522248449	0.000226874	0.013423545
NHLH1	7.21870972	5.518164155	8.40E-06	0.001066477
CFAP54	7.1036377	5.493383068	7.29E-05	0.005993158
TMEM51	18.8344328	5.4891308	1.39E-06	0.000276168
RAPGEFL1	7.02778648	5.484900326	1.06E-05	0.001273112
SLC7A7	7.03528976	5.475640448	8.94E-05	0.007104663
SATB2	7.00424653	5.475608728	0.000241602	0.013971558
FBLIM1	19.2129781	5.450721195	1.17E-06	0.000246086
CCDC146	6.88285598	5.449862577	0.001546544	0.045695546
ITGB6	6.88137561	5.448263968	2.45E-06	0.000409654
LRRC4	6.80485062	5.434404068	0.004581027	0.087946409
LFNG	11.3684528	5.426528013	0.004365276	0.08580807
DCST2	11.3227384	5.423800429	0.003533456	0.07469961
LOC1027240	6.625912	5.396051647	7.08E-05	0.005896531
CCER2	6.45401727	5.353177411	0.000120648	0.008807878
PRRG4	6.41051007	5.349715808	0.00017164	0.010928332
LAMA2	17.4480266	5.326802735	8.44E-07	0.000189947
C2orf16	6.27687611	5.317739796	0.002566722	0.0614726
GPSM1	6.28588362	5.316696901	0.000424382	0.01971758
SPATA12	6.23666555	5.308374653	0.001012617	0.035337576
ZCCHC24	6.20048072	5.298800715	0.002677671	0.063056992
GMPR	6.08814814	5.279500535	1.13E-05	0.00133892
ZXDA	10.2685292	5.278627136	0.004707258	0.089551559
FBXL14	6.09803826	5.274546844	0.002293085	0.057612248
PATL2	6.08284243	5.271812084	0.000904739	0.03260984
PCSK4	6.04407904	5.266607082	0.00056994	0.024367764
IL15RA	5.90484093	5.228214331	0.002760592	0.064052505
RAPSN	5.91092204	5.227230514	3.31E-05	0.003224591
A2M	5.79514194	5.205912019	0.000504426	0.022245301
ATCAY	5.79026172	5.198967391	0.00123745	0.040360147
FBXL13	5.75527368	5.188589541	0.004993109	0.092750191
ENGASE	15.2118729	5.186544291	0.000908799	0.03260984
MED12L	9.32253342	5.146467487	4.83E-05	0.004568603
LINC01687	5.52127508	5.136255906	3.23E-05	0.00320238
PRKCG	9.0931535	5.103120536	0.00148971	0.044644085
COL18A1	15.0023828	5.097990915	5.23E-06	0.000779015
MAML3	5.35693651	5.08872919	0.003392158	0.072975776

USO1_Normal vs Fragmented_Upregulated

LINC00926	5.30309865	5.072169837	3.40E-05	0.003292515
GLI1	5.27155854	5.063493351	0.000916941	0.032777614
SLC44A3	5.23365116	5.055397156	0.00523966	0.095179602
ANKRD55	5.25136033	5.055245068	0.001116447	0.037353336
CNIH2	5.18802071	5.043249485	0.000352204	0.017619534
RHBDL2	5.1925931	5.04178955	0.000893573	0.03237061
PAQR8	5.18444648	5.039295786	0.000114223	0.008470448
GMFG	5.14889165	5.032781831	0.00454664	0.087820108
KLLN	5.13157523	5.027112528	0.000466217	0.020941007
COL25A1	5.12905357	5.01878973	3.56E-05	0.003430159
RAPGEF4	14.1189772	5.009679491	6.73E-06	0.000935158
ELMO3	4.99774649	4.989046434	0.001088447	0.036939717
PIWIL3	4.99427554	4.98375884	0.000134867	0.009445715
HCG27	4.98635278	4.976739179	0.000170783	0.010910465
TAF4	27.7991222	4.972340315	8.73E-10	1.03E-06
PTGS1	8.2596266	4.960121732	2.95E-05	0.003027454
CCDC87	4.8994329	4.955609241	0.001012849	0.035337576
NEBL	4.81250644	4.938342766	0.000929702	0.033046378
NIPSNAP3B	4.82588617	4.933236735	0.004712271	0.089556825
ATXN2-AS	4.81118653	4.928168796	0.000279234	0.015593626
POU5F1P4	4.75935372	4.914052082	0.00015961	0.010430298
SLC45A2	4.75109508	4.909025546	0.000231248	0.013538409
LOC1053765	4.61740899	4.872315477	0.000134782	0.009445715
MLYCD	7.71133977	4.852623801	2.87E-05	0.002960903
ANKHD1	7.65843517	4.847646543	5.18E-05	0.004726922
LINC01671	4.54731554	4.846822825	0.000166417	0.010703911
BEST4	7.63172453	4.846425545	0.000426349	0.019760431
CAMK2A	4.54052477	4.845467265	0.001425523	0.043903315
QPCT	12.9954477	4.842416724	0.000121899	0.008831828
KCNIP2-AS1	7.60887199	4.842162409	0.005019163	0.093121231
ICA1L	7.28273797	4.796128479	5.14E-05	0.004726922
USP27X-AS1	4.36548564	4.791583049	0.000915427	0.032777614
LOC1019290	4.35798158	4.791241844	0.001329066	0.042310833
SERTAD4	4.28698157	4.763627716	0.001337995	0.042381046
LOC339059	4.22037995	4.742873002	0.005156776	0.094582571
LINC01136	4.1780605	4.739416738	0.001412203	0.043850182
LSM14B	7.06058868	4.724118911	0.005096238	0.094032265
CD34	4.16842041	4.722458528	0.001485543	0.044644085
FSTL1	3.98051267	4.66702627	0.003084437	0.069025675
KCNRG	3.92662847	4.636290745	0.002562136	0.0614726
BRWD1-AS2	3.90675442	4.633447659	0.002177667	0.055874739
LINC01679	9.89205533	4.62155759	0.000269595	0.01517272
NCRNA00250	3.84951198	4.613989119	0.002577369	0.061615728
ARHGAP44	3.8301963	4.602811763	0.003338124	0.072429651
MAMDC4	10.8904185	4.59250471	0.000153402	0.010107413

USO1_Normal vs Fragmented_Upregulated

PNLDC1	6.39709573	4.587307436	0.000760528	0.028995126
HDAC11	30.0820736	4.580238178	2.12E-07	6.61E-05
OTUD1	3.7243534	4.570803333	0.000645678	0.026318693
MNX1	6.19276479	4.552545561	0.001217256	0.039893093
SEMA3F	6.2796169	4.55049849	0.003253225	0.071222975
FLJ31356	3.56496331	4.496134454	0.004793702	0.09067821
LOC1053724	3.47743665	4.465422066	0.000712504	0.027953224
REPS2	23.4103797	4.457913555	2.18E-08	1.01E-05
SNORD15B	3.47969626	4.456208736	0.001912323	0.052257273
DGKQ	9.28845393	4.453314025	0.000560224	0.024022311
PITPNM2	16.1295822	4.426513395	1.45E-05	0.001655487
LOC440700	5.69099023	4.423430445	0.000553692	0.023903807
MEIS3	5.65597438	4.403085231	0.000471454	0.021126037
KIAA1107	9.4616385	4.396424349	0.000146373	0.009751403
LHB	5.63699238	4.392429585	0.001102167	0.037217815
TWIST2	9.29392052	4.335587063	0.000812629	0.030470613
LOC1019293	3.12176863	4.307724258	0.001116619	0.037353336
THEM5	3.09662295	4.304350866	0.003126449	0.06955429
CYP2E1	5.26876285	4.300525819	0.000460665	0.020805965
ROBO2	3.09380123	4.295832536	0.005293652	0.095844317
ELFN2	3.07988438	4.280017583	0.004448304	0.086451619
TMEM106A	5.15808697	4.276488497	0.000500581	0.022195533
CPNE2	5.18732543	4.27405585	0.00527764	0.095685695
TAS2R20	2.93404281	4.215375225	0.001860138	0.051257352
ALDH1A2	2.92063547	4.204651311	0.002568131	0.0614726
SCARNA6	2.67814699	4.086237771	0.00498802	0.092750191
ADAM20	2.66114951	4.072343882	0.005664281	0.099887464
SLC26A5	4.52819828	4.060388463	0.002055513	0.054060837
SLC9A7	2.61577414	4.05545853	0.005184982	0.09500777
H6PD	44.3366121	4.048144269	7.59E-08	2.76E-05
TFF1	74.8991205	4.043955593	7.42E-07	0.000171208
PNPLA7	11.8517633	4.00451458	0.000363663	0.018002257
TOLLIP-AS1	24.9238848	4.002147251	1.79E-06	0.000328107
VAC14	39.8519453	3.99416951	1.19E-05	0.001404968
RGS5	15.6477822	3.983838313	5.51E-05	0.004919105
TNIK	6.47836754	3.962497628	0.000383737	0.018417439
GPR82	4.04630447	3.922077645	0.004925504	0.092127866
LPAR2	6.88948642	3.920540806	0.000490604	0.021880466
KCNJ18	77.9710454	3.902089035	0.000152137	0.010059133
VMAC	15.6735524	3.84734373	6.41E-05	0.005531202
CCR10	9.7597866	3.828614223	0.000367322	0.018008322
ALG10B	22.0179998	3.797492767	1.96E-05	0.002115239
ISG15	2612.85242	3.782843191	0.005027857	0.093121231
TSPYL4	48.1470318	3.767629282	6.53E-06	0.000915345
COL4A3	13.555746	3.76132462	0.00102623	0.035672813

USO1_Normal vs Fragmented_Upregulated

CAVIN4	13.8647106	3.747812223	0.001728895	0.048506546
HECA	22.2093487	3.732283118	1.15E-08	6.21E-06
LOC440028	21.2014742	3.683697349	0.000139588	0.009546736
LINC00854	11.4409854	3.590778069	0.000176261	0.011094508
LBX2-AS1	7.64919581	3.498980603	0.004268986	0.084353735
RALGAPA2	20.341344	3.45488581	0.000684874	0.027150868
SDC3	52.9428082	3.441656577	6.82E-08	2.53E-05
PAQR6	11.0480184	3.434722295	0.000827342	0.030797308
LOC731157	7.27338984	3.430396369	0.002410671	0.058967572
PRPH	13.2245001	3.429751125	0.001322771	0.042181434
TRANK1	13.848876	3.419456684	0.001432566	0.043955439
SYTL3	16.5821757	3.413268055	0.000695464	0.027455597
PURB	9.59960195	3.409799128	0.000622536	0.025759627
SPSB1	33.0438033	3.400572688	0.001560179	0.04588334
KDM4B	16.6046906	3.397148311	0.000647384	0.026318693
DCDC2B	9.83803666	3.386371267	0.000579007	0.024604529
HIST3H2BB	7.09665842	3.351997041	0.001053818	0.036298159
HIST1H3E	6.52570069	3.346662033	0.002299459	0.057612248
NEB	12.671785	3.32585306	0.00034806	0.017551514
ETS1	35.2964291	3.313896166	0.000644807	0.026318693
LINC01759	22.0332958	3.267006603	0.000676141	0.027068615
SLC2A4	14.5250155	3.228409564	0.002374841	0.058626945
UVSSA	20.9987165	3.177502949	0.002195191	0.056171948
SPATC1L	15.1719881	3.171279801	0.000305253	0.016445411
ACP5	10.2829197	3.160783654	0.004535453	0.087694691
LINC01600	8.13774291	3.159398631	0.001677646	0.047705681
DYNLRB2	19.9331647	3.149562968	1.01E-05	0.001235197
PLXNC1	16.8309175	3.130251674	0.000295087	0.01603473
SRGAP3	27.1482526	3.129545257	0.000103716	0.007845089
SELENON	14.8676054	3.091476268	0.000219771	0.013215209
POU6F1	18.1586821	3.032492766	0.001519765	0.045319114
IQSEC1	39.9949269	2.996280418	3.06E-05	0.00311314
SAP30L	38.0578738	2.962210279	3.05E-08	1.31E-05
ANKRD1	27.3042746	2.934413687	0.000680156	0.027088473
SPATA32	6.60090661	2.925146642	0.003411724	0.073230085
IFIT3	374.166382	2.914874281	0.002093075	0.054820011
KLF13	35.9122479	2.907488772	2.33E-05	0.002465276
SLC25A27	18.9672323	2.904654512	0.000138852	0.009546736
STX3	104.664258	2.892329638	0.000677073	0.027068615
PCAT7	13.2949049	2.881653595	0.003794366	0.078021318
ATG16L2	49.7788842	2.863965125	1.07E-05	0.00128585
GALNT10	58.6363523	2.84542546	1.83E-08	8.90E-06
VSIG10L	11.4431832	2.839919494	0.000501189	0.022195533
DDC	11.6869703	2.836621266	0.00548051	0.098061022
LRCH1	14.68848	2.823399976	0.00052284	0.022780907

USO1_Normal vs Fragmented_Upregulated

DPH6-DT	9.41854937	2.79345678	0.003837097	0.078495951
TTC3-AS1	6.64919354	2.79306996	0.004240468	0.084172199
CASC10	17.4735184	2.786312697	0.00026957	0.01517272
ANKRD16	10.9337799	2.781174252	0.00225966	0.057355943
DNMT3A	11.0642006	2.779615053	0.000603534	0.025249625
ZC3H11A	34.5213267	2.774583107	3.10E-05	0.003119931
OMD	10.1020882	2.771955015	0.005326356	0.096223047
SNORD3B-1	11.8088647	2.750464709	0.00034307	0.017486417
CROCCP3	16.859123	2.692898539	0.000668801	0.026965959
SH2B3	14.3347561	2.677424831	0.003399443	0.073049396
ATP2C2-AS1	11.9722722	2.670954528	0.004509438	0.087459976
MIR374C	9.31849244	2.63528347	0.001669171	0.047607867
DNAH1	19.7206475	2.63170564	0.000446296	0.020434527
HEATR5B	153.806711	2.533454734	0.000220836	0.013215209
LINC01588	55.912074	2.531004375	0.003280109	0.071624546
MB	92.6541607	2.517435545	1.19E-10	1.73E-07
LINC00707	30.8948317	2.516966219	0.003970077	0.080207429
MIRLET7BHG	41.873803	2.508023228	0.001340792	0.042398639
ANKRD33B	42.211361	2.503579721	0.004818806	0.09085107
SCARA3	67.6049091	2.469237496	5.85E-05	0.005120343
RNFT2	29.7767916	2.405325829	0.004811317	0.090800408
LOC1019287	9.40811684	2.390229194	0.004228377	0.084078461
SPATA5L1	115.166205	2.354400512	0.000209931	0.012723697
HOXC-AS2	25.0272908	2.354039309	0.004552339	0.087820108
KIAA1211L	24.8961581	2.329685466	0.004893523	0.091802112
NPHP4	105.047389	2.324019483	0.00164143	0.047311115
LOC1027237	10.0386138	2.307771994	0.003591165	0.075448866
SPECC1L	85.9844528	2.303728637	0.001115087	0.037353336
ABHD6	38.7180209	2.270706945	0.004571562	0.087853904
DVL1	17.9225369	2.267191197	3.26E-05	0.003207504
TUBA4B	23.7471338	2.2554255	0.003950746	0.080159454
TNFAIP3	487.033993	2.204473705	1.72E-06	0.000324419
ZNF620	37.4034581	2.193599029	6.89E-05	0.005818614
ZNF8	31.4379413	2.175665424	0.001924199	0.052430272
SMAD6	7.63333669	2.160797061	0.004564148	0.087820108
PLD4	13.4025609	2.156979671	0.002914749	0.066567513
TYMP	88.4522146	2.0881035	0.002688312	0.063228837
RS1	64.089412	2.087379632	0.003438347	0.073634357
TPM3P9	61.4642314	2.06489758	0.001031719	0.035757171
ZMYM6	46.8996989	2.052305487	0.00267069	0.063044227
RAD51B	104.087063	2.049152647	0.000201108	0.012267608
BMPR2	44.6169118	2.048598582	0.000180819	0.011306616
PRKACA	34.3685252	2.047346228	1.28E-08	6.57E-06
NDST1	138.03998	2.043840952	0.004482022	0.087017498
TBC1D25	44.1608277	2.041729342	0.002760341	0.064052505

USO1_Normal vs Fragmented_Upregulated

TMEM129	57.1969965	2.021274454	0.001161335	0.038663462
MCF2L2	12.8765533	2.016611276	0.005109387	0.094089485
NSMF	100.445301	2.004729487	7.29E-06	0.000978015
FHL1	417.831899	1.944981504	0.00236628	0.058584726
LINC00355	119.370162	1.916538528	4.95E-07	0.000124823
TRIM41	67.8037424	1.854838444	0.002484336	0.060147639
TEPSIN	68.6115933	1.846981137	0.005572636	0.098946987
LOC1005074	73.6881332	1.787172918	0.00145376	0.044055442
NOM1	79.1166447	1.786227887	1.69E-12	8.01E-09
ATL1	44.9534351	1.680077512	0.002942118	0.067030675
KIAA0930	95.9935172	1.670030639	0.000753581	0.028902768
SH2D3A	81.090542	1.669100888	0.001268335	0.041139314
PCNX1	147.396098	1.625475559	7.02E-06	0.000960453
SPATA2L	51.8533627	1.589594762	0.000950785	0.03354356
PIP5K1C	51.9984202	1.588325688	0.000932602	0.03308724
MIR3074	21.5416097	1.58753687	0.003584698	0.075402272
ZNF594	58.4365611	1.574779826	3.21E-06	0.00050971
ZSCAN29	162.83567	1.570323418	0.001345164	0.042465862
HIST2H2BC	13.871024	1.563867827	0.004690028	0.089502202
LOC644135	27.5984545	1.552489638	0.001084102	0.036939717
LSS	440.602113	1.546293764	5.00E-09	3.50E-06
IL32	321.366372	1.535609555	0.000902129	0.03260984
POLH	319.328084	1.530353423	8.93E-09	5.12E-06
PSRC1	595.176034	1.508805181	0.001415371	0.043876508
PLXNA1	152.730853	1.503820574	0.003015785	0.067810331
MYCBP2	386.37018	1.488803567	2.64E-08	1.16E-05
RPS6KA3	101.860905	1.477685793	0.000921647	0.032851454
SNAPC1	90.3438282	1.425159235	1.15E-06	0.000244665
TEX2	249.625985	1.413479536	0.00195082	0.052700018
RILPL1	63.8026076	1.398107358	0.002405272	0.058967572
TRAK1	122.49686	1.386321325	0.000315351	0.016724279
LRRC47	126.775111	1.283638686	0.00067553	0.027068615
TRIM24	113.49818	1.279165348	9.94E-05	0.007639138
LCMT2	182.235699	1.278581056	0.002361768	0.058584726
AHNAK2	338.487424	1.267403515	2.92E-06	0.000468941
TAF5L	94.4188971	1.253785158	0.002103435	0.05498819
COL4A3BP	142.698865	1.237103447	0.002882197	0.06590368
REXO4	205.828671	1.198142022	0.003008297	0.067803214
ARSB	126.417684	1.196822106	5.88E-09	3.84E-06
MKRN1	345.534542	1.186899312	0.000330695	0.017274681
KDM1A	127.258646	1.173560989	0.000283076	0.015744035
CAPRN2	77.6838107	1.164180127	5.44E-05	0.004876681
LIMS2	35.7205001	1.162624277	0.005109989	0.094089485
USP24	175.646548	1.156515701	0.001424177	0.043903315
TCIRG1	157.451503	1.141025949	0.00314324	0.069763691

USO1_Normal vs Fragmented_Upregulated

CARD14	380.10199	1.125896751	3.21E-08	1.35E-05
PRKAG2	272.178836	1.111130879	0.003389211	0.072975776
AHNAK	893.680677	1.09604482	6.80E-09	4.29E-06
RNF146	155.127624	1.082310448	0.002171194	0.055798805
EFHC1	135.678392	1.063891774	0.001966453	0.052856143
FMNL1	194.477773	1.060541136	0.002706144	0.063499675
CNPPD1	200.360293	1.058982638	1.29E-09	1.36E-06
FCHSD2	85.2704581	1.0520337	0.00074486	0.028863308
ZC3H12A	299.206545	1.041660533	0.000338043	0.017465549
SCPEP1	345.157308	1.038810579	9.61E-07	0.000211336
APOL2	1049.83133	1.034782137	0.002167857	0.055798805
POLK	208.804871	1.021680889	0.003654699	0.076280753
PRRT3-AS1	72.5363345	1.013882538	0.000141603	0.009546736
CDK10	226.945267	0.999405641	1.54E-07	5.12E-05
PKIG	155.843766	0.994088928	0.003871675	0.078978826
FAM214A	74.4269155	0.990934874	0.000460096	0.020805965
FUOM	384.652596	0.983518531	0.003598883	0.075448866
CKAP2L	491.652141	0.977350778	0.005023386	0.093121231
TADA2A	186.479285	0.969134109	0.001117807	0.037353336
USP2	268.438583	0.968049875	8.32E-05	0.006697562
PSMB8-AS1	311.553415	0.958287131	0.002751131	0.063990013
CREB3L1	445.490444	0.949672747	0.000414144	0.019336937
SPATA20	553.722019	0.943961844	7.81E-15	4.92E-11
ANKRD28	329.558244	0.941220615	0.003529807	0.07469961
SEMA4G	117.873906	0.932300098	0.005425857	0.097346262
TAP1	1707.45304	0.931533779	0.002006454	0.053289399
SBF2-AS1	229.761586	0.92735074	0.000141863	0.009546736
IFNGR1	513.882428	0.912024749	5.39E-05	0.004872331
TRIM16L	1182.77228	0.874156586	0.002270405	0.057397536
TMCO4	500.637119	0.858954593	0.004166597	0.083199947
SOD2	1454.24084	0.84929949	5.53E-06	0.000797662
ADAMTSL5	152.850821	0.848052438	0.001862179	0.051257352
TMEM53	185.543491	0.845989009	0.002019462	0.053451067
ZSCAN16-AS	211.787245	0.845245683	0.000458288	0.020805965
PLK2	2072.23897	0.841505166	5.79E-06	0.000822736
SP100	411.374555	0.829247549	7.86E-06	0.001024635
LOC171391	91.7155247	0.828945013	0.004881694	0.09167114
ATP6V1A	725.596105	0.824186015	0.00014068	0.009546736
WFDC21P	656.299599	0.817786502	0.003775801	0.077948027
LINC00339	223.741374	0.812404803	0.003015653	0.067810331
LIPE	68.0560332	0.795563279	0.002859207	0.065616022
NEK1	242.929448	0.792630678	0.005564991	0.09890411
ZNF557	237.266689	0.782078184	0.003067217	0.068803181
PBX1	143.610437	0.774320747	0.003179041	0.070252767
SLC25A37	731.470266	0.76656209	0.000103614	0.007845089

USO1_Normal vs Fragmented_Upregulated

MTCL1	143.95853	0.765508635	0.001051985	0.036298159
CENPL	697.813478	0.761255465	0.003135929	0.069683225
ZNF623	215.134777	0.756081371	0.004939838	0.092213556
STX7	194.492744	0.747234301	0.000123609	0.008887645
GLA	1789.86675	0.743998144	5.60E-09	3.78E-06
DNAJC6	171.830506	0.743090794	0.002706544	0.063499675
SNX2	1556.21588	0.739056415	0.002225316	0.056789102
NEFH	597.611458	0.735868893	0.000137191	0.009537775
LMAN2L	683.566545	0.726049411	0.000238715	0.013846925
LRRFIP2	578.502918	0.725743726	0.000521859	0.022780907
ZNF322	106.099148	0.719913465	0.00058771	0.024862617
C15orf39	202.031176	0.717177697	1.49E-05	0.001691227
CEP72	548.101477	0.716279309	0.00396275	0.080207429
TNFAIP2	230.39251	0.715180907	0.000346879	0.017538702
PPP1R35	225.048134	0.715038231	0.00346966	0.073886567
ARSJ	144.483633	0.713895699	0.00059078	0.02488116
WASHC3	585.166321	0.712285707	0.000287676	0.015906318
RAB30	219.895253	0.712057723	0.00023123	0.013538409
ZBTB38	1473.5339	0.711892397	6.89E-06	0.000950947
PISD	1180.03356	0.707078926	0.002458339	0.059675481
LOC1053718	315.889866	0.706308326	0.000906934	0.03260984
GCAT	944.423158	0.705026004	9.44E-05	0.007320269
SELENOM	2891.99657	0.700924663	0.000723407	0.028263689
FNBP1L	1150.39751	0.699451035	0.00210822	0.05498819
PSME2	2381.26671	0.696260885	0.001942698	0.052700018
LMO7	629.676513	0.695225621	0.005058974	0.093514376
ACAA1	925.315328	0.694886698	0.001095856	0.037070917
PBRM1	285.376093	0.694535532	0.000583134	0.024724366
MAP2K3	3566.63843	0.691619885	0.000516337	0.022601676
HBB	491.387981	0.686977884	0.001488783	0.044644085
EEA1	344.841025	0.685101239	5.91E-05	0.005149252
GBAP1	187.746469	0.680361761	0.000349449	0.017555296
PRSS23	11232.4416	0.677387604	0.001715139	0.04840789
ANKRD49	328.157576	0.672903109	0.003165145	0.070085346
SPIN2B	108.203462	0.671119499	0.00026529	0.015110361
PPP2R1B	1000.1495	0.670347207	0.000662963	0.026845044
KYNU	1812.04851	0.663950907	0.003155645	0.069956903
SERHL	274.551787	0.656034009	5.57E-05	0.004945475
LAMB3	968.565967	0.650244869	0.00279302	0.064409772
CYP51A1	211.613672	0.629029851	0.000141833	0.009546736
TMBIM1	591.222685	0.608368931	0.000199553	0.012212098
SRGAP1	601.174376	0.605765208	0.001434967	0.043955439
DHRX	737.114838	0.603247851	0.001540229	0.045651607
RITA1	1506.21898	0.595525165	0.001960807	0.05281889
ERG28	777.607571	0.595515029	0.000802427	0.030287221

USO1_Normal vs Fragmented_Upregulated

NFS1	1140.12733	0.592401485	6.81E-07	0.000160974
STK38L	1096.68126	0.59021653	0.000192003	0.011826643
PRPF38A	1315.18523	0.583050915	0.001422418	0.043903315

Normal vs. Fragmented_Downregulated

symbol	baseMean	log2FoldChange	pvalue	padj
N4BP2L2-IT2	53.56118504	-8.689032179	0.004524173	0.087566123
SYNE4	30.4907175	-8.552129888	0.005222816	0.0951142
HCP5	14.08655156	-7.922804458	0.001701605	0.048169682
PPFIA4	11.30389238	-7.605995351	0.004950853	0.092328037
GAL3ST1	7.098080936	-6.44407994	0.000680435	0.027088473
WFIKKN1	4.463278896	-5.749899341	0.00249622	0.060208562
NDUFA4L2	193.0987489	-5.240049595	1.75E-09	1.65E-06
PRSS37	36.65350678	-5.092847674	0.000342972	0.017486417
SSC5D	14.27166805	-4.979983603	0.000248212	0.014223312
TEX53	12.30312871	-4.765619017	0.005340843	0.096223047
LRFN3	11.96881109	-4.644820084	2.93E-06	0.000468941
SNORA13	6.138564559	-4.100202982	0.002733874	0.063887682
PLCB4	11.9952435	-4.01437484	0.003716739	0.076980874
RGS22	10.59787241	-3.825888468	0.000333755	0.017291246
KNDC1	9.903346679	-3.809461585	0.002628539	0.062287808
ESPNL	19.71732756	-3.418176005	0.004795252	0.09067821
GCNT7	11.37652933	-3.366326692	6.78E-05	0.005775605
LINC02361	14.84174085	-3.339675653	0.002243885	0.057032077
ZNF205	11.46209679	-3.316369727	0.000186677	0.011573944
FCRLB	34.43830229	-3.191306802	0.001642774	0.047311115
TJP3	33.01056406	-3.144095262	0.000510687	0.022458348
TEDC1	29.83714195	-2.694301623	0.004432778	0.086402101
ME3	142.4157283	-2.652746583	5.50E-10	6.94E-07
TTC6	28.38916544	-2.622658614	0.00041195	0.019336937
ADORA2A-AS1	19.24201347	-2.561802722	4.90E-07	0.000124823
WDR59	83.57629347	-2.508744006	0.000524809	0.022814121
VPS26B	99.76745497	-2.481033309	0.003180136	0.070252767
FOXB1	14.0847591	-2.446658666	0.003257952	0.071222975
TTBK2	72.38154372	-2.380099607	0.000359659	0.017897761
TSSK3	52.19781972	-2.328527782	0.005235896	0.095179602
NACC1	60.67944402	-2.271801942	4.11E-06	0.000626334
LMBR1	89.48661808	-2.161088755	0.00193836	0.052664353
SOS2	23.13347807	-2.144812994	0.002413585	0.058967572
MINDY4	20.36769827	-2.041982031	5.05E-05	0.004725925
LOC284930	46.98691582	-2.023349532	0.002586216	0.061674951
HIST2H2BE	46.19806661	-2.001127868	0.005592841	0.099066922
SLC9A5	54.91423454	-1.995266579	8.28E-05	0.006687815
WEE1	225.8189529	-1.991888363	1.36E-05	0.00158621
CD27-AS1	32.78837731	-1.975698363	0.000146452	0.009751403
COL6A6	28.67461615	-1.966554544	0.00245131	0.059581331
SCRIB	60.83843688	-1.959299343	0.003688846	0.076655038
TMEM260	150.9682505	-1.943525059	0.002164685	0.055798805
VLDLR	149.5859808	-1.927651866	9.45E-05	0.007320269
2-Mar	86.83866413	-1.917557093	0.004255617	0.084353589

Normal vs. Fragmented_Downregulated

SLC45A4	100.3656922	-1.913148567	0.003530683	0.07469961
EID2	46.64248262	-1.907715052	0.00441678	0.086371563
CCNJ	79.74920541	-1.817764028	0.000448136	0.020469187
LIG4	135.8808255	-1.785193715	0.00085081	0.031386856
METRNL	83.42908531	-1.716438218	0.002088547	0.054777277
FIZ1	42.33700692	-1.699321613	0.002717332	0.063594985
GOLGA8A	228.0250601	-1.687808271	0.000607689	0.025311453
CPSF4	194.9569794	-1.672755605	0.002790875	0.064409772
SDCBP2-AS1	105.3671106	-1.666854485	0.003218087	0.070760504
KCTD15	302.439998	-1.642247304	5.20E-05	0.004726922
FILIP1L	29.95728101	-1.626252256	0.000411473	0.019336937
RYR3	43.36425528	-1.569547571	0.003308261	0.072072839
KIAA1958	61.12973654	-1.548712725	0.003956838	0.080197009
TMEM62	81.51179994	-1.525296554	0.005390086	0.096980522
SMURF2	75.75935247	-1.49721224	2.06E-05	0.002200497
BRPF3	148.9486498	-1.484576828	1.09E-06	0.000236647
MCMDC2	55.97084695	-1.470456877	3.05E-05	0.00311314
ATP2A1-AS1	49.18088993	-1.464815823	0.000476881	0.021318704
ING2	139.493492	-1.464375731	0.000494933	0.022021627
YJEFN3	76.26450336	-1.447155219	0.004630526	0.088716557
CCDC85B	90.22614225	-1.445819616	0.004695198	0.089502202
HELB	83.33005126	-1.444525331	0.002880503	0.06590368
GXYLT1	107.3707796	-1.436204386	0.001660136	0.047547686
UBE2D1	141.7797107	-1.433586104	0.000298906	0.016195755
HEIH	63.85186353	-1.431322847	0.001975999	0.052926541
AKTIP	99.46570302	-1.425967288	6.72E-08	2.53E-05
COPRS	203.5642902	-1.411674313	0.004059072	0.081569652
ATPAF1	68.30577347	-1.41102324	0.004779089	0.09055368
FAM219B	159.9028848	-1.401149237	0.001396933	0.043496916
CHST14	55.33100405	-1.399815089	0.004293544	0.084750426
CEP162	138.9470668	-1.399195181	0.000577323	0.024588249
FAM207A	46.21237896	-1.389971021	0.000648164	0.026318693
SLC35G1	315.6815122	-1.382226571	0.001651601	0.047464703
LDLRAP1	307.6969761	-1.380183729	0.000367595	0.018008322
VAMP1	151.1294075	-1.354655262	0.002448241	0.059581331
TOMM70	259.1875565	-1.344329422	0.001553217	0.0458211
ADM2	64.34480389	-1.337868305	0.001980218	0.052964517
LYSMD4	109.5999044	-1.337271892	0.000869231	0.031790619
AGRN	64.85451817	-1.32011879	0.002787439	0.064409772
GABRE	633.8816752	-1.30607727	0.000813731	0.030470613
CROCCP2	106.9189595	-1.30387436	4.68E-05	0.004473059
CHAC1	349.9173052	-1.279282487	0.003256385	0.071222975
PKN3	161.3170927	-1.27867409	0.003358906	0.072757058
TMEM231	106.8855739	-1.273368342	0.002627639	0.062287808
KANK2	545.2912779	-1.269977107	0.005406328	0.097180291

Normal vs. Fragmented_Downregulated

C16orf46	38.4855733	-1.260147266	0.002243698	0.057032077
IDNK	132.1208021	-1.254983089	0.001450996	0.044042259
MATR3	112.7947109	-1.250780471	0.003124077	0.06955429
LZTS2	236.4689796	-1.211569933	0.001613373	0.047009067
MARCKSL1	148.5076722	-1.206764914	4.43E-07	0.000119539
TMEM250	162.4035704	-1.203755617	0.004559657	0.087820108
PPFIA3	136.5560252	-1.176089547	0.005425505	0.097346262
ARFGEF1	126.0527109	-1.168503525	0.004802994	0.09073389
HSPA1B	287.2944025	-1.166691284	2.92E-06	0.000468941
PRSS56	1417.899661	-1.15686985	1.91E-05	0.002077712
SLC19A2	234.0731871	-1.154097922	0.000612579	0.025459041
TAF1C	489.2820596	-1.142712381	0.000866992	0.031790619
PPP1R3C	199.5640404	-1.140473092	0.001273364	0.041231687
NPDC1	194.420123	-1.137984731	0.000952982	0.033558438
TRIM35	282.9948648	-1.134395827	0.001448356	0.044042259
RPP25	375.8444145	-1.126588169	3.43E-07	9.74E-05
SPNS2	45.41337194	-1.124002782	0.001085658	0.036939717
NOP14	204.3121126	-1.121180453	0.001873578	0.051496152
HSPA1A	2795.20706	-1.117329883	1.86E-05	0.002035077
NUDT16	98.6782567	-1.116251013	0.003798369	0.078021318
NR2F6	946.8757533	-1.097325476	0.002266492	0.057397425
EYS	53.3660648	-1.094992811	0.002336312	0.058361495
ZNF397	301.9130535	-1.09258887	1.29E-06	0.000260214
PLEKHH1	106.1452628	-1.083587281	0.002286198	0.057565923
PLEKHF2	145.27493	-1.078652337	0.002673795	0.063044227
DNAJC25	118.7766567	-1.074329691	1.39E-09	1.38E-06
CHTF18	153.5642196	-1.073130924	0.001259589	0.040996266
SLC25A40	146.2367259	-1.068577927	0.005481253	0.098061022
DNAJB9	1574.398981	-1.044853139	2.34E-07	7.03E-05
KANSL1L	106.5141798	-0.980594487	0.000615575	0.025527445
LOX	557.7551136	-0.975786195	1.62E-07	5.28E-05
ZNF74	242.745452	-0.973386736	8.55E-06	0.001078067
OLMALINC	225.3357437	-0.960887561	0.001996562	0.053107294
PTPN4	182.7039682	-0.960712118	0.001947169	0.052700018
GAS5-AS1	141.3277674	-0.960578319	0.00029161	0.015913536
TTN-AS1	76.00765786	-0.956419674	0.003794364	0.078021318
PAPOLA	640.9331758	-0.94777438	0.002825	0.065067905
OPA3	403.0695835	-0.945623245	0.000726835	0.028339062
B4GALT2	221.2120946	-0.942970462	0.001502621	0.044959752
ELAVL1	347.6746465	-0.927712584	0.000122735	0.008858444
PIGX	189.0086695	-0.915896793	9.39E-06	0.001160305
PRKCI	165.7992348	-0.913561359	0.003818424	0.078230109
RECK	273.8915892	-0.892816701	7.53E-06	0.0010025
WDR53	546.6551255	-0.886802594	0.003598281	0.075448866
POLM	260.6094393	-0.882131259	0.00434979	0.085681809

Normal vs. Fragmented_Downregulated

TULP3	881.7776161	-0.866121368	0.000743862	0.028863308
GRPEL2-AS1	81.83039232	-0.863185739	0.000851447	0.031386856
P4HA2	572.029448	-0.854943371	0.002619761	0.062235783
LOC101927027	219.2952677	-0.845689307	0.00043194	0.019956744
FAM117B	113.1652462	-0.843751359	0.000183262	0.011399622
CCDC117	475.5738703	-0.839495079	0.002015728	0.053451067
CHSY1	151.9389124	-0.837123915	0.001749279	0.049005737
CPD	352.2013519	-0.830001487	0.000341633	0.017486417
BNIP3	2357.555156	-0.819707044	0.001698773	0.048161603
LOC648987	416.8185836	-0.816249834	0.001568063	0.045985109
GPC5	107.5609003	-0.816130345	0.004021915	0.081081454
XPR1	336.7405388	-0.813010149	0.000570858	0.024367764
STK4	451.3459623	-0.812609381	2.37E-05	0.002491542
EDC4	325.8674984	-0.811247106	0.005221734	0.0951142
C21orf58	164.6010344	-0.80441626	0.001184823	0.039173045
ARL5B	399.5930869	-0.783805068	0.00075933	0.028995126
TPD52	948.3442421	-0.77857117	7.67E-05	0.006282273
NKAPD1	467.3590546	-0.777546866	9.23E-05	0.007238453
UBA5	227.8221579	-0.775788815	0.001612135	0.047009067
IGF2R	159.7998237	-0.767599458	0.000844393	0.031308763
PAXBP1	162.2082086	-0.761532522	9.01E-05	0.007125523
SPTY2D1	571.4278797	-0.754721105	0.00053042	0.02300516
KLHL11	665.2394795	-0.75136498	0.0027389	0.063887682
GRPEL2	773.6755639	-0.750347499	0.000439626	0.020177957
DSC2	380.7933268	-0.74979778	0.002381968	0.058726232
MPZL2	276.2206413	-0.748187342	0.000290387	0.015913536
ABCA5	163.7868538	-0.748085549	0.005342898	0.096223047
RPUSD2	580.8510838	-0.740341082	0.004011545	0.080958711
RPS6KA5	146.1854061	-0.730198754	0.001336551	0.042381046
PRICKLE3	207.1827782	-0.727825271	0.001355456	0.042719442
OTUD6B	408.7628146	-0.72765782	0.001449269	0.044042259
HSPH1	1418.875387	-0.725487311	0.005117804	0.094141706
GPRC5C	982.5845903	-0.723355549	0.002185989	0.056012265
CHST12	261.9483834	-0.721167084	0.003812122	0.078185713
ABRAXAS1	550.9535594	-0.720549086	0.001834302	0.050800769
SLC35E1	433.0362793	-0.716756094	0.005543921	0.098622345
ZNF302	296.3395022	-0.715823301	0.000218305	0.013188943
SLC18A2	294.6640664	-0.715016607	0.001568503	0.045985109
TSC22D2	322.1256123	-0.71409253	0.000863977	0.031785601
GMCL1	595.66171	-0.713437849	9.37E-06	0.001160305
TAOK3	751.0619418	-0.709931463	0.002952597	0.067107701
FAM217B	862.5031708	-0.693030758	0.000754803	0.028902768
OTUD6B-AS1	444.6751802	-0.692620305	0.005132959	0.094237138
RPP38	1264.558648	-0.691675949	0.004844833	0.091069373
PPDPF	330.8438616	-0.688678758	0.002984219	0.06758274

Normal vs. Fragmented_Downregulated

TMED7	561.1174162	-0.683863624	0.00035345	0.017635214
SMC6	761.1715497	-0.682568189	4.74E-11	9.95E-08
TAOK1	505.9666478	-0.682041619	2.50E-09	2.15E-06
OTULINL	183.4796107	-0.678142159	0.001957192	0.052796714
GTPBP6	89.41345602	-0.668507903	0.003754303	0.077588935
ACTR6	341.0463224	-0.664541507	0.002025477	0.05349408
ASH2L	619.0710261	-0.664050186	0.00405362	0.081546751
TDP1	383.378096	-0.658144352	0.004706279	0.089551559
SLC22A5	455.5052307	-0.656543574	0.005210205	0.0951142
ZCRB1	775.2542604	-0.652220375	0.000369726	0.018017208
ZNF672	397.503624	-0.646295244	8.10E-05	0.006577441
RTN4IP1	359.3653848	-0.644386867	0.005263234	0.095516076
PPP1CB	3080.979171	-0.636729608	0.000791238	0.029924623
HOOK2	594.8433867	-0.636653427	0.004027562	0.081108827
CDC42EP1	574.4342915	-0.633726141	0.002782894	0.064409772
GTF3C3	821.5148954	-0.630303859	5.20E-05	0.004726922
TMEM192	403.2927755	-0.629015295	0.000160618	0.010437406
PTEN	2439.16491	-0.626370477	0.000786878	0.029819381
EEF1E1	1093.261566	-0.623199367	0.000309776	0.016594537
ATXN2	530.7363131	-0.621931064	0.00046101	0.020805965
IRF3	845.036855	-0.620714618	0.002171757	0.055798805
SLC1A5	4423.441032	-0.615428923	0.001558642	0.04588334
SLC39A8	314.2581401	-0.608043436	0.003505561	0.074455031
BRWD1	802.5308646	-0.605617292	2.07E-06	0.000358447
CHERP	609.7186493	-0.604471034	0.003839701	0.078495951
CEP290	309.4470117	-0.603157704	0.002829616	0.065094938
NPTX1	622.6397647	-0.601766052	0.002434695	0.059330006
SLC9A3R1	1795.207546	-0.593493938	0.000412993	0.019336937
MILR1	472.2565236	-0.592401538	0.001164208	0.038690976
HPF1	698.5352291	-0.584075089	0.000104859	0.0078999
POLD1	673.2463208	-0.580030064	0.002237023	0.05701093

CHAPTER 7

BIBLIOGRAPHY

BIBLIOGRAPHY

- [1] James E Rothman and Lelio Orci. “Molecular dissection of the secretory pathway”. In: *Nature* 355.6359 (1992), p. 409.
- [2] George Palade. “Intracellular aspects of the process of protein synthesis”. In: *Science* 189.4200 (1975), pp. 347–358.
- [3] Peter Novick, Susan Ferro, and Randy Schekman. “Order of events in the yeast secretory pathway”. In: *Cell* 25.2 (1981), pp. 461–469.
- [4] George E Palade. “The endoplasmic reticulum”. In: *The Journal of biophysical and biochemical cytology* 2.4 (1956), p. 85.
- [5] John F Presley et al. “ER-to-Golgi transport visualized in living cells”. In: *Nature* 389.6646 (1997), p. 81.
- [6] Annika Budnik and David J Stephens. “ER exit sites—localization and control of COPII vesicle formation”. In: *FEBS letters* 583.23 (2009), pp. 3796–3803.
- [7] Meta J Kuehn, Johannes M Herrmann, and Randy Schekman. “COPII—cargo interactions direct protein sorting into ER-derived transport vesicles”. In: *Nature* 391.6663 (1998), p. 187.
- [8] C Barlowe, C d’Enfert, and R Schekman. “Purification and characterization of SAR1p, a small GTP-binding protein required for transport vesicle formation from the endoplasmic reticulum.” In: *Journal of Biological Chemistry* 268.2 (1993), pp. 873–879.
- [9] Alessandra Pagano et al. “Sec24 proteins and sorting at the endoplasmic reticulum”. In: *Journal of Biological Chemistry* 274.12 (1999), pp. 7833–7840.
- [10] Ken Matsuoka et al. “COPII-coated vesicle formation reconstituted with purified coat proteins and chemically defined liposomes”. In: *Cell* 93.2 (1998), pp. 263–275.
- [11] Charles Barlowe et al. “COPII: a membrane coat formed by Sec proteins that drive vesicle budding from the endoplasmic reticulum”. In: *Cell* 77.6 (1994), pp. 895–907.

- [12] Judith Klumperman. “Transport between ER and Golgi”. In: *Current opinion in cell biology* 12.4 (2000), pp. 445–449.
- [13] Christian Appenzeller-Herzog and Hans-Peter Hauri. “The ER-Golgi intermediate compartment (ERGIC): in search of its identity and function”. In: *Journal of cell science* 119.11 (2006), pp. 2173–2183.
- [14] Rainer Duden. “ER-to-Golgi transport: Cop I and Cop II function”. In: *Molecular membrane biology* 20.3 (2003), pp. 197–207.
- [15] Anne Eugster et al. “COP I domains required for coatomer integrity, and novel interactions with ARF and ARF-GAP”. In: *The EMBO journal* 19.15 (2000), pp. 3905–3917.
- [16] R Beck et al. “The COPI system: molecular mechanisms and function”. In: *FEBS letters* 583.17 (2009), pp. 2701–2709.
- [17] Anne Spang. “ARF1 regulatory factors and COPI vesicle formation”. In: *Current opinion in cell biology* 14.4 (2002), pp. 423–427.
- [18] Nelson B Cole et al. “Retrograde transport of Golgi-localized proteins to the ER”. In: *The Journal of cell biology* 140.1 (1998), pp. 1–15.
- [19] Jennifer Lippincott-Schwartz et al. “Microtubule-dependent retrograde transport of proteins into the ER in the presence of brefeldin A suggests an ER recycling pathway”. In: *Cell* 60.5 (1990), pp. 821–836.
- [20] Charles K Barlowe and Elizabeth A Miller. “Secretory protein biogenesis and traffic in the early secretory pathway”. In: *Genetics* 193.2 (2013), pp. 383–410.
- [21] Peter Watson and David J Stephens. “ER-to-Golgi transport: form and formation of vesicular and tubular carriers”. In: *Biochimica et Biophysica Acta (BBA)-Molecular Cell Research* 1744.3 (2005), pp. 304–315.
- [22] Markus Elsner, Hitoshi Hashimoto, and Tommy Nilsson. “Cisternal maturation and vesicle transport: join the band wagon!” In: *Molecular membrane biology* 20.3 (2003), pp. 221–229.
- [23] Benjamin S Glick, Timothy Elston, and George Oster. “A cisternal maturation mechanism can explain the asymmetry of the Golgi stack”. In: *FEBS letters* 414.2 (1997), pp. 177–181.
- [24] Benjamin S Glick and Alberto Luini. “Models for Golgi traffic: a critical assessment”. In: *Cold Spring Harbor perspectives in biology* 3.11 (2011), a005215.
- [25] Eugene Losev et al. “Golgi maturation visualized in living yeast”. In: *Nature* 441.7096 (2006), p. 1002.
- [26] Benjamin S Glick and Akihiko Nakano. “Membrane traffic within the Golgi apparatus”. In: *Annual Review of Cell and Developmental* 25 (2009), pp. 113–132.

- [27] Gareth Griffiths et al. “Exit of newly synthesized membrane proteins from the trans cisterna of the Golgi complex to the plasma membrane.” In: *The Journal of Cell Biology* 101.3 (1985), pp. 949–964.
- [28] Juan S Bonifacino and Benjamin S Glick. “The mechanisms of vesicle budding and fusion”. In: *cell* 116.2 (2004), pp. 153–166.
- [29] Alberto Luini et al. “Morphogenesis of post-Golgi transport carriers”. In: *Histochemistry and cell biology* 129.2 (2008), pp. 153–161.
- [30] Geri Kreitzer et al. “Three-dimensional analysis of post-Golgi carrier exocytosis in epithelial cells”. In: *Nature cell biology* 5.2 (2003), p. 126.
- [31] Patrick Keller and Kai Simons. “Post-Golgi biosynthetic trafficking”. In: *Journal of cell science* 110.24 (1997), pp. 3001–3009.
- [32] A Rambourg, D Segretain, and Y Clermont. “Tridimensional architecture of the Golgi apparatus in the atrial muscle cell of the rat”. In: *American journal of anatomy* 170.2 (1984), pp. 163–179.
- [33] Mark S Ladinsky et al. “Golgi structure in three dimensions: functional insights from the normal rat kidney cell”. In: *The Journal of cell biology* 144.6 (1999), pp. 1135–1149.
- [34] Enrica San Pietro et al. “Group IV phospholipase A2 α controls the formation of inter-cisternal continuities involved in intra-Golgi transport”. In: *PLoS biology* 7.9 (2009), e1000194.
- [35] Catherine L Jackson. “Mechanisms of transport through the Golgi complex”. In: *Journal of cell science* 122.4 (2009), pp. 443–452.
- [36] James Shorter and Graham Warren. “Golgi architecture and inheritance”. In: *Annual review of cell and developmental biology* 18.1 (2002), pp. 379–420.
- [37] A Rambourg and Y Clermont. “Three-dimensional structure of the Golgi apparatus in mammalian cells”. In: *The Golgi Apparatus*. Springer, 1997, pp. 37–61.
- [38] Werner W Franke et al. “Inter- and intracisternal elements of the Golgi apparatus”. In: *Zeitschrift für Zellforschung und Mikroskopische Anatomie* 132.3 (1972), pp. 365–380.
- [39] EDWARD B Cluett and WILLIAM J Brown. “Adhesion of Golgi cisternae by proteinaceous interactions: intercisternal bridges as putative adhesive structures”. In: *Journal of cell science* 103.3 (1992), pp. 773–784.
- [40] Cedric BOUCHET-MARQUIS, Vytaute Starkuviene, and Markus Grabenbauer. “Golgi apparatus studied in vitreous sections”. In: *Journal of microscopy* 230.2 (2008), pp. 308–316.
- [41] Johan Thyberg and Stanislaw Moskalewski. “Microtubules and the organization of the Golgi complex”. In: *Experimental cell research* 159.1 (1985), pp. 1–16.

- [42] Brad J Marsh. “Reconstructing mammalian membrane architecture by large area cellular tomography”. In: *Methods in cell biology* 79 (2007), pp. 193–220.
- [43] Martin Lowe. “Structural organization of the Golgi apparatus”. In: *Current opinion in cell biology* 23.1 (2011), pp. 85–93.
- [44] Manojkumar A Puthenveedu et al. “GM130 and GRASP65-dependent lateral cis-ternal fusion allows uniform Golgi-enzyme distribution”. In: *Nature cell biology* 8.3 (2006), p. 238.
- [45] Kevin Mowbrey and Joel B Dacks. “Evolution and diversity of the Golgi body”. In: *FEBS letters* 583.23 (2009), pp. 3738–3745.
- [46] James E Rothman. “The Golgi apparatus: two organelles in tandem”. In: *Science* 213.4513 (1981), pp. 1212–1219.
- [47] Yanzhuang Wang et al. “Golgi cisternal unstacking stimulates COPI vesicle budding and protein transport”. In: *PLoS One* 3.2 (2008), e1647.
- [48] Smita Yadav, Sapna Puri, and Adam D Linstedt. “A primary role for Golgi positioning in directed secretion, cell polarity, and wound healing”. In: *Molecular biology of the cell* 20.6 (2009), pp. 1728–1736.
- [49] Antonino Colanzi and Daniela Corda. “Mitosis controls the Golgi and the Golgi controls mitosis”. In: *Current opinion in cell biology* 19.4 (2007), pp. 386–393.
- [50] Christine Sütterlin et al. “Fragmentation and dispersal of the pericentriolar Golgi complex is required for entry into mitosis in mammalian cells”. In: *Cell* 109.3 (2002), pp. 359–369.
- [51] Kristien JM Zaal et al. “Golgi membranes are absorbed into and reemerge from the ER during mitosis”. In: *Cell* 99.6 (1999), pp. 589–601.
- [52] Martin Lowe et al. “Cdc2 kinase directly phosphorylates the cis-Golgi matrix protein GM130 and is required for Golgi fragmentation in mitosis”. In: *Cell* 94.6 (1998), pp. 783–793.
- [53] Vladimir Litvak et al. “Mitotic phosphorylation of the peripheral Golgi protein Nir2 by Cdk1 provides a docking mechanism for Plk1 and affects cytokinesis completion”. In: *Molecular cell* 14.3 (2004), pp. 319–330.
- [54] Stephen A Jesch et al. “Mitotic phosphorylation of Golgi reassembly stacking protein 55 by mitogen-activated protein kinase ERK2”. In: *Molecular biology of the cell* 12.6 (2001), pp. 1811–1817.
- [55] David T Shima et al. “Partitioning of the Golgi apparatus during mitosis in living HeLa cells”. In: *The Journal of cell biology* 137.6 (1997), pp. 1211–1228.
- [56] Magnus AB Axelsson and Graham Warren. “Rapid, endoplasmic reticulum-independent diffusion of the mitotic Golgi haze”. In: *Molecular biology of the cell* 15.4 (2004), pp. 1843–1852.

- [57] Eija Jokitalo et al. “Golgi clusters and vesicles mediate mitotic inheritance independently of the endoplasmic reticulum”. In: *J Cell Biol* 154.2 (2001), pp. 317–330.
- [58] John M Lucocq et al. “A mitotic form of the Golgi apparatus in HeLa cells”. In: *The Journal of cell biology* 104.4 (1987), pp. 865–874.
- [59] Carolina Tångemo et al. “A novel laser nanosurgery approach supports de novo Golgi biogenesis in mammalian cells”. In: *J Cell Sci* 124.6 (2011), pp. 978–987.
- [60] Sapna Puri and Adam D Linstedt. “Capacity of the Golgi apparatus for biogenesis from the endoplasmic reticulum”. In: *Molecular biology of the cell* 14.12 (2003), pp. 5011–5018.
- [61] Benjamin S Glick. “Can the Golgi form de novo?” In: *Nature Reviews Molecular Cell Biology* 3.8 (2002), p. 615.
- [62] Brooke J Bevis et al. “De novo formation of transitional ER sites and Golgi structures in *Pichia pastoris*”. In: *Nature cell biology* 4.10 (2002), p. 750.
- [63] Jen-Hsuan Wei and Joachim Seemann. “Golgi ribbon disassembly during mitosis, differentiation and disease progression”. In: *Current opinion in cell biology* 47 (2017), pp. 43–51.
- [64] Tommy Nilsson, Catherine E Au, and John JM Bergeron. “Sorting out glycosylation enzymes in the Golgi apparatus”. In: *FEBS letters* 583.23 (2009), pp. 3764–3769.
- [65] Catherine Rabouille et al. “Mapping the distribution of Golgi enzymes involved in the construction of complex oligosaccharides”. In: *Journal of cell science* 108.4 (1995), pp. 1617–1627.
- [66] William G Dunphy et al. “Early and late functions associated with the Golgi apparatus reside in distinct compartments”. In: *Proceedings of the National Academy of Sciences* 78.12 (1981), pp. 7453–7457.
- [67] Linna Tu et al. “Signal-mediated dynamic retention of glycosyltransferases in the Golgi”. In: *Science* 321.5887 (2008), pp. 404–407.
- [68] Massimo Micaroni et al. “The SPCA1 Ca²⁺ pump and intracellular membrane trafficking”. In: *Traffic* 11.10 (2010), pp. 1315–1333.
- [69] Ludwig Missiaen et al. “Calcium in the Golgi apparatus”. In: *Cell calcium* 41.5 (2007), pp. 405–416.
- [70] Nick J Dolman and Alexei V Tepikin. “Calcium gradients and the Golgi”. In: *Cell calcium* 40.5-6 (2006), pp. 505–512.
- [71] Nelson B Cole et al. “Golgi dispersal during microtubule disruption: regeneration of Golgi stacks at peripheral endoplasmic reticulum exit sites.” In: *Molecular biology of the cell* 7.4 (1996), pp. 631–650.

- [72] Mónica Bettencourt-Dias and David M Glover. “Centrosome biogenesis and function: centrosomics brings new understanding”. In: *Nature reviews Molecular cell biology* 8.6 (2007), p. 451.
- [73] Karine Chabin-Brion et al. “The Golgi complex is a microtubule-organizing organelle”. In: *Molecular biology of the cell* 12.7 (2001), pp. 2047–2060.
- [74] Sabrina Rivero et al. “Microtubule nucleation at the cis-side of the Golgi apparatus requires AKAP450 and GM130”. In: *The EMBO journal* 28.8 (2009), pp. 1016–1028.
- [75] Paul M Miller et al. “Golgi-derived CLASP-dependent microtubules control Golgi organization and polarized trafficking in motile cells”. In: *Nature cell biology* 11.9 (2009), p. 1069.
- [76] Michele Sallese, Monica Giannotta, and Alberto Luini. “Coordination of the secretory compartments via inter-organelle signalling”. In: *Seminars in cell & developmental biology*. Vol. 20. 7. Elsevier. 2009, pp. 801–809.
- [77] Kerry Inder et al. “Activation of the MAPK module from different spatial locations generates distinct system outputs”. In: *Molecular biology of the cell* 19.11 (2008), pp. 4776–4784.
- [78] Vi K Chiu et al. “Ras signalling on the endoplasmic reticulum and the Golgi”. In: *Nature cell biology* 4.5 (2002), p. 343.
- [79] Ignacio Perez de Castro et al. “Ras activation in Jurkat T cells following low-grade stimulation of the T-cell receptor is specific to N-Ras and occurs only on the Golgi apparatus”. In: *Molecular and cellular biology* 24.8 (2004), pp. 3485–3496.
- [80] David Matallanas et al. “Distinct utilization of effectors and biological outcomes resulting from site-specific Ras activation: Ras functions in lipid rafts and Golgi complex are dispensable for proliferation and transformation”. In: *Molecular and cellular biology* 26.1 (2006), pp. 100–116.
- [81] Alan Charest et al. “Oncogenic targeting of an activated tyrosine kinase to the Golgi apparatus in a glioblastoma”. In: *Proceedings of the National Academy of Sciences* 100.3 (2003), pp. 916–921.
- [82] Kenneth L Scott et al. “GOLPH3 modulates mTOR signalling and rapamycin sensitivity in cancer”. In: *Nature* 459.7250 (2009), p. 1085.
- [83] Teodoro Pulvirenti et al. “A traffic-activated Golgi-based signalling circuit coordinates the secretory pathway”. In: *Nature cell biology* 10.8 (2008), p. 912.
- [84] Denis M Schewe and Julio A Aguirre-Ghiso. “ATF6 α -Rheb-mTOR signaling promotes survival of dormant tumor cells in vivo”. In: *Proceedings of the National Academy of Sciences* 105.30 (2008), pp. 10519–10524.

- [85] Christopher R McMaster. “Lipid metabolism and vesicle trafficking: more than just greasing the transport machinery”. In: *Biochemistry and cell biology* 79.6 (2001), pp. 681–692.
- [86] Jay D Horton, Joseph L Goldstein, and Michael S Brown. “SREBPs: activators of the complete program of cholesterol and fatty acid synthesis in the liver”. In: *The Journal of clinical investigation* 109.9 (2002), pp. 1125–1131.
- [87] Juro Sakai et al. “Sterol-regulated release of SREBP-2 from cell membranes requires two sequential cleavages, one within a transmembrane segment”. In: *Cell* 85.7 (1996), pp. 1037–1046.
- [88] Jin Ye et al. “ER stress induces cleavage of membrane-bound ATF6 by the same proteases that process SREBPs”. In: *Molecular cell* 6.6 (2000), pp. 1355–1364.
- [89] Satomi Nadanaka et al. “Analysis of ATF6 activation in Site-2 protease-deficient Chinese hamster ovary cells”. In: *Cell structure and function* (2006), pp. 0611150002–0611150002.
- [90] Anna Godi et al. “ARF mediates recruitment of PtdIns-4-OH kinase- β and stimulates synthesis of PtdIns (4, 5) P 2 on the Golgi complex”. In: *Nature cell biology* 1.5 (1999), p. 280.
- [91] Thomas Porstmann et al. “SREBP activity is regulated by mTORC1 and contributes to Akt-dependent cell growth”. In: *Cell metabolism* 8.3 (2008), pp. 224–236.
- [92] Xiangyu Liu and XF Steven Zheng. “Endoplasmic reticulum and Golgi localization sequences for mammalian target of rapamycin”. In: *Molecular biology of the cell* 18.3 (2007), pp. 1073–1082.
- [93] Giovanni D’Angelo et al. “The multiple roles of PtdIns (4) P—not just the precursor of PtdIns (4, 5) P2”. In: *Journal of Cell Science* 121.12 (2008), pp. 1955–1963.
- [94] Mirco Capitani and Michele Sallese. “The KDEL receptor: new functions for an old protein”. In: *FEBS letters* 583.23 (2009), pp. 3863–3871.
- [95] David J Gill et al. “Regulation of O-glycosylation through Golgi-to-ER relocation of initiation enzymes”. In: *The Journal of cell biology* 189.5 (2010), pp. 843–858.
- [96] Collin Bachert and Adam D Linstedt. “Dual anchoring of the GRASP membrane tether promotes trans pairing”. In: *Journal of Biological Chemistry* 285.21 (2010), pp. 16294–16301.
- [97] Yanzhuang Wang et al. “A direct role for GRASP65 as a mitotically regulated Golgi stacking factor”. In: *The EMBO journal* 22.13 (2003), pp. 3279–3290.
- [98] Yi Xiang and Yanzhuang Wang. “GRASP55 and GRASP65 play complementary and essential roles in Golgi cisternal stacking”. In: *The Journal of cell biology* 188.2 (2010), pp. 237–251.

- [99] Yanzhuang Wang, Ayano Satoh, and Graham Warren. “Mapping the functional domains of the Golgi stacking factor GRASP65”. In: *Journal of Biological Chemistry* 280.6 (2005), pp. 4921–4928.
- [100] Yi Xiang and Yanzhuang Wang. “New components of the Golgi matrix”. In: *Cell and tissue research* 344.3 (2011), pp. 365–379.
- [101] Debrup Sengupta et al. “Organelle tethering by a homotypic PDZ interaction underlies formation of the Golgi membrane network”. In: *The Journal of cell biology* 186.1 (2009), pp. 41–55.
- [102] Danming Tang, Hebao Yuan, and Yanzhuang Wang. “The role of GRASP65 in Golgi cisternal stacking and cell cycle progression”. In: *Traffic* 11.6 (2010), pp. 827–842.
- [103] Fen Hu et al. “Structural basis for the interaction between the Golgi reassembly-stacking protein GRASP65 and the Golgi matrix protein GM130”. In: *Journal of Biological Chemistry* 290.44 (2015), pp. 26373–26382.
- [104] Yanbin Feng et al. “Structural insight into Golgi membrane stacking by GRASP65 and GRASP55 proteins”. In: *Journal of Biological Chemistry* 288.39 (2013), pp. 28418–28427.
- [105] Timothy N Feinstein and Adam D Linstedt. “GRASP55 regulates Golgi ribbon formation”. In: *Molecular biology of the cell* 19.7 (2008), pp. 2696–2707.
- [106] Intaek Lee et al. “Membrane adhesion dictates Golgi stacking and cisternal morphology”. In: *Proceedings of the National Academy of Sciences* 111.5 (2014), pp. 1849–1854.
- [107] MJ Fritzler et al. “Molecular characterization of two human autoantigens: unique cDNAs encoding 95-and 160-kD proteins of a putative family in the Golgi complex.” In: *Journal of Experimental Medicine* 178.1 (1993), pp. 49–62.
- [108] Vladimir Lupashin and Elizabeth Sztul. “Golgi tethering factors”. In: *Biochimica et Biophysica Acta (BBA)-Molecular Cell Research* 1744.3 (2005), pp. 325–339.
- [109] Alison K Gillingham and Sean Munro. “Long coiled-coil proteins and membrane traffic”. In: *Biochimica et Biophysica Acta (BBA)-Molecular Cell Research* 1641.2-3 (2003), pp. 71–85.
- [110] Sean Munro. “The golgin coiled-coil proteins of the Golgi apparatus”. In: *Cold Spring Harbor perspectives in biology* 3.6 (2011), a005256.
- [111] Irene Barinaga-Rementería Ramirez and Martin Lowe. “Golgins and GRASPs: holding the Golgi together”. In: *Seminars in cell & developmental biology*. Vol. 20. 7. Elsevier. 2009, pp. 770–779.

- [112] Cecilia Alvarez et al. “The p115-interactive proteins GM130 and giantin participate in endoplasmic reticulum-Golgi traffic”. In: *Journal of Biological Chemistry* 276.4 (2001), pp. 2693–2700.
- [113] Joachim Seemann, Eija Jämsä Jokitalo, and Graham Warren. “The role of the tethering proteins p115 and GM130 in transport through the Golgi apparatus in vivo”. In: *Molecular biology of the cell* 11.2 (2000), pp. 635–645.
- [114] Stephanie K Sapperstein et al. “p115 is a general vesicular transport factor related to the yeast endoplasmic reticulum to Golgi transport factor Uso1p.” In: *Proceedings of the National Academy of Sciences* 92.2 (1995), pp. 522–526.
- [115] Cecilia Alvarez et al. “ER to Golgi transport: requirement for p115 at a pre-Golgi VTC stage”. In: *The Journal of cell biology* 147.6 (1999), pp. 1205–1222.
- [116] Theresa H Ward et al. “Maintenance of Golgi structure and function depends on the integrity of ER export”. In: *The Journal of cell biology* 155.4 (2001), pp. 557–570.
- [117] Manojkumar A Puthenveedu and Adam D Linstedt. “Gene replacement reveals that p115/SNARE interactions are essential for Golgi biogenesis”. In: *Proceedings of the National Academy of Sciences* 101.5 (2004), pp. 1253–1256.
- [118] Susie Kim et al. “Golgi disruption and early embryonic lethality in mice lacking USO1”. In: *PloS one* 7.11 (2012), e50530.
- [119] Nobuhiro Nakamura. “Emerging new roles of GM130, a cis-Golgi matrix protein, in higher order cell functions”. In: *Journal of pharmacological sciences* (2010), pp. 1002260359–1002260359.
- [120] Eliza Vasile et al. “Structural integrity of the Golgi is temperature sensitive in conditional-lethal mutants with no detectable GM130”. In: *Traffic* 4.4 (2003), pp. 254–272.
- [121] Adam D Linstedt and Hans-Peter Hauri. “Giantin, a novel conserved Golgi membrane protein containing a cytoplasmic domain of at least 350 kDa.” In: *Molecular biology of the cell* 4.7 (1993), pp. 679–693.
- [122] Birte Sönnichsen et al. “A role for giantin in docking COPI vesicles to Golgi membranes”. In: *The Journal of cell biology* 140.5 (1998), pp. 1013–1021.
- [123] Adam D Linstedt et al. “Binding relationships of membrane tethering components The giantin N terminus and the GM130 N terminus compete for binding to the p115 C terminus”. In: *Journal of Biological Chemistry* 275.14 (2000), pp. 10196–10201.
- [124] Mayuko Koreishi et al. “The golgin tether giantin regulates the secretory pathway by controlling stack organization within Golgi apparatus”. In: *PloS one* 8.3 (2013), e59821.

- [125] Carlos Infante et al. “GMAP-210, A cis-Golgi network-associated protein, is a minus end microtubule-binding protein”. In: *The Journal of cell biology* 145.1 (1999), pp. 83–98.
- [126] Guillaume Drin et al. “Asymmetric tethering of flat and curved lipid membranes by a golgin”. In: *Science* 320.5876 (2008), pp. 670–673.
- [127] Karin Pernet-Gallay et al. “The overexpression of GMAP-210 blocks anterograde and retrograde transport between the ER and the Golgi apparatus”. In: *Traffic* 3.11 (2002), pp. 822–832.
- [128] Peristera Roboti, Keisuke Sato, and Martin Lowe. “The golgin GMAP-210 is required for efficient membrane trafficking in the early secretory pathway”. In: *J Cell Sci* 128.8 (2015), pp. 1595–1606.
- [129] Benjamin Short, Alexander Haas, and Francis A Barr. “Golbins and GTPases, giving identity and structure to the Golgi apparatus”. In: *Biochimica et Biophysica Acta (BBA)-Molecular Cell Research* 1744.3 (2005), pp. 383–395.
- [130] Cemal Gurkan et al. “Large-scale profiling of Rab GTPase trafficking networks: the membrome”. In: *Molecular biology of the cell* 16.8 (2005), pp. 3847–3864.
- [131] Ragna Sannerud, Jaakko Saraste, and Bruno Goud. “Retrograde traffic in the biosynthetic-secretory route: pathways and machinery”. In: *Current opinion in cell biology* 15.4 (2003), pp. 438–445.
- [132] Suzanne Pfeffer and Dikran Aivazian. “Targeting Rab GTPases to distinct membrane compartments”. In: *Nature reviews Molecular cell biology* 5.11 (2004), p. 886.
- [133] Daniel F Markgraf, Karolina Peplowska, and Christian Ungermann. “Rab cascades and tethering factors in the endomembrane system”. In: *FEBS letters* 581.11 (2007), pp. 2125–2130.
- [134] George Galea and Jeremy C Simpson. “High-content screening and analysis of the Golgi complex”. In: *Methods in cell biology*. Vol. 118. Elsevier, 2013, pp. 281–295.
- [135] George Galea and Jeremy C Simpson. “High-content analysis of Rab protein function at the ER-Golgi interface”. In: *Bioarchitecture* 5.3-4 (2015), pp. 44–53.
- [136] Dong Fu. “Where is it and how does it get there—intracellular localization and traffic of P-glycoprotein”. In: *Frontiers in oncology* 3 (2013), p. 321.
- [137] Dirk Fasshauer et al. “Conserved structural features of the synaptic fusion complex: SNARE proteins reclassified as Q- and R-SNAREs”. In: *Proceedings of the national academy of sciences* 95.26 (1998), pp. 15781–15786.
- [138] Thomas C Südhof and James E Rothman. “Membrane fusion: grappling with SNARE and SM proteins”. In: *Science* 323.5913 (2009), pp. 474–477.
- [139] James A McNew et al. “Compartmental specificity of cellular membrane fusion encoded in SNARE proteins”. In: *Nature* 407.6801 (2000), p. 153.

- [140] Christina G Schuette et al. “Determinants of liposome fusion mediated by synaptic SNARE proteins”. In: *Proceedings of the National Academy of Sciences* 101.9 (2004), pp. 2858–2863.
- [141] Rose Willett, Daniel Ungar, and Vladimir Lupashin. “The Golgi puppet master: COG complex at center stage of membrane trafficking interactions”. In: *Histochemistry and cell biology* 140.3 (2013), pp. 271–283.
- [142] Joshua A Lees et al. “Molecular organization of the COG vesicle tethering complex”. In: *Nature structural & molecular biology* 17.11 (2010), p. 1292.
- [143] Ellen Reynders et al. “How Golgi glycosylation meets and needs trafficking: the case of the COG complex”. In: *Glycobiology* 21.7 (2010), pp. 853–863.
- [144] Miwa Sohda et al. “The interaction of two tethering factors, p115 and COG complex, is required for Golgi integrity”. In: *Traffic* 8.3 (2007), pp. 270–284.
- [145] Daniel Ungar et al. “Characterization of a mammalian Golgi-localized protein complex, COG, that is required for normal Golgi morphology and function”. In: *J Cell Biol* 157.3 (2002), pp. 405–415.
- [146] Jennifer Lippincott-Schwartz. “Cytoskeletal proteins and Golgi dynamics”. In: *Current opinion in cell biology* 10.1 (1998), pp. 52–59.
- [147] TE Kreis et al. “Golgi apparatus-cytoskeleton interactions”. In: *The Golgi Apparatus*. Springer, 1997, pp. 179–193.
- [148] Ferran Valderrama et al. “Actin microfilaments are essential for the cytological positioning and morphology of the Golgi complex”. In: *European journal of cell biology* 76.1 (1998), pp. 9–17.
- [149] Gustavo Egea et al. “Actin acting at the Golgi”. In: *Histochemistry and cell biology* 140.3 (2013), pp. 347–360.
- [150] Kenneth A Beck et al. “Golgi spectrin: identification of an erythroid beta-spectrin homolog associated with the Golgi complex.” In: *The Journal of cell biology* 127.3 (1994), pp. 707–723.
- [151] Kim Brownhill, Laura Wood, and Viki Allan. “Molecular motors and the Golgi complex: staying put and moving through”. In: *Seminars in cell & developmental biology*. Vol. 20. 7. Elsevier. 2009, pp. 784–792.
- [152] Claudia G Almeida et al. “Myosin 1b promotes the formation of post-Golgi carriers by regulating actin assembly and membrane remodelling at the trans-Golgi network”. In: *Nature Cell Biology* 13.7 (2011), p. 779.
- [153] Manuel H Taft et al. “Functional characterization of human myosin-18A and its interaction with F-actin and GOLPH3”. In: *Journal of Biological Chemistry* 288.42 (2013), pp. 30029–30041.

- [154] Gustavo Egea, Francisco Lázaro-Diéguéz, and Montserrat Vilella. “Actin dynamics at the Golgi complex in mammalian cells”. In: *Current opinion in cell biology* 18.2 (2006), pp. 168–178.
- [155] Gustavo Egea et al. “Cytoskeleton and Golgi-apparatus interactions: a two-way road of function and structure”. In: *Cell Health and Cytoskeleton* 7 (2015), p. 37.
- [156] Xiaodong Zhu and Irina Kaverina. “Golgi as an MTOC: making microtubules for its own good”. In: *Histochemistry and cell biology* 140.3 (2013), pp. 361–367.
- [157] Jingchao Wu et al. “Molecular pathway of microtubule organization at the Golgi apparatus”. In: *Developmental cell* 39.1 (2016), pp. 44–60.
- [158] Anna AWM Sanders and Irina Kaverina. “Nucleation and dynamics of Golgi-derived microtubules”. In: *Frontiers in neuroscience* 9 (2015), p. 431.
- [159] Tom Misteli. “The concept of self-organization in cellular architecture”. In: *J Cell Biol* 155.2 (2001), pp. 181–186.
- [160] Eric Karsenti. “Self-organization in cell biology: a brief history”. In: *Nature reviews Molecular cell biology* 9.3 (2008), p. 255.
- [161] Paolo Ronchi et al. “Positive feedback between Golgi membranes, microtubules and ER exit sites directs de novo biogenesis of the Golgi”. In: *J Cell Sci* 127.21 (2014), pp. 4620–4633.
- [162] Christian E Schuberth et al. “Self-organization of core Golgi material is independent of COPII-mediated endoplasmic reticulum export”. In: *J Cell Sci* 128.7 (2015), pp. 1279–1293.
- [163] Masashi Tachikawa and Atsushi Mochizuki. “Golgi apparatus self-organizes into the characteristic shape via postmitotic reassembly dynamics”. In: *Proceedings of the National Academy of Sciences* 114.20 (2017), pp. 5177–5182.
- [164] Yukio Fujita et al. “Fragmentation of Golgi apparatus of nigral neurons with α -synuclein-positive inclusions in patients with Parkinson’s disease”. In: *Acta neuropathologica* 112.3 (2006), pp. 261–265.
- [165] Atsushi Sakurai et al. “Fragmentation of the Golgi apparatus of the ballooned neurons in patients with corticobasal degeneration and Creutzfeldt-Jakob disease”. In: *Acta neuropathologica* 100.3 (2000), pp. 270–274.
- [166] Anirban Maitra and Paul J Thuluvath. “GP73 and liver disease: a (Golgi) complex enigma”. In: *The American journal of gastroenterology* 99.6 (2004), p. 1096.
- [167] Mariana Bexiga and Jeremy Simpson. “Human diseases associated with form and function of the Golgi complex”. In: *International journal of molecular sciences* 14.9 (2013), pp. 18670–18681.
- [168] Meir Aridor and Lisa A Hannan. “Traffic jams II: an update of diseases of intracellular transport”. In: *Traffic* 3.11 (2002), pp. 781–790.

- [169] Gunjan Joshi et al. “A β -induced Golgi fragmentation in Alzheimer’s disease enhances A β production”. In: *Proceedings of the National Academy of Sciences* 111.13 (2014), E1230–E1239.
- [170] Antony A Cooper et al. “ α -Synuclein blocks ER-Golgi traffic and Rab1 rescues neuron loss in Parkinson’s models”. In: *Science* 313.5785 (2006), pp. 324–328.
- [171] I Ferrer et al. “Dementia of frontal lobe type and motor neuron disease. A Golgi study of the frontal cortex.” In: *Journal of Neurology, Neurosurgery & Psychiatry* 54.10 (1991), pp. 932–934.
- [172] Daniel Ungar. “Golgi linked protein glycosylation and associated diseases”. In: *Seminars in cell & developmental biology*. Vol. 20. 7. Elsevier. 2009, pp. 762–769.
- [173] Matthew D Buschman, Juliati Rahajeng, and Seth J Field. “GOLPH3 links the Golgi, DNA damage, and cancer”. In: *Cancer research* 75.4 (2015), pp. 624–627.
- [174] Shuanzeng Wei et al. “GOLPH2 and MYO6: putative prostate cancer markers localized to the Golgi apparatus”. In: *The Prostate* 68.13 (2008), pp. 1387–1395.
- [175] Robert Jan Veldman et al. “Altered sphingolipid metabolism in multidrug-resistant ovarian cancer cells is due to uncoupling of glycolipid biosynthesis in the Golgi apparatus”. In: *The FASEB Journal* 16.9 (2002), pp. 1111–1113.
- [176] Sakari Kellokumpu, Raija Sormunen, and Ilmo Kellokumpu. “Abnormal glycosylation and altered Golgi structure in colorectal cancer: dependence on intra-Golgi pH”. In: *FEBS letters* 516.1-3 (2002), pp. 217–224.
- [177] Yukinobu Hino, Akira Asano, and Ryo Sato. “Biochemical Studies on Rat Liver Golgi Apparatus: II. Further Characterization of Isolated Golgi Fraction”. In: *The Journal of Biochemistry* 83.4 (1978), pp. 925–934.
- [178] Tomohiko Taguchi, Marc Pypaert, and Graham Warren. “Biochemical sub-fractionation of the mammalian Golgi apparatus”. In: *Traffic* 4.5 (2003), pp. 344–352.
- [179] Brian Burke et al. “A monoclonal antibody against a 135-K Golgi membrane protein.” In: *The EMBO Journal* 1.12 (1982), pp. 1621–1628.
- [180] Lelio Orcl et al. “Brefeldin A, a drug that blocks secretion, prevents the assembly of non-clathrin-coated buds on Golgi cisternae”. In: *Cell* 64.6 (1991), pp. 1183–1195.
- [181] Paolo Ronchi and Rainer Pepperkok. “Golgi depletion from living cells with laser nanosurgery”. In: *Methods in cell biology*. Vol. 118. Elsevier, 2013, pp. 311–324.
- [182] Roman S Polishchuk et al. “Ultrastructure of long-range transport carriers moving from the trans Golgi network to peripheral endosomes”. In: *Traffic* 7.8 (2006), pp. 1092–1103.
- [183] Daphne Preuss et al. “Characterization of the *Saccharomyces* Golgi complex through the cell cycle by immunoelectron microscopy.” In: *Molecular biology of the cell* 3.7 (1992), pp. 789–803.

- [184] Joanne Chia et al. “RNAi screening reveals a large signaling network controlling the Golgi apparatus in human cells”. In: *Molecular systems biology* 8.1 (2012).
- [185] Matteo Pasetto et al. “Whole-genome RNAi screen highlights components of the endoplasmic reticulum/Golgi as a source of resistance to immunotoxin-mediated cytotoxicity”. In: *Proceedings of the National Academy of Sciences* 112.10 (2015), E1135–E1142.
- [186] David E Gordon et al. “A targeted siRNA screen to identify SNAREs required for constitutive secretion in mammalian cells”. In: *Traffic* 11.9 (2010), pp. 1191–1204.
- [187] Jeremy C Simpson et al. “Genome-wide RNAi screening identifies human proteins with a regulatory function in the early secretory pathway”. In: *Nature cell biology* 14.7 (2012), p. 764.
- [188] Vytaute Starkuviene et al. “High-content screening microscopy identifies novel proteins with a putative role in secretory membrane traffic”. In: *Genome research* 14.10a (2004), pp. 1948–1956.
- [189] Benjamin S Glick. “Organization of the Golgi apparatus”. In: *Current opinion in cell biology* 12.4 (2000), pp. 450–456.
- [190] Richard D Klausner, Julie G Donaldson, and Jennifer Lippincott-Schwartz. “Brefeldin A: insights into the control of membrane traffic and organelle structure.” In: *The Journal of cell biology* 116.5 (1992), pp. 1071–1080.
- [191] Regis B Kelly. “Microtubules, membrane traffic, and cell organization”. In: *Cell* 61.1 (1990), pp. 5–7.
- [192] Michael Held et al. “CellCognition: time-resolved phenotype annotation in high-throughput live cell imaging”. In: *Nature methods* 7.9 (2010), p. 747.
- [193] Simone Picelli et al. “Smart-seq2 for sensitive full-length transcriptome profiling in single cells”. In: *Nature methods* 10.11 (2013), p. 1096.
- [194] Michael I Love, Wolfgang Huber, and Simon Anders. “Moderated estimation of fold change and dispersion for RNA-seq data with DESeq2”. In: *Genome biology* 15.12 (2014), p. 550.
- [195] Anne E Carpenter et al. “CellProfiler: image analysis software for identifying and quantifying cell phenotypes”. In: *Genome biology* 7.10 (2006), R100.
- [196] Fedor V Subach et al. “Photoactivatable mCherry for high-resolution two-color fluorescence microscopy”. In: *Nature methods* 6.2 (2009), p. 153.
- [197] Nadya G Gurskaya et al. “Engineering of a monomeric green-to-red photoactivatable fluorescent protein induced by blue light”. In: *Nature biotechnology* 24.4 (2006), p. 461.
- [198] Lucas Pelkmans. “Using cell-to-cell variability—a new era in molecular biology”. In: *Science* 336.6080 (2012), pp. 425–426.

- [199] Efthymia Papalexi and Rahul Satija. “Single-cell RNA sequencing to explore immune cell heterogeneity”. In: *Nature Reviews Immunology* 18.1 (2018), p. 35.
- [200] Berend Snijder and Lucas Pelkmans. “Origins of regulated cell-to-cell variability”. In: *Nature reviews Molecular cell biology* 12.2 (2011), p. 119.
- [201] Steven J Altschuler and Lani F Wu. “Cellular heterogeneity: do differences make a difference?” In: *Cell* 141.4 (2010), pp. 559–563.
- [202] John A Follit et al. “The Golgin GMAP210/TRIP11 anchors IFT20 to the Golgi complex”. In: *PLoS genetics* 4.12 (2008), e1000315.
- [203] Dae-Hyun Seog et al. “Uso1 protein contains a coiled-coil rod region essential for protein transport from the ER to the Golgi apparatus in *Saccharomyces cerevisiae*”. In: *The Journal of Biochemistry* 116.6 (1994), pp. 1341–1345.
- [204] Carolyn E Machamer. “The Golgi complex in stress and death”. In: *Frontiers in neuroscience* 9 (2015), p. 421.
- [205] Oliver Stegle, Sarah A Teichmann, and John C Marioni. “Computational and analytical challenges in single-cell transcriptomics”. In: *Nature Reviews Genetics* 16.3 (2015), p. 133.
- [206] Antoine-Emmanuel Saliba et al. “Single-cell RNA-seq: advances and future challenges”. In: *Nucleic acids research* 42.14 (2014), pp. 8845–8860.
- [207] Keisuke Sato et al. “Coupling of vesicle tethering and Rab binding is required for in vivo functionality of the golgin GMAP-210”. In: *Molecular biology of the cell* 26.3 (2015), pp. 537–553.
- [208] Tomasz M Witkos and Martin Lowe. “The golgin family of coiled-coil tethering proteins”. In: *Frontiers in cell and developmental biology* 3 (2016), p. 86.
- [209] Jennifer Hirst and Margaret S Robinson. “Clathrin and adaptors”. In: *Biochimica et Biophysica Acta (BBA)-Molecular Cell Research* 1404.1-2 (1998), pp. 173–193.
- [210] Willem Stoorvogel, Viola Oorschot, and Hans J Geuze. “A novel class of clathrin-coated vesicles budding from endosomes.” In: *The Journal of cell biology* 132.1 (1996), pp. 21–33.
- [211] Felicia Yu Hsuan Teng, Ya Wang, and Bor Luen Tang. “The syntaxins”. In: *Genome biology* 2.11 (2001), reviews3012–1.
- [212] Norihiro Nakamura et al. “Syntaxin 7 mediates endocytic trafficking to late endosomes”. In: *Journal of Biological Chemistry* 275.9 (2000), pp. 6523–6529.
- [213] Nikunj Sharma et al. “Apical targeting of syntaxin 3 is essential for epithelial cell polarity”. In: *The Journal of cell biology* 173.6 (2006), pp. 937–948.
- [214] Edward L Huttlin et al. “Architecture of the human interactome defines protein communities and disease networks”. In: *Nature* 545.7655 (2017), p. 505.

- [215] Wendy J van Zuylen et al. “Proteomic profiling of the TRAF3 interactome network reveals a new role for the ER-to-Golgi transport compartments in innate immunity”. In: *PLoS pathogens* 8.7 (2012), e1002747.
- [216] Oded Behar et al. “Semaphorin III is needed for normal patterning and growth of nerves, bones and heart”. In: *Nature* 383.6600 (1996), p. 525.
- [217] Wiebke Schultze et al. “Semaphorin4F interacts with the synapse-associated protein SAP90/PSD-95”. In: *Journal of neurochemistry* 78.3 (2001), pp. 482–489.
- [218] Rigney E Turnham and John D Scott. “Protein kinase A catalytic subunit isoform PRKACA; History, function and physiology”. In: *Gene* 577.2 (2016), pp. 101–108.
- [219] Yoav Benjamini and Yosef Hochberg. “Controlling the false discovery rate: a practical and powerful approach to multiple testing”. In: *Journal of the Royal statistical society: series B (Methodological)* 57.1 (1995), pp. 289–300.

CHAPTER 8

LISTS OF ABBREVIATIONS, FIGURES AND TABLES

ACBD3	Acyl-CoA binding domain containing 3
AKAP9	A-Kinase Anchoring Protein 9
AP2B1	Adaptor Related Protein Complex 2 Subunit Beta 1
Arf1	ADP-ribosylation factor 1
ATF6	Activating Transcription Factor 6
BICD2	Bicaudal D homolog 2
BSA	Bovine Serum Albumin
CAMSAP2	Calmodulin regulated spectrin associated protein family member 2
CCDC146	Coiled-coil domain containing 146
Cdk1	Cyclin dependent kinase 1
CLASP2	Cytoplasmic Linker Associated Protein 2
CLIP	CLIP domain-containing serine protease 2
COG	Conserved Oligomeric Golgi
COPB2	Coatomer protein complex, subunit beta 2 (beta prime)
COPG1	Coatomer protein complex, subunit gamma 1
COPI, COPII	COat Protein I,II
DAPI	4,6-diamidino-2-phenylindole
DMEM	Dulbecco's Modified Eagle's Medium
DMF	Dimethylformamid
DMSO	DiMethyl Sulphoxide
DNA	Deoxyribonucleic acid
DNAJC6	DnaJ Heat Shock Protein Family (Hsp40) Member C6
dNTP	deoxy Nucleotide TriPhosphate
EDTA	Ethylenediaminetetraacetic Acid
ER	Endoplasmic Reticulum
ERES	ER-Exit Sites
FACS	Fluorescence-activated cell sorting

FCHSD2	FCH And Double SH3 Domains 2
FCS	Fetal Calf Serum
FDR	False Discovery Rate
FNBP1L	Formin Binding Protein 1 Like
FPKM	Fragments Per Kilobase Million
GAK	Cyclin G associated kinase
GAP	Guanosine Associated Phosphatase
GC	Golgi Complex
GCC1	GRIP and coiled-coil domain containing 1
GCC185	GRIP and coiled-coil domain-containing protein 2
GDP	Guanosine DiPhosphate
GEF	Guanosine Exchange Factor
GM130	Golgin subfamily A member 2
GOLGA1	Golgi Autoantigen, Golgin Subfamily A, 1 (Golgin 97)
GOLGA5	Golgin A5 (Golgin 84)
GOLGB1	Golgin B1 (Giantin)
GOLM1	Golgi membrane protein 1
GOLPH3	Golgi Phosphoprotein 3
GPR107	G Protein-Coupled Receptor 107
GRASP55/65	Golgi Reassembly-Stacking Protein of 55 kDa /65 kDa
GFP	Green fluorescent protein
GO	Gene Ontology
H2B	Histone H2B
IF	Immunofluorescence
KD	Knockdown
KDEL	Lys-Asp-Glu-Leu
KIAA1107	AP2-interacting clathrin-endocytosis protein

MAPK	Mitogen Activated Protein Kinase
MgCl₂	Magnesium Chloride
MT	Microtubules
MTOC	Microtubule Organizing Center
mTOR	mammalian Target of Rapamycin
NGS	Next-generation sequencing
PBS	Phosphate Buffer Saline
PCA	Principal Component Analysis
PFA	Paraformaldehyde
PGC	Progastricin
PI4P	Phosphatidylinositol 4-phosphate
PIP5K1C	phosphatidylinositol-4-phosphate 5-kinase type 1
Plk1	Polo-like kinase 1
PRKACA	Protein Kinase CAMP-Activated Catalytic Subunit Alpha
qPCR	Quantitative polymerase chain reaction
RAS	Ras (Rat sarcoma) oncoprotein
RASGEF1A	RasGEF domain family, member 1A
RNA	Ribonucleic acid
RNAi	RNA interference
SCAP	SREBP Cleavage Activating Protein
SDS	Sodium Dodecyl Sulphate
Sec23	Secretory 23
SEM	Standard error of the mean
SEM4F	Semaphorin 4F
SERCA	sarco/endoplasmic reticulum Ca ²⁺ -ATPase
SFM	Serum Free Media
SNAREs	SNAP Receptors

SPCA	Calcium-transporting ATPase
SPRI	Solid Phase Reversible Immobilization
SREBP	Sterol Regulatory Element-Binding Protein
SYNGR2	Synaptogyrin 2
TGN	Trans Golgi Network
TLR	Toll-like receptor
TMCO3	Transmembrane and coiled-coil domains 3
TMEM165	Transmembrane protein 165
TMF1	TATA element modulatory factor 1
TRAPP	TRANsport Protein Particle
TRIF	TIR-domain-containing adapter-inducing interferon- β
TRIP11	Thyroid Hormone Receptor Interactor 11
TSO	Template Switching Oligo
USO1	General vesicular transport factor p115
VTC's	Vesicular Tubular Structures
WASL	WASP Like Actin Nucleation Promoting Factor

LIST OF FIGURES

1.1	Overview of the Secretory Pathway	20
1.2	COPI and COPII coat proteins	21
1.3	Two main models of membrane traffic.	22
1.4	Organization of the Golgi Complex	24
1.5	Electron micrograph of the Golgi Complex	25
1.6	Change in Golgi morphology during mitosis	27
1.7	MAP Kinase signaling at the Golgi	29
1.8	Many factors effect Golgi Organization	31
1.9	Stacking by GRASP proteins	32
1.10	Various Golgins serve as Golgi tethers	34
1.11	Golgi regulation by Rab proteins	35
1.12	Role of the COG complex in vesicle tethering	36
1.13	Actin and associated proteins in Golgi organization	38
1.14	Effect of the Microtubule network on Golgi organization	39
2.1	Golgi Phenotypes on different siRNA treatment	45
2.2	Variability within the same siRNA treatment	46
2.3	Hypothesis	47
2.4	Experimental design for hypothesis testing	49
2.5	SiRNAs with an effect on Golgi morphology	50
2.6	Analysis of Antibody intensity in siRNA treatments	51
2.7	Defining knockdown populations in siRNA treatments	51
2.8	Schematic Overview of the Pipeline	53
2.9	Schematic Workflow of CellCognition	54
2.10	Aquisition of training set and manual annotation	56
2.11	Testing classifier on a new image set	57
2.12	Probability of classification in two-channels	57

2.13	H2b-PAmCherry as a selective marker	58
2.14	Optimizing transfection of H2b-PAmCherry	59
2.15	Optimizing photo-activation parameters in live cells	59
2.16	Photo-activation of single-cells	60
2.17	Automation of Phenotype recognition and photo-activation	62
2.18	Cell loss between microscopy and flow cytometry	63
2.19	FACS plot of non-activated cells	64
2.20	FACS plot of activated normal phenotype	65
2.21	FACS plot of activated fragmented phenotype	66
2.22	Overview of processing for transcriptome sequencing	68
2.23	Bioanalyzer analysis of isolated nucleic acids	69
2.24	Total number of genes detected per sample	71
2.25	PCA plot of global transcriptome analysis	72
2.26	Changes in global transcriptome upon siRNA knockdown	72
2.27	Functional clusters in siAKAP9	73
2.28	Functional clusters in siTRIP11	73
2.29	Functional clusters in siUSO1	74
2.30	Up-regulated pathways in siAKAP9	75
2.31	Up-regulated pathways in siTRIP11	76
2.32	Up-regulated pathways in siUSO1	77
2.33	PCA plot of phenotype-based transcriptome analysis	79
2.34	PCA plot after removal of sample 'Fragmented 2'	80
2.35	Variability within Fragmented samples	81
2.36	Variability within Normal samples	82
2.37	USO1 expression in both phenotypes	83
2.38	Genes involved in clathrin-dependent endocytosis	89
6.1	Golgi proteins selected for siRNA treatment	127

LIST OF TABLES

2.1	Parameters for photo-activation	58
2.2	Samples for global transcriptomics	70
2.3	USO1 expression vs. median expression	83
2.4	Number of differently expressed genes	84
2.5	Genes involved in clathrin-mediated endocytosis	85
2.6	USO1 interactors	86
2.7	Differential expression of kinases and phosphatases	87
2.8	Biological process upregulated	88
2.9	Biological processes downregulated	88
5.1	Bacterial Cell Culture Reagents	107
5.2	Mammalian Cell Culture Reagents	107
5.3	Media Composition	107
5.4	Lab Equipment	108
5.5	Lab Reagents	108
5.6	Primary Antibodies	109
5.7	Secondary Antibodies	109
5.8	Oligonucleotides	110
5.9	Plasmids	110
5.10	List of reagents for cDNA library preparation	112
5.11	List of Oligos for cDNA library preparation	112
5.12	List of kits	113
5.13	List of analyzers used	113
5.14	List of software used	113

